

PhD Thesis

Interactions between bed material and biomass ash in dual fluid bed gasification

ausgeführt zum Zwecke der Erlangung des akademischen Grades eines
Doktors der technischen Wissenschaften (Dr. techn.)

unter der Leitung von
Prof. Hermann Hofbauer

Institut für Verfahrenstechnik, Umwelttechnik und technische Biowissenschaften
E 166

eingereicht an der Technischen Universität Wien
Fakultät für Maschinenwesen und Betriebswissenschaften

von
Matthias Kuba
Matrikelnummer: 0727381
Sprengersteig 11, 1160 Wien

Wien, am 11. November 2016

.....

Abstract

A promising way to substitute fossil fuels for production of not only electricity and heat, but also fuels for transportation and synthetic chemicals is steam gasification of biogenous feedstocks in a dual fluidized bed (DFB). The principle of this technology is the separation of combustion and gasification into two reactors. Bed material, nowadays, olivine, circulates between those reactors and acts both as heat carrier and catalyst. Interactions between biomass ash and bed material leading to layer formation on the surface of bed particles have been observed in the past. It was found that layer formation can have different consequences on the process. On the one hand, enrichment of ash components on the surface of bed particles can lead to agglomeration. On the other hand, Ca-rich layers showed a high catalytic activity towards tar reduction in DFB gasification.

Beside olivine no other suitable bed material for DFB gasification has been identified so far. Alternative bed materials could lead to an economical improvement of the process due to various reasons, e.g. finding an heavy-metal free bed material would lead to a reduction of deposition costs of the biomass ash. Furthermore, when installing DFB gasifiers in other regions locally available materials could be used as bed materials which would improve the economics of the operation.

In this work, three major aspects of the interaction between bed materials and biomass ash have been addressed. First, the influence of bed particle layers on possible alternative materials on the tendency toward agglomeration and deposit build-up in industrial-scale DFB gasification. Second, the catalytic activity of different layered bed particles regarding the reduction of undesirable tars. And third, the identification of mechanisms underlying layer formation on different bed particles. It was found that the admixing of foreign matter from biomass feedstock (e.g. quartz) into the olivine bed leads to increased deposit build-up due to enrichment of undesired compounds in the combustion reactor. Furthermore, promising characteristics regarding the thermal stability of its

layer have been observed for K-feldspar, a possible candidate for an alternative bed material. In addition, it could be proven that once a Ca-rich layer has formed, even non-catalytic materials, such as e.g. quartz, develop a satisfying catalytic activity. Steam reforming of different tar model compounds has been performed as well as the water-gas-shift reaction. All experiments showed a similar trend proving the comparably high catalytic activity of the Ca-rich layer. Pure CaO, used as benchmark material for the highest catalytic activity reachable for layered particles, showed promising catalytic properties for DFB gasification.

A layer formation mechanism for olivine was proposed and compared to the already known mechanism of layer formation on quartz. It was shown, that layer formation on olivine is based on a fundamentally different mechanism, where a solid-solid reaction leads to the substitution of Mg^{2+} and Fe^{2+} ions in the crystal structure of olivine with Ca^{2+} from the biomass ash. Due to this incorporation of Ca^{2+} into the crystal structure of olivine the bed materials keeps its low tendency toward agglomeration even during layer build-up. Thus, an alternative bed material should follow a similar layer formation mechanism than that of olivine. Such similarities were found for K-feldspar, however, more detailed research is yet needed to verify these first observations.

Finally, an outlook of future research fields regarding the interaction of biomass ash and bed material is given.

Kurzfassung

Die Dampfvergasung von Biomasse in einer Zweibettwirbelschicht ist eine vielversprechende Technologie hinsichtlich der Substitution von fossilen Energieträgern für die Produktion von Strom, Wärme, Treibstoffen und synthetischen Chemikalien. Das Prinzip der Technologie basiert auf der Trennung von Verbrennung und Vergasung in zwei separaten Reaktoren. Bettmaterial, derzeit Olivin, zirkuliert zwischen diesen beiden Reaktoren und dient sowohl als Wärmeträger als auch als Katalysator. Interaktionen zwischen der Biomasseasche und dem Bettmaterial führen zu Schichtbildung auf der Oberfläche der Bettpartikel und wurden bereits in der Vergangenheit beobachtet. Diese Bettmaterialschichten haben unterschiedliche Auswirkungen auf den Prozess. Einerseits führt diese Anreicherung von Aschekomponenten auf der Bettmaterialoberfläche zu Agglomeration, andererseits weisen die Ca-reichen Schichten eine hohe katalytische Aktivität hinsichtlich der Reduktion von Teeren im Zweibettwirbelschichtverfahren auf.

Neben Olivin wurden bisher noch keine anderen geeigneten Bettmaterialien identifiziert. Alternative Bettmaterialien könnten zu einer Reduktion der Betriebskosten führen. Ein schwermetallfreies Bettmaterial könnte beispielsweise die Entsorgungskosten der Ascherückstände senken. Darüber hinaus könnten lokal verfügbare Materialien die Wirtschaftlichkeit dezentraler Anlagen verbessern.

In dieser Arbeit wurden drei zentrale Aspekte der Interaktion zwischen Biomasseasche und Bettmaterial behandelt. Der erste Aspekt war der Einfluss der Bettmaterialschichten auf die Agglomeration und das Anbackungswachstum in industriellen Zweibettwirbelschichtanlagen. Bei dem zweiten Aspekt handelte es sich um die katalytische Aktivität der Bettmaterialschichten hinsichtlich der Reduktion von Teeren. Der dritte Aspekt war die Identifikation von Schichtwachstumsmechanismen unterschiedlicher Materialien.

Es konnte gezeigt werden, dass Fremdstoffe, beispielsweise Quarz, welche über den Brennstoff

in das Olivinbett gelangen, zu erhöhtem Anbackungswachstum führen. Darüber hinaus konnte eine Anreicherung unerwünschter Fremdstoffe im Verbrennungsreaktor festgestellt werden. Des Weiteren konnten vielversprechende Charakteristiken hinsichtlich der thermischen Stabilität der Bettmaterialschichten beim Einsatz von K-Feldspat beobachtet werden, welcher als mögliches alternatives Bettmaterial identifiziert wurde.

Es konnte ebenfalls gezeigt werden, dass Ca-reiche Schichten eine zufriedenstellende katalytische Aktivität vorweisen, unabhängig von dem ursprünglichen Bettmaterial. Daher konnte bei Vorliegen einer Ca-reichen Schicht auch für nicht-katalytische Materialien wie Quarz eine zufriedenstellende katalytische Aktivität beobachtet werden. Die Dampfreformierung unterschiedlicher Teer-Modellsubstanzen sowie die Wassergas-Shift-Reaktion wurden untersucht. Alle Experimente zeigten, dass Ca-reiche Schichten eine hohe katalytische Aktivität besitzen. Reines Kalziumoxid, welches als Benchmark-Material verwendet wurde, besaß die höchste katalytische Aktivität.

Ein Mechanismus für das Schichtwachstum für Olivin wurde vorgestellt und mit dem bereits bekannten Mechanismus des Schichtwachstums für Quarz verglichen. Es konnte gezeigt werden, dass das Schichtwachstum für Olivin auf einem grundsätzlich unterschiedlichen Mechanismus basiert. Eine Feststoff-Feststoff-Reaktion führt zu einer Substitution von Mg^{2+} und Fe^{2+} Ionen in der Kristallstruktur mit Ca^{2+} aus der Biomasseasche. Die Einlagerung von Ca^{2+} in die Kristallstruktur von Olivin führt zu keiner erhöhten Agglomerationstendenz durch diese Interaktion mit Biomasseasche. Ein alternatives Bettmaterial sollte also einem ähnlichen Schichtwachstumsmechanismus folgen wie Olivin. K-Feldspat wies Ähnlichkeiten zu Olivin in dessen Schichtwachstum auf. Allerdings ist noch weitere Forschung notwendig, um diese ersten Beobachtungen fundiert belegen zu können.

Abschließend werden zukünftige Forschungsbereiche, welche eng mit dem Thema der Interaktion zwischen Biomasseasche und Bettmaterial verwandt sind, vorgestellt und diskutiert.

Acknowledgements

I would like to express my sincerest thanks to everyone who has contributed to this work.

First and foremost, I would like to thank Prof. Hermann Hofbauer for giving me the opportunity to work in the field of biomass gasification. I greatly value the countless discussions, his encouragement and constructive criticism which leads to constant improvement. His passion for the field of biomass utilization and gasification in particular has motivated me from the time I started in his group as a master's student. I am now looking forward to the times ahead with the same motivation.

I own special thanks to my colleague Fritz Kirnbauer for his steady support and his mentoring over the past three years. Uncountable discussions – about scientific matters and much more – have made the time of my thesis extremely instructive and fascinating. His criticism and his way of turning my drafts of scientific papers upside down have taught me to view scientific ideas from different angles. Moreover, I am thankful for the nice and relaxed atmosphere in our shared office.

Prof. Marcus Öhman greatly supported this work and I would like to express my thanks for inviting me to join his research group in Luleå more than once during the last years. I am glad that we have started such a productive collaboration and I am looking forward to many exciting years to follow.

I would also like to thank Prof. Dan Boström for welcoming me in his research group in Umeå. I am thankful for his scientific contributions and that he shared his expertise with me. I am looking forward to deepen my knowledge about crystal structures under his guidance in the years to come.

Moreover, I would like to thank my close colleague Nils Skoglund from Luleå and Umeå for the joint work we have performed. There is a lot where we have just scratched the surface and where

we will continue to work on.

I thank my co-worker in Sweden, Hanbing He, for the pleasant time we spent during our joint work and for making the long hours in the SEM room so diverting.

Furthermore, I would like to express my thanks to Frank Maierhans, who has contributed greatly to this thesis by challenging the research with his experience of gasification in industrial scale and his drive to constantly improve the current state of the technology. Additionally, I thank Christian Bischof, Steffen Schneider, Sebastian Allgaier, Jürgen Müller and the whole team at the power plant in Senden for the good cooperation.

Also, I would like to thank Klaus Bosch for the close cooperation at the power plants in Oberwart and Heiligenkreuz and for the many interesting discussions we had over the last years.

In addition, I would like to thank all other colleagues in Luleå and Umeå for the great times while I was up there and all my colleagues at Bioenergy2020+ and TU Wien for the wonderful times here in Vienna. I especially thank Stephan Kraft for bringing me up to speed when I started in our research group and Markus Deutsch for the thought-provoking discussions we had in the past years.

Finally, the greatest thanks of all belong to my parents Trixi and Kersten, my sister Birgit and my girlfriend Paula for their encouragement and motivation, which have made all of this possible in the first place. Their open ears throughout the process of working myself into the topic, conducting my research and finally writing the thesis were indispensable for me and I will always be grateful for their unconditional support.

Contents

| | |
|---|-------------|
| Abstract | i |
| Acknowledgements | v |
| List of appended journal papers | ix |
| Author's contributions | xi |
| Other scientific publications of relevance | xiii |
| 1 Introduction | 1 |
| 1.1 Fundamentals and state-of-the-art | 1 |
| 1.1.1 The role of biomass in future technologies | 1 |
| 1.1.2 Biomass gasification in fluidized beds | 5 |
| 1.1.3 Interaction between bed material and biomass ash | 10 |
| 1.2 Objective and scope of this work | 13 |
| 2 Materials and Methods | 15 |
| 2.1 Experimental equipment in lab scale | 15 |
| 2.1.1 Set-up for magnetic bed material separation | 15 |
| 2.1.2 Apparatus for catalytic measurements | 16 |
| 2.2 Sampling from industrial scale power plants | 20 |
| 2.2.1 Dual fluidized bed gasification plant in Senden, Germany | 21 |
| 2.2.2 Dual fluidized bed gasification plant in Oberwart, Austria | 24 |
| 2.2.3 Bubbling fluidized bed combustion plant in Heiligenkreuz, Austria | 25 |
| 2.3 Analysis methods and equipment | 26 |

| | | |
|----------|--|-----------|
| 2.3.1 | Ashing of feedstock samples | 26 |
| 2.3.2 | X-ray fluorescence | 26 |
| 2.3.3 | Environmental scanning electron microscope with energy-dispersive spectroscopy | 27 |
| 2.3.4 | X-ray diffraction | 28 |
| 2.4 | Thermochemical equilibrium calculations | 28 |
| 3 | Summary of findings in appended journal papers | 29 |
| 4 | Results and Discussion | 33 |
| 4.1 | The role of bed particle layers in agglomeration and deposit build-up | 33 |
| 4.2 | Catalytic activity of bed particle layers | 41 |
| 4.3 | Mechanisms underlying bed particle layer formation | 51 |
| 5 | Future work | 61 |
| 5.1 | Clarifying bed particle layer formation mechanisms of different alternatives | 61 |
| 5.2 | Influence of different biomass feedstock on bed particle layer formation | 62 |
| 5.3 | Introduction of alternative bed material in industrial scale DFB power plants | 63 |
| 5.4 | Further utilization of biomass ashes from dual fluid gasification | 63 |
| 6 | Conclusion | 67 |
| | List of Figures | 69 |
| | List of Tables | 72 |
| | Bibliography | 73 |
| A | Journal Papers | 85 |
| A.1 | Paper I | 85 |
| A.2 | Paper II | 97 |
| A.3 | Paper III | 109 |
| A.4 | Paper IV | 123 |
| A.5 | Paper V | 135 |

List of appended journal papers

The work presented here is based on the following five peer-reviewed journal papers. Highlights of the results from the papers will be presented and put into context regarding the big picture of the research field. Details and deep insights are given in the corresponding journal papers. Throughout the thesis the papers are mentioned based on the Roman numerals assigned in the following list:

- Paper I** Deposit build-up and ash behavior in dual fluid bed steam gasification of logging residues in an industrial power plant
Kuba, M., He, H., Kirnbauer, F., Boström, D., Öhman, M., Hofbauer, H.
Fuel Processing Technology, **2015**, 139, 33-41.
doi:10.1016/j.fuproc.2015.08.017
- Paper II** Influence of bed material coatings on the water-gas-shift reaction and steam reforming of toluene as tar model compound of biomass gasification
Kuba, M., Havlik, F., Kirnbauer, F., Hofbauer, H.
Biomass and Bioenergy, **2016**, 89, 40-49.
doi:10.1016/j.biombioe.2015.11.029
- Paper III** Influence of coated olivine on the conversion of intermediate products from decomposition of biomass tars during gasification
Kuba, M., Kirnbauer, F., Hofbauer, H.
Biomass Conversion and Biorefinery, **2016**, 1-11.
doi:10.1007/s13399-016-0204-z

Paper IV Thermal stability of bed particle layers on naturally occurring minerals from dual fluid bed gasification of woody biomass

Kuba, M., He, H., Kirnbauer, F., Skoglund, N., Boström, D., Öhman, M., Hofbauer, H.

Energy and Fuels, **2016**, 1-11.

Paper V Mechanism of layer formation on olivine bed particles in industrial scale dual fluid bed gasification of wood

Kuba, M., He, H., Kirnbauer, F., Skoglund, N., Boström, D., Öhman, M., Hofbauer, H.

Energy and Fuels, **2016**, 1-11.

Author's contributions

- Paper I** Matthias Kuba planned and carried out the sampling of feedstock, bed material and ash fractions at the industrial scale power plant in Senden/Ulm, Germany. Furthermore, Matthias Kuba conducted the sample preparation, ESEM analysis and evaluation of the results. In addition, Matthias Kuba wrote the scientific paper.
- Paper II** Matthias Kuba planned and carried out the sampling of bed material at the industrial scale power plants in Senden/Ulm, Germany, and Heiligenkreuz, Austria. Matthias Kuba planned the experimental work and contributed in carrying it out as well as in the data evaluation. In addition, Matthias Kuba wrote the scientific paper.
- Paper III** Matthias Kuba planned the experimental work, reconstructed the lab-scale apparatus and carried out the experiments. Moreover, Matthias Kuba did the evaluation of results and wrote the paper.
- Paper IV** Matthias Kuba planned and carried out the sampling of feedstock and bed material at the industrial scale power plant in Senden/Ulm, Germany. Furthermore, Matthias Kuba conducted the sample preparation, ESEM analysis and evaluation of the results. In addition, Matthias Kuba wrote the scientific paper.
- Paper V** Matthias Kuba planned the sampling of feedstock and bed material at the industrial scale power plant in Oberwart, Austria. Furthermore, Matthias Kuba conducted the sample preparation, ESEM analysis and evaluation of the results. Moreover, Matthias Kuba wrote the scientific paper.

Other scientific publications of relevance

- Paper 1** Optimization of a 50 MW bubbling fluidized bed biomass combustion chamber by means of computational particle fluid dynamics
Kraft, S., Kuba, M., Kirnbauer, F., Bosch, K., Hofbauer, H.
Biomass and Bioenergy, **2016**, 89, 31-39.
doi:10.1016/j.biombioe.2016.02.020
- Paper 2** State of the art biomass gasification for CHP production – the Ulm plant
Kirnbauer, F., Maierhans, F., Kuba, M., Hofbauer, H.
Proceedings: International Conference on Renewable Energy Gas Technology, **2015**.
- Paper 3** Optimization of a 50 MW bubbling fluidized bed biomass combustion furnace by means of computational particle fluid dynamics
Kraft, S., Kuba, M., Kirnbauer, F., Bosch, K., Hofbauer, H.
Proceedings: European Biomass Conference and Exhibition, **2015**.
- Paper 4** Investigations on the catalytic activity of bed material coating regarding the water–gas–shift reaction and the steam reforming of model compounds for lighter and heavier hydrocarbons
Kuba, M., Havlik, F., Kirnbauer, F., Hofbauer, H.
Proceedings: European Biomass Conference and Exhibition, **2015**.

Paper 5 The role of 1H-Indene in product gas of biomass gasification

Kuba, M., Kirnbauer, F., Hofbauer, H.

Contribution: Asian Bioenergy Conference (IBSCE), **2015**.

Paper 6 Influence of calcium-rich coatings on the catalytic activity of bed materials in
CO₂-gasification of biomass

Kuba, M., Kirnbauer, F., Hofbauer, H.

Proceedings: European Biomass Conference and Exhibition, **2016**.

Chapter 1

Introduction

1.1 Fundamentals and state-of-the-art

Greenhouse gas concentrations in the atmosphere have reached levels unprecedented in at least the last 800,000 years and are still rising. The current scientific knowledge strongly indicates that rising concentrations of gases such as carbon dioxide (CO₂) and methane (CH₄) are likely to be the main cause of global warming [1]. Reducing CO₂, a long-lived climate pollutant, has been set a major goal in the framework of the Kyoto Protocol and was also the basis for the definition of the two degrees Celsius goal [2]. At the 21st session of the Conference of the Parties, which was held in Paris, France, in 2015 a new agreement was reached: The man-made temperature increase was limited to a value of 1.5 °C [3]. This awareness of the consequences of human-caused climate change leads to the development of technologies using renewable sources. The substitution of fossil fuels by renewable energy carriers is therefore a necessity to cover the global demand of energy. Biomass needs to play a role in achieving this goal, as it is the only renewable carbon based fuel and as such CO₂-neutral [4]. The utilization of biogenous residues in thermo-chemical conversion processes is a great potential and will be explained and discussed in further detail later on.

1.1.1 The role of biomass in future technologies

Sustainable use of biomass for the production of electricity or heat can be beneficial in economic and environmental matters. As biomass naturally stores energy, it can be understood as a constantly available energy carrier in contrast to solar or wind systems. Therefore, biomass plays an important role in balancing the rising share of fluctuating renewable electricity production [5].

Figure 1.1 shows the development of the shares of energy sources regarding the gross electricity generation in the European Union [6]. As it can be seen, the share of renewables increased significantly in the past ten years. In the year 2013 the share of renewables was the highest in the mix for electricity production. Figure 1.2 shows the distribution of the different types of renewable energy sources [6]. Comparing the trend of renewables in Figure 1.1 to that of hydro power in Figure 1.2, it can be seen that until 2002 hydro-power was the only significant renewable energy source in the mix. Starting from 2002, the share of wind power as well as biomass and renewable wastes has increased significantly. Biomass is currently the third most important renewable energy source for the production of electricity after hydro-power and wind-power and still has a significantly higher contribution than solar-power. Moreover, the share of biomass in the mix is constantly rising and it will play an important role in the energy generation of the EU in the foreseeable future. Figure 1.1 and Figure 1.2 also show an interesting milestone in Europe's policy: the introduction of a novel energy concept by the German government in 2010 [7] has boosted the share of solar-power and further increased the rise of wind-power. At the same time it led to a significant decrease of natural gas while solid fuels (mainly coal) have reversed their decrease. Biomass, however, has not been strongly influenced by this change of circumstances and has proven to be an energy carrier which continues to rise in a similar manner to the time from 2002 to 2010, which was the time before the policy in Germany has changed.

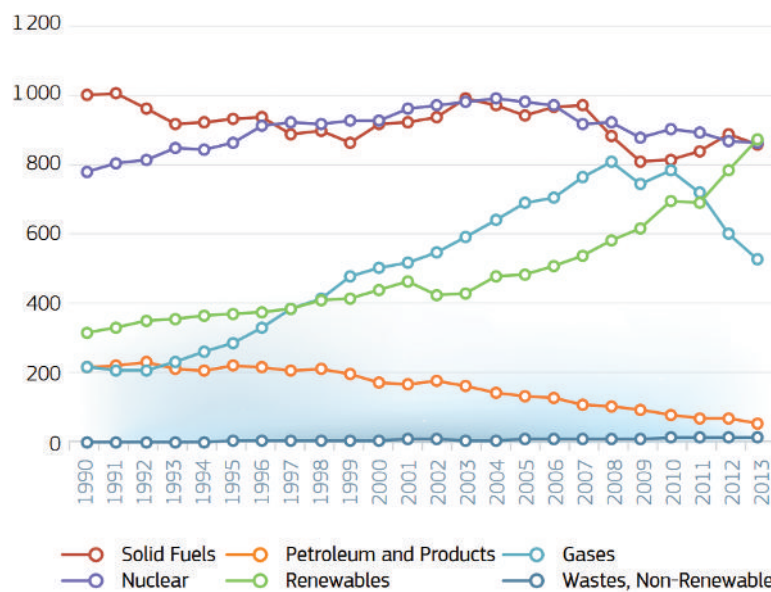


Figure 1.1: Gross electricity generation in the EU in TWh [6]

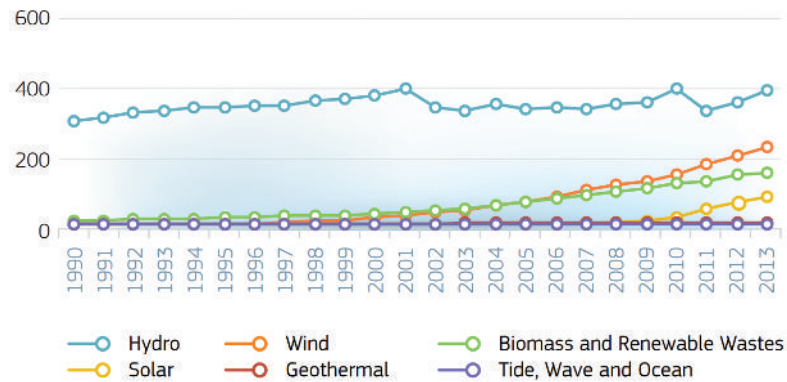


Figure 1.2: Electricity generation by renewable fuels in the EU in TWh [6]

In addition, the utilization of biomass can lead to a de-central energy supply, as locally available biogenous materials can be used as feedstock for pyrolysis, gasification, combustion or biogas systems. Thus, the transport ways of the input fuels could be minimized, and regionally added value could be created. If sustainably produced and used in an efficient way, biomass leads to significant savings of greenhouse gases compared to the use of fossil fuels. Furthermore, increasing awareness of the value of biomass as feedstock helps to motivate small forest owners to carry out sustainable forest management [5].

As biomass is the only renewable carbon carrier, its utilization in gasification systems possesses great potential. Further use of the product gas, gained from gasifying biogenous feedstock, for the production of e.g. transport fuels or green chemicals is a promising option for future use of biomass in addition to the production of electricity and heat [4]. Systems in which more than one product is gained are referred to as poly-generation. Thus, biomass could be used to balance variable energy sources at times when it is necessary and produce valuable secondary energy carriers when wind or solar power provide enough electricity [8].

Figure 1.3 shows an outlook for the bioenergy demand (in Mtoe) of the EU. A forecast of the demand in 2020 is compared to the demands of 2005, 2010 and 2015 [5]. As it can be seen, the most significant increase in the demand is that for biofuels. Thus, gasification is one of the most suitable and most promising technologies to cover the demands of the foreseeable future.

Sustainable use of biomass comprises not only the utilization of its stored energy, but includes also issues such as recovery of valuable materials (e.g. phosphorus), the utilization of certain ash fractions as fertilizers and the minimization of biogenous waste streams. Figure 1.4 shows the planetary boundaries, as defined by Steffen et al. [9]. The planetary boundary framework



Figure 1.3: Outlook for the bioenergy demand of the EU in Mtoe [5]

is based on critical processes that ensure the functionality of the Earth system. As shown, climate change is only one of the boundaries which are already in a state of uncertainty or even worse. Biogeochemical flows such as phosphorus or nitrogen are already in a state of high risk. Therefore, including the recovery of valuables and the further utilization of certain ash fractions is of high importance in a global scale and will be further addressed in depth later on. Sustainable utilization of biomass in thermo-chemical conversion processes such as gasification can address multiple issues to ensure the Earth system.

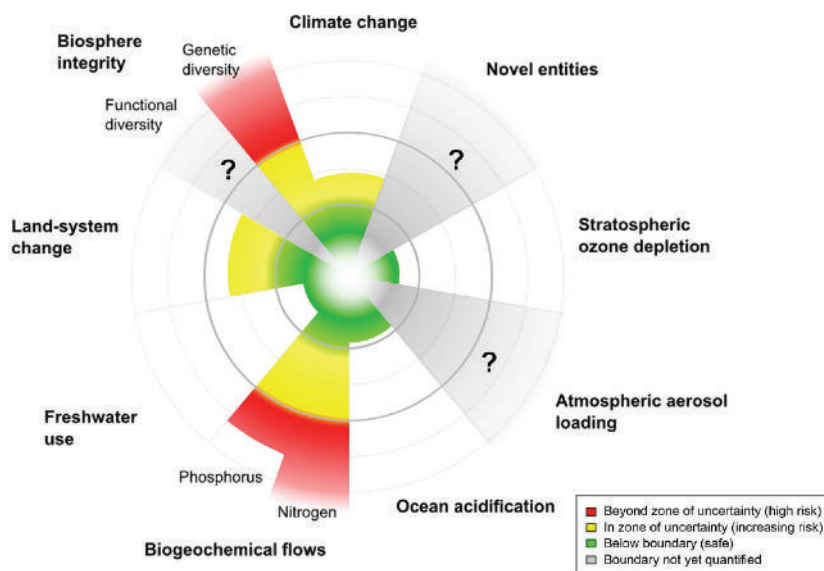


Figure 1.4: Current status of the nine planetary boundaries as proposed by Steffen et al. [9]

As described above, biomass feedstock is suitable for different technologies, such as pyrolysis, combustion, gasification or biogas production. Research performed within this work has been done in the field of gasification. Thus, further explanations will focus on gasification of biogenous

feedstock. The gas which leaves the gasifier – before it is further cleaned or upgraded – is referred to as product gas [4, 10]. Gas cleaning equipment downstream of the gasifier might be able to further adjust the gas composition, and therefore the gas stream might be called differently (e.g. synthesis gas) at later stages of the process.

1.1.2 Biomass gasification in fluidized beds

Gasification of solid fuels was first developed for coal as feedstock and went into operation in industrial scale for the first time in 1926 (Werk Leuna, BASF). The principle idea of gasification is to add value to a solid feedstock by converting it to a valuable secondary energy carrier, referred to as product gas. This gas contains desired components, such as carbon monoxide, hydrogen and methane, which can be further used [11].

The following reactions are typical for the gasification of a solid biomass feedstock:

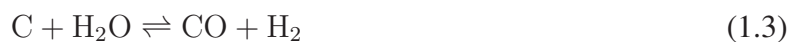
Oxidation:



Partial oxidation:



Heterogeneous water-gas reaction:



Boudouard reaction:



Hydrogenating gasification:



Gasification can be realized in fixed bed, fluidized bed or entrained flow systems. In the frame of this thesis only fluidized bed gasification will be addressed. Fluidization is a state, in which solid particles behave like a fluid through continuous contact with a gaseous medium. Fluidized bed systems have advantageous characteristics for gasification processes, such as a uniform temperature distribution throughout the bed or a fuel flexibility including fuels with comparably

high ash contents [11].

In biomass gasification fluidized bed systems have been proven to be suitable, as both bubbling fluidized bed systems and circulating fluidized bed systems are currently operated in industrial scale [12].

A dual fluidized bed (DFB) gasification system was developed at the TU Wien, Austria. Separation of endothermic gasification from exothermic combustion is the main principle underlying this technology, as shown in Figure 1.5. Separation is achieved using two separate reactors connected by a circulating bed material which acts as both heat carrier and catalyst in the process. Combustion provides the heat necessary for gasification [8]. Olivine, a naturally occurring magnesium-iron silicate, is currently used as bed material in the DFB process. It is characterised by a good performance avoiding agglomeration and defluidization [13]. Gas released from biomass feedstock in the gasifier contains heavier hydrocarbons, which are also referred to as tars. Up to this day there is no uniform definition of tar. Usually tar is understood to be every substance with a molecular weight larger than benzene. In gasification these tars are found in the product gas leaving the gasifier. They are highly problematic in downstream equipment once they condensate. As a result, slagging and fouling of downstream equipment can occur, which can lead to shut-downs of the whole process. Thus being another reason for the choice of olivine as bed material, as it has been shown to possess a catalytic activity towards reducing tars [14, 15, 16].

This technology has been developed from lab-scale to pilot-scale at the facilities of TU Wien, and was further scaled-up to industrial-scale. Since 2001 the process has been successfully demonstrated at the biomass power plant in Güssing, Austria, which has a fuel power of 8 MW_{th}. In Oberwart, Austria, a biomass power plant with fuel power of 8.5 MW_{th} has been in operation since 2007. At Senden, near Ulm in Germany, a plant with fuel power of 15 MW_{th} is operated since 2011. Details about the operation of the power plant in Senden will be given in further depth in Section 2.2.1.

Product gas obtained from gasifying solid feedstock can be used for the generation of electricity, district heat or the production of hydrogen, methane, Fischer-Tropsch diesel, or mixed alcohols, etc.

Hydrogen separation from product gas has been conducted at the industrial-scale power plant in Oberwart, Austria, where different process chains including a water-gas-shift, a membrane and a pressure swing adsorption unit have been successfully tested [17, 18, 19, 20, 21]. In addition,

hydrogen production using a water-gas-shift unit has been investigated at the industrial-scale power plant in Güssing, Austria [22]. Methanation of product gas has been first demonstrated using real product gas from a dual fluidized bed gasifier in Güssing [23]. An industrial-scale methanation plant was then installed downstream of the DFB gasification plant GoBiGas in Gothenburg, Sweden [24]. Fischer-Tropsch synthesis for the production of a 2nd generation bio-diesel has been investigated in lab-scale in Güssing [25, 26] and is currently under scale-up to a 1 barrel/day demonstration plant, which is also being erected in Güssing. Another possible upgrading technology of the product gas results in the production of mixed alcohols [27]. As a result of the flexibility of the process, it can quickly react to a fast changing energy market [8].

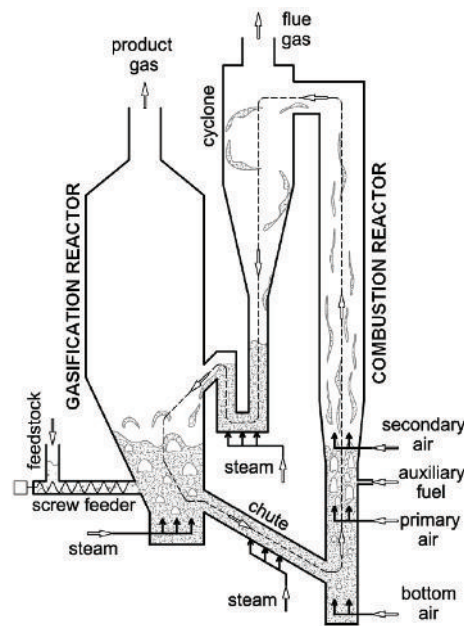


Figure 1.5: Dual fluid bed gasification as developed at TU Wien [8]

Next generation dual fluidized bed gasification is currently under investigation at the TU Wien [28, 29, 30]. The main renewal over the already established system is the novel design of the gasification reactor, which is based on the improvement of the solid-gas contact between catalytically active bed material and volatiles released from the biomass feedstock. A counter-current flow column with neckings is installed above the bubbling fluidized bed, where the released gas from the biomass feedstock has to pass through, increasing the intensity of contact in each necking, as shown in Figure 1.6. This counter-current column is supposed to decrease the tar content in the product gas significantly. However, the design of the gasifier is only one of the angles to approach the reduction of tars in the product gas. To explain other angles the formation and decomposition of biomass tars will be addressed in more detail first.

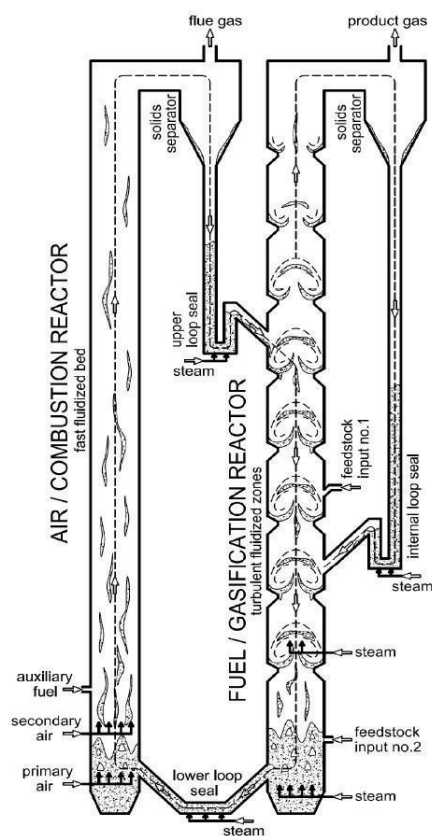


Figure 1.6: Novel dual fluid bed gasification system [28]

Tars are primarily produced in the pyrolysis stage due to breakage of the three main macro molecules of biomass: cellulose, hemicellulose and lignin. As a result, primary tars such as phenols and creosols are formed. At temperatures above 500 °C, these primary tars recombine into heavier molecules, referred to as secondary tars. A further temperature increase leads to the destruction of primary and secondary tars, resulting in the production of tertiary tars, such as naphthalene or pyrene. These are highly undesirable by-products as they can easily condense in downstream equipment [10]. Therefore, reducing these compounds is necessary to obtain a valuable product gas. The mechanism behind tar decomposition has been investigated in the past [31, 32, 33]. Figure 1.8 shows the decomposition mechanism of naphthalene [31]. As it can be seen, stable intermediate products such as 1H-indene, toluene, and benzene, are formed which have to be further converted to produce smaller gaseous molecules, such as CO, H₂, or CH₄. The conversion of toluene has been investigated in detail and findings can be found in the literature [34, 35, 36]. Toluene is a suitable tar model compound due to its molecular structure. Figure 1.7 shows the molecular structure of toluene, consisting of a CH₃ group attached to a phenyl group. It is an aromatic hydrocarbon and its composition can, therefore, be compared to a certain extent to higher tars.

The typical gaseous products that form during biomass steam gasification are carbon monoxide (CO), hydrogen (H₂), methane (CH₄), and carbon dioxide (CO₂). In lesser amounts, the product gas also contains larger molecules, such as ethene (C₂H₄). Table 1.1 shows the typical gas composition of the product gas, as measured at the industrial scale DFB gasification power plant in Oberwart [17].

Table 1.1: Typical product gas composition for DFB gasification of woody biomass [17]

| H ₂ (%) | CO (%) | CO ₂ (%) | CH ₄ (%) | C ₂ H _y (%) |
|-----------------------|------------|------------------------|------------------------|--------------------------------------|
| 38.6 ± 1.5 | 24.9 ± 1.3 | 22.3 ± 1.2 | 10.1 ± 0.6 | 2.7 ± 0.3 |

In addition, the product gas contains impurities such as H₂S, HCl, NH₃, their amount in the product gas highly depends on the presence of S, Cl and N in the feedstock. The molecules CO, H₂ and CO₂ are the result of steam reforming reactions and the water-gas shift reaction, which is explained in more detail in Section 2.1.2. The occurrence of CH₄ is most likely a consequence of both direct release from solid biomass feedstock [37] and the decomposition of heavier hydrocarbons [38]. Intermediate decomposition products, such as 1H-indene, are of special interest as they should not exist in significant amounts in the product gas, if sufficient contact with catalytically active bed material was ensured.

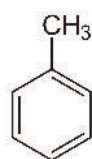


Figure 1.7: Molecular structure of toluene

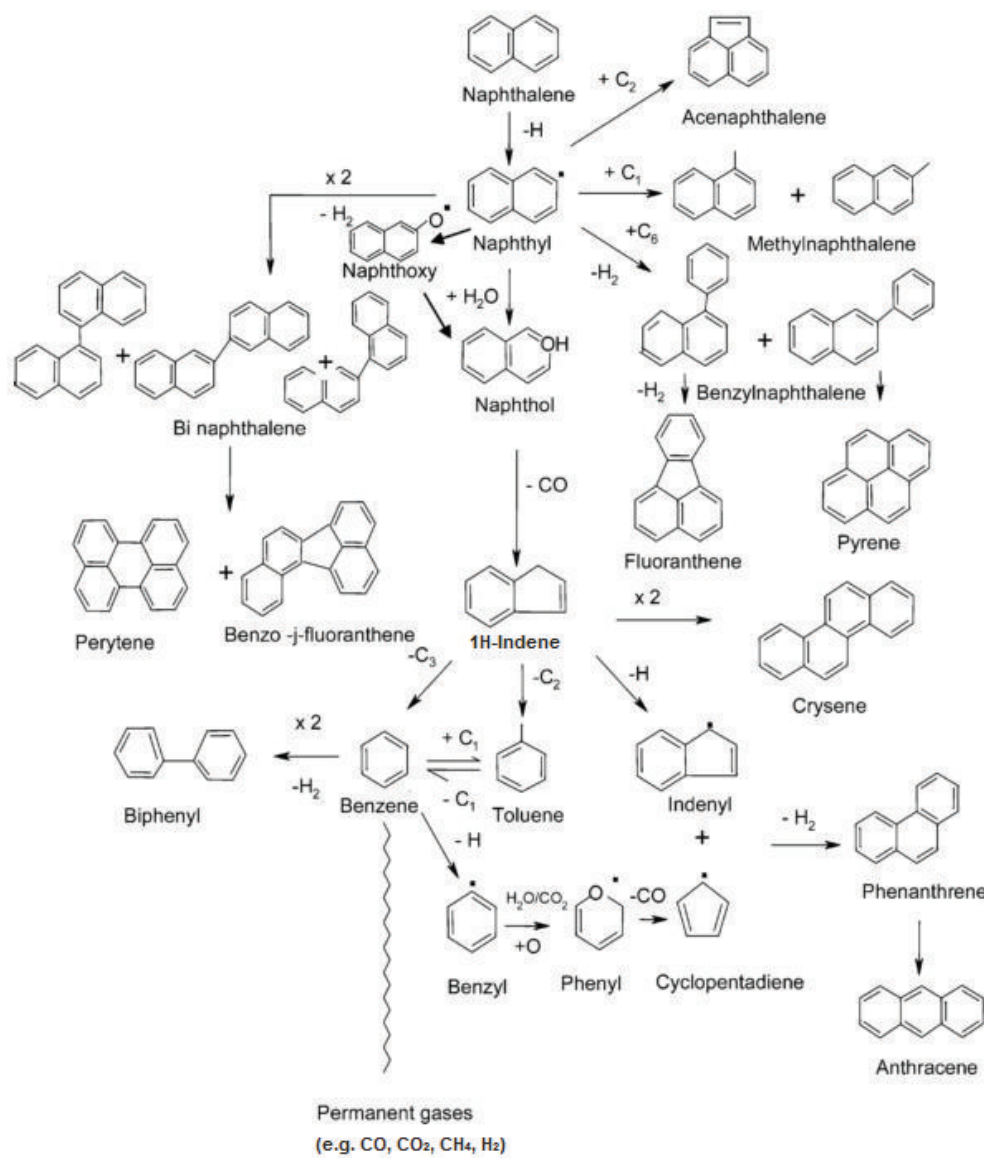


Figure 1.8: Decomposition mechanism of naphthalene as proposed by Devi et al. [31] (adapted)

1.1.3 Interaction between bed material and biomass ash

It has been found that biomass ash and bed materials interact at elevated temperatures, e.g. above 750 °C, in fluidized bed combustion or gasification. This interaction leads to the formation of bed particle layers, which have been observed for the first time on quartz particles in fluidized bed combustion [39, 40, 41, 42]. Layer formation on quartz particles has been identified to be initiated by alkali-attack from the gas phase [43] leading to low-melting eutectic mixtures with free silica from the quartz particle [44]. These low-melting particle surfaces play a critical role in agglomeration and deposit build-up during operation of fluidized beds [45, 40, 42, 46, 47]. Figure 1.9 shows agglomeration of quartz particles due to layer formation, as the bed particle

layers result in necks which act as glue in the fluidized bed and lead to defluidization. In the image, which originates from analysis in a scanning electron microscope, the black area is the background, grey areas are particles and white areas are necks between those particles.

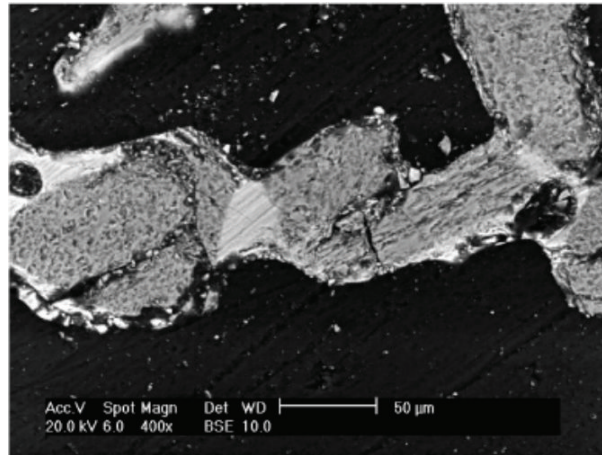


Figure 1.9: Agglomeration of quartz particles as observed by Brus et al. [48]

He et al. have observed layer formation on quartz particles in combustion of biomass over time describing the initiating step to be potassium (K) attacking the particle surface from gas phase. Over time calcium (Ca) diffused into the first K-dominated layer and a second outer layer starts to form. This outer layer grows outwards and calcium diffuses also further inwards into the inner particle layer [49]. It was shown that the tendency towards agglomeration could not be solely attributed to bed materials, but rather to the interaction between the bed materials and the ash components from the biomass feedstock. Depending on the biomass used, agglomeration, which leads to defluidization, varies significantly [44, 50, 51]. De Geyter et al. have investigated different combinations of feedstocks and bed materials and observed significant differences in layer formation and defluidization tendencies [52]. Free Si in the biomass ash is a strong reaction partner for K or Na and therefore tends to form K-silicates or Na-silicates, which lead to low melting ash. This might inhibit or decelerate the formation of particle layers. Agglomeration during combustion of woody biomass in quartz beds can, therefore, occur either as a result of bed particle coatings, which is referred to as coating-induced, or as a consequence of biomass ash melting, which is referred to as melt-induced [43, 53, 54].

Layers on olivine particles in dual fluidized bed gasification were investigated for the first time by Kirnbauer and Hofbauer [55] by analysing samples from the power plant in Güssing. Figure 1.10 shows the inner and outer layer on olivine particles. Results of the composition and morphology

of these olivine particle layers have been published and will be addressed later on. The main observation was the significant enrichment of Ca on the particle's surface [55].

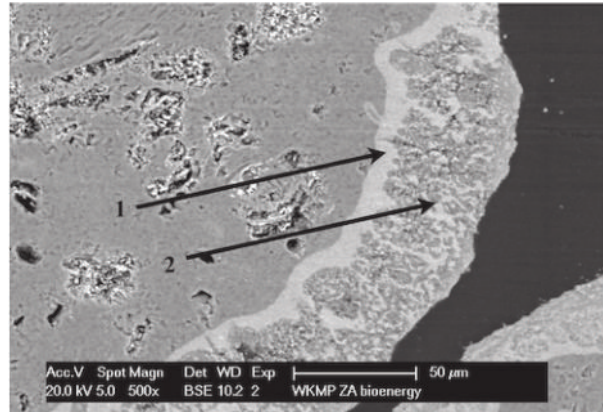


Figure 1.10: Bed particle layers on olivine in DFB gasification as observed by Kirnbauer and Hofbauer [55] showing an inner (1) and an outer (2) layer

These calcium-rich layers around the olivine particles were found to dramatically increase the catalytic activity regarding the reduction of biomass tars in comparison to the fresh olivine particles [56]. The tests were performed at the power plant in Güssing, the catalytic activity of those bed particle layers were further proven in lab-scale test-runs investigating the water-gas-shift reaction [57]. Moreover, resembling results regarding the activity of aged olivine particles were found during experiments at the Chalmer's gasifier [58]. Similar findings regarding the formation of a calcium-rich layer on olivine particles were also found when miscanthus was used as feedstock in fluidized bed gasification [59, 60]. Layer formation on olivine seems to be based on a different mechanism as layer formation on quartz particles. Kirnbauer and Hofbauer have given first insights into the mechanism of layer formation on olivine particles, describing a low driving force of potassium to retain in the crystal structure of olivine [61], which was also observed by Grimm et al. in their studies [13]. Calcium seems to play a more important role than potassium in the layer formation on olivine, however, the exact mechanism has not been stated. The increased catalytic activity of layered, used, olivine particles could be traced back to the increased amount of calcium on the particle surface [56]. However, different ash components are known to possess a certain catalytic activity towards gasification reaction, especially components such as potassium or calcium, but also e.g. sulphur. Thus, by using biomass feedstock, such components are brought into the system, which displays a great potential if they can be controlled [62, 63, 58]. As layer formation is based on interaction between inorganic components

of biomass ash and bed material, layer growth is highly dependent on the ash chemistry in the process. Different feedstocks and bed materials have different inorganic components, and therefore different reactions will take place. Understanding the ash chemistry for the used feedstock and bed material is therefore essential to control layer formation, thus, increasing the catalytic activity and at the same time inhibit agglomeration and deposit build-up. Possible reactions between the main ash forming elements determine the availability of inorganic components to react with the bed material leading to bed particle layer formation. Ash chemistry is therefore the basis for studying the inorganic components in fluidized beds [64, 65, 66, 67].

Interactions between inorganic compounds in biomass ash and bed particles have been investigated for different possible bed materials, such as bauxite or ilmenite resulting in different paths of ash-bed particle interaction [68, 69].

1.2 Objective and scope of this work

The main objective of this work is to investigate the interaction of biomass ash and bed material in dual fluid bed gasification. Thus, positive and negative consequences of layer formation are investigated.

Positive consequences are the increase of the catalytic activity of the bed material towards tar reduction. Therefore, a non-catalytic bed material, quartz, which has developed a Ca-rich layer due to interaction with biomass ash, is compared to olivine regarding its catalytic activity towards tar decomposition. Moreover, the enhancement of the conversion of intermediate tar decomposition products, such as 1H-indene, are investigated for layered bed particles in comparison to fresh ones. Catalytic investigations are benchmarked to pure CaO, as bed particles can enhance their catalytic activity maximally to that of pure CaO when developing Ca-rich layers.

Negative consequences of layer formation are agglomeration and deposit build-up, as layer formation can mainly be understood as an enrichment of biomass ash (essentially an enrichment of certain biomass ash components) on the bed particle surfaces. Thus, the risk of melting processes leading to agglomeration or deposit build-up increases. The influence of foreign matter (e.g. quartz particles) in the olivine bed is investigated and evaluated. Moreover, the thermal stability of particle layers on different naturally occurring bed materials is addressed and explained.

The key to replace olivine in the DFB gasification process is understanding the principle for-

mation mechanism of the layers. As olivine shows satisfying characteristics in its performance when used in DFB gasification, the exact mechanism of layer formation on olivine particles is discussed.

Deriving from the knowledge of this mechanism and from findings of the thermal stability of layers on different particles, essential characteristics for possible alternative bed materials are suggested, allowing for targeted search of suitable alternative materials.

Finally, an outlook of research topics, which emerge from the basis laid with this work, will be given and future research tasks will be presented.

In this thesis the following three research questions will be answered:

1. How do bed particle layers influence agglomeration and deposit-build up in dual fluid bed gasification?
2. What is the consequence of Ca-rich particle layers on the catalytic activity towards tar reduction?
3. What are the different mechanisms underlying the formation of bed particle layers?

Chapter 2

Materials and Methods

In this section the equipment, which was used for investigations, is explained in detail. Laboratory test-rigs and the operation procedures are described as well. Moreover, industrial scale power plants, where bed material samples were collected, are described. As operational data from the power plants was used for the evaluation of the research conducted with the bed samples, insights into the operational procedure are given (especially for the power plant in Senden, Germany). Furthermore, analysis equipment and thermochemical calculation tools are explained.

2.1 Experimental equipment in lab scale

Experimental equipment in lab-scale was used to investigate the catalytic activity of bed particle layers. Thus, before used for catalytic investigations the olivine bed material from industrial plants had to be separated from foreign matter to ensure the targeted investigation of olivine particle layers.

2.1.1 Set-up for magnetic bed material separation

Separation of olivine particles from foreign matter, which was present in bed material due to admixing of minerals from the feedstock with the fluidized olivine bed, was performed by a lab-scale separation device. The separator was developed for this specific application and was based on the magnetic properties of olivine. Since olivine is an iron-magnesium-silicate a certain magnetic force could be assigned to olivine particles which is not present for foreign matter (mainly quartz or feldspar particles). Therefore a magnetic separator has been installed and applied to gain a pure olivine particle fraction before further catalytic investigations, which are

presented in detail in Paper II and Paper III.

Figure 2.1 shows a simplified flow sheet of the particle separator. In the figure the ideal case for 100 % separation is shown. The bed material was transported by a vibrating chute and fell into a storage bucket. Falling bed material passed a neodymium magnet, which deflected olivine particles into a separate bucket. As the separation did not occur ideally, the fraction which was not deflected was then brought to the shaker again and the procedure was repeated. In total, each bed material charge was led through the separator six to eight times.

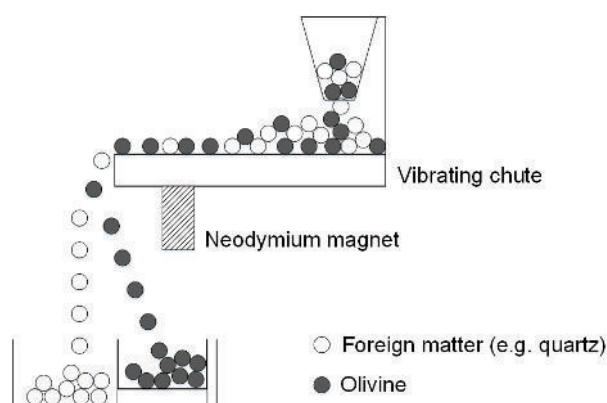


Figure 2.1: Scheme of the lab-scale magnetic separator

2.1.2 Apparatus for catalytic measurements

Investigations in Paper II and Paper III regarding the catalytic activity of bed particle layers towards tar reduction were performed with a lab-scale apparatus, which will be explained in the following: Figure 2.2 shows a flow chart of the employed test-rig. Model tar components, such as toluene or 1H-indene, could be introduced in liquid state via a syringe pump, as shown in Figure 2.2 – (1). Liquids were pumped into an evaporator where complete transformation of the model tar into the gaseous state took place. The temperature of the evaporator was chosen according to the model tar. A carrier gas stream was brought into the evaporator to drag the evaporated tar compound to the reactor zone. Nitrogen was used as the carrier gas for all experiments included in this thesis, since it is inert and therefore does not interfere with the reactions to a noteworthy extent but merely dilutes the produced gas.

Demineralized water (Figure 2.2 – (2)) was transported separately to the reactor. Pressurized nitrogen pushes the water from a reservoir through a liquid mass flow controller. Then, it was brought to a controlled evaporator mixer (CEM) from Bronkhorst, where it was transformed

completely into steam and was mixed with a carrier gas. The evaporator was operated at a constant temperature of 135 °C. Nitrogen was used as the carrier gas, analogous to the model tar carrier gas stream. The mixture of water and the carrier gas could be either led directly to the reactor zone or switched to a bypass. All pipes leading to the reactor were trace heated to 200 °C to avoid premature condensation.

It was possible to introduce up to six different gases (Figure 2.2 – (3)) into the reactor simultaneously. The gas streams were introduced via mass flow controllers (MFCs). All gas streams could be separately switched to a bypass or led to the reactor zone. Bypassing the gas mixtures was necessary for calibration of the gas measurement unit and ensured its functionality right before each experiment. Calibration was conducted by the certified Test Laboratory for Combustion Systems of the TU Wien.

Figure 2.3 shows a more detailed scheme of the reactor part. A quartz glass tube with an inner diameter of 1.0 cm and an outer diameter of 1.2 cm was used as reactor. Quartz glass was chosen as it merely influences the water-gas-shift or steam reforming reactions. Moreover, it is suitable at temperatures between 700 - 900 °C, which was the intended temperature range, as explained in more detail later on. For the experiments around 10 grams of bed particles were inserted as a fixed bed, resulting in a bed height of about 7.4 cm. Quartz wool inside the quartz glass reactor held the particles in position. Gas always streamed downwards from top to bottom during the experiments.

A heating furnace was placed around the quartz glass reactor and a thermocouple continuously measured and the bed temperature inside. A second thermocouple was placed outside the quartz glass reactor which continuously measured the outside wall temperature of the reactor of the fixed bed. This second thermocouple was used to constantly check the functionality of the thermocouple inside the reactor. When an increasing offset of the temperature measurement inside the reactor was observed, the experiment was stopped, the thermocouple cleaned and the experimental run restarted. The temperature was continuously controlled and therefore constant temperature levels were ensured throughout the experiments. Quartz wool was installed as insulation outside of the reactor to reduce heat losses during operation.

Gas leaving the reactor was either led to through a Liebig cooler or through impinger bottles, depending on the model tar. When toluene was used as model tar the gas stream passed a Liebig cooler in which both water and toluene condensed. The cooling medium of the Liebig cooler was kept at a temperature of 0.1 °C. Condensed liquids were collected in a reservoir. As toluene

and water hardly intermix the two phases could be easily separated from each other for further measurement.

In the case of 1H-indene as tar model compound, the gas stream was led through two consecutive impinger bottles which were placed inside a cryostat. During the experiments of this work the cryostat was kept at a temperature of -8 °C. Tar sampling from the lab-scale test rig was similar to the Tar Sampling Guidelines [70], but was adapted for the apparatus. Gas was led through two consecutive impinger bottles in bypass mode at all times. The impinger bottles were filled with toluene as the solvent instead of a mixture of dry ice with isopropanol as suggested in the guidelines, since measuring 1H-indene was the primary goal. Time-defined tar sampling was performed by switching to two separate bottles, when a constant composition was measured for the produced gas. Time-defined tar sampling was conducted for 30 min. Pipes connecting the reactor outlet and the inlet to the bottles were constantly trace heated to a temperature of 200 °C to avoid losses through condensation. Figure 2.4 shows the set-up of 1H-indene sampling.

Measurement of collected samples was performed by the certified Test Laboratory for Combustion Systems at the TU Wien using a GC/MS to identify single tar components.

After condensation and sampling of tar components the gas stream was led to the gas analysis, which consisted of a five component Rosemount NGA 2000 online gas analyzer and an automatic data recording unit. Measurement of CO, CO₂, CH₄, H₂ and O₂ was carried out by the online analyzer and data was recorded every ten seconds. Before the off gas was finally released through a vent, the volume flow was measured by a gas meter.

Evaluation of gas compositions and conversion efficiencies was performed for steady state operation. Therefore, experiments were conducted until constant values were observed for a minimum of 40 min. Results from that time were then statistically evaluated. Each experiment was conducted three times to ensure reproducibility of the results.

The following reactions have been investigated using the lab-scale apparatus for measurements of the catalytic activity of bed materials. The exact procedures (e.g. flow rates) for the single reactions are given in the appended journal papers.

1. Water-gas-shift reaction:



2. Steam reforming of ethene (model compound for lighter hydrocarbons):



3. Steam reforming of toluene (model compound for heavier hydrocarbons):



4. Steam reforming of 1H-indene (model compound for heavier hydrocarbons / model compound for intermediate product of tar decomposition):



5. Steam reforming of methane:

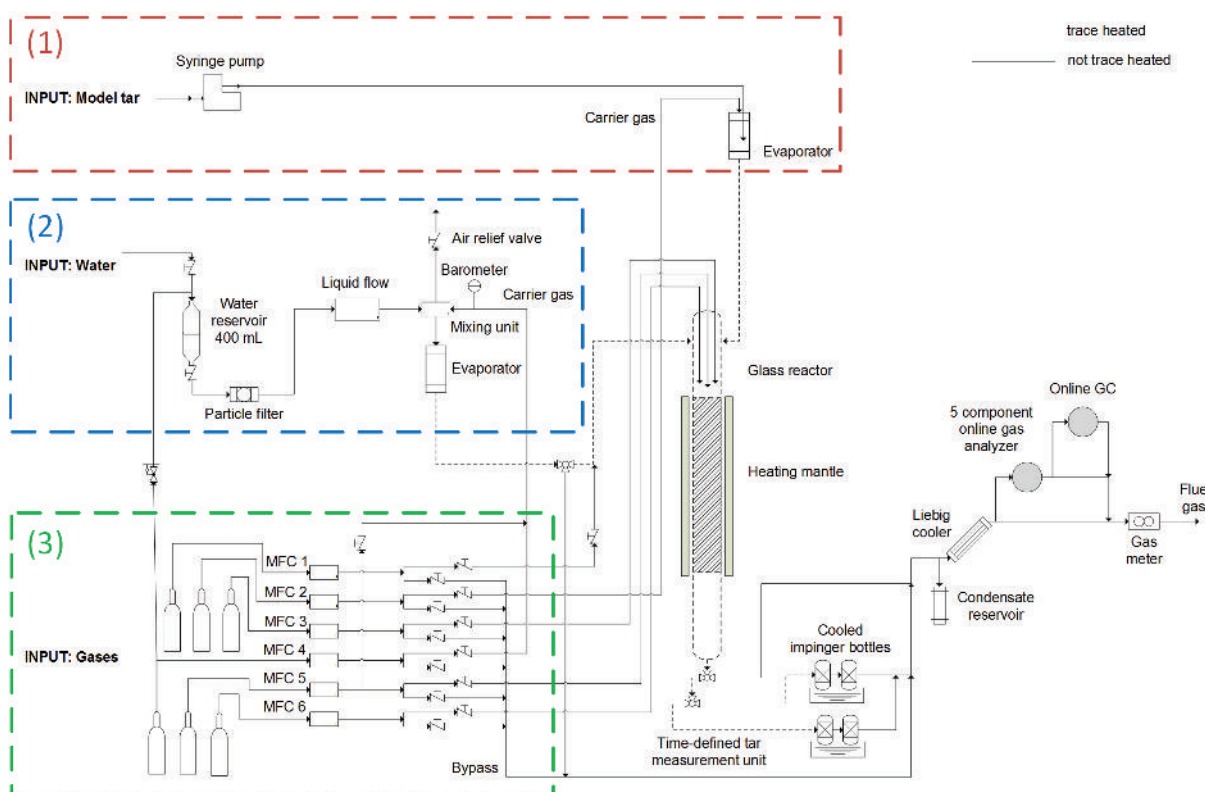


Figure 2.2: Flow-sheet of the lab-scale apparatus for catalytic measurements

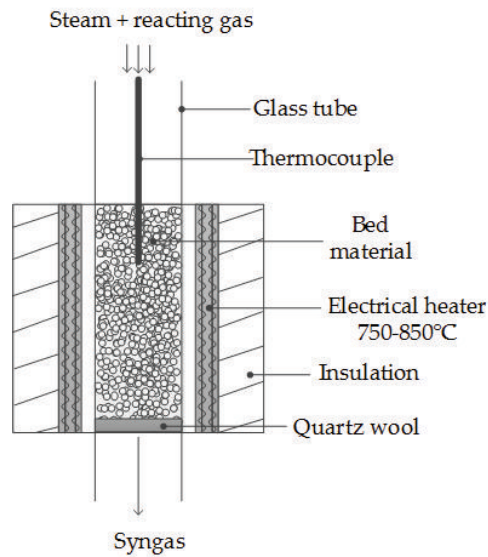


Figure 2.3: Scheme of the reactor part

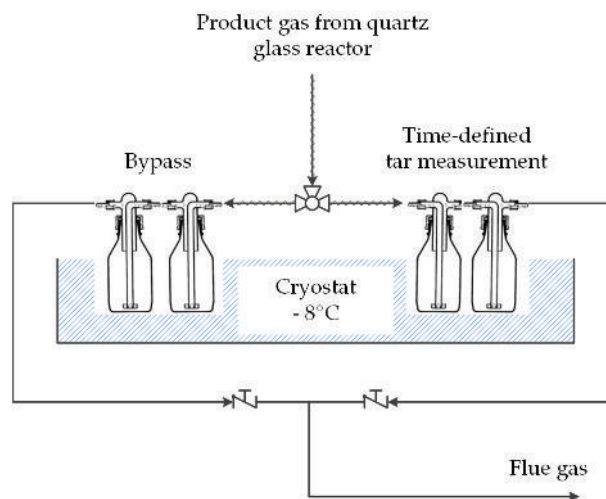


Figure 2.4: Set-up for sampling of the tar model compound 1H-indene

2.2 Sampling from industrial scale power plants

Long-term effects of the interaction between bed material and biomass ash were investigated using samples from industrial scale power plants. Olivine bed material and ash samples were collected from two different dual fluidized bed gasification plants, whereas quartz particles were collected from a bubbling fluidized bed combustion plant. Those three power plants will be described in the following sub-chapters.

2.2.1 Dual fluidized bed gasification plant in Senden, Germany

For investigations regarding the layer formation on olivine particles, samples were collected at the industrial scale power plant in Senden, near Ulm, Germany. Samples collected on-site in Senden were used for Paper I, Paper II, Paper III and Paper IV.

The power plant has a fuel power of 15 MW_{th}, generates electricity of about 5.1 MW_{el} in two gas engines and an organic rankine cycle (ORC) and also produces district heating of about 6.4 MW_{th} at full capacity. Logging residues, including cut-off root ends, tops, and branches, are used as biogenous feedstock. This feedstock comprises on average 15% of bark and 15% of needles; therefore, only 70% of the used fuel is wood chips. Because of decentered chipping, mainly conducted by the forest industry, the particle size distribution and water content vary considerably. The feedstock is collected in four storage silos before it is fed into the biomass dryer. Hence, a good fuel mixing can be achieved before the feedstock is put into the gasifier. The specifications mentioned above are constantly monitored by a feedstock management process executed by the staff of the power plant on site.

Figure 2.5 shows a flow sheet of the power plant. Feedstock enters the gasification reactor via a screw conveyor, where the biomass is led directly into the bubbling fluidized bed. Therefore, gases released from the biomass are immediately in contact with catalytically active bed material. Olivine is used as bed material. It has two major roles in the process. First, it acts as a circulating heat carrier between the combustion reactor and the gasifier. Second, it performs as a catalyst regarding the decomposition of tars. The bubbling bed is kept at a temperature of around 850 °C and steam is used as a gasifying agent. Calcite is brought into the system as an additive to enhance the catalytic activity of the olivine. Bed material is transported together with char from the solid feedstock from the gasifier into the combustion reactor via a chute. In this reactor air is used for fluidization and nearly full oxidation is achieved. As a result, bed material particles are heated up and temperatures over 1000 °C are reached. After it has been transported through the fast fluidized combustion reactor, the bed material enters a cyclone which separates the bed material from flue gas. Small particles which are not separated from the gas stream by the cyclone enter the post-combustion chamber. Air is added at the inlet of the chamber to secure oxidation of flue gas. Since the post-combustion chamber is widened after the inlet, the gas stream is slowed down and then it is further redirected by 180 ° before leaving the chamber. The gas stream is then led through a radiation channel where the temperature of the flue gas is cooled down to about 630 °C. Particles in the gas stream are again separated by a gravitational separation unit.

Bigger particles are recirculated back into the combustion reactor and are referred to as coarse ash. Smaller particles are dragged to a flue gas filter by the gas stream and are collected as fine ash. This fine ash is finally removed from the system.

Small biomass particles which are entrained out of the gasifier together with the product gas stream are referred to as fly coke. The product gas is cooled down by heat exchangers before passing through a product gas filter, where fly coke is separated. Impurities in the product gas which cannot be separated by the filter, such as tars, ammonia or sulphur components, are captured in a product gas scrubber filled with methyl ester of rapeseed (RME). Collected fly coke is transported back into the combustion reactor, since it still contains combustible compounds. The cleaned product gas is utilized in gas engines to generate electricity and heat. A small amount of product gas is brought back to control the temperature of the combustion zone. Used, layered, olivine is periodically replaced by fresh olivine to make up for bed material losses owed to attrition. Therefore, used (aged) olivine is taken out of the combustion reactor at the bottom and fresh olivine enters together with coarse ash and fly coke.

Samples of bed material, fly ash, coarse ash and fine ash were taken during steady state operation of the power plant at different times. The exact sampling procedures are explained in further detail in Paper I, Paper II, Paper III and Paper IV. Bed material and coarse ash samples sieved into the desired fractions before further use in lab-scale equipment. Thus, only a part of those samples was used in the investigations. As fly coke and fine ash were only used for XRF and XRD analysis, no sieving of the materials was necessary.

Figure 2.6 shows a more detailed illustration of the DFB reactors. The zones which are most likely to be critical regarding the thermal stability of bed particle layers and deposit build-up are highlighted. Critically high temperatures of up to 1100 °C and consequently high potentials for deposit build-up and slagging occur in the combustion path. Zones, which are critical regarding deposit build-up, were identified at the outlet of the combustion reactor, the cyclone and the post-combustion chamber. Table 2.1 shows average measured temperatures in those zones. It has to be stated here that the measured temperatures are gas temperatures at the corresponding position, thus, the temperatures are displayed here only as guide values for the tendency toward agglomeration and deposit build-up. The temperatures in the combustion path are compared to the temperature in the gasifier bed, which shows the significant temperature difference that is characteristic for the DFB system. Temperature peaks will be discussed in Section 4.1.

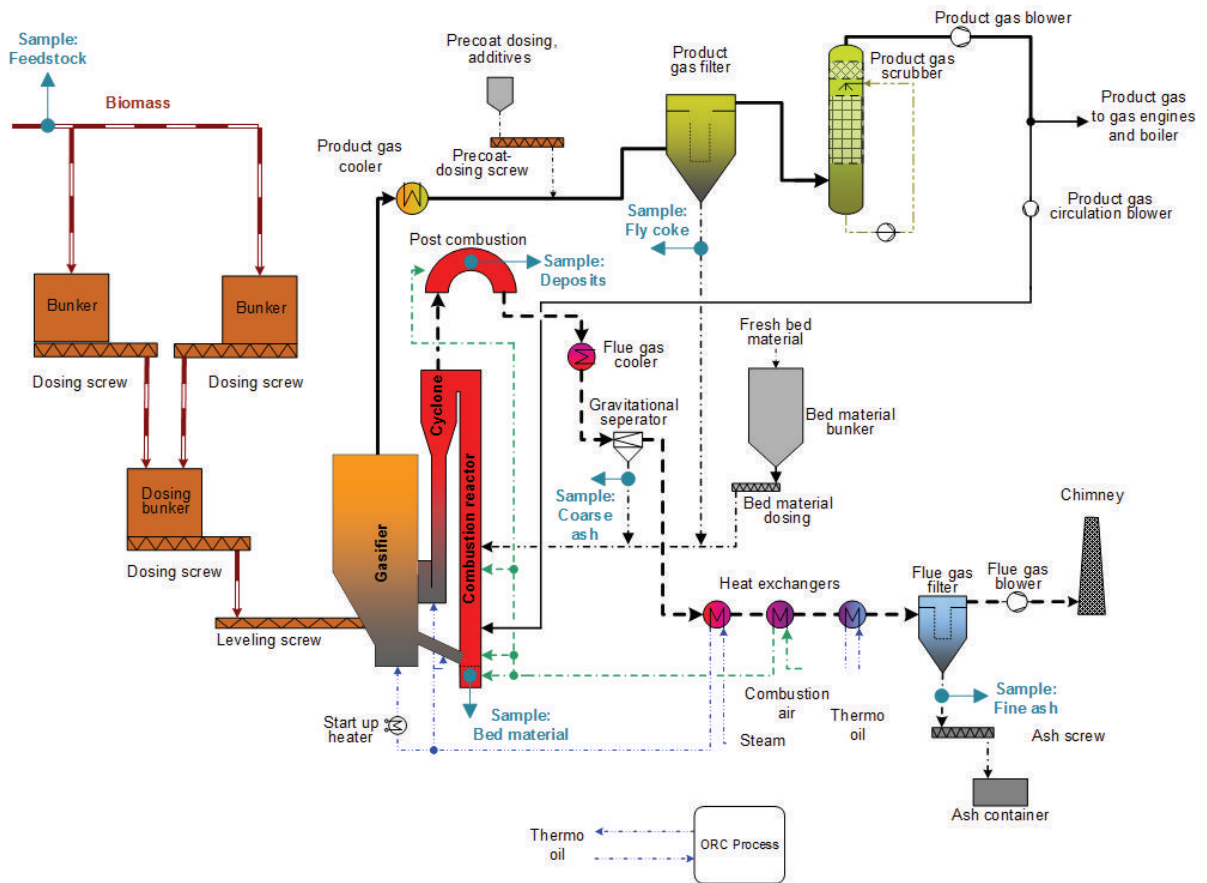


Figure 2.5: Simplified flow sheet of the dual fluidized bed gasification plant in Senden/Ulm

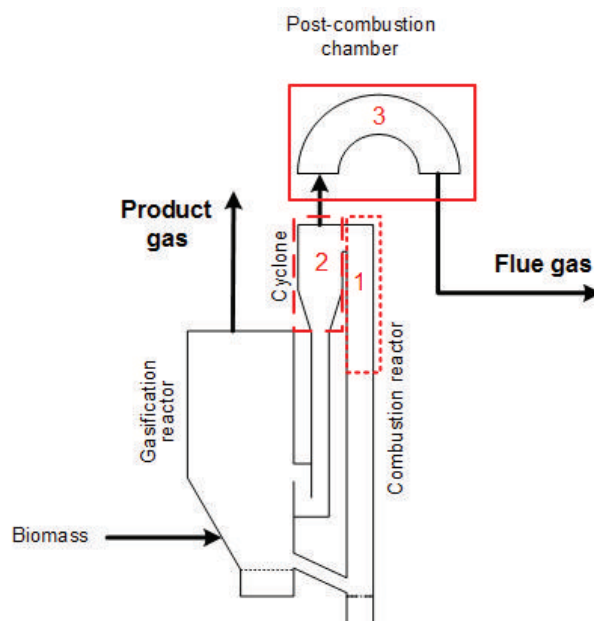


Figure 2.6: Zones with critically high temperatures (1) upper part of the combustion reactor, (2) cyclone, (3) post-combustion chamber

Table 2.1: Average temperatures in the gasification and the combustion reactor

| | Gasifier bed | Upper part of the combustion chamber | Cyclone outlet | Outlet of the post-combustion chamber |
|--------------------------------------|--------------|--------------------------------------|----------------|---------------------------------------|
| | °C | °C | °C | °C |
| Average | 856 | 884 | 1018 | 922 |
| Standard deviation (+/- 1 σ) | 5.6 | 5.9 | 26.8 | 37.5 |

σ ... standard deviation

2.2.2 Dual fluidized bed gasification plant in Oberwart, Austria

Investigations regarding the time-dependent layer formation on olivine particles under gasification circumstances were based on bed material samples from the industrial scale power plant in Oberwart, Austria. Results from these investigations can be found in Paper V.

The set-up of the power plant is almost analogous to the plant in Senden/Ulm, which is explained in Section 2.2.1 and therefore is not described in further detail here. A simplified flow sheet of the power plant is shown in Figure 2.7. Differences in certain parts of the power plants are of no further interest for the investigations of bed particle layer formation, which were performed in the course of this work.

The main difference between the two power plants is their size, as the plant in Oberwart only has a fuel power of 8 MW_{th} and generates electricity of around 2.5 MW_{el} in two gas engines and in an organic rankine cycle (ORC) and has the capacity to produce district heating of 4 MW_{th}.

Sampling of bed material was conducted periodically over the course of 17 days after the start-up of the power plant. The power plant was started up with fresh bed material, therefore, the formation of bed particle layers due to interaction with biomass ash could be observed in the investigated time-frame. Bed particle samples were sieved into the desired fractions before further use in lab-scale equipment. Thus, only a certain part of the samples was used in the investigations.

The sampling position of the bed material is shown in Figure 2.7, bed material was sampled with recirculated coarse ash. Thus, it might come to enrichment of certain compounds in the recirculation stream. However, this accumulation only occurs to a critical extend over long-term operation, therefore, the representativeness of the sampling of bed material can be evaluated as reliable, as the power plant was started with fresh bed material and no significant amounts of foreign matter were in the power plant at this time.

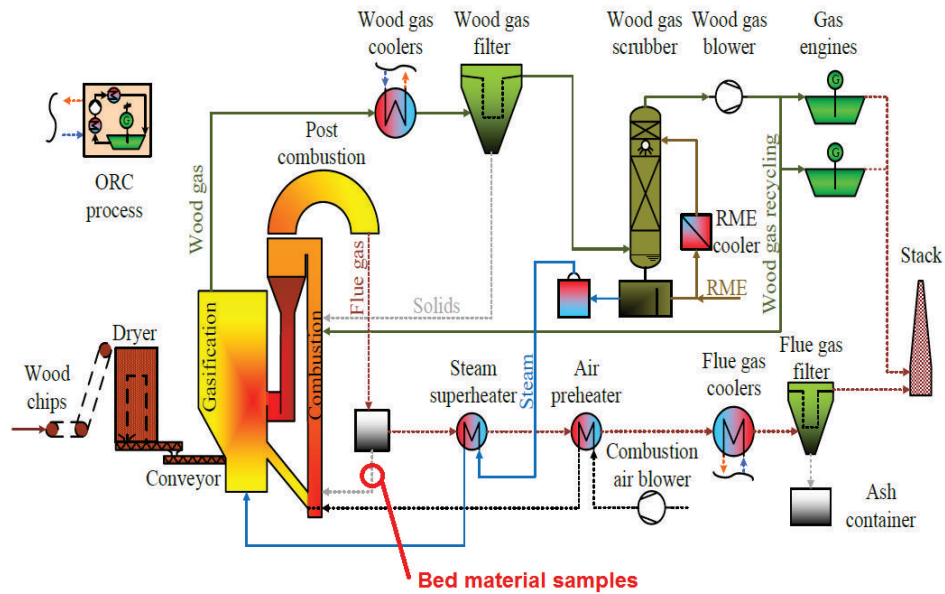


Figure 2.7: Simplified flow sheet of the dual fluidized bed gasification plant in Oberwart

2.2.3 Bubbling fluidized bed combustion plant in Heiligenkreuz, Austria

Samples of used, layered, quartz particles, which were investigated in Paper II regarding their catalytic activity towards the reduction of tars, were collected at the bubbling fluidized bed (BFB) combustion plant in Heiligenkreuz, Austria. The power plant has a fuel power of $48 \text{ MW}_{\text{th}}$. A simplified scheme of the combustion reactor is shown in Figure 2.8. The power plant comprises the combustion reactor, flue gas cooling, flue gas cleaning and the steam process including the steam turbine for generation of electricity. The combustion reactor is operated in gasification mode, which means that the bubbling fluidized bed is operated under-stoichiometric. Therefore, a burnable gas is produced out of the biomass, which is further combusted using secondary air in the freeboard. Therefore, the interaction between quartz sand and biomass ash in the bubbling fluidized bed occurs in gasification atmosphere (air-fuel equivalence ratio $\lambda < 1$).

Samples were collected before the start-up of the plant (fresh quartz bed samples) and during steady state operation by discharging bed particles from the bottom of the combustion reactor. Samples collected from the industrial-scale power plant were sieved into the desired fractions before further use in lab-scale equipment. Thus, only a part of the collected bed material was used in the investigations.

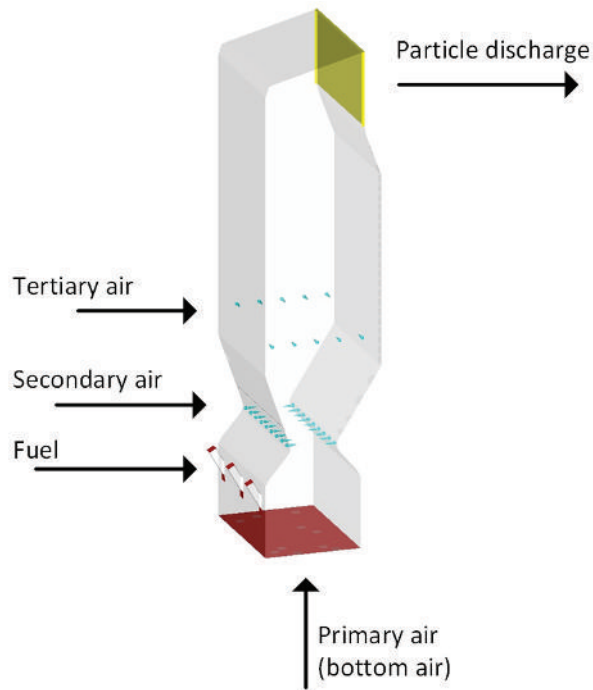


Figure 2.8: 3D- model of the bubbling fluidized bed combustion reactor in Heiligenkreuz [71] (adapted)

2.3 Analysis methods and equipment

In the following subsections analysis methods and used equipment will be explained. Procedures for specific cases are explained in further depth in the appended journal papers.

2.3.1 Ashing of feedstock samples

Feedstock samples were transformed into ash according to DIN CEN/TS 14775. Wood samples were heated up to a temperature of 250 °C. This temperature was maintained for 60 min. Then the temperature was increased to 550 °C and maintained until transformation of the biomass into ash was completed. The ash produced from the feedstock was then subjected to X-ray fluorescence (XRF) analysis.

2.3.2 X-ray fluorescence

The ash samples were melted in a Merck Spectromelt at 1050 °C and placed on a stainless steel plate at a temperature of 400 °C. Using the Spectromelt ensured that no evaporation of e.g. sodium or potassium took place. The XRF analysis was then carried out by a PANalytical Axios Advanced analyzer. This analyzer works in a vacuum with a rhodium anode, an excitation

voltage of 50 kV, and a tube current of 50 mA. Results of XRF analysis indicated the elemental composition of the total sample, all of which is present as oxides.

As the investigations regarding bed particle layer formation in this work are all done for woody biomass, typical fuel compositions of the CHP power plants in Senden and Oberwart are shown in Table 2.2. The power plant in Oberwart and the power plant in Heiligenkreuz use similar wood and as consequences of the layer formation regarding the fuel type will only be discussed for samples from Oberwart, the fuel composition from Heiligenkreuz is not included here.

It can be seen that the main compounds in the woody biomass ash are SiO_2 , K_2O , CaO , MgO and P_2O_5 . Also significant amounts of Al_2O_3 and SO_3 are present in the ash in both samples.

Table 2.2: Fuel ash composition (expressed as oxides) identified with XRF analysis

| | CHP plant Senden | CHP plant Oberwart |
|-------------------------|--------------------------|---------------------------|
| | mass ratio in (%) | |
| NiO | 0.0 | 1.5 |
| Fe_2O_3 | 0.7 | 2.0 |
| Cr_2O_3 | 0.0 | 0.0 |
| CaO | 55.6 | 35.4 |
| K_2O | 12.6 | 12.3 |
| SO_3 | 2.9 | 4.4 |
| P_2O_5 | 4.8 | 7.3 |
| SiO_2 | 13.4 | 19.8 |
| Al_2O_3 | 3.3 | 4.8 |
| MgO | 5.0 | 10.1 |
| Na_2O | 0.8 | 1.4 |
| Others | 0.9 | 1.0 |
| <i>Sum</i> | 100.0 | 100.0 |

2.3.3 Environmental scanning electron microscope with energy-dispersive spectroscopy

Collected samples were mounted in epoxy, cross-sectioned and polished. The chemical composition and morphology of the samples were determined by an environmental scanning electron microscope (ESEM) combined with energy dispersive X-ray spectroscopy (EDS). Elemental composition of different parts of the samples was determined by spot analysis of different fragments in the cross-section. Each fragment was analysed at three or four different points (EDS spot analysis) and numerous fragments from each sample were analysed (more than 10

per sample). The collected data was then statistically evaluated. Corresponding bed material and coarse ash samples from the same operational time were analysed in the same manner. Bed material layers with different thickness were investigated in detail.

2.3.4 X-ray diffraction

XRD data collections were performed with a Bruker d8 Advance instrument in $\Theta - \Theta$ mode with an optical configuration consisting of Cu $K\alpha$ radiation, and a Vantec-1 detector. Continuous scans were made; therefore, the total data collection time for each sample was more than 6 h. The PDF-2 databank with Bruker software was used to gain initial qualitative identifications. The data were then further analyzed by the Rietveld technique and structure data from the Inorganic Crystal Structure Database (ICSD). As a result, semi-quantitative information on the present crystalline phases was gained.

2.4 Thermochemical equilibrium calculations

Chemical equilibrium model calculations were performed to interpret the findings from experimental analysis regarding melt fragments and furthermore to gain insights into the mechanism of layer formation. Calculations were based on results gained from EDS analyses of the samples. Average values from the analyses were used. Fact-Sage 6.3 was used to investigate the thermodynamic driving force behind the formation of melt fragments. The program uses the minimization method of the total Gibbs free energy of a chemical system. Thermodynamic data were employed from the Fact database regarding gaseous compounds, stoichiometric condensed phases and non-ideal solutions.

Table 2.3: Elements and solution models used in the thermochemical equilibrium calculations

| | |
|------------------------|---|
| Elements | C, H, N, O, K, Na, Ca, Mg, Si, Fe, Al |
| Solution models | Slag: SLAGA (MgO, SiO ₂ , CaO, K ₂ O, Fe ₂ O ₃ , FeO, Al ₂ O ₃) Olivine (Mg, Fe, Ca//SiO ₃) MulF (Mullite Al ₆ Si ₂ O ₁₃ , Fe ₆ Si ₂ O ₁₃) Mel (Melilite Ca ₂ MgSi ₂ O ₇ , Ca ₂ Al ₂ SiO ₇ , Ca ₂ FeSi ₂ O ₇ , Ca ₂ Fe ₂ SiO ₇) Salt melt: MELTA (K, Na // CO ₃ , OH salt melt) LCSO (K, Ca // CO ₃ melt) SCSO (K, Ca // CO ₃ solid solution) |

Chapter 3

Summary of findings in appended journal papers

The main points from the appended journal papers relating to interaction between bed materials and biomass ash are summarized below. The focus lies on the development of bed particle layers and the consequences for biomass gasification processes.

The short summaries of findings in the journal papers give an overview of the results on which the following discussion in Chapter 4 is based.

Paper I

Olivine bed material and ash fractions from the dual fluidized bed gasification power plant in Senden/Ulm, Germany, were characterized based on elemental and crystallographic analysis. The build-up of deposits in the post-combustion chamber was investigated in detail clarifying the role of olivine and biomass ash. Impurities, such as quartz, diluting the fluidized olivine bed were found to have a major influence on deposit build-up due to reaction between potassium from the biomass ash with free silicon in quartz particles resulting in low melting eutectic mixtures. Olivine bed materials and especially layer fragments from aged olivine particles were found to be embedded in the deposits. An enrichment of critical components, especially melt fractions originated from impurities such as quartz, was observed in the combustion reactor. The enrichment occurs due to recirculation of coarse ash, which is separated from the flue gas stream, back to the combustion reactor. A solution for the operation of the power plant was proposed, namely periodical discharge of coarse ash from the system.

Paper II

The increase of the catalytic activity from fresh to layered olivine was compared to that from fresh to layered quartz sand. Both materials showed Ca-rich particle layers after long-term interaction with biomass ash. It could be proven that once a Ca-rich layer has developed, the bed material possesses a significantly higher catalytic activity regarding tar reduction (tested with the model compound toluene) and the water-gas-shift reaction, independent from the catalytic characteristics of the original particle. Thus showing that a non-catalytic material (in this case quartz sand) can develop satisfying catalytic activity over time when exposed to biomass ash in the process. The materials were compared to the benchmark material CaO, which represented the highest activity a Ca-rich particle layer could achieve, showing the importance of the Ca-content in the outer particle layer.

Paper III

The influence of Ca-rich particle layers on the decomposition of heavier hydrocarbons was investigated. Increased conversion of the model compound 1H-Indene, which is an intermediate product of the decomposition of heavier tars, when using layered instead of fresh olivine showed the importance of the bed material state. 1H-Indene could further be identified as important indicator substance in tar measurements regarding the catalytic behaviour of the fluidized catalyst bed. Problems regarding e.g. insufficient contact time between the catalytically active bed material and the tar-rich gas released from the biomass feedstock can be judged by measuring the content of the intermediate decomposition product 1H-Indene in the gas.

Paper IV

Bed material layers on three different materials, namely olivine, quartz and K-feldspar, have been investigated regarding their thermal stability in DFB gasification in industrial scale. Bed particle layers on olivine showed a low tendency towards agglomeration due to comparably high melting points. However, cracks in the particle layer led to breakage and as a consequence fragments in the process. Layer build-up on quartz particles takes place via the formation of low-melting potassium silicates leading to a high tendency towards agglomeration. Thus, quartz sand is not suitable as bed material for DFB gasification. K-feldspar showed promising characteristics due

to comparably high melting points of their particle layers. Furthermore, no crack formation could be observed and therefore no fragmentation of the particle layers took place. Thus, K-feldspar could be identified as possible alternative bed material in DFB gasification of biomass.

Paper V

Time dependent particle layer formation on olivine from an industrial scale gasification power plant has been investigated. From analysis of the bed material samples and supporting thermodynamic equilibrium calculations a mechanism describing the layer formation on olivine particles could be derived. The proposed mechanism is based on a substitution reaction in which Ca^{2+} ions are incorporated into the crystal structure of olivine. This occurs at one of the exchangeable sites M1 or M2 which is occupied by either a Mg^{2+} or a Fe^{2+} ion. Mg expelled from the crystal structure when replaced by Ca could be detected in a separate zone of the olivine particle layer. The proposed mechanism can explain numerous findings from literature and is therefore in good accordance with observations of biomass ash and olivine interactions.

Chapter 4

Results and Discussion

This chapter summarizes results regarding the three research questions investigated in the frame of this work, which are repeated at this point:

1. How do bed particle layers influence agglomeration and deposit-build up in dual fluid bed gasification?
2. What is the consequence of Ca-rich particle layers on the catalytic activity towards tar reduction?
3. What are the different mechanisms underlying the formation of bed particle layers?

Only highlights from the results will be presented here, detailed information on the findings are given in the corresponding journal papers. First, short summaries of the findings in the papers will be given. Moreover, findings will be presented across the single papers regarding the above mentioned cross-cutting topics.

4.1 The role of bed particle layers in agglomeration and deposit build-up

Agglomeration plays a significant role in fluidized bed systems, as explained in Section 1.1.3. In DFB gasification there exist zones of elevated temperatures exist, such as the cyclone or the post-combustion chamber. Figure 4.1 shows a histogram of the temperature measurements at the outlet of the cyclone and the inlet of the post-combustion chamber at the industrial-scale power plant in Senden. As it can be seen, the peak in frequency of the measurements is at

around 1020 °C, however more than 10 % of the measurements showed values above 1050 °C with maximum temperatures of 1100 °C. Deposit-build up has been observed during operation of the power plant. Thus, interaction between biomass ash and bed material may have critical consequences regarding agglomeration and deposit build-up.

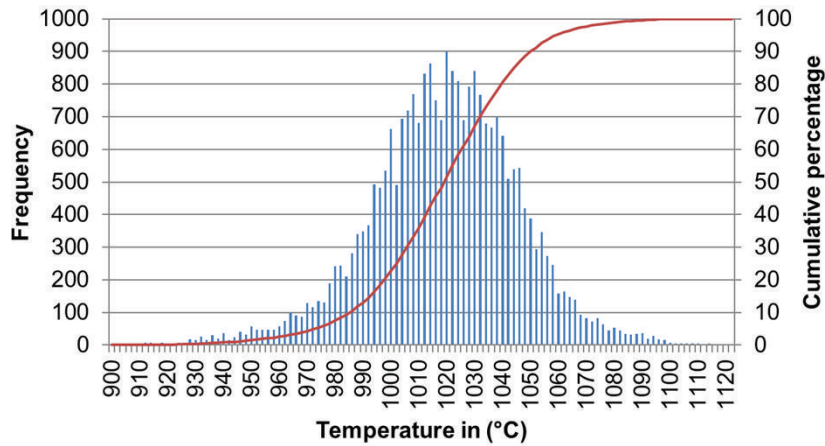


Figure 4.1: Histogram of temperature measurements at the outlet of the cyclone and respectively the inlet of the post-combustion chamber

In industrial-scale power plants using low-cost woody feedstocks, such as logging residues as used in the power plant in Senden, numerous impurities (e.g quartz particles) are brought into the gasifier together with the biomass feedstock. The influence of those particles which become mixed into the fluidized bed and dilute the olivine bed ESEM analysis performed for samples collected on-site in Senden showed a greater variety of different particles in the coarse ash than in the bed material fraction from the bottom of the combustion reactor. Higher amounts of impurities from the feedstock, such as quartz and feldspar particles, than in the bed material samples could be observed. XRF analysis of the samples are shown in Table 4.1. As it can be seen, impurities are characterised by increased amounts of potassium.

Numerous melt fragments and layered impurities with high amounts of potassium could be found, but XRD analysis did not detect the presence of potassium in crystalline structures to a significant extent, as shown in Table 4.2. Therefore, potassium seems to exist in an amorphous state rather than in crystallite structures. This indicates that melting processes proceed in areas with elevated temperatures, such as the post-combustion chamber. Chemical equilibrium calculations also showed comparably high amounts of melt at elevated temperatures for those fragments because of the relatively high content of potassium. It is noteworthy to mention that the samples showed

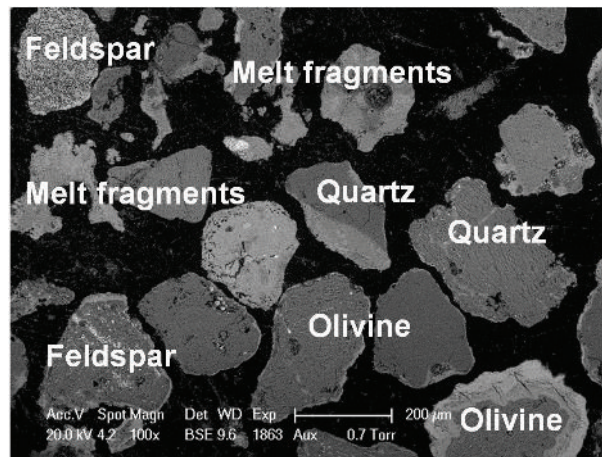


Figure 4.2: ESEM image showing the presence of impurities, such as quartz or feldspar particles, in the coarse ash fraction

a clear resemblance to the results for bed material analysis. High amounts of forsterite as well as lime and periclase characterized the coarse ash samples.

XRD analysis of deposits, as also presented in Table 4.2, showed occurrence of crystal structures which are typical of olivine, such as forsterite, Mg_2SiO_4 . Compounds with Ca and Si, such as larnite, Ca_2SiO_4 , and especially wollastonite, CaSiO_3 , could be found. Furthermore, a significant number of compounds with Ca, Mg and Si could be detected, such as akermanite, $\text{Ca}_2\text{MgSi}_2\text{O}_7$, merwinite, $\text{Ca}_3\text{Mg}(\text{SiO}_4)_2$ and bredigite, $\text{Ca}_7\text{Mg}(\text{SiO}_4)_4$. In addition, comparably high amounts of kalsilite, KAlSiO_4 , could be detected. Three different deposit samples from different positions in the post-combustion chamber were analysed.

Structures with high amounts of silica, aluminum and potassium, such as kalsilite, KAlSiO_4 , are most likely formed through an interaction between biomass ash and impurities. Thus, indicating that e.g. feldspar dissolved into the melt and formed new crystallite structures.

It is likely that melts from biomass ash and layered impurities get stuck on the olivine particles. Reaction with Ca-rich layers and Mg-rich areas seems to proceed. These attached fragments can easily break off the olivine particle and be found as fragments in the deposits. A high probability of breakage of these fragments is further supported by another observation. Numerous breakage areas for aged olivine particles could be detected in the coarse ash.

Particle size fractionation analysis of bed material and coarse ash showed that the average particle diameter is significantly smaller for particles recirculated with the coarse ash. As a consequence, these particles have a higher probability of leaving the system through the cyclone and entering the post-combustion chamber before they can enter again the gasification zone.

Table 4.1: Elemental composition (expressed as oxides) identified with XRF analysis

| | Deposit average | Bed material average | Coarse ash average | Fine ash average | Fly coke average | Impurities average |
|------------------------------------|--------------------------|-----------------------------|---------------------------|-------------------------|-------------------------|---------------------------|
| | mass ratio in (%) | | | | | |
| <i>NiO</i> | 0.0 | 0.2 | 0.2 | 0.0 | 0.2 | 1.6 |
| <i>Fe₂O₃</i> | 2.4 | 6.8 | 6.3 | 2.0 | 6.5 | 2.5 |
| <i>Cr₂O₃</i> | 0.1 | 0.2 | 0.2 | 0.1 | 0.2 | 0.6 |
| <i>CaO</i> | 34.0 | 13.8 | 11.0 | 54.6 | 16.5 | 22.9 |
| <i>K₂O</i> | 5.1 | 0.7 | 0.9 | 2.9 | 0.9 | 8.2 |
| <i>SO₃</i> | 0.1 | 0.1 | 0.1 | 0.4 | 0.1 | 0.3 |
| <i>P₂O₅</i> | 0.9 | 0.3 | 0.3 | 1.5 | 0.3 | 0.4 |
| <i>SiO₂</i> | 40.8 | 34.3 | 38.1 | 22.8 | 34.6 | 47.0 |
| <i>Al₂O₃</i> | 4.3 | 0.9 | 1.1 | 3.1 | 1.0 | 5.6 |
| <i>MgO</i> | 10.5 | 39.5 | 40.5 | 10.3 | 38.2 | 4.7 |
| <i>Na₂O</i> | 1.1 | 2.2 | 0.8 | 1.0 | 0.9 | 3.9 |
| <i>Others</i> | 0.7 | 1.0 | 0.5 | 1.3 | 0.6 | 2.3 |
| <i>Sum</i> | 100.0 | 100.0 | 100.0 | 100.0 | 100.0 | 100.0 |

Thus, a circulation of critical components in the coarse ash is created between the combustion chamber, the cyclone and the post-combustion chamber. This means that critical components, such as potassium-rich fragments leading to ash mixtures close to the eutectic point, are not only kept in the system, but seem to be mainly circulated in the combustion part of the dual fluidized bed. As a result, the recirculated particles have only a slight impact on the catalytic activity of the fluidized bed in the gasification zone as they are not frequently found there.

The formation of such critical potassium-rich layers on impurities, such as quartz, originates from interaction with potassium from biomass ash. The potassium searches for reaction partners and can form potassium-silicates with the free Si in quartz. This leads to comparably high amounts of potassium in the layers of these impurities. As the reaction between K and Si is likely to occur, the potassium which is bound in the feedstock has a high probability of reacting with impurities to form potassium-silicate compounds. These can be observed as brighter areas either as inner layer or along cracks where potassium can attack the inner particle surface, see Figure 4.3. Potassium reduces the melting temperature of the compound and is, therefore, critical regarding slagging and the build-up of deposits. Temperatures above 1000 °C in the post-combustion chamber lead to melting of the potassium-rich layers of the impurities and, as a consequence, make them sticky. These sticky layers are a critical factor in agglomeration and as a result defluidization of beds. In the outlet of the cyclone of the dual fluidized bed process temperatures of around 1020 °C are typical but that temperature fluctuations can cause peaks

Table 4.2: Crystalline phases identified with XRD analysis (samples from the plant in Senden)

| | | Deposit average | Bed material average | Coarse ash average | Fine ash average | Fly coke average |
|--------------------------|--|----------------------------|-------------------------------------|-----------------------------------|---------------------------------|---------------------------------|
| mass ratio in (%) | | | | | | |
| quartz | SiO ₂ | 1 | 3 | 4 | 1.5 | 4 |
| microcline | KAlSi ₃ O ₈ | n.d. | n.d. | n.d. | n.d. | 2 |
| forsterite | Mg ₂ SiO ₄ | 5 | 76.5 | 69.5 | n.d. | 32.5 |
| lime | CaO | n.d. | 3.5 | 6.5 | 27.5 | 3.5 |
| periclase | MgO | 1.5 | 3 | 5 | 4 | 2.5 |
| portlandite | Ca(OH) ₂ | 2 | n.d. | n.d. | n.d. | 15 |
| calcite | CaCO ₃ | 2 | 1.5 | n.d. | 45.5 | 21.5 |
| fairchildite | CaK ₂ (CO ₃) ₂ | n.d. | n.d. | n.d. | n.d. | n.d. |
| anhydrite | CaSO ₄ | 2 | n.d. | n.d. | n.d. | n.d. |
| gypsum | CaSO ₄ ·2H ₂ O | 2 | n.d. | n.d. | n.d. | n.d. |
| archanite | K ₂ SO ₄ | n.d. | 1.5 | 1.5 | n.d. | n.d. |
| apatite | Ca ₅ (PO ₄) ₃ (OH) | 1 | n.d. | n.d. | 1.5 | 1 |
| larnite | Ca ₂ SiO ₄ | 5.3 | 4 | 4.5 | 5.5 | 4.5 |
| wollastonite | CaSiO ₃ | 15.7 | n.d. | n.d. | n.d. | n.d. |
| rankinite | Ca ₃ Si ₂ O ₇ | 8.7 | n.d. | n.d. | n.d. | n.d. |
| akermanite | Ca ₂ MgSi ₂ O ₇ | 21 | n.d. | n.d. | n.d. | n.d. |
| merwinite | Ca ₃ Mg(SiO ₄) ₂ | 8 | 2.5 | 3 | 5.5 | 2.5 |
| bredigite | Ca ₇ Mg(SiO ₄) ₄ | 10 | 1.5 | 1 | 5 | 2.5 |
| kalsilite | KAlSiO ₄ | 9.3 | 1 | n.d. | 2 | 3.5 |
| | K ₂ MgSiO ₄ | 2.5 | 1 | 2.5 | n.d. | n.d. |
| | K ₂ MgSi ₅ O ₁₂ | 2 | n.d. | n.d. | n.d. | n.d. |
| hematite | Fe ₂ O ₃ | 1 | n.d. | n.d. | 1 | 2 |
| maghemite | Fe ₂ O ₃ | n.d. | 1 | 1.5 | 1 | 3 |
| magnetite | Fe ₃ O ₄ | n.d. | n.d. | n.d. | n.d. | n.d. |
| cristobalite | SiO ₂ | n.d. | n.d. | 1 | n.d. | n.d. |
| n.d. | not detected | | | | | |
| Sum | | 100 | 100 | 100 | 100 | 100 |

up to 1100 °C in the cyclone. Furthermore, smaller particles which are not separated from the flue gas stream by the cyclone pass through the post-combustion chamber, where the flue gas stream is redirected by 180°, as shown in Figure 2.5. Particles with sticky surfaces have a high probability of building up deposits through collision with the wall. Some of these particles are recirculated back to the combustion reactor after leaving the post-combustion chamber, where temperatures are still around 920 °C, and so stay in the system [63].

In combustion systems counter-measures include the dilution of critical components such as potassium in the bed and the replacement of old bed particles by fresh ones [72]. However, since the Ca-rich layers are necessary in gasification due to their catalytic activity, as explained in more detail in Section 4.2, such replacement would be counter-productive in terms of tar reduction. For this reason layer build-up is desirable and, therefore, bed particles should be kept in the system as long as possible. Thus using quartz sand as a bed material or quartz polluted fuel such as logging residues for dual fluid bed gasification is problematic as regards bed material agglomeration, slagging, and deposit build-up.

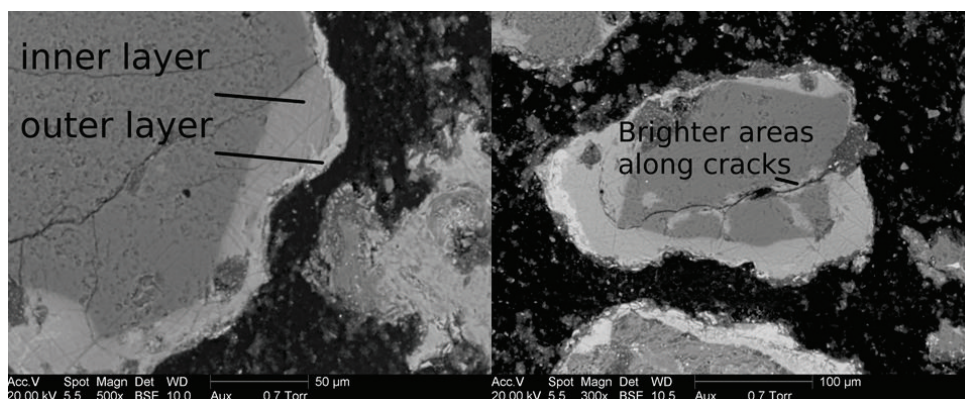


Figure 4.3: ESEM image of layers on and cracks in quartz particles

Certain deposit fragments – also referred to as melt fragments in the ESEM images – showed magnesium amounts of around 10 wt.%, which indicates the presence of olivine in the melt. Olivine itself is not prone to forming deposits; the particles are only embedded in a melt, as shown in Figure 4.4. Therefore, depositions with significant amounts of magnesium (around 10 wt.%) have to emerge from an interaction between olivine and impurity-driven melt, since significant amounts of Al and K could also be detected in those fragments. XRD analysis showed significant amounts of compounds with Si, Ca and Mg, such as akermanite, $\text{Ca}_2\text{MgSi}_2\text{O}_7$, merwinite, $\text{Ca}_3\text{Mg}(\text{SiO}_4)_2$ and bredigite, $\text{Ca}_7\text{Mg}(\text{SiO}_4)_4$, which also indicates an interaction

between olivine and biomass ash. Attachments of melt fragments to the olivine particles showed almost identical composition as the melt fragments, which are comparably rich in Mg, see Table 4.3. Thus showing, that melt fragments – most likely originated from interaction of biomass ash with impurities (e.g. quartz) – can collide with olivine particles and stick to them, which leads to interaction with the olivine. This results in an enrichment of Mg in the melt fragments. As they are attached to the olivine particles and stick out, there is a high probability for them to break off again, explaining the presence of Mg-rich melt fragments in the deposits. Investigations of the thermal stability of olivine particle layers performed in the frame of this work showed a low melting tendency of the layers due to a stable crystal structure containing of Ca, Mg and Si as the main components.

Table 4.3: Average elemental compositions on a C- and O-free basis of attached melt fragments

| | Mg-rich deposit (melt) fragments | Attached melt fragments |
|-----------|---|------------------------------------|
| | [wt%] | [wt%] |
| Na | 1.3 (+/- 0.3) | 0.2 (+/- 0.2) |
| Mg | 11.4 (+/- 1.3) | 11.0 (+/- 1.0) |
| Al | 3.7 (+/- 0.4) | 3.6 (+/- 1.0) |
| Si | 31.0 (+/- 0.8) | 30.9 (+/- 1.2) |
| P | 1.2 (+/- 0.2) | 0.6 (+/- 0.1) |
| S | 0.3 (+/- 0.2) | 0.2 (+/- 0.0) |
| Cl | 1.9 (+/- 0.8) | 0.4 (+/- 0.1) |
| K | 7.7 (+/- 0.9) | 7.4 (+/- 1.1) |
| Ca | 36.0 (+/- 2.5) | 40.7 (+/- 1.4) |
| Mn | 0.7 (+/- 0.1) | 0.8 (+/- 0.1) |
| Fe | 4.8 (+/- 0.7) | 4.2 (+/- 0.6) |

Due to the development of layers on bed material particles the surface stability changes relative to the original particle. Thermal changes of bed particles and their layers can lead to fragmentation and as a result to an increase of undesired fines in the system. Even though olivine particles did not show any signs of crack formation inside and satisfying characteristics towards agglomeration, calcium-rich particle layers were characterized by the development of cracks which led to breakage of parts of the layer. As a result, fragments of the layers exist loosely in the dual fluid bed system which increases the fines in the system.

Other impurities than quartz particles, e.g. K-feldspar, were also brought into the gasifier with the biomass feedstock in the power plant in Senden. Investigations of the layer formation on

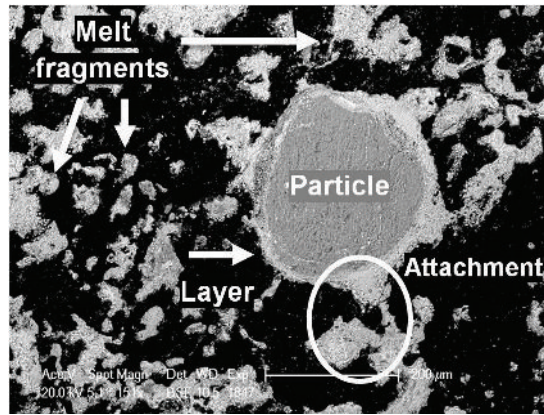


Figure 4.4: ESEM image showing an olivine particle embedded in a melt phase with melt attachments on its surface

K-feldspar showed clear differences to those on quartz particles.

Investigated K-feldspar particles, which have been in the system and already developed particle layers, were characterized by increasing amounts of Ca and decreasing amounts of K towards the particle surface. Further explanations regarding the layer formation on K-feldspar will be discussed in more detail in Section 4.3. The calcium-enrichment during layer formation preserves a stable crystal structure. Thermodynamic equilibrium calculations predicted that this composition should have a significantly lower tendency towards coating-induced agglomeration than quartz, as the closer to the surface the lower the melt fraction gets. Feldspars used as bed material have been reported to decrease defluidization problems compared to quartz in fluidized bed combustion [73, 74, 75]. In comparison to the inner layer of olivine the melt fraction was slightly higher. However due to the increasing Ca content near the surface the tendency towards agglomeration is expected to be a minor issue.

K-feldspar did not show any stability problems in DFB gasification. Furthermore, no crack formation was observed in K-feldspar or its layers, which should decrease fractionation of bed material compared to quartz and fractionation of bed particle layers compared to olivine. Thus, K-feldspar could therefore lead to an improvement in controlling inorganic streams in the system.

In summary it can be stated that olivine and K-feldspar showed only a limited tendency toward agglomeration and deposit build-up in DFB gasification. However, impurities mixed into the bed together with the feedstock can have a major influence on the interaction between biomass ash and bed material. Low melting points of K-rich particle layers on quartz lead to sticky surfaces and can be understood as seed initiating agglomeration or deposit build-up. Furthermore, fractionation of bed particles and their layers can lead to an enrichment of the smaller share in

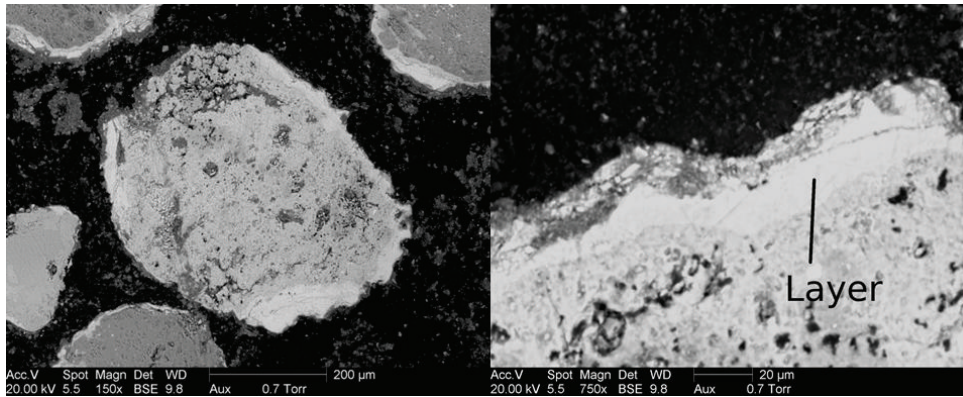


Figure 4.5: ESEM image of layers on K-feldspar particles

the system. Quartz particles showed fractionation and olivine showed the development of cracks in the layers. Only K-feldspar showed satisfying resistance towards cracking and fractionation. An accumulation of critical components, such as K-rich impurities, melt fragments and fine share could be detected in the coarse ash fraction. Thus, periodically discharging the coarse ash from the system leads to a decrease of troublesome components in the system.

4.2 Catalytic activity of bed particle layers

This chapter addresses the catalytic activity of bed material layers. The influence of Ca-rich bed particle layers will be discussed for different reactions, namely the water-gas-shift reaction (Reaction 2.1), and steam reforming of ethene, toluene and 1H-indene (Reactions 2.2, 2.3 and 2.4) as well as steam reforming of methane (Reaction 2.5). Moreover, the influence of bed particle layers on different materials, olivine from DFB gasification and quartz from fluidized bed combustion, will be compared to each other, to the fresh materials and to the benchmark material CaO.

Since operation parameters in combustion in bubbling fluidized bed systems differ significantly from those in DFB gasification, the two used bed materials were compared regarding their layers. Operating temperature, how long the bed material stayed in the system, and the composition of the biomass ash (amongst other parameters) have an influence on the formation of layers. Therefore, layers on particles from different industrial power plants can differ significantly from each other. Hence, layered bed materials were characterized and compared.

Table 4.4 shows the elemental composition of used quartz and olivine bulk samples. The main ash forming elements are displayed; the fraction referred to as "others" includes SnO, MoO₃,

Nb_2O_5 , ZrO_2 , PbO , As_2O_3 , ZnO , CuO , Co_3O_4 , Cr_2O_3 , V_2O_5 , TiO_2 , Cl and SO_3 . These are not of particular interest in terms of characterization because of the low amounts in particle layers and are, therefore, not included in further discussion.

Figures 4.6 and 4.7 show ESEM images of the used materials. As it can be seen, the layer thickness of used olivine is much higher than that of used quartz. Thus, it can not be stated with certainty that the layer coverage on quartz particles is existent to the same extent as on olivine particles. This is also evident from elemental analysis on the particle surfaces shown in Table 4.5 as olivine shows higher contents of Ca on its surface than quartz. Comparing fresh olivine and fresh quartz, we can see that both of them only have a mass fraction of around 1 % of Ca. Thus, calcium is only added once the bed material interacts with biomass ash. The difference of layer coverage between used olivine and used quartz has to be kept in mind when evaluating the results.

Table 4.4: Elemental composition (expressed as oxides) of used particles

| Components | used quartz from combustion plant | used olivine from gasification plant |
|-------------------------|--------------------------------------|---|
| | Mass fraction (%) | |
| Fe_2O_3 | 1.6 | 11.1 |
| CaO | 11.9 | 15.4 |
| K_2O | 6.8 | 1.3 |
| SiO_2 | 69.7 | 28.5 |
| Al_2O_3 | 2.1 | 0.6 |
| MgO | 2.3 | 41.6 |
| Na_2O | 1.5 | 0.5 |
| NiO | 1.3 | 0.3 |
| P_2O_5 | 0.9 | 0.2 |
| Others | 1.9 | 0.5 |

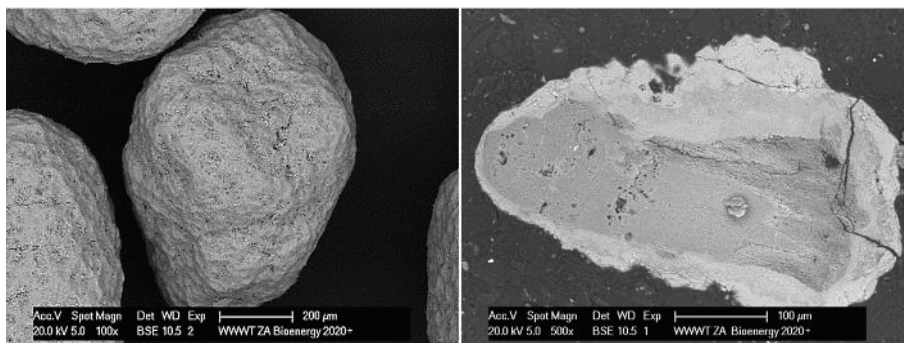


Figure 4.6: ESEM images of used olivine, left: surface of particle layer, right: cross-section

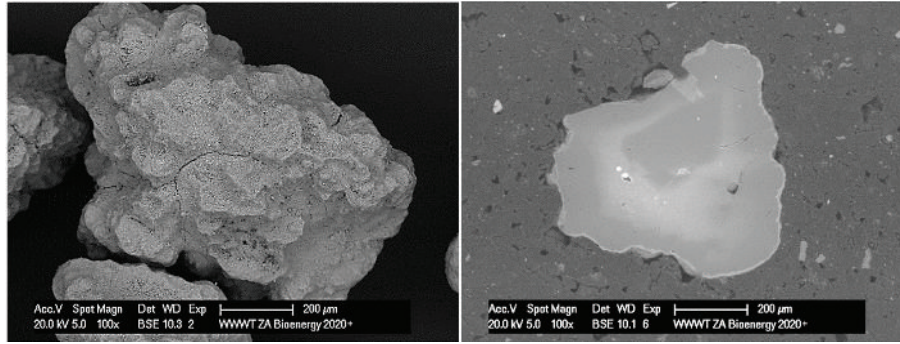


Figure 4.7: ESEM images of used quartz, left: surface of particle layer, right: cross-section

Table 4.5: Elemental surface composition of main components of bed materials

| | fresh quartz | fresh olivine | used quartz | used olivine | CaO |
|--------------------------|--------------|---------------|-------------|--------------|------|
| Mass fraction (%) | | | | | |
| Mg | 0.7 | 46.8 | 11.7 | 6.4 | 0.8 |
| Al | 2.7 | 1.4 | 2.0 | 2.0 | 0.5 |
| Si | 90.4 | 39.8 | 8.9 | 10.6 | 1.8 |
| P | 0.4 | 0.1 | 5.8 | 3.2 | 0.1 |
| K | 0.8 | 0.3 | 1.9 | 1.0 | 0.2 |
| Ca | 1.0 | 1.1 | 64.7 | 73.0 | 95.9 |
| Mn | 1.2 | 0.2 | 3.2 | 1.0 | 0.2 |
| Fe | 2.8 | 10.3 | 1.8 | 2.8 | 0.5 |

First, the catalytic activity of bed particle layers regarding the water-gas-shift reaction will be discussed. Here, the catalytic activity of both fresh and used quartz and olivine particles has been investigated and compared to CaO. Fresh quartz sand did not show significant catalytic activity. Fresh olivine showed some catalytic activity, however it was significantly lower than that of coated bed materials. Used quartz had notably higher catalytic activity than fresh olivine. Used olivine had a slightly higher activity than used quartz sand, however still lower than that of CaO. The difference between fresh and used quartz sand was especially notable since fresh quartz sand did not possess any catalytic activity. CaO almost reached the equilibrium of the reaction. As already mentioned, CaO was used as benchmark material for satisfying conversion. All materials except CaO showed higher production of H₂ at higher temperatures. Furthermore, Figure 4.8 shows the CO concentration on a dry basis in the produced gas (outlet of the reactor) in dependence of the temperature. As it can be seen, at a temperature of 850 °C used olivine almost reached the same catalytic activity. CaO, used as benchmark material, showed high reactivity by almost reaching equilibrium in water-gas-shift test reactions. As expected, fresh quartz sand did not show any significant catalytic effect on the reaction. Therefore, these two

materials constitute extreme cases regarding their catalytic activity. The gas composition of the produced gas is shown in Table 4.6, the content of H₂O is not measured but calculated from the reaction formula.

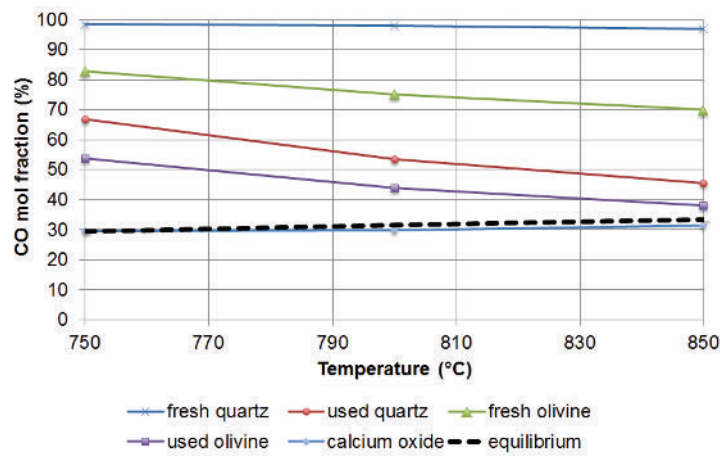


Figure 4.8: CO mol ratio (dry gas) at the outlet of the reactor for the water-gas-shift reaction

Table 4.6: Wet gas composition at the outlet of the reactor for the water-gas-shift reaction, (*) H₂O content calculated from chemical equation (equimolar)

| | °C | H ₂ O(*) | CO | CO ₂ | H ₂ |
|----------------------|-----|---------------------|------|-----------------|----------------|
| CaO | 750 | 24.0 | 24.0 | 25.7 | 26.3 |
| | 800 | 24.3 | 24.3 | 25.8 | 25.6 |
| | 850 | 25.6 | 25.6 | 24.5 | 24.4 |
| used olivine | 750 | 36.0 | 36.0 | 14.1 | 13.9 |
| | 800 | 30.8 | 30.8 | 19.3 | 19.1 |
| | 850 | 28.1 | 28.1 | 22.0 | 21.8 |
| used quartz | 750 | 40.4 | 40.4 | 9.7 | 9.5 |
| | 800 | 38.0 | 38.0 | 12.1 | 11.9 |
| | 850 | 35.8 | 35.8 | 14.3 | 14.1 |
| fresh olivine | 750 | 45.7 | 45.7 | 4.4 | 4.2 |
| | 800 | 43.5 | 43.5 | 6.5 | 6.5 |
| | 850 | 41.8 | 41.8 | 8.2 | 8.2 |
| fresh quartz | 750 | 49.7 | 49.7 | 0.3 | 0.3 |
| | 800 | 49.6 | 49.6 | 0.3 | 0.5 |
| | 850 | 49.3 | 49.3 | 0.7 | 0.7 |

Steam reforming of toluene has been investigated as a model of steam reforming of biomass tars. Again, the catalytic activity of both fresh and used quartz and olivine particles has been investigated and compared with CaO.

Table 4.7 shows the conversion efficiency for steam reforming of toluene of the different bed

materials. The conversion of toluene was measured by comparing the amount of condensed toluene after the reactor to the amount of toluene which was introduced as input stream. For used, layered, particles a significantly higher catalytic activity towards toluene conversion could be observed than for fresh particles. The benchmark material CaO reached a conversion efficiency of 82% of the equilibrium concentration at 850 °C. All materials showed an increasing conversion efficiency with increasing temperature. Table 4.8 shows the dry gas composition of steam reforming of toluene performed with the different bed materials. H₂ content remained relatively constant between 60.6% and 69.7% depending on the bed material and slightly decreased with rising temperature. Materials with lower catalytic activity such as fresh olivine or fresh quartz showed significantly higher amounts of CO compared to CO₂ and vice versa for materials with higher catalytic activity such as used olivine or CaO. Used quartz showed amounts of both CO and CO₂ between 14 and 18.2% and the difference between them was much lower than that of the other particles. Between 1 and 2.7% of methane could be observed. The only exception was fresh olivine at 850 °C, where 6.6% could be observed. Conversion of toluene with CaO shows a conversion of up to 82% at 850 °C. Coll et al. investigated the conversion of toluene by steam reforming using two commercial catalysts (containing about 15% nickel on a support consisting mainly of alumina) and achieved similar conversions with one of them [10]. Swierczynski et al. measured higher conversion of toluene by steam reforming for Ni/olivine of around 90% at 850 °C [11]. This shows that pure CaO has a catalytic activity, which is similar to that of commercial catalysts in the investigated conditions. Fresh quartz did not show any catalytic activity, low conversion of toluene is most likely a result of thermal rather than catalytic decomposition. Even though the catalytic activities of used olivine and quartz were significantly increased compared to the fresh particles, conversion of toluene was notably lower compared to when CaO was used.

Used, layered, quartz and olivine particles showed a much higher selectivity towards the production of CO₂ whereas fresh particles favored the production of CO, as displayed in Table 4.8. Therefore, it was shown that the higher the catalytic activity of the bed material, the higher is the content of CO₂ in the produced gas.

The comparison, displayed in Figures 4.9 to 4.11, shows that the catalytic activity of used particles regarding the H₂-yield in the produced gas is increased for the water-gas-shift reaction and the steam reforming of the model compound for lighter hydrocarbons ethene and the tar model compound toluene. For the following display of results the amount of H₂, which could

| | CaO | used olivine | used quartz | fresh olivine | fresh quartz |
|-----|------------|---------------------|--------------------|----------------------|---------------------|
| °C | η (%) | η (%) | η (%) | η (%) | η (%) |
| 750 | 60 | 19 | 12 | 5 | 2 |
| 800 | 75 | 35 | 30 | 10 | 3 |
| 850 | 82 | 56 | 45 | 22 | 5 |

Table 4.7: Conversion efficiency of bed materials regarding toluene steam reforming

| | | CO | CO ₂ | CH ₄ | H ₂ |
|----------------------|-----|------------------------|-----------------|-----------------|----------------|
| | °C | Gas composition (100%) | | | |
| CaO | 750 | 2.2 | 29.5 | 1.2 | 67.1 |
| | 800 | 4.2 | 28.1 | 1.2 | 66.5 |
| | 850 | 5.5 | 27.0 | 1.9 | 65.6 |
| used olivine | 750 | 3.7 | 25.6 | 1.0 | 69.7 |
| | 800 | 4.4 | 25.1 | 1.1 | 69.4 |
| | 850 | 5.0 | 24.9 | 1.3 | 68.8 |
| used quartz | 750 | 15.1 | 16.0 | 1.5 | 67.4 |
| | 800 | 17.0 | 14.4 | 1.7 | 66.9 |
| | 850 | 18.2 | 14.1 | 1.3 | 66.4 |
| fresh olivine | 750 | 22.9 | 9.2 | 1.8 | 66.1 |
| | 800 | 26.7 | 7.5 | 2.7 | 63.1 |
| | 850 | 27.6 | 5.2 | 6.6 | 60.6 |

Table 4.8: Dry gas composition of toluene steam reforming

be achieved when CaO was used as catalyst was chosen as reference base of the definition of H₂-yield, rather than the theoretically maximum amount. Therefore, the H₂-yield is presented relative to CaO. The catalytic activity seems to be related to the Ca-content on the surface of the particle, as a comparison with 4.5 shows. Since both olivine and quartz particles were characterized by Ca-rich surfaces, the catalytic activity could be assigned to the layer, independent of the original particle. Increasing amounts of CaO detected in XRF analysis of bulk samples, shown in Table 4.4, suggest that it is the active site responsible for increased catalytic activity of the coating. Pure CaO represents therefore the maximal catalytic activity a Ca-rich bed particle coating can achieve. Poorer performance of used quartz sand than that of used olivine could have been caused by reduced coverage of layers around the particles and a lower CaO-amount on the layer surface. Therefore, lesser active surface sites were available for catalytic reactions.

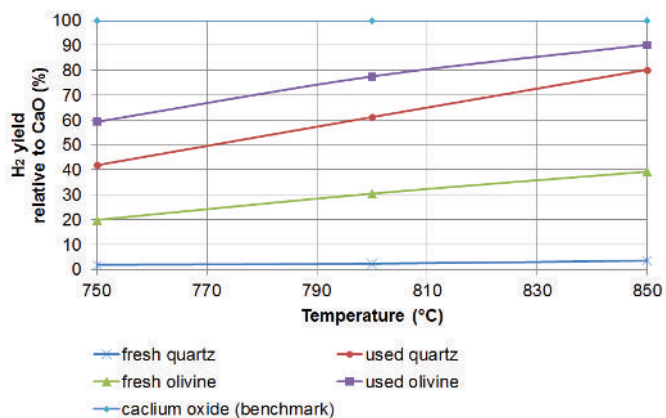


Figure 4.9: H₂ yield of the water-gas-shift reaction relative to CaO (benchmark)

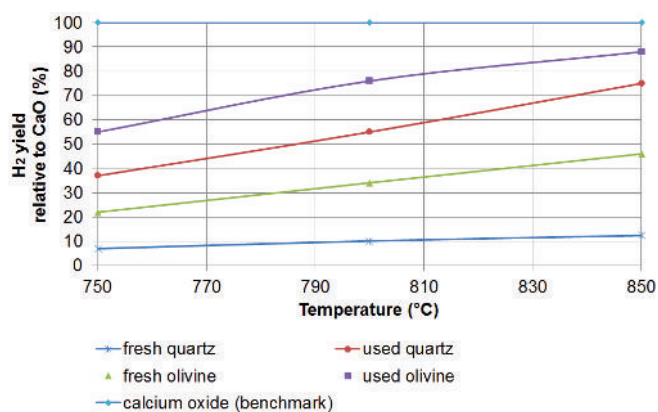


Figure 4.10: H₂ yield of steam reforming of ethene relative to CaO (benchmark)

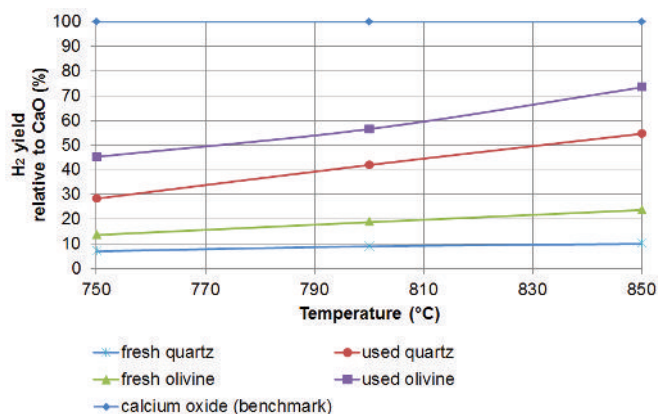


Figure 4.11: H₂ yield of steam reforming of toluene relative to CaO (benchmark)

As a result, it was shown that Ca-rich particle layers are responsible for the catalytic activity of the material even if the material itself does not show any significant activity, as in the case of quartz sand. This leads to the conclusion that the catalytic activity of the original particle is

substituted by that of the layer. Therefore, the activity of specific catalysts - whether naturally occurring or synthetically created - will eventually be replaced once a layer has developed. Hence, potassium and calcium containing feedstock will lead to substitution of the catalytic activity of the original catalyst thanks to their ability to develop particle layers. However, layer build-up on bed particles could easily lead to agglomeration or slagging phenomena [48] and, therefore, to operational problems in DFB gasification of biomass when other materials than olivine are used. Non-quartz minerals were investigated regarding their agglomeration tendency [52] and it was shown that the influence of different bed materials regarding layer build-up and slagging varies significantly.

Furthermore, it is not yet clear if the full potential of the catalytic activity of Ca-rich layers was tapped with the investigated samples. The difference between layered quartz and layered olivine shows the importance of sufficient coverage of Ca-rich layers around the particles. Moreover, it is not clear if the activity of fully covered particles could be further increased to reach the activity of pure CaO.

In additional experiments the influence of the catalytic activity of bed particle layers regarding the transformation of 1H-indene was investigated. As shown in Figure 1.8, 1H-indene is an intermediate product from the decomposition of heavier tars. Thus, if there is a satisfying catalytic activity of the bed material and the gas-solid contact time is sufficient, this intermediate product 1H-indene should not be present. Conversion of 1H-indene at 800 °C in the presence of different bed materials is shown in Figure 4.12. Fresh feldspar, used as inert bed material in these experimental runs, did not show noteworthy catalytic activity towards the reduction of 1H-indene. Fresh olivine reached more than 20 % conversion; however, this was significantly less than used, layered, olivine which converted more than 70 % of 1H-indene. As already observed in the previous experiments, almost complete conversion could be achieved when using the benchmark material CaO.

Table 4.9 shows the dry gas composition (CO, CO₂, CH₄, H₂) of the produced gas (outlet of the reactor) of steam reforming of 1H-indene performed with the different bed materials. It has to be stated here that the carrier gas N₂ is not included in the composition. The H₂ composition rose with increasing catalytic activity. Materials with lower catalytic activity, such as fresh feldspar and fresh olivine, showed significantly higher selectivity toward CO compared to CO₂. In comparison, for used olivine and CaO, which possess higher catalytic activity, increased amounts of CO₂ compared to CO were detected. The amounts of CH₄ were close to the detection limit

for all investigated samples. These limited amounts of CH_4 which were detected in the produced gas are most likely the results of thermal decomposition of 1H-indene rather than the outcome of steam reforming.

Again, the calcium-rich bed particle coating of used olivine led to a significant increase in its catalytic activity. 1H-indene conversion of more than 70 % was achieved during these experiments. Pure CaO used as the benchmark showed conversion of almost 100 %. As a consequence, it can be stated that the bed material, once it is in its active state with a calcium-rich coating, acts as an effective catalyst regarding the conversion of 1H-indene. If this active state is reached, ensuring sufficient contact time between tars and catalyst due to uniform mixing of solid biomass and bed material in the fluidized bed leads to decreasing amounts of intermediate tar decomposition products. The higher catalytic activity of the material leads to increased amounts of CO_2 compared to CO. This is most likely a consequence of the water-gas-shift reaction, which occurs as a follow-up reaction.

In addition to 1H-indene and gaseous compounds, such as CO, CO_2 and CH_4 , the tar chrysene was detected in the produced gas. As shown in Figure 1.8, chrysene is formed through recombination of two 1H-indene molecules. Thus, it could be shown that there is not a one-way decomposition of tars towards smaller molecules, but at the same time also recombination of molecules to larger compounds.

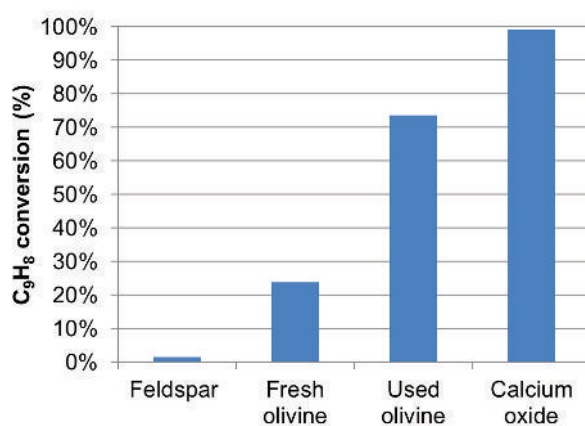


Figure 4.12: Conversion of 1H-indene during steam reforming at 800 °C

Table 4.9: Dry gas composition (main components, total 100%) of steam reforming of 1H-indene at 800 °C

| | CO | CO ₂ | CH ₄ | H ₂ |
|-----------------------------|------|-----------------|-----------------|----------------|
| Average gas composition (%) | | | | |
| Feldspar | 22 | 5.7 | 0.4 | 71.9 |
| Fresh olivine | 15.8 | 9.6 | 0.2 | 74.4 |
| Used olivine | 6 | 18.5 | 0.5 | 75 |
| CaO | 3.1 | 18.8 | 0.2 | 77.9 |

Table 4.10: Formation of chrysene during steam reforming of 1H-indene at 800 °C

| | Feldspar | Fresh olivine | Used olivine | CaO |
|--------------------|----------|---------------|--------------|---------|
| (%) of total input | | | | |
| Chrysene | 2.1 | 1.9 | 1.1 | 0.2 |
| | +/- 0.3 | +/- 0.4 | +/-0.2 | +/- 0.1 |

To evaluate the reduction of CH₄, which could be observed during e.g. the decomposition of 1H-indene, when using layered bed particles, experiments were conducted using solely CH₄ and steam (together with the carrier gas N₂). By isolating this reaction and performing experiments only on the steam reforming of CH₄, no other effects or reactions blurred the findings. Figure 4.13 shows the results gained from these investigations, comparing fresh and used olivine particles. It is evident that Ca-enrichment on the particle surface does not significantly increase the catalytic activity towards the steam reforming of CH₄. Thus, CH₄ is much less influenced by in-bed catalytic conversion than the other investigated compounds, which is due to its stable structure.

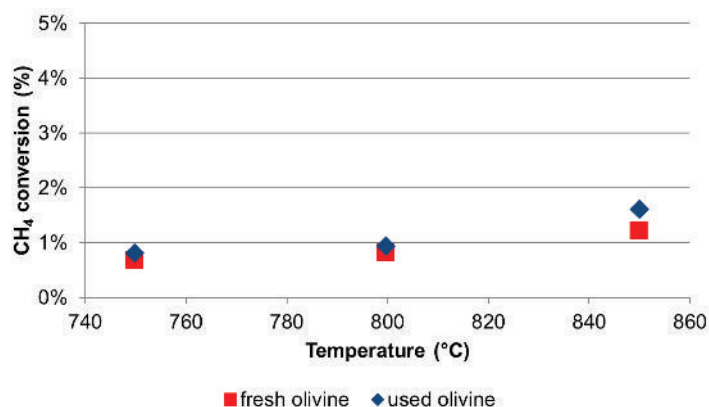


Figure 4.13: Methane conversion during steam reforming at 800 °C using fresh and used olivine particles

4.3 Mechanisms underlying bed particle layer formation

In this chapter investigations regarding the mechanisms underlying layer formation on olivine and K-feldspar particles will be presented. Understanding the reactions which occur during the formation of ash layers is essential to find alternative bed materials to olivine. Thus, the first step of the investigations has been the clarification of the mechanism for layer formation on olivine particles.

Investigations were based on olivine bed samples collected at the DFB gasification power plant in Oberwart. Time-dependence of layer formation was investigated allowing to draw conclusions of the single steps leading to the formation of the already known Ca-rich particle layers.

The first traces of layer formation after 4 and 8 hours of operation showed increasing amounts of Ca while no K was detected. The absence of K and presence of Ca in olivine layer formation was further confirmed by chemical equilibrium calculations. These findings suggest that the initial step of layer formation is based on a solid-solid reaction between CaO and olivine. It should be noted that ash forming elements introduced with the fuel may form melted K-silicates that can act as an adhesive between surrounding ash and the olivine bed particles. Several K-Mg-silicates exist that are conceivably products of such a reaction [76]. Such initial melts may constitute an intermediate that facilitates Ca^{2+} transport into the olivine.

The low concentration of potassium retained in the particle layer is in good accordance to previous studies conducted by Kirnbauer and Hofbauer [61] and by Grimm et al. [13]. This leads to the proposal of the following mechanism for olivine particle layer formation: This solid-solid reaction between CaO and olivine is a substitution reaction where Ca^{2+} is incorporated into the crystal structure of olivine.

The crystal structures in Figure 4.14 are taken from reference structures [77, 78] using Mercury 3.8 [79] and show the changes in the crystal structure as the olivine bed material changes from olivine [77] to calcium magnesium silicate [78]. The calcium magnesium silicate monticellite (MgCaSiO_4) is shown in Figure 4.14 on the bottom. However, two other phases, merwinite ($\text{Ca}_3\text{Mg}(\text{SiO}_4)_2$) and bredigite ($\text{Ca}_7\text{Mg}(\text{SiO}_4)_4$) are also stable intermediates. In Figure 4.14 the yellow sphere in the middle of the structures represents a Si-atom. The red spheres are O-atoms.

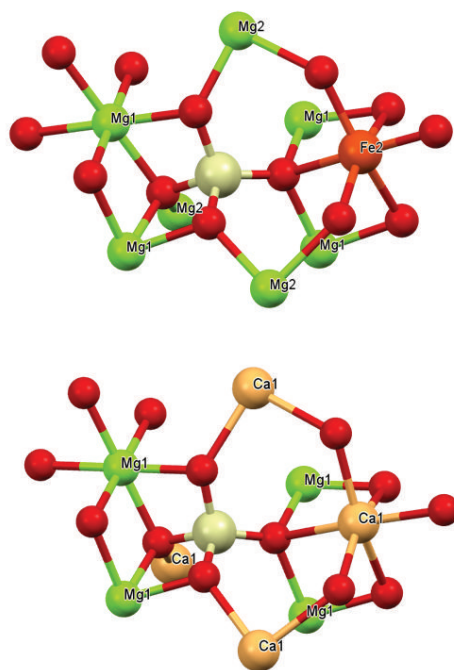


Figure 4.14: Steps of the substitution mechanism: (1) olivine, $\text{Mg}_{1.8}\text{Fe}_{0.2}\text{SiO}_4$ (top), and (2) CaMgSiO_4 (bottom).

The incorporation of Ca^{2+} into the crystal structure proceeds at one of the exchangeable sites M1 or M2, which are occupied by either Mg^{2+} or Fe^{2+} . Ca^{2+} will preferably occupy the site M2 as it is slightly larger than M1. For a Ca^{2+} ion to be incorporated, a Mg^{2+} or a Fe^{2+} ion has to be expelled from the structure, either accompanied by an O^{2-} from the SiO_4^{4-} or by reacting with the oxygen carried by CaO . This replacement is expected to be due to an ion substitution of a Mg^{2+} or Fe^{2+} by a Ca^{2+} ion. Fe^{2+} is statistically more likely to be replaced than Mg as described by Smyth [80], and is, therefore, statistically replaced first, before Mg is substituted. Fe is then not present in crystal form anymore. Besides, it should be noted here, that the oxidation of Fe^{2+} when exposed to air at elevated temperatures is also likely to take place. As a consequence, so long as not every Mg^{2+} in the crystal structure is replaced by a Ca^{2+} atom, there exist intermediate states which are mainly composed of Ca-Mg-silicates.

The observed separation of the inner layer into an inner and an outer zone in the ESEM analysis, as shown in Figure 4.16, therefore, appears to be based on the substitution of Mg by Ca . As a result of being expelled from the olivine structure, Mg^{2+} accumulates and is trapped between the inner and the outer layers forming on the particle surface and the outer zone of the inner layer is formed. EDS analysis confirms a relatively high amount of Mg in the outer zone of the inner layer. Thermochemical equilibrium calculations have shown the tendency of Mg^{2+} to form MgO .

Therefore, EDS analysis in ESEM investigations has shown a comparably high amount of Mg in the outer zone of the inner layer. Kirnbauer and Hofbauer [61], using XRD analysis, also noted the presence of MgO in used layered olivine particles. At the time this could not be explained. Further addition of calcium leads to a Ca-silicate dominated crystal structure as Ca^{2+} is incorporated at all available exchangeable sites M1 and M2. Once all exchangeable sites are occupied by Ca^{2+} ions the crystal structure α -di-calcium silicate [81] is present. This is shown in Figure 4.15. The three light green spheres shown in the middle of the figure are Si-atoms and red spheres are O-atoms. The exchangeable sites M1 and M2 are now all occupied by Ca^{2+} , represented by the pink spheres.

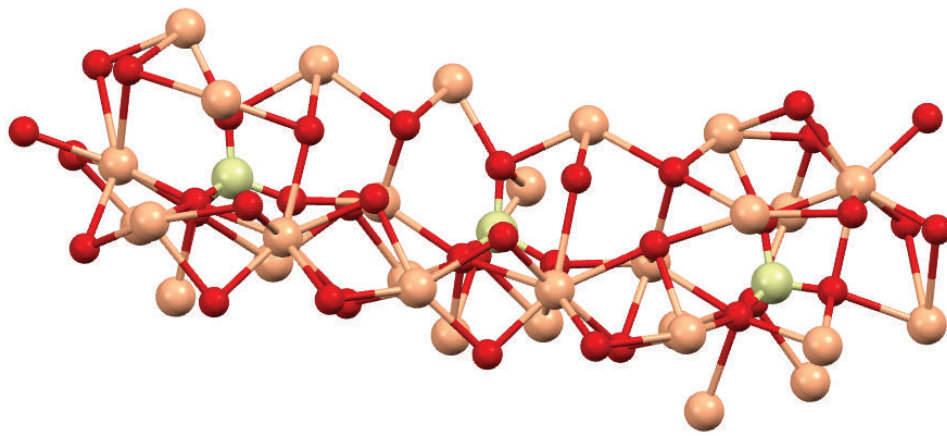


Figure 4.15: Crystal structure of α -di-calcium silicate

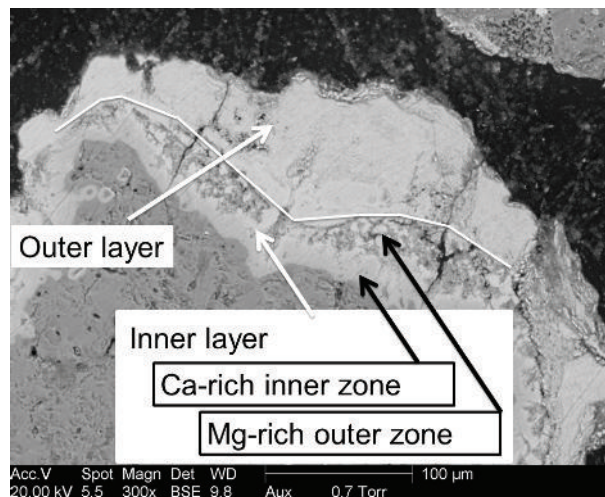


Figure 4.16: ESEM image of a typical cross section of the olivine bed particle layer taken after about 400 h showing distinguishable zones of the inner particle layer

The substitution of Mg by Ca also results in the formation of cracks perpendicular to the surface of the particles, as shown in Figure 4.17. It has to be stated at this point that it cannot be excluded

with certainty, that some of the cracks might have occurred during the polishing of the samples. However, as explained later on, certain chemical substitution reactions, which could be observed in the ESEM, strongly indicate that most of these cracks were formed during operation. The substitution of calcium into the olivine has a dramatic initial effect on the unit cell volume per formula unit, i.e. the volume of the smallest repeating unit in the crystal normalized against the amount of formula units in the unit cell. The 17% increase is a direct effect of the difference in bond lengths between metal ions and oxygen atoms in the silicate anion. The Mg/Fe – O distance in olivine ranges from 2.075 to 2.145 Å in the Mg/Fe position M1 and between 2.062 and 2.225 Å in the Mg/Fe position M2. In CaMgSiO_4 the corresponding distance for Mg – O is 2.086 to 2.191 Å but it is significantly larger for Ca – O at 2.301 to 2.480 Å. As Mg^{2+} is fully substituted by Ca^{2+} to form Ca_2SiO_4 (most likely $\alpha\text{-Ca}_2\text{SiO}_4$ at the relevant process temperatures) the volume per formula unit increases by 6% compared to CaMgSiO_4 . Also, the unit cell axis changes significantly creating further strain in the structure which may promote crack formation.

There are several other modifications of Ca_2SiO_4 which may also induce further strain in the layers formed on the surface of fluidized bed particles. As can be seen in Figure 4.14, this change is probably induced by going from an octahedral configuration of oxygens surrounding Ca^{2+} in CaMgSiO_4 where four oxygen atoms are located in the same plane and the other two oxygen atoms are almost orthogonal to that plane. This symmetrical configuration surrounding the Ca^{2+} is lost in $\alpha\text{-Ca}_2\text{SiO}_4$ as seen in Figure 4.15. These changes in bond distances and angles are the likely causes of crack formation and will be further exacerbated by physical conditions such as temperature changes and abrasion.

Due to these cracks the surface becomes exposed and further intrusion of Ca into the particle is possible. The mechanism of the intrusion is identical to the proposed layer formation mechanism, since Ca^{2+} is again substituting either Fe^{2+} or Mg^{2+} at the same exchangeable sites in the crystal structure. This phenomenon can be observed in the ESEM and EDS analyses as the separation of Ca and Mg can be detected at the intrusion area and along the cracks. Ca^{2+} is incorporated into the crystal structure at the exposed surface and Mg accumulates along the cracks indicating that it has been expelled from the olivine structure. This accumulation of Mg along the cracks, shown in Table 4.11, is, therefore, equivalent to the outer zone of the inner layer. Such an enrichment could also clearly be observed on the surface of the particle layers, as shown in Figure 4.18.

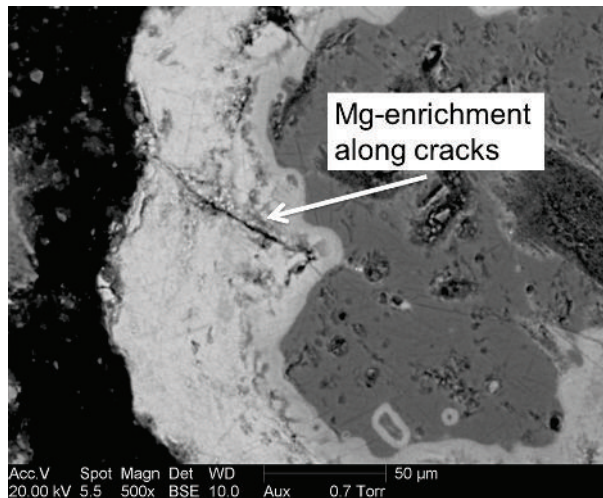


Figure 4.17: ESEM image of cracks in the olivine bed particle layer perpendicular to the surface and the typical Mg-enrichment along cracks in the particle layer

Table 4.11: Comparison of the compositions in the inner and outer zone of the inner layer and at the intrusion into the surface and along the cracks (sampled after 400 h of operation)

| | inner layer (inner zone) | inner layer (outer zone) | intrusion into the surface | along the cracks |
|----|-------------------------------------|-------------------------------------|---------------------------------------|-----------------------------|
| | Mass fraction in (%) | | | |
| Na | 1.2 (+/- 0.1) | 1.6 (+/- 0.2) | 1.4 (+/- 0.2) | 1.7 (+/- 0.2) |
| Mg | 20.9 (+/- 0.4) | 29.3 (+/- 2.1) | 23.9 (+/- 1.2) | 29.9 (+/- 1.6) |
| Al | 0.8 (+/- 0.1) | 0.7 (+/- 0.1) | 1.0 (+/- 0.1) | 1.0 (+/- 0.2) |
| Si | 22.0 (+/- 1.1) | 18.9 (+/- 0.6) | 27.1(+/- 0.8) | 25.6 (+/- 1.0) |
| P | 0.7 (+/- 0.1) | 0.6 (+/- 0.1) | 0.5 (+/- 0.1) | 0.5 (+/- 0.1) |
| S | 0.2 (+/- 0.1) | 0.1 (+/- 0.0) | 0.2 (+/- 0.0) | 0.2 (+/- 0.0) |
| Cl | 0.2 (+/- 0.0) | 0.2 (+/- 0.0) | 0.3 (+/- 0.0) | 0.3 (+/- 0.0) |
| K | 0.6 (+/- 0.1) | 0.7 (+/- 0.2) | 1.4 (+/- 0.2) | 0.8 (+/- 0.1) |
| Ca | 47.2 (+/- 1.6) | 40.8 (+/- 2.1) | 36.4 (+/- 2.7) | 31.9 (+/- 2.1) |
| Cr | 0.4 (+/- 0.1) | 0.3 (+/- 0.1) | 0.9 (+/- 0.2) | 0.3 (+/- 0.0) |
| Mn | 0.5 (+/- 0.2) | 0.7 (+/- 0.1) | 0.7 (+/- 0.1) | 0.7 (+/- 0.1) |
| Fe | 5.3 (+/- 0.5) | 6.1 (+/- 0.4) | 6.2 (+/- 1.2) | 7.1 (+/- 2.1) |

Due to these cracks the surface becomes exposed and further intrusion of Ca into the particle is possible. The mechanism of the intrusion is identical to the proposed layer formation mechanism, since Ca^{2+} is again substituting either Fe^{2+} or Mg^{2+} at the same exchangeable sites in the crystal structure. This phenomenon can be observed in the ESEM and EDS analyses as the separation of Ca and Mg can be detected at the intrusion area and along the cracks. Ca^{2+} is incorporated into the crystal structure at the exposed surface and Mg accumulates along the cracks indicating that it has been expelled from the olivine structure. This accumulation of Mg along the cracks is, therefore, equivalent to the outer zone of the inner layer.

Crack formation can also be observed on the borderline between the Mg-rich outer zone of the inner layer and the Ca-rich outer layer. Those cracks, which spread out parallel to the particle surface, shown in Figure 4.19, seem to be critical regarding layer breakage. They originate at the borderline of Mg which is present in the form of oxide and the Ca-rich outer ash layer, since there is no interaction between those two stable structures. They result in a clear physical separation of the outer layer, which is likely to break off during operation.

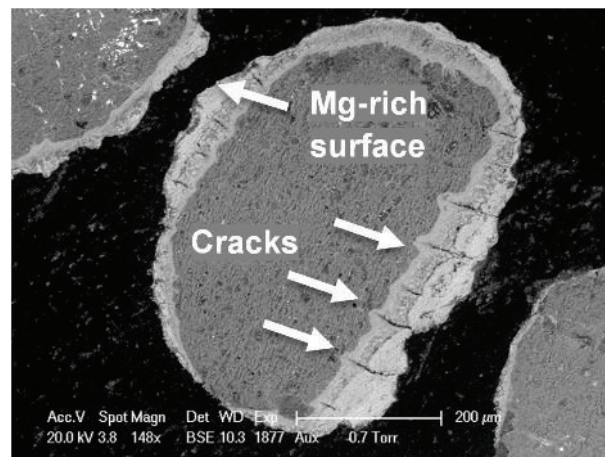


Figure 4.18: ESEM image of Mg-enrichment on the surface of the particle layers on olivine (sampled after 180 h of operation)

Thermochemical equilibrium calculations suggest that further increases in Ca levels result in increasing amounts of $\text{Ca}_3\text{MgSi}_2\text{O}_8$ while CaMgSiO_4 concentrations decrease. This is further evidence of Ca incorporation into the originally Mg-rich olivine structure. The change from CaMgSiO_4 to $\text{Ca}_3\text{MgSi}_2\text{O}_8$ represents an increase of the Ca:Mg ratio during ongoing substitution of Mg by Ca. With even further increases in Ca levels no Ca-Mg-structures will be present at all, but only Ca_2SiO_4 . At this stage Mg will have been completely expelled from the crystal structure and will only be present in the form of MgO. An increase in the level of CaO marks the

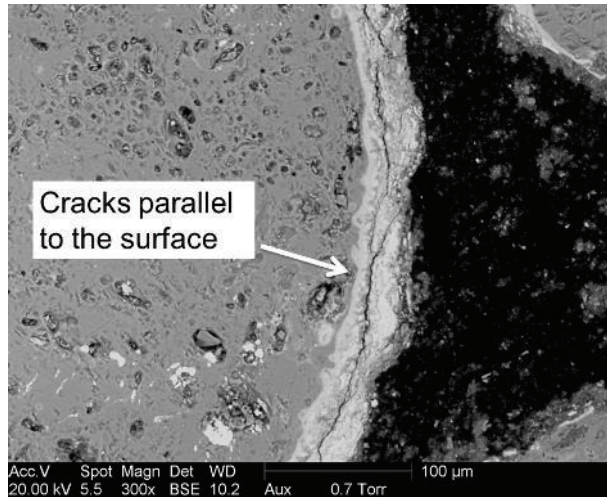


Figure 4.19: ESEM image of cracks in the olivine bed particle layer parallel to the surface (sampled after 180 h of operation)

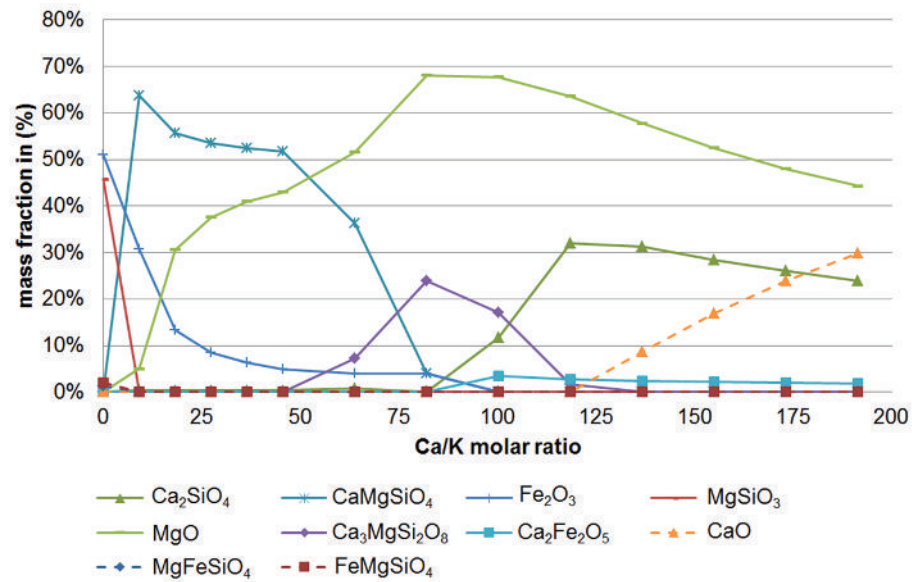


Figure 4.20: Mass fraction of crystal structures present at varying Ca/K molar ratios at a K to bed (olivine) molar ratio of 1/200

last step of layer formation. Increasing amounts of Ca on the particle surface are essential for the catalytic effectiveness of the bed material in tar reduction.

The proposed mechanism explains the layer formation on olivine particles and shows that layer formation mechanisms can differ significantly from material to material – as they differ for e.g. olivine and quartz. Knowledge of the mechanism of layer formation is an important step to the understanding of the ash chemistry in the system. It is an essential basis for the successful replacement of olivine by alternative bed material and also for future ash utilization and recovery of valuables from the ash.

Therefore, the mechanism for layer formation needs to be understood for all potential bed materials. In the frame of this work first insights into the layer formation mechanism of K-feldspar were gained. However, the complete mechanism is yet not clear. First results show similarities to the layer formation on olivine, however, the exact differences are yet to be investigated. For K-feldspar, typically KAlSi_3O_8 , the formation of clearly separated particle layers could not be detected when investigating the elemental composition with EDS analysis. Thus, Figure 4.21 shows an example of a so called mapping which was conducted for numerous K-feldspar particles. Table 4.12 shows the composition of the single spots. Starting from the particle itself (x1) numerous spot analyses were taken along a line going outwards towards the layer surface (x2- x9). As it can be seen, layer formation around feldspar particles was observed to be rather fluent than clearly distinguished. Outer areas of the layer contained notably higher amounts of calcium. Layers on K-feldspar were characterized by increasing amounts of Ca and decreasing amounts of K towards the particle surface, which might be caused by replacement of K and incorporation of Ca into the crystal structure. This substitution leading to a simultaneously increase of Ca and decrease of K results in the build-up of a stable crystal structure. The suspected substitution shows similarities to the substitution reaction observed during the layer formation of olivine. However, since K^{1+} has a different charge than Ca^{2+} , the reaction is most likely a coupled ion substitution. Layer formation on K-feldspar seems to be connected to the release of K from the particle itself. It is unclear to this point which other ions are involved in this substitution reaction.

The similarity in the layer formation mechanism – and the low tendency towards agglomeration, which seems to be a consequence of the layer formation mechanism, as no low melting K-silicates are formed during the substitution with Ca – could be an indicator that olivine and K-feldspar show similar characteristics when used as bed material in a fluidized bed.

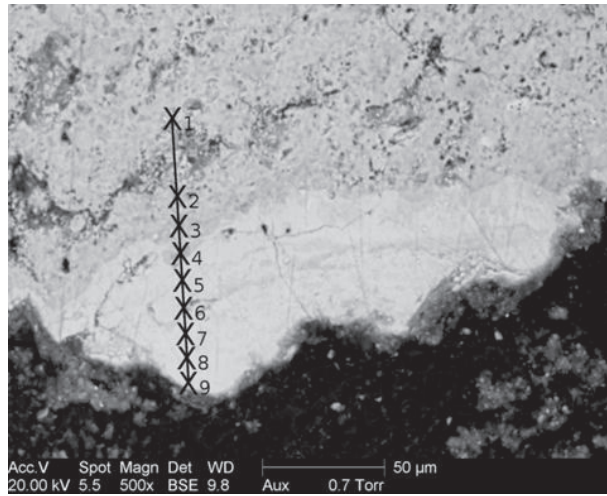


Figure 4.21: ESEM image of mapping along a typical cross-section of a K-feldspar layer

Table 4.12: Average elemental composition on a C- and O-free basis across K-feldspar particle layers

| | x1 | x2 | x3 | x4 | x5 | x6 | x7 | x8 | x9 |
|----|-----------|-----------|-----------|-----------|-----------|-----------|-----------|-----------|-----------|
| | wt% |
| Na | 1.4 | 0.0 | 0.8 | 1.2 | 0.6 | 0.9 | 0.8 | 0.7 | 1.1 |
| Mg | 4.8 | 5.3 | 4.5 | 6.4 | 3.7 | 5.4 | 7.5 | 9.7 | 9.8 |
| Al | 14.1 | 11.6 | 11.1 | 3.4 | 4.2 | 2.9 | 2.5 | 2.7 | 2.7 |
| Si | 32.7 | 34.2 | 33.4 | 40.4 | 35.3 | 24.9 | 8.4 | 10.6 | 11.3 |
| P | 0.3 | 0.2 | 0.6 | 0.6 | 0.5 | 0.9 | 1.8 | 2.6 | 2.5 |
| S | 0.2 | 0.0 | 0.2 | 0.0 | 0.2 | 0.1 | 0.2 | 0.2 | 0.2 |
| Cl | 0.2 | 0.3 | 0.3 | 0.0 | 0.4 | 0.2 | 0.3 | 0.1 | 0.3 |
| K | 32.5 | 29.3 | 17.8 | 12.3 | 8.8 | 3.7 | 2.9 | 2.6 | 2.8 |
| Ca | 4.6 | 8.8 | 26.5 | 32.5 | 41.9 | 56.8 | 71.5 | 66.3 | 64.6 |
| Cr | 0.1 | 0.4 | 0.3 | 0.3 | 0.2 | 0.0 | 0.3 | 0.3 | 0.4 |
| Mn | 0.4 | 0.7 | 0.5 | 0.3 | 0.3 | 0.3 | 0.9 | 0.7 | 0.5 |
| Fe | 8.7 | 9.2 | 4.0 | 2.6 | 3.9 | 3.9 | 2.9 | 3.5 | 3.8 |

Chapter 5

Future work

In this chapter possible next steps for the research in the field of bed material – biomass ash interaction in DFB gasification, based on results of this work, will be explained and discussed. This shall show both the short-term and long-term goals of the bed material and biomass ash research in dual fluid bed gasification of biomass, put the findings from this work in context and show the bigger picture.

5.1 Clarifying bed particle layer formation mechanisms of different alternatives

Findings from this work showed the difference in layer formation between quartz and olivine particles when interacting with biomass ash in a fluidized bed. Understanding the mechanism underlying layer formation was identified to be crucial for the replacement of olivine as bed material. Therefore, it will be necessary to clarify possible other mechanisms when using different bed materials. As described in Section 4.3, the mechanism underlying the formation of particle layers for K-feldspar might be closely related to that of olivine. It is of high importance to understand the single steps on an atomic level to evaluate the suitability of possible alternative bed materials.

It is likely that different materials can be grouped according to their initial layer formation mechanism. A possible classification scheme could be as follows:

1. Group A: K-silicate formation: e.g. K reacts with free Si (quartz)
2. Group B: Simple substitution: e.g. Mg^{2+} or Fe^{2+} is substituted by Ca^{2+} (olivine)

3. Group C: Coupled substitution: e.g. K^{1+} is involved in the substitution by Ca^{2+} , mechanism not yet clear (K-feldspar)
4. Group X_i : Possible alternative mechanisms

On the basis of such an classification, bed materials could maybe even be grouped according to their crystal structure. This would allow for predictions regarding the layer formation behaviour in fluidized bed gasification or combustion of biomass for different materials.

However, this is only a very raw draft of a possible classification. Much more information on layer formation mechanisms on different materials has to be collected before such a classification can be made. Moreover, the composition of the biomass feedstock highly influences the layer formation due to competing reactions. Here is an example: If free Si is available in the biomass ash, K might react with this free Si in the biomass ash rather than with bed material. Therefore, the predictions of layer formation would have to be specifically made for the used feedstock. Thus, the influence of biomass feedstock will be addressed in the following sub-chapter.

5.2 Influence of different biomass feedstock on bed particle layer formation

Investigations performed in this work were done using woody biomass as feedstock. This is a limitation of the work as the results are not necessarily adaptable for other feedstocks. When using lower-cost biogenous feedstock, the ash composition will vary significantly from that of woody biomass. Therefore, the ash chemistry will be determined by certain reactive components in the ash. As an example, the use of phosphorus(P)-rich biomass as feedstock will be explained here. Skoglund et al. [82] have shown the strong tendency of P to form compounds with alkali, such as K and Na, and earth alkali, such as Ca and Mg. Thus, the bed material will be in competition to the ash from the feedstock regarding the reaction with alkali and/or earth alkali. Thus, lower-cost biogenous feedstock could lead to inhibition of layer formation.

In previous studies from Skoglund et al. [83] they experimented with fuel mixtures to obtain certain ash compositions. The idea behind this fuel design [84], as it is referred to by the authors, is to mix the fuels in such a way, that one can gain defined ratios of critical ash forming elements. Thus, the ash chemistry in the system can be controlled.

Adapting this method for fluidized bed gasification and including Ca-rich additives into the fuel

mixtures might be essential to control ash-related problems and, at the same time to form Ca-rich particle layers.

5.3 Introduction of alternative bed material in industrial scale DFB power plants

The next step in realizing the substitution of olivine in dual fluidized bed gasification of biomass would be the implementation of an alternative bed material in an industrial scale power plant. Once the mechanisms of bed particle layer formation for an alternative bed material are understood, a step-wise replacement of olivine with the alternative bed material should be performed. The two consequences of layer formation should be evaluated – agglomeration and catalytic activity. Once 100 % of the olivine is replaced and the operation with the alternative bed material is stable, intensive ash analysis should be conducted to evaluate the potential regarding further utilization of the different biomass ash fractions, as it will be discussed in more detail in the following section.

5.4 Further utilization of biomass ashes from dual fluid gasification

One of the unique characteristics of the dual fluid bed gasification process is the existence of different ash fractions from both the gasification and the combustion reactor. Only a few examples for further ash utilization will be discussed in the following to show the potential of making the different ash fraction available to further applications.

Ash, regained from the product gas filter after the gasifier – referred to as fly coke – is characterised by comparably high amounts of unburnt carbon as it originates from gasification of the biomass in the gasification reactor. Nowadays, the fly coke is recirculated to the combustion reactor and burnt there. However, in future application a discharge of the fly coke from the system and further utilization of this ash fraction could be advantageous. Due to its C-rich composition it could be used as biochar for different applications, e.g. as soil amendment, carbon sink or for water retention, this application will be explained in more detail. Biochar, used as soil amendment, can be understood as soil conditioner, which has to role of improving its physical qualities, mainly resulting in an improvement of its ability to provide nutrients to plants.

However, the C-rich fly coke from dual fluid bed gasification of biomass has to fulfill certain characteristics before it can be used as biochar [85, 86, 87, 88]. Furthermore, it can play an important role as a carbon sink. Figure 5.1 shows the implementation of biochar - in this case gained from pyrolysis - into the carbon cycle. Biochar is reluctant against decomposition and remains in the soil for many centuries. Thus, carbon can be effectively and sustainably stored in the pedosphere [89, 90]. Moreover, Abel et al. [91] could prove that the addition of biochar to the soil increases the water content significantly. The retention of water is essential for sustainable regrowth of plants.

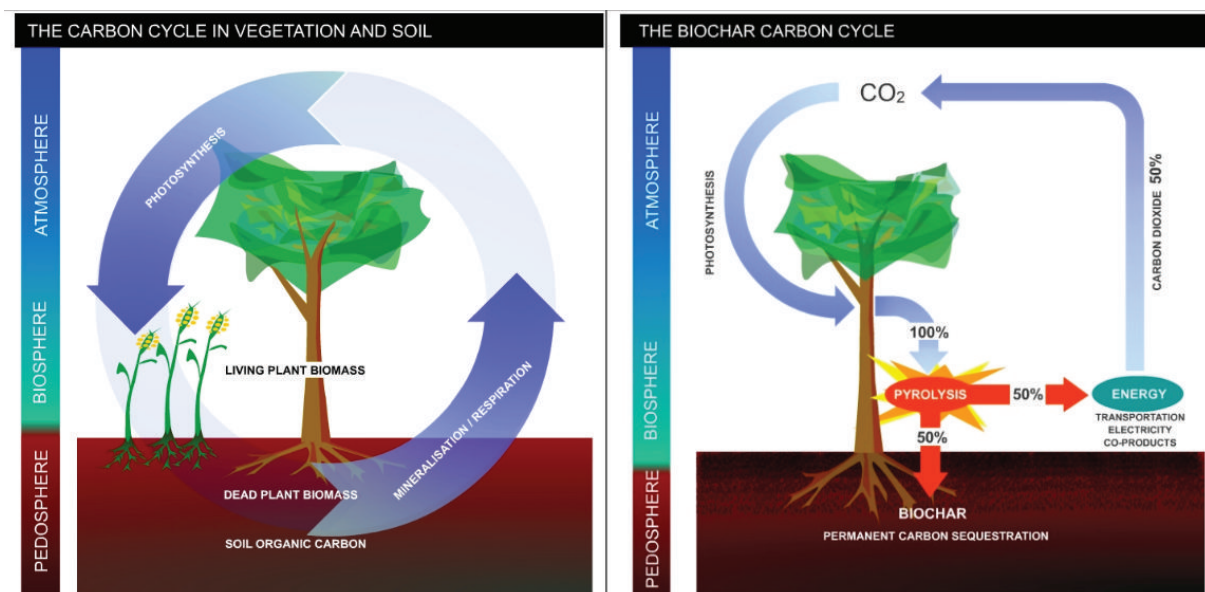


Figure 5.1: Comparison between the simple carbon cycle (left) and the manipulated carbon cycle with biochar (right) as proposed by Steiner [89]

Ash, regained from the flue gas filter after the combustion reactor - referred to as fine ash - differs significantly from the fly char. Further utilization as fertilizer is promising, once olivine is replaced as bed material in the system. However, more investigations regarding possible accumulation of undesirable components from the biomass in the fine ash are necessary to evaluate its suitability as fertilizer.

The feedstock has a great impact on the further utilization of the ash fraction from the DFB process. Using lower-cost biomass feedstock will result in different ash compositions as those already known from gasification of woody biomass. Phosphorus-rich biomass will play an important role regarding the further utilization of biomass ash [92, 93, 84]. As described in Section 1.1.1, phosphorus is a limited resource, which has already been exploited to a significant

amount. Recovery of phosphorus will, therefore, be necessary in the future. Phosphorus possesses comparably high fertilizing effects [94] and is one of the main ash forming compounds in biomass ash [64]. Thus, P-rich biomass will play a central role in future ash utilization.

Chapter 6

Conclusion

Interaction between bed materials and biomass ash leads to the formation of particle layers. While layer formation can be troublesome regarding agglomeration or deposit build-up, the Ca-enrichment on the particle surface leads to a desirable catalytic activity towards tar reduction. Therefore, layer formation has a positive impact on biomass gasification.

Olivine, which is used as bed material nowadays, contains certain amounts of heavy metals, thus, the ash cannot be further used after the process. Replacing olivine by a heavy metal-free and widely available alternative bed material would lead to an improvement of the process (reducing costs for disposal of the ash and making further ash utilization possible).

In this work, both aspects of layer formation – agglomeration and catalytic activity – have been investigated for olivine and possible alternative bed materials – quartz and K-feldspar. It was shown that layer formation on quartz particles leads to significantly lower melting points due to the formation of low-temperature eutectica, compared to when olivine is used. K-feldspar showed promising characteristics regarding the thermal stability and its low tendency to form agglomerates and can be considered as a possible alternative bed material for biomass gasification in a dual fluid bed.

Investigations regarding the catalytic activity of bed particle layers showed that once a Ca-rich layer has formed the catalytic activity toward tar reduction is satisfying, independent on what material was used. Thus, non-catalytic materials, such as quartz and K-feldspar can develop a satisfying catalytic activity by in-situ interaction with biomass ash in the fluidized bed. It was also shown that the Ca-rich layers influence different reactions, such as the water-gas-shift reaction, steam reforming of lighter hydrocarbons (such as ethene) and steam reforming of heavier hydrocarbons (such as toluene and 1H-indene) in a similar matter whereas steam

reforming of CH_4 was not strongly influenced due to the stable structure of CH_4 . 1H-indene was also identified as indicator compound for incomplete tar reduction as it is an intermediate product from the decomposition of heavier hydrocarbons. The investigations showed that CaO was responsible for high catalytic activity, rising catalytic activity could be matched with increasing amounts of CaO in the particle layer. Thus, pure CaO was used as benchmark material for catalytic investigations. Pure CaO showed the highest catalytic activity for the materials tested and can be understood as the maximum catalytic activity layered bed particles could achieve, as CaO seems to be the active component. This also leads to the conclusion that pure CaO is a highly promising candidate for a bed material in future DFB gasification, if the particle separation can be adjusted to a smoother separation. However, due to its low hardness it is not suitable in already existing power plants where cyclones are used for particle separation.

The layer formation mechanism of olivine was investigated and found to be based on a solid-solid substitution reaction, where Fe^{2+} and Mg^{2+} ions located exchangeable sites (M1 and M2) in the crystal structure of olivine are replaced by Ca^{2+} . Understanding the mechanism of layer formation has been identified to be essential for evaluating the suitability of alternative bed materials. First insights into the layer formation mechanism of K-feldspar were presented, showing similarities to that of olivine. Thus, showing that K-feldspar is also a promising candidate regarding the mechanism underlying layer formation.

In summary, it can be stated that the research performed in the frame of this work has laid a basis for further investigations to replace olivine as bed material in DFB gasification. Future work includes testing of promising bed material candidates in DFB-gasification conditions and as a consequence the examination of the potential of further utilization of biomass ash disposed of the process.

List of Figures

| | | |
|------|--|----|
| 1.1 | Gross electricity generation in the EU in TWh [6] | 2 |
| 1.2 | Electricity generation by renewable fuels in the EU in TWh [6] | 3 |
| 1.3 | Outlook for the bioenergy demand of the EU in Mtoe [5] | 4 |
| 1.4 | Current status of the nine planetary boundaries as proposed by Steffen et al. [9] . . | 4 |
| 1.5 | Dual fluid bed gasification as developed at TU Wien [8] | 7 |
| 1.6 | Novel dual fluid bed gasification system [28] | 8 |
| 1.7 | Molecular structure of toluene | 9 |
| 1.8 | Decomposition mechanism of naphthalene as proposed by Devi et al. [31] (adapted) | 10 |
| 1.9 | Agglomeration of quartz particles as observed by Brus et al. [48] | 11 |
| 1.10 | Bed particle layers on olivine in DFB gasification as observed by Kirnbauer and Hofbauer [55] showing an inner (1) and an outer (2) layer | 12 |
| 2.1 | Scheme of the lab-scale magnetic separator | 16 |
| 2.2 | Flow-sheet of the lab-scale apparatus for catalytic measurements | 19 |
| 2.3 | Scheme of the reactor part | 20 |
| 2.4 | Set-up for sampling of the tar model compound 1H-indene | 20 |
| 2.5 | Simplified flow sheet of the dual fluidized bed gasification plant in Senden/Ulm . . | 23 |
| 2.6 | Zones with critically high temperatures (1) upper part of the combustion reactor, (2) cyclone, (3) post-combustion chamber | 23 |
| 2.7 | Simplified flow sheet of the dual fluidized bed gasification plant in Oberwart | 25 |
| 2.8 | 3D- model of the bubbling fluidized bed combustion reactor in Heiligenkreuz [71] (adapted) | 26 |

| | | |
|------|---|----|
| 4.1 | Histogram of temperature measurements at the outlet of the cyclone and respectively the inlet of the post-combustion chamber | 34 |
| 4.2 | ESEM image showing the presence of impurities, such as quartz or feldspar particles, in the coarse ash fraction | 35 |
| 4.3 | ESEM image of layers on and cracks in quartz particles | 38 |
| 4.4 | ESEM image showing an olivine particle embedded in a melt phase with melt attachments on its surface | 40 |
| 4.5 | ESEM image of layers on K-feldspar particles | 41 |
| 4.6 | ESEM images of used olivine, left: surface of particle layer, right: cross-section . . | 42 |
| 4.7 | ESEM images of used quartz, left: surface of particle layer, right: cross-section . . | 43 |
| 4.8 | CO mol ratio (dry gas) at the outlet of the reactor for the water-gas-shift reaction . . | 44 |
| 4.9 | H ₂ yield of the water-gas-shift reaction relative to CaO (benchmark) | 47 |
| 4.10 | H ₂ yield of steam reforming of ethene relative to CaO (benchmark) | 47 |
| 4.11 | H ₂ yield of steam reforming of toluene relative to CaO (benchmark) | 47 |
| 4.12 | Conversion of 1H-indene during steam reforming at 800 °C | 49 |
| 4.13 | Methane conversion during steam reforming at 800 °C using fresh and used olivine particles | 50 |
| 4.14 | Steps of the substitution mechanism: (1) olivine, Mg _{1.8} Fe _{0.2} SiO ₄ (top), and (2) CaMgSiO ₄ (bottom). | 52 |
| 4.15 | Crystal structure of α -di-calcium silicate | 53 |
| 4.16 | ESEM image of a typical cross section of the olivine bed particle layer taken after about 400 h showing distinguishable zones of the inner particle layer | 53 |
| 4.17 | ESEM image of cracks in the olivine bed particle layer perpendicular to the surface and the typical Mg-enrichment along cracks in the particle layer | 55 |
| 4.18 | ESEM image of Mg-enrichment on the surface of the particle layers on olivine (sampled after 180 h of operation) | 56 |
| 4.19 | ESEM image of cracks in the olivine bed particle layer parallel to the surface (sampled after 180 h of operation) | 57 |
| 4.20 | Mass fraction of crystal structures present at varying Ca/K molar ratios at a K to bed (olivine) molar ratio of 1/200 | 57 |
| 4.21 | ESEM image of mapping along a typical cross-section of a K-feldspar layer | 59 |

5.1 Comparison between the simple carbon cycle (left) and the manipulated carbon cycle with biochar (right) as proposed by Steiner [89] 64

List of Tables

| | | |
|------|--|----|
| 1.1 | Typical product gas composition for DFB gasification of woody biomass [17] . . . | 9 |
| 2.1 | Average temperatures in the gasification and the combustion reactor | 24 |
| 2.2 | Fuel ash composition (expressed as oxides) identified with XRF analysis | 27 |
| 2.3 | Elements and solution models used in the thermochemical equilibrium calculations | 28 |
| 4.1 | Elemental composition (expressed as oxides) identified with XRF analysis | 36 |
| 4.2 | Crystalline phases identified with XRD analysis (samples from the plant in Senden) | 37 |
| 4.3 | Average elemental compositions on a C- and O-free basis of attached melt fragments | 39 |
| 4.4 | Elemental composition (expressed as oxides) of used particles | 42 |
| 4.5 | Elemental surface composition of main components of bed materials | 43 |
| 4.6 | Wet gas composition at the outlet of the reactor for the water-gas-shift reaction, (*) H ₂ O content calculated from chemical equation (equimolar) | 44 |
| 4.7 | Conversion efficiency of bed materials regarding toluene steam reforming | 46 |
| 4.8 | Dry gas composition of toluene steam reforming | 46 |
| 4.9 | Dry gas composition (main components, total 100%) of steam reforming of 1H- indene at 800 °C | 50 |
| 4.10 | Formation of chrysene during steam reforming of 1H-indene at 800 °C | 50 |
| 4.11 | Comparison of the compositions in the inner and outer zone of the inner layer and at the intrusion into the surface and along the cracks (sampled after 400 h of operation) | 55 |
| 4.12 | Average elemental composition on a C- and O-free basis across K-feldspar particle layers | 59 |

Bibliography

- [1] IPCC 2014, “Climate Change 2014: Synthesis Report. Contribution of Working Groups I, II and III to the Fifth Assessment Report of the Intergovernmental Panel on Climate Change,” tech. rep., UNEP, Geneva, Switzerland, 2014.
- [2] The World Bank and The International Cryosphere Climate Initiative, “On Thin Ice - How Cutting Pollution Can Slow Warming and Save Lives,” tech. rep., The World Bank, Washington DC, USA, 2013.
- [3] United Nations - Framework Convention on Climate Change, “Adoption of the Paris Agreement,” in *Conference of the Parties, 21st session*, vol. 21932, 2015.
- [4] M. Kaltschmitt, H. Hartmann, and H. Hofbauer, *Energie aus Biomasse*. Berlin, Heidelberg: Springer Berlin Heidelberg, 2001.
- [5] European Commission, “State of play on the sustainability of solid and gaseous biomass used for electricity, heating and cooling in the EU,” 2014.
- [6] European Commission, *EU Energy in Figures*. 2015.
- [7] Deutscher Bundestag, “Gesetz zur Neuregelung des Rechts der Erneuerbaren Energien im Strombereich und zur Änderung damit zusammenhängender Vorschriften,” 2008.
- [8] H. Hofbauer, R. Rauch, G. Loeffler, S. Kaiser, E. Fercher, and H. Tremmel, “Six years experience with the FICFB-gasification process,” in *Proceedings of the 12th European Conference and Technology Exhibition on Biomass for Energy, Industry and Climate Protection*, (Amsterdam, The Netherlands), pp. 982–985, 2002.

- [9] W. Steffen, K. Richardson, J. Rockström, S. E. Cornell, I. Fetzer, E. M. Bennett, R. Biggs, S. R. Carpenter, W. de Vries, C. A. de Wit, C. Folke, D. Gerten, J. Heinke, G. M. Mace, L. M. Persson, V. Ramanathan, B. Reyers, and S. Sörlin, “Sustainability. Planetary boundaries: guiding human development on a changing planet.,” *Science (New York, N.Y.)*, vol. 347, p. 1259855, feb 2015.
- [10] P. Basu, *Biomass Gasification and Pyrolysis*. Oxford: Elsevier Inc., 2010.
- [11] H. Knoef, *Handbook of biomass gasification*. BTG Biomass Technology Group BV, 1 ed., 2005.
- [12] M. Bolhàr-Nordenkamp, *Techno-Economic Assessment on the Gasification of Biomass on the Large Scale for Heat and Power Production*. PhD thesis, Vienna University of Technology, Austria, 2004.
- [13] A. Grimm, M. Öhman, T. Lindberg, A. Fredriksson, and D. Boström, “Bed agglomeration characteristics in fluidized-bed combustion of biomass fuels using olivine as bed material,” *Energy and Fuels*, vol. 26, no. 7, pp. 4550–4559, 2012.
- [14] S. Koppatz, C. Pfeifer, and H. Hofbauer, “Comparison of the performance behaviour of silica sand and olivine in a dual fluidised bed reactor system for steam gasification of biomass at pilot plant scale,” *Chemical Engineering Journal*, vol. 175, pp. 468–483, nov 2011.
- [15] C. Christodoulou, D. Grimekis, K. Panopoulos, E. Pachatouridou, E. Iliopoulou, and E. Kakaras, “Comparing calcined and un-treated olivine as bed materials for tar reduction in fluidized bed gasification,” *Fuel Processing Technology*, vol. 124, pp. 275–285, aug 2014.
- [16] R. Rauch, K. Bosch, H. Hofbauer, D. Świerczyński, and C. Courson, “Comparison of different olivines for biomass steam gasification,” in *Science in Thermal and Chemical Biomass Conversion*, pp. 799–809, 2006.
- [17] M. Kraussler, M. Binder, S. Fail, K. Bosch, M. Hackel, and H. Hofbauer, “Performance of a water gas shift pilot plant processing product gas from an industrial scale biomass steam gasification plant,” *Biomass and Bioenergy*, dec 2015.

- [18] M. Kraussler, M. Binder, S. Fail, K. Bosch, M. Hackel, and H. Hofbauer, "Performance of a Water-Gas-Shift Unit Processing Product Gas from Biomass Steam Gasification," in *23rd European Biomass Conference and Exhibition*, no. June, pp. 1–4, 2015.
- [19] M. Kraussler, M. Binder, S. Fail, A. Plaza, A. Cortes, and H. Hofbauer, "Variation of a Kinetic Model for the Catalyzed Water-Gas-Shift Reaction Applying a Fe/Cr Catalyst Processing Product Gas from Biomass Steam Gasification," *23rd European Biomass Conference and Exhibition*, no. June, pp. 1–4, 2015.
- [20] F. Benedikt, M. Kraussler, D. Konlechner, K. Bosch, M. Hackel, and H. Hofbauer, "Poly-generation at the Biomass Steam Gasification Plant Oberwart - Evaluation of Process Chains to Produce Hydrogen, Electricity and Heat," in *Proceedings of the 23rd European Biomass Conference and Exhibition*, (Vienna, Austria), pp. 1–4, 2015.
- [21] S. Fail, N. Diaz, F. Benedikt, M. Kraussler, J. Hinteregger, K. Bosch, M. Hackel, R. Rauch, and H. Hofbauer, "Wood Gas Processing To Generate Pure Hydrogen Suitable for PEM Fuel Cells," *ACS Sustainable Chemistry and Engineering*, vol. 2, no. 12, pp. 2690–2698, 2014.
- [22] S. Chianese, J. Loipersböck, M. Malits, R. Rauch, H. Hofbauer, A. Molino, and D. Musmarra, "Hydrogen from the high temperature water gas shift reaction with an industrial Fe/Cr catalyst using biomass gasification tar rich synthesis gas," *Fuel Processing Technology*, vol. 132, pp. 39–48, 2015.
- [23] B. Rehling, H. Hofbauer, R. Rauch, and C. Aichernig, "BioSNG-process simulation and comparison with first results from a 1-MW demonstration plant," *Biomass Conversion and Biorefinery*, vol. 1, no. 2, pp. 111–119, 2011.
- [24] J. Agerborg and E. Lingehed, *Integration of Power-to-Gas in Gasendal and GoBiGas*. PhD thesis, Master's Thesis, Chalmers University of Technology, 2013.
- [25] R. Rauch, J. Hrbek, and H. Hofbauer, "Biomass gasification for synthesis gas production and applications of the syngas," *Wiley Interdisciplinary Reviews: Energy and Environment*, vol. 3, no. 4, pp. 343–362, 2014.
- [26] A. Sauciuc, Z. Abosteif, G. Weber, A. Potetz, R. Rauch, H. Hofbauer, G. Schaub, and I. Dumitrescu, "Influence of pressure on the performance of biomass based Fischer-Tropsch

synthesis,” in *Proceedings of the International Conference on Polygeneration Strategies (ICPS)*, (Vienna, Austria), 2011.

- [27] G. Weber, R. Rauch, and H. Hofbauer, “Influence of ethylene on the formation of mixed alcohols over a MoS₂ catalyst using biomass-derived synthesis gas,” *Biomass Conversion and Biorefinery*, vol. 07, pp. 85–94, 2014.
- [28] J. C. Schmid, T. Pröll, C. Pfeifer, and H. Hofbauer, “Improvement of Gas - Solid Interaction in Dual Circulating Fluidized Bed Systems,” in *Proceedings of the 9th European Conference on Industrial Furnaces and Boilers (INFUB)*, (Estoril, Portugal), pp. 1–13, 2011.
- [29] J. C. Schmid, C. Pfeifer, H. Kitzler, T. Pröll, and H. Hofbauer, “A new dual fluidized bed gasifier design for improved in situ conversion of hydrocarbons,” in *Proceedings of the International Conference on Polygeneration Strategies (ICPS)*, (Vienna, Austria), pp. 1–10, 2011.
- [30] C. Pfeifer, J. C. Schmid, T. Pröll, and H. Hofbauer, “Next Generation Biomass Gasifier,” in *Proceedings of the 19th European Biomass Conference and Exhibition*, (Berlin, Germany), pp. 1–7, 2011.
- [31] L. Devi, K. J. Ptasinski, and F. J. J. G. Janssen, “Decomposition of Naphthalene as a Biomass Tar over Pretreated Olivine: Effect of Gas Composition, Kinetic Approach, and Reaction Scheme,” *Industrial & Engineering Chemistry Research*, vol. 44, no. 24, pp. 9096–9104, 2005.
- [32] L. Devi, K. J. Ptasinski, F. J. Janssen, S. V. Van Paasen, P. C. Bergman, and J. H. Kiel, “Catalytic decomposition of biomass tars: use of dolomite and untreated olivine,” *Renewable Energy*, vol. 30, no. 4, pp. 565–587, 2005.
- [33] S. A. Nair, K. Yan, A. J. M. Pemen, E. J. M. van Heesch, K. J. Ptasinski, and A. A. H. Drinkenburg, “Tar Removal from Biomass-Derived Fuel Gas by Pulsed Corona Discharges. A Chemical Kinetic Study,” *Industrial & Engineering Chemistry Research*, vol. 43, no. 7, pp. 1649–1658, 2004.
- [34] I. Zamboni, C. Courson, D. Niznansky, and A. Kiennemann, “Simultaneous catalytic H₂ production and CO₂ capture in steam reforming of toluene as tar model compound from

- biomass gasification,” *Applied Catalysis B: Environmental*, vol. 145, no. 2, pp. 63–72, 2014.
- [35] B. Zhao, X. Zhang, L. Chen, R. Qu, G. Meng, X. Yi, and L. Sun, “Steam reforming of toluene as model compound of biomass pyrolysis tar for hydrogen,” *Biomass and Bioenergy*, vol. 34, no. 1, pp. 140–144, 2010.
- [36] M. Kong, Q. Yang, J. Fei, and X. Zheng, “Experimental study of Ni/MgO catalyst in carbon dioxide reforming of toluene, a model compound of tar from biomass gasification,” *International Journal of Hydrogen Energy*, vol. 37, pp. 13355–13364, sep 2012.
- [37] E. Biagini, F. Barontini, and L. Tognotti, “Devolatilization of biomass fuels and biomass components studied by TG/FTIR technique,” *Industrial and Engineering Chemistry Research*, vol. 45, pp. 4486–4493, 2006.
- [38] D. Swierczynski, C. Courson, and A. Kiennemann, “Study of steam reforming of toluene used as model compound of tar produced by biomass gasification,” *Chemical Engineering and Processing: Process Intensification*, vol. 47, no. 3, pp. 508–513, 2008.
- [39] T. Valmari, T. M. Lind, E. I. Kauppinen, G. Sfiris, K. Nilsson, and W. Maenhaut, “Field study on ash behavior during circulating fluidized-bed combustion of biomass. 1. Ash formation,” *Energy and Fuels*, vol. 13, no. 2, pp. 379–389, 1999.
- [40] A. C. Tranvik, M. Öhman, and M. Sanati, “Bed material deposition in cyclones of wood fuel fired circulating fluidized beds (CFBs),” *Energy and Fuels*, vol. 21, no. 1, pp. 104–109, 2007.
- [41] M. Öhman and A. Nordin, “The Role of Kaolin in Prevention of Bed Agglomeration during Fluidized Bed Combustion of Biomass Fuels,” *Energy {&} Fuels*, vol. 14, no. 3, pp. 618–624, 2000.
- [42] M. Zevenhoven-Onderwater, R. Backman, B.-J. Skrifvars, and M. Hupa, “The ash chemistry in fluidised bed gasification of biomass fuels. Part I: predicting the chemistry of melting ashes and ash–bed material interaction,” *Fuel*, vol. 80, pp. 1489–1502, aug 2001.
- [43] M. Öhman, L. Pommer, and A. Nordin, “Bed agglomeration characteristics and mechanisms during gasification and combustion of biomass fuels,” *Energy and Fuels*, vol. 19, no. 4, pp. 1742–1748, 2005.

- [44] E. Brus, M. Öhman, and A. Nordin, “Mechanisms of bed agglomeration during fluidized-bed combustion of biomass fuels,” *Energy and Fuels*, vol. 19, no. 3, pp. 825–832, 2005.
- [45] L. Fryda, K. Panopoulos, and E. Kakaras, “Agglomeration in fluidised bed gasification of biomass,” *Powder Technology*, vol. 181, no. 3, pp. 307–320, 2008.
- [46] B. Gatternig and J. Karl, “Investigations on the Mechanisms of Ash-Induced Agglomeration in Fluidized-Bed Combustion of Biomass,” *Energy & Fuels*, vol. 29, pp. 931–941, 2015.
- [47] M. Bartels, W. Lin, J. Nijenhuis, F. Kapteijn, and J. R. van Ommen, “Agglomeration in fluidized beds at high temperatures: Mechanisms, detection and prevention,” *Progress in Energy and Combustion Science*, vol. 34, pp. 633–666, oct 2008.
- [48] E. Brus, M. Öhman, A. Nordin, D. Boström, H. Hedman, and A. Eklund, “Bed agglomeration characteristics of biomass fuels using blast-furnace slag as bed material,” *Energy and Fuels*, vol. 18, no. 4, pp. 1187–1193, 2004.
- [49] H. He, D. Boström, and M. Öhman, “Time Dependence of Bed Particle Layer Formation in Fluidized Quartz Bed Combustion of Wood-Derived Fuels,” *Energy & Fuels*, vol. 28, no. 6, pp. 3841–3848, 2014.
- [50] A. Grimm, N. Skoglund, D. Boström, and M. Öhman, “Bed agglomeration characteristics in fluidized quartz bed combustion of phosphorus-rich biomass fuels,” *Energy and Fuels*, vol. 25, no. 3, pp. 937–947, 2011.
- [51] V. Barišić and M. Hupa, “On changes in bed-material particles from a 550MWth CFB boiler burning coal, bark and peat,” *Fuel*, vol. 86, pp. 464–468, feb 2007.
- [52] S. De Geyter, M. Öhman, D. Boström, M. Eriksson, and A. Nordin, “Effects of non-quartz minerals in natural bed sand on agglomeration characteristics during fluidized bed combustion of biomass fuels,” *Energy and Fuels*, vol. 21, no. 5, pp. 2663–2668, 2007.
- [53] G. Olofsson, Z. Ye, I. Bjerle, and A. Andersson, “Bed Agglomeration Problems in Fluidized-Bed Biomass Combustion,” *Ind. Eng. Chem. Res.*, vol. 41, no. 12, pp. 2888–2894, 2002.
- [54] H. J. M. Visser, S. C. van Lith, and J. H. A. Kiel, “Biomass Ash – Bed Material Interactions Leading to Agglomeration in FBC,” pp. 563–570, 2003.

- [55] F. Kirnbauer and H. Hofbauer, "Investigations on bed material changes in a dual fluidized bed steam gasification plant in Güssing, Austria," *Energy and Fuels*, vol. 25, no. 8, pp. 3793–3798, 2011.
- [56] F. Kirnbauer, V. Wilk, H. Kitzler, S. Kern, and H. Hofbauer, "The positive effects of bed material coating on tar reduction in a dual fluidized bed gasifier," *Fuel*, vol. 95, pp. 553–562, 2012.
- [57] S. Kern, C. Pfeifer, and H. Hofbauer, "Reactivity tests of the water-gas shift reaction on fresh and used fluidized bed materials from industrial DFB biomass gasifiers," *Biomass and Bioenergy*, vol. 55, pp. 227–233, 2013.
- [58] J. Marinkovic, H. Thunman, P. Knutsson, and M. Seemann, "Characteristics of olivine as a bed material in an indirect biomass gasifier," *Chemical Engineering Journal*, vol. 279, pp. 555–566, 2015.
- [59] J. Kaknics, F. Defoort, and J. Poirier, "Inorganic Phase Transformation in Miscanthus Ash," *Energy and Fuels*, vol. 29, no. 10, pp. 6433–6442, 2015.
- [60] J. Kaknics, R. Michel, and J. Poirier, "Miscanthus ash transformation and interaction with bed materials at high temperature," *Fuel Processing Technology*, vol. 141, pp. 178–184, 2016.
- [61] F. Kirnbauer and H. Hofbauer, "The mechanism of bed material coating in dual fluidized bed biomass steam gasification plants and its impact on plant optimization," *Powder Technology*, vol. 245, pp. 94–104, 2013.
- [62] M. S. Masnadi, J. R. Grace, X. T. Bi, C. J. Lim, N. Ellis, Y. H. Li, and A. P. Watkinson, "From coal towards renewables: Catalytic/synergistic effects during steam co-gasification of switchgrass and coal in a pilot-scale bubbling fluidized bed," *Renewable Energy*, vol. 83, pp. 918–930, 2015.
- [63] F. Kirnbauer, M. Koch, R. Koch, C. Aichernig, and H. Hofbauer, "Behavior of Inorganic Matter in a Dual Fluidized Steam Gasification Plant," *Energy & Fuels*, vol. 27, no. 6, pp. 3316–3331, 2013.

- [64] D. Boström, N. Skoglund, A. Grimm, C. Boman, M. Öhman, M. Broström, and R. Backman, “Ash transformation chemistry during combustion of biomass,” *Energy and Fuels*, vol. 26, no. 1, pp. 85–93, 2012.
- [65] M. Hupa, “Ash-related issues in fluidized-bed combustion of biomasses: Recent research highlights,” *Energy and Fuels*, vol. 26, no. 1, pp. 4–14, 2012.
- [66] Y. Niu, H. Tan, and S. Hui, “Ash-related issues during biomass combustion: Alkali-induced slagging, silicate melt-induced slagging (ash fusion), agglomeration, corrosion, ash utilization, and related countermeasures,” *Progress in Energy and Combustion Science*, vol. 52, pp. 1–61, oct 2016.
- [67] M. Tapley and D. Jolley, “Ash Research from Palm Coast, Florida to Banff, Canada: Entry of Biomass in Modern Power Boilers,” *British Journal of General Practice*, vol. 62, no. 594, pp. 38–38, 2012.
- [68] J. Marinkovic, M. Seemann, G. L. Schwebel, and H. Thunman, “Impact of Biomass Ash-Bauxite Bed Interactions on an Indirect Biomass Gasifier,” *Energy and Fuels*, vol. 30, no. 5, pp. 4044–4052, 2016.
- [69] A. Corcoran, J. Marinkovic, F. Lind, H. Thunman, P. Knutsson, and M. Seemann, “Ash Properties of Ilmenite Used as Bed Material for Combustion of Biomass in a Circulating Fluidized Bed Boiler,” *Energy & Fuels*, vol. 28, no. 12, pp. 7672–7679, 2014.
- [70] S. V. van Paasen, J. H. Kiel, J. Neeft, H. Knoef, G. Buffinger, U. Zielke, K. Sjöström, C. Brage, P. Hasler, P. Simell, M. Suomalainen, M. Dorrington, and L. Thomas, “Guideline for Sampling and Analysis of Tar and Particles in Biomass Producer Gases,” tech. rep., ECN, 2002.
- [71] S. Kraft, M. Kuba, F. Kirnbauer, K. Bosch, and H. Hofbauer, “Optimization of a 50 MW Bubbling Fluidized Bed Biomass Combustion Furnace by means of Computational Particle Fluid Dynamics,” in *Proceedings of the 23rd European Biomass Conference and Exhibition*, no. June, pp. 1–4, Elsevier Ltd, 2015.
- [72] M. F. Llorente and R. E. Cuadrado, “Influence of the amount of bed material on the distribution of biomass inorganic elements in a bubbling fluidised bed combustion pilot plant,” *Fuel*, vol. 86, pp. 867–876, mar 2007.

- [73] M. Almark and M. Hiltunen, "Alternative bed materials for high alkali fuels," in *Proceedings of the 18th International Conference on Fluidized Bed Combustion*, (Toronto, Ontario, Canada), 2005.
- [74] D. Vamvuka, D. Zografos, and G. Alevizos, "Control methods for mitigating biomass ash-related problems in fluidized beds.," *Bioresource technology*, vol. 99, no. 9, pp. 3534–44, 2008.
- [75] D. Vamvuka, M. Pitharoulis, G. Alevizos, E. Repouskou, and D. Pentari, "Ash effects during combustion of lignite/biomass blends in fluidized bed," *Renewable Energy*, vol. 34, no. 12, pp. 2662–2671, 2009.
- [76] E. Roedder, "The system $K_2O-MgO-SiO_2$, Part 1," *Am. J. Sci.*, vol. 249, pp. 97 – 130, 1951.
- [77] T. C. McCormick, J. R. Smyth, and G. E. Lofgren, "Site occupancies of minor elements in synthetic olivines as determined by channeling-enhanced X-ray emission," *Physics and Chemistry of Minerals*, vol. 14, no. 4, pp. 368–372, 1987.
- [78] H. Onken, "Verfeinerung der Kristallstruktur von Monticellit," *Naturwissenschaften*, vol. 51, no. 14, p. 334, 1964.
- [79] C. F. Macrae, I. J. Bruno, J. A. Chisholm, P. R. Edgington, P. McCabe, E. Pidcock, L. Rodriguez-Monge, R. Taylor, J. van de Streek, and P. A. Wood, "Mercury CSD 2.0 - new features for the visualization and investigation of crystal structures," *Journal of Applied Crystallography*, vol. 41, pp. 466–470, apr 2008.
- [80] J. R. Smyth, "High Temperature Crystal Chemistry of Fayalite," *American Mineralogist*, vol. 60, pp. 1092–1097, 1975.
- [81] W. Mumme, L. Cranswick, and B. Chakoumakos, "Rietveld crystal structure refinements from high temperature neutron powder diffraction data for the polymorphs of dicalcium silicate.," *Neues Jahrbuch fuer Mineralogie-Abhandlungen*, vol. 170, no. 2, pp. 171–188, 1996.
- [82] N. Skoglund, A. Grimm, M. Öhman, and D. Boström, "Combustion of biosolids in a bubbling fluidized bed, part 1: Main ash-forming elements and ash distribution with a focus on phosphorus," *Energy and Fuels*, vol. 28, no. 2, pp. 1183–1190, 2014.

- [83] N. Skoglund, A. Grimm, M. Öhman, and D. Boström, “Effects on Ash Chemistry when Co-firing Municipal Sewage Sludge and Wheat Straw in a Fluidized Bed: Influence on the Ash Chemistry by Fuel Mixing,” *Energy and Fuels*, vol. 27, no. 10, pp. 5725–5732, 2013.
- [84] N. Skoglund, *Ash chemistry and fuel design focusing on combustion of phosphorus-rich biomass*. PhD thesis, Umea University, 2014.
- [85] A. Demeyer, J. Voundi Nkana, and M. Verloo, “Characteristics of wood ash and influence on soil properties and nutrient uptake: an overview,” *Bioresource Technology*, vol. 77, no. 3, pp. 287–295, 2001.
- [86] M. Moilanen, A. Saarsalmi, M. Kukkola, and J. Issakainen, “Effects of stabilized wood ash on nutrient status and growth of Scots pine – Comparison between uplands and peatlands,” *Forest Ecology and Management*, vol. 295, pp. 136–144, 2013.
- [87] J. Ulyett, R. Sakrabani, M. Kibblewhite, and M. Hann, “Impact of biochar addition on water retention, nitrification and carbon dioxide evolution from two sandy loam soils,” *European Journal of Soil Science*, vol. 65, pp. 96–104, jan 2014.
- [88] A. Saarsalmi, A. Smolander, M. Kukkola, M. Moilanen, and J. Saramäki, “30-Year effects of wood ash and nitrogen fertilization on soil chemical properties, soil microbial processes and stand growth in a Scots pine stand,” *Forest Ecology and Management*, vol. 278, pp. 63–70, 2012.
- [89] C. Steiner, “Biochar Carbon Sequestration,” *Report - University of Georgia, Biorefining and Carbon Cycling Program*, 2003.
- [90] J. Lehmann, J. Gaunt, and M. Rondon, “Bio-char Sequestration in Terrestrial Ecosystems – A Review,” *Mitigation and Adaptation Strategies for Global Change*, vol. 11, pp. 395–419, jun 2006.
- [91] S. Abel, A. Peters, S. Trinks, H. Schonsky, M. Facklam, and G. Wessolek, “Impact of biochar and hydrochar addition on water retention and water repellency of sandy soil,” *Geoderma*, vol. 202, pp. 183–191, 2013.
- [92] B. E. Yusiharni, “An Evaluation of Chicken Litter Ash , Wood Ash and Slag for Use as Lime and Phosphate Soil Amendments,” *Soil Science*, 2007.

- [93] E. E. Codling, R. L. Chaney, and J. Sherwell, "Poultry Litter Ash as a Potential Phosphorus Source for Agricultural Crops," *Journal of Environmental Quality*, vol. 31, no. 3, pp. 954–961, 2002.
- [94] K. Schiemenz and B. Eichler-Löbermann, "Biomass ashes and their phosphorus fertilizing effect on different crops," *Nutrient Cycling in Agroecosystems*, vol. 87, pp. 471–482, jul 2010.

Appendix A

Journal Papers

A.1 Paper I

**Deposit build-up and ash behavior in dual fluid bed steam gasification of logging residues
in an industrial power plant**



Research article

Deposit build-up and ash behavior in dual fluid bed steam gasification of logging residues in an industrial power plant



Matthias Kuba^{a,*}, Hanbing He^c, Friedrich Kirnbauer^a, Dan Boström^d, Marcus Öhman^c, Hermann Hofbauer^b

^a Bioenergy 2020 + GmbH, Wiener Straße 49, A-7540 Güssing, Austria

^b Vienna University of Technology, Institute of Chemical Engineering, Getreidemarkt 9/166, 1060 Vienna, Austria

^c Luleå University of Technology, Energy Engineering, Division of Energy Science, SE-971 87 Luleå, Sweden

^d Umeå University, Energy Technology and Thermal Process Chemistry, SE-901 87 Umeå, Sweden

ARTICLE INFO

Article history:

Received 25 June 2015

Received in revised form 11 August 2015

Accepted 12 August 2015

Available online 28 August 2015

Keywords:

Biomass gasification

Deposit build-up

Olivine

Bed material agglomeration

Logging residues

ABSTRACT

A promising way to substitute fossil fuels for production of electricity, heat, fuels for transportation and synthetic chemicals is biomass steam gasification in a dual fluidized bed (DFB). Using lower-cost feedstock, such as logging residues, instead of stemwood, improves the economic operation. In Senden, near Ulm in Germany, the first plant using logging residues is successfully operated by Stadtwerke Ulm. The major difficulties are slagging and deposit build-up. This paper characterizes inorganic components of ash forming matter and draws conclusions regarding mechanisms of deposit build-up. Olivine is used as bed material. Impurities, e.g., quartz, brought into the fluidized bed with the feedstock play a critical role. Interaction with biomass ash leads to formation of potassium silicates, decreasing the melting temperature. Recirculation of coarse ash back into combustion leads to enrichment of critical fragments. Improving the management of inorganic streams and controlling temperature levels is essential for operation with logging residues.

© 2015 Elsevier B.V. All rights reserved.

1. Introduction

A steadily rising CO₂ concentration in the atmosphere, which is linked to climate change, has increased the demand for the development of multiple technologies using renewable energy sources. Using solid biomass as a resource is one way to raise the ratio of renewable energy in our energy system. As a CO₂-neutral carbon source it is suited for usage in pyrolysis, gasification and combustion systems. Steam gasification of biomass is a promising technology for generating electricity and heat as well as synthetic products such as bio-fuels or chemicals. A dual fluidized bed (DFB) steam gasification process was developed at the Vienna University of Technology which is able to produce a product gas that can be further used to generate electricity, heat, fuels for transportation and synthetic chemicals. Thanks to the flexibility of the technology it can quickly adapt to changes in the energy market.

The principle underpinning this process is the separation of endothermic gasification and exothermic combustion. Heat which is necessary for gasification is provided by a circulating bed material from the combustion to the gasification zone. Steam is used as fluidizing agent for the bubbling bed in the gasification zone. Fast fluidization in the combustion zone is realized by using air. Part of the biomass is combusted to provide the heat necessary for gasification [1–4]. Since 2001 the process has been successfully demonstrated at the biomass

power plant in Güssing, Austria, which has a fuel power of 8 MW_{th}. In Oberwart, Austria, a biomass power plant with fuel power of 8.5 MW_{th} has been in operation since 2007. At Senden, near Ulm in Germany, a plant with fuel power of 15 MW_{th} has been in operation since 2011. Next generation dual fluid bed gasification is currently investigated at the Vienna University of Technology [5–7].

In contrast with all other gasification power plants the Senden plant is operated with logging residues together with wood chips as feedstock. As regards this lower-cost biomass, the major difficulties of operation are deposit build-up and slagging. Avoiding build-up of deposits may increase the availability and consequently the operation time further and is therefore important as regards the optimization of the plant. Previous studies showed an interaction between bed particles and ash during combustion of biomass feedstock. As a consequence of this interference calcium-rich layers are built around bed particles [8–10]. Investigations of time dependence regarding layer formation on quartz sand particles from a 30 MW_{th} bubbling fluidized bed biomass combustion plant showed several steps of layer growth. On the first day of operation only one thin Ca-, Si- and K-rich homogeneous layer with a relatively high K/Ca molar ratio could be observed. Particles aged one day to two weeks also showed an outer Ca-rich layer. During the initial phase of layer formation, the growth rate was relatively high, but decreased over time [11].

A correlation between bed particle layer formation and bed agglomeration has been established, mainly focusing on combustion of wood fuels [8,9,12–15]. Since layers on particles originate from biomass ash,

* Corresponding author.

E-mail address: matthias.kuba@bioenergy2020.eu (M. Kuba).

they have a high probability of melting in zones of elevated temperatures. Partly melted layers act as glue and cause particles to stick together [16–18]. Biomass ash leading to deposits has been investigated in the past for biomass combustion systems [19–23]. Depositions found in circulated fluidized bed combustion of woody biomass consisted mainly of bed particles embedded in a homogeneous melt. Potassium species from the feedstock interact with quartz sand bed particles to form sticky alkali-rich silicates. These sticky silicate melts can adhere to the walls of the cyclone or the return legs. Ordinary bed particles can deposit on the surface of those melts [24]. Impurities such as quartz and feldspar further enhance slag formation [25–27].

Similar findings can be observed for dual fluid bed gasification of biomass. During long-term operation of the biomass DFB gasification plant in Güssing two calcium-rich layers formed on the bed material. The inner layer mainly consisted of calcium silicates and the outer layer had a composition similar to fine ash. The formation of calcium-rich layers is owed to the high calcium content of the woody feedstock and addition of calcium-rich additives to the reactor. This formation may arise from intensive contact with burning char particles. Molten ash components stick on the surface and calcium diffuses into the particles. The smooth surface of the layer indicates that the formation occurs with a molten surface [28]. Layers on olivine have a positive catalytic influence in the gasification process. They increase its catalytic activity enhancement of gasification reactions and reduce tar dramatically. Measurements at the biomass gasification reactor at the Vienna University of Technology showed a significant decrease of tars when layered olivine was used [29,30]. The water–gas–shift reaction is enhanced, which leads to higher hydrogen and carbon dioxide content in the product gas [31].

This paper focuses on the characterization of inorganic compounds in dual fluid bed biomass gasification of logging residues. X-ray fluorescence (XRF) analysis of different ash fractions in the systems was conducted. Results from these analyses were compared with other investigations with an environmental scanning electron microscope (ESEM) and X-ray diffraction (XRD). As a result, tracking of critical components regarding deposit built-up could be realized. Chemical equilibrium calculations were performed to evaluate melting behavior of compounds appertaining to slagging phenomena. Particle size fractionation enhanced knowledge of particle pathways in the system. Therefore, critical compounds could be assigned to certain parts of the reactor set-up. From the results of these analyses conclusions regarding the mechanisms of deposit build-up in the combustion area of the DFB system are drawn.

2. Materials and methods

2.1. Description of the industrial biomass DFB gasification plant

Samples for investigation were taken from the biomass combined heat and power (CHP) plant in Senden, Germany. It has fuel power of 15 MW_{th}, generates electricity of about 5.1 MW_{el} in two gas engines and an organic rankine cycle (ORC) and also produces district heating of about 6.4 MW_{th}. Logging residues, including cut-off root ends, tops, and branches, are used as feedstock. This lower-cost feedstock comprises on average 15% of bark and 15% of needles; therefore, only 70% of the used fuel is wood chips. Because of decentered chipping, mainly by the forest industry, the particle size distribution and water content vary considerably. The feedstock is collected in four storage silos before it is fed into the biomass dryer. Hence, a good fuel mixing can be achieved before the feedstock is put into the gasifier. The specifications mentioned above are constantly monitored by a feedstock management process executed by the staff of the power plant on site.

Fig. 1 shows a flow sheet of the power plant. Feedstock enters the gasification reactor via a screw conveyor, where the biomass is led directly into the bubbling fluidized bed. Therefore, gases released from the biomass are immediately in contact with catalytically active bed

material. Olivine is used as bed material. It has two major roles in the process. First, it acts as a circulating heat carrier between the combustion reactor and the gasifier. Second, it performs as a catalyst regarding the decomposition of tars. The bubbling bed is kept at a temperature of around 850 °C and steam is used as a gasifying agent. Calcite is brought into the system as an additive to enhance the catalytic activity of the olivine. Bed material is transported together with char from the solid feedstock from the gasifier into the combustion reactor via a chute. In this zone air is used for fluidization and full oxidation is achieved. As a result, bed material particles are heated up and temperatures of up to 950 °C are reached. After it has been transported through the fast fluidized combustion reactor the bed material enters a cyclone which separates the bed material from flue gas. Small particles which are not separated from the gas stream by the cyclone enter the post-combustion chamber. Air is added at the inlet of the chamber to secure complete oxidation of flue gas. Since the post-combustion chamber is widened after the inlet, the gas stream is slowed down and further redirected by 180° before leaving the chamber. The gas stream is then led through a radiation channel where the temperature of the flue gas is cooled down to about 630 °C. Particles in the gas stream are again divided by a gravitational separation unit. Bigger particles are recirculated back into the combustion reactor and are referred to as coarse ash. Smaller particles are dragged to a flue gas filter by the gas stream and are collected as fine ash. This fine ash is finally removed from the system.

Small biomass particles which are entrained out of the gasifier together with the product gas stream are referred to as fly coke. The product gas is cooled down by heat exchangers before passing through a product gas filter, where fly coke is separated. Impurities in the product gas which cannot be separated by the filter, such as tars, ammonia or sulfur components, are captured in a product gas scrubber filled with methyl ester of rapeseed (RME). Collected fly coke is transported back into the combustion reactor, since it still contains combustible compounds. The cleaned product gas is utilized in gas engines to generate electricity and heat. A small amount of product gas is brought back to control the temperature of the combustion zone. Used, layered olivine is periodically replaced by fresh olivine to make up bed material losses owed to attrition. Therefore used (aged) olivine is let out of the combustion reactor at the bottom and fresh olivine enters together with coarse ash and fly coke.

2.2. Sampling

Sampling was conducted during and after two different operation periods. On both occasions the power plant was continuously operated for around 1200 h without cooling off. Fig. 1 shows the sampling locations in the power plant. Deposition samples were taken out of the post-combustion chamber on two different dates during the shutdown of the power plant after the operation periods. On each of the dates samples from three different positions were collected. From each position two samples were investigated. Thus, a total of 12 deposition samples were analyzed. Samples of bed material, coarse ash, fine ash, fly coke and feedstock were taken during the corresponding operation periods of the power plant which led to the build-up of the deposits. To obtain representative values samples from two different days of the operation period were collected. Sampling of bed material, coarse ash, fine ash and fly coke was conducted during steady-state operation. Bed material samples were collected at the bottom of the combustion reactor. Samples of coarse ash and fine ash were both taken after the gravitational separation of the two ash streams. The sampling point of the coarse ash was located below the gravitational separation chamber and that of the fine ash at the flue gas filter. Fly coke was collected from the product gas filter. Biomass feedstock was taken for every delivery at the power plant over a day. In total, eight trucks delivered the wood chips to the plant each day. A sample corresponding to the amount of biomass

present crystalline phases was gained. In total, three deposit samples and two samples each of fly coke, fine ash, coarse ash and bed material were analyzed.

2.7. Optical particle size fractionation

Particle size distribution was carried out with a Camsizer XT from Retsch Technologies. The camsizer uses dynamic image analysis (ISO 1322-2). In comparison with conventional particle size fractionation, such as sieving, dynamic image analysis delivers additional detailed particle shape information. Bed material and coarse ash samples were investigated and compared with each other with the same analysis settings. The measured parameters were the smallest diameter and the spherical equivalent diameter (area) with a selected measuring range between 1 μm and 1.4 mm. Particles with a diameter above 1.4 mm were collected separately.

2.8. Chemical equilibrium calculation

Chemical equilibrium model calculations were performed to interpret the findings from experimental analysis regarding melt fragments in the depositions and the coarse ash. Those calculations were based on results gained from EDXS analysis of the samples. Average values from the analyses were used. Fact-Sage 6.3 was used to investigate the thermodynamic driving force behind the formation of melt fragments. The program uses the minimization method of the total Gibbs free energy of a chemical system. Thermodynamic data were employed from the Fact database regarding gaseous compounds, stoichiometric condensed phases and non-ideal solutions. Table 1 presents the data used in Fact-Sage 6.3. Calculations were performed for temperatures between 800 °C and 1100 °C in 25 °C steps with an access air ratio of 1.2.

3. Results

An overview of the findings for each fraction based on the different analysis methods is presented. The focus lies on the characterization of inorganic components in different fractions and the interaction between them.

3.1. Ash of feedstock

Average results of the elemental composition of the collected feedstock ash samples are shown in Table 2. Only the main elements are displayed, and the mathematical remainder of 0.85 wt.% (called "others") includes the components SnO, MoO₃, Nb₂O₅, ZrO₂, PbO, As₂O₃, ZnO, CuO, Co₃O₄, V₂O₅, TiO₂, and Cl. They are of no further interest regarding the investigation of deposit build-up and are therefore not included in the results of this paper.

The feedstock ash is characterized by comparably high amounts of K₂O of about 12.6 wt.% and relatively high amounts of SiO₂ of about 13.4 wt.%. Ash from stemwood usually contains around 6 wt.% K₂O [32].

Table 1
Elements and solution models used in the chemical equilibrium model calculations.

| Elements | C, H, N, O, K, Na, Ca, Mg, Si, Fe, Al |
|-----------------|--|
| Solution models | Slag: SLAGA (MgO, SiO ₂ , CaO, K ₂ O, Fe ₂ O ₃ , FeO, Al ₂ O ₃) Olivine (Mg, Fe, Ca//SiO ₄) MullF (Mullite Al ₆ Si ₂ O ₁₃ , Fe ₆ Si ₂ O ₁₃) Mel (Melilite Ca ₂ MgSi ₂ O ₇ , Ca ₂ Al ₂ SiO ₇ , Ca ₂ FeSi ₂ O ₇ , Ca ₂ Fe ₂ SiO ₇) Salt melt: MELTA (K, Na//CO ₃ , OH salt melt) LCSO (K, Ca//CO ₃ melt) SCSO (K, Ca//CO ₃ solid solution) |

3.2. Deposits

XRF analysis of deposits as average value is shown in Table 2. Relatively high amounts of SiO₂, CaO and MgO could be detected in the investigated samples. However, significant amounts of K₂O over 5 wt.% could also be found. Furthermore, amounts of more than 4 wt.% of Al₂O₃ were detected.

Fig. 2 shows an ESEM/EDXS image of typical deposits in the post-combustion chamber. The black background is epoxy and therefore not the sample itself. It was possible to differentiate between particles – darker areas – which were embedded in a molten phase. Other areas showed higher amounts of molten fragments with different structures. Analysis of the darker areas showed typical composition of olivine particles. Around olivine particles an area with a composition typical of olivine layers could be detected [28]. Results of analyses are shown in Table 4. These layered particles were found embedded in a melt phase. Areas with high amounts of Mg characterize the surface of the outer particle layer. The morphology of these areas was less dense than that from the layers or the particle itself. Enrichment in Mg was not consistent everywhere. It varied heavily in terms of both thickness and coverage of the surface.

The composition of the melt was not homogeneous for all investigated fragments. However, it was possible to differentiate between four types of fragments. Spot analysis showed that the composition of each of the types was homogeneous. Analyses of the fragments are presented in Table 4. Statistically, most of the fragments (~75%) had the composition named deposit fragments A and B. Those fragments contained mainly Ca, Si, Mg, K, Fe, Al and O. The amount of potassium was either around 7.5 wt.% or around 3 wt.%. A significant amount (~20%) of the fragments showed the composition named deposit fragments C. They are comparably high in Al and K. Only a comparably small percentage (~5%) of the investigated samples showed the composition named deposit fragments D. No Mg could be detected in these fragments, and they are dominated by Si, Ca and O. Those four types (A, B, C, D) of fragments could be detected in all deposit samples. Regardless of the position of the deposit in the post-combustion chamber, the investigated samples showed similarities. Melt fragments attached to bed particles, as seen in Fig. 2, were investigated in detail. These attached melt fragments had the same composition – shown in Table 5 – as fragments A. The morphology of those attached fragments varied heavily.

XRD analysis of deposits, as presented in Table 3, showed occurrence of crystal structures which are typical of olivine, such as forsterite, Mg₂SiO₄. Compounds with Ca and Si, such as larnite, Ca₂SiO₄, and especially wollastonite, CaSiO₃, could be found. Furthermore, a significant number of compounds with Ca, Mg and Si could be detected, such as akermanite, Ca₂MgSi₂O₇, merwinite, Ca₃Mg(SiO₄)₂ and bredigite, Ca₇Mg(SiO₄)₄. In addition, comparably high amounts of kalsilite, KAlSi₄O₈, could be detected. The three samples were taken from different positions in the post-combustion chamber. Chemical equilibrium calculations of melted fragments in the deposits showed a content of melt fractions of about 18 to 22 wt.% for fragments A and B. Those are the fragments with higher potassium content. However, the difference between those two fragments regarding the melt fraction is comparably low, even though the potassium content varies from 7.7 wt.% in fragment A to 16.9 wt.% in fragment B. The deposit melt fragments C and D possess a melt fraction of 5 to 8.5 wt.%. Increasing the temperature leads to rising numbers of melt fragments, temperatures above 1000 °C show the highest amounts of molten fragments.

3.3. Bed material

Table 2 shows a typical elemental composition for used olivine, as already known from previous work [29].

Typical back-scattered electron images of cross-sectional analysis with ESEM/EDXS of bed material samples are shown in Fig. 3. Bed material samples were characterized by high numbers of olivine particles.

Table 2
Elemental composition (expressed as oxides) identified with XRF analysis.

| Component | Feedstock ash average [wt.%] | Deposit average [wt.%] | Bed material average [wt.%] | Coarse ash average [wt.%] | Fine ash average [wt.%] | Fly coke average [wt.%] | Impurities average [wt.%] |
|--------------------------------|---------------------------------|---------------------------|--------------------------------|------------------------------|----------------------------|----------------------------|------------------------------|
| NiO | 0.0% | 0.0% | 0.2% | 0.2% | 0.0% | 0.2% | 1.6% |
| Fe ₂ O ₃ | 0.7% | 2.4% | 6.8% | 6.3% | 2.0% | 6.5% | 2.5% |
| Cr ₂ O ₃ | 0.0% | 0.1% | 0.2% | 0.2% | 0.1% | 0.2% | 0.6% |
| CaO | 55.6% | 34.0% | 13.8% | 11.0% | 54.6% | 16.5% | 22.9% |
| K ₂ O | 12.6% | 5.1% | 0.7% | 0.9% | 2.9% | 0.9% | 8.2% |
| SO ₃ | 2.9% | 0.1% | 0.1% | 0.1% | 0.4% | 0.1% | 0.3% |
| P ₂ O ₅ | 4.8% | 0.9% | 0.3% | 0.3% | 1.5% | 0.3% | 0.4% |
| SiO ₂ | 13.4% | 40.8% | 34.3% | 38.1% | 22.8% | 34.6% | 47.0% |
| Al ₂ O ₃ | 3.3% | 4.3% | 0.9% | 1.1% | 3.1% | 1.0% | 5.6% |
| MgO | 5.0% | 10.5% | 39.5% | 40.5% | 10.3% | 38.2% | 4.7% |
| Na ₂ O | 0.8% | 1.1% | 2.2% | 0.8% | 1.0% | 0.9% | 3.9% |
| Others | 0.8% | 0.8% | 0.8% | 0.5% | 1.2% | 0.6% | 2.3% |
| | 100.0% | 100.0% | 100.0% | 100.0% | 100.0% | 100.0% | 100.0% |

The layers of the particles differed in thickness, from fresher particles with no or only thin layers to older particles with thick layers. The composition of the inner and outer layers of the olivine particles is shown in Table 6. A smaller proportion of the investigated particles showed divergent composition. Those particles could be identified as quartz and feldspars amongst others and are further referred to as impurities.

Corresponding to the findings from the XRF analysis bed material showed a comparably high correlation with findings from previous work on XRD analysis, as shown in Table 3 [29]. Two bed material samples were investigated. They are characterized by forsterite, Mg₂SiO₄, periclase, MgO and lime, CaO. In addition, around 3% of quartz could be detected. Traces of potassium could only be detected in crystallite phases as for instance K₂MgSiO₄. This compound is, however, only a suggestion and it cannot be stated with certainty that it really occurs.

3.4. Coarse ash

Elemental analysis with XRF also shows a similar composition of coarse ash and bed material samples, with slightly higher amounts of SiO₂ in the coarse ash. Impurities were analyzed in detail. Table 2 shows the elemental composition of the XRF analyses. The foreign matter was composed of a broader variety of elements than bed material or coarse ash. Na₂O amounts to around 4 wt.% and Al₂O₃ amounts to around 5.5 wt.% could be detected. Furthermore, the K₂O was elevated to values of around 8 wt.%.

Coarse ash samples showed higher amounts of impurities from the feedstock, such as quartz and feldspar particles, than the bed material samples. A typical cross-section image of the sample can be seen in

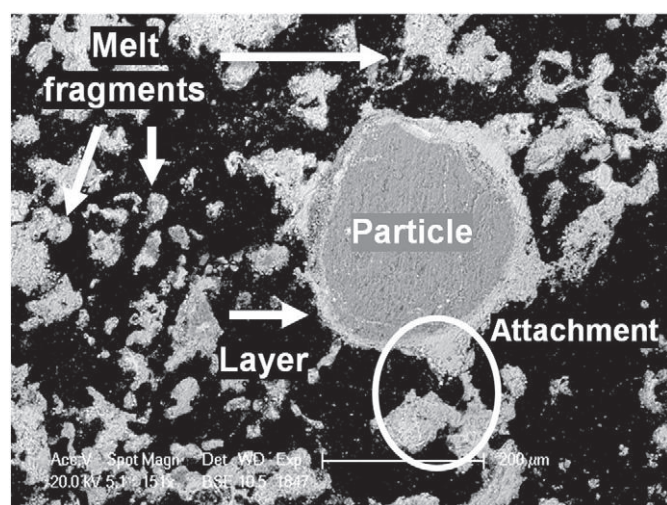


Fig. 2. ESEM image of the deposits.

Fig. 4. It presents the diversity of different particles. Table 6 presents the composition of the inner and outer layers of those quartz and feldspar particles. Layers, especially the inner layers, of quartz and feldspars were significantly richer in potassium than those of olivine. In addition, melt fragments could be found in the sample. Two different compositions could be detected and are also presented in Table 6. Melt fragments varied in size and shape; some of them were attached to particles or even caused agglomeration of particles. Olivine particles in the coarse ash were characterized by thick layers. In those thick layers cracks could be observed. The cracks could only be found in the layers, not in the olivine particle itself. The particle surface, however, seems to be affected by the formation of cracks. Even though the cracks seem to end at the surface, an inner layer intrudes a little further into the particle at those spots. This phenomenon was observed for numerous olivine particles in the coarse ash. Fig. 5 shows an example of an olivine particle with the described cracks in the layer. Furthermore, a comparably high number of layer breakage areas could be detected in olivine particles in the coarse ash, but not for any of the impurities. These

Table 3
Crystalline phases identified with XRD analysis.

| | | Deposit average [wt.%] | Bed material average [wt.%] | Coarse ash average [wt.%] | Fine ash average [wt.%] | Fly coke average [wt.%] |
|----------------|--|---------------------------|--------------------------------|------------------------------|----------------------------|----------------------------|
| Quartz | SiO ₂ | 1.0 | 3 | 4 | 1.5 | 4 |
| Microcline | KAlSi ₃ O ₈ | n.d. | n.d. | n.d. | n.d. | 2 |
| Forsterite(Fe) | Mg ₂ SiO ₄ | 5.0 | 76.5 | 69.5 | n.d. | 32.5 |
| Lime | CaO | n.d. | 3.5 | 6.5 | 27.5 | 3.5 |
| Periclase | MgO | 1.5 | 3 | 5 | 4 | 2.5 |
| Portlandite | Ca(OH) ₂ | 2.0 | n.d. | n.d. | n.d. | 15 |
| Calcite | CaCO ₃ | 2.0 | 1.5 | n.d. | 45.5 | 21.5 |
| Fairchildite | CaK ₂ (CO ₃) ₂ | n.d. | n.d. | n.d. | n.d. | n.d. |
| Anhydrite | CaSO ₄ | 2.0 | n.d. | n.d. | n.d. | n.d. |
| Gypsum | CaSO ₄ ×2H ₂ O | 2.0 | n.d. | n.d. | n.d. | n.d. |
| Archanite | K ₂ SO ₄ | n.d. | 1.5 | 1.5 | n.d. | n.d. |
| Apathite | Ca ₅ (PO ₄) ₃ (OH) | 1.0 | n.d. | n.d. | 1.5 | 1 |
| Larnite | Ca ₂ SiO ₄ | 5.3 | 4 | 4.5 | 5.5 | 4.5 |
| Wollastonite | CaSiO ₃ | 15.7 | n.d. | n.d. | n.d. | n.d. |
| Rankinite | Ca ₃ Si ₂ O ₇ | 8.7 | n.d. | n.d. | n.d. | n.d. |
| Akermanite | Ca ₂ MgSi ₂ O ₇ | 21.0 | n.d. | n.d. | n.d. | n.d. |
| Merwinite | Ca ₃ Mg(SiO ₄) ₂ | 8.0 | 2.5 | 3 | 5.5 | 2.5 |
| Bredigite | Ca ₇ Mg(SiO ₄) ₄ | 10.0 | 1.5 | 1 | 5 | 2.5 |
| Kalsilite | KAlSiO ₄ | 9.3 | 1 | n.d. | 2 | 3.5 |
| | K ₂ MgSiO ₄ | 2.5 | 1 | 2.5 | n.d. | n.d. |
| | K ₂ MgSi ₅ O ₁₂ | 2.0 | n.d. | n.d. | n.d. | n.d. |
| Hematite | Fe ₂ O ₃ | 1.0 | n.d. | n.d. | 1 | 2 |
| Maghemite | Fe ₂ O ₃ | n.d. | 1 | 1.5 | 1 | 3 |
| Magnetite | Fe ₃ O ₄ | n.d. | n.d. | n.d. | n.d. | n.d. |
| Cristobalite | SiO ₂ | n.d. | n.d. | 1 | n.d. | n.d. |
| n.d. | not detected | | | | | |
| SUM | | 100.0 | 100.0 | 100.0 | 100.0 | 100.0 |

Table 4
Average elemental compositions on a C- and O free basis in the deposition sample.

| | Particle | Layer | Deposit fragments A | Deposit fragments B | Deposit fragments C | Deposit fragments D |
|----|---------------|---------------|---------------------|---------------------|---------------------|---------------------|
| | | [wt.%] | [wt.%] | [wt.%] | [wt.%] | [wt.%] |
| Na | 1.9 (+/-0.1) | 1.1 (+/-0.1) | 1.3 (+/-0.3) | 1.1 (+/-0.2) | 0.8 (+/-0.2) | 0.3 (+/-0.1) |
| Mg | 41.7 (+/-1.1) | 13.0 (+/-0.2) | 11.4 (+/-1.3) | 10.9 (+/-0.5) | 5.2 (+/-1.0) | 1.3 (+/-0.2) |
| Al | 1.2 (+/-0.1) | 1.9 (+/-0.5) | 3.7 (+/-0.4) | 1.9 (+/-0.2) | 9.2 (+/-0.9) | 1.6 (+/-0.3) |
| Si | 37.6 (+/-0.4) | 27.3 (+/-0.5) | 31.0 (+/-0.8) | 34.1 (+/-1.2) | 34.1 (+/-0.9) | 37.4 (+/-1.5) |
| P | 0.4 (+/-0.1) | 0.5 (+/-0.0) | 1.2 (+/-0.2) | 0.8 (+/-0.2) | 0.5 (+/-0.0) | 0.6 (+/-0.1) |
| S | 0.2 (+/-0.0) | 0.1 (+/-0.1) | 0.3 (+/-0.2) | 0.1 (+/-0.1) | 0.2 (+/-0.1) | 0.1 (+/-0.1) |
| Cl | 0.4 (+/-0.0) | 0.5 (+/-0.1) | 1.9 (+/-0.8) | 0.4 (+/-0.1) | 0.4 (+/-0.1) | 0.3 (+/-0.1) |
| K | 1.5 (+/-0.4) | 1.6 (+/-0.4) | 7.7 (+/-0.9) | 2.8 (+/-0.4) | 16.9 (+/-1.1) | 3.1 (+/-0.7) |
| Ca | 9.1 (+/-2.6) | 47.6 (+/-2.7) | 36.0 (+/-2.5) | 45.5 (+/-1.8) | 26.6 (+/-2.4) | 53.6 (+/-1.8) |
| Mn | 0.6 (+/-0.0) | 0.7 (+/-0.2) | 0.7 (+/-0.1) | 0.5 (+/-0.1) | 0.5 (+/-0.1) | 0.5 (+/-0.1) |
| Fe | 9.6 (+/-1.4) | 5.7 (+/-2.2) | 4.9 (+/-0.7) | 1.9 (+/-0.2) | 5.7 (+/-0.8) | 1.0 (+/-0.2) |

breakages could be detected for olivine with thick layers, as seen in Fig. 6. The particle itself seems to be untouched, but part of the layer is missing.

Results of XRD analysis of coarse ash are shown in Table 3. Two samples were investigated. A clear resemblance to the results for bed material analysis can be seen. High amounts of forsterite as well as lime and periclase characterize the coarse ash samples. Chemical equilibrium calculations show varying amounts of molten fractions at elevated temperatures. Coarse ash melt fragments A have a melt fraction of around 70 to 71 wt.%, whereas the melt fraction in the fragments B varies from 33 to 43 wt.%, rising with increasing temperature.

The particle size distribution for coarse ash samples was compared with those of bed material. The mean diameter D_{50} of bed material for the spherical equivalent diameter is about 605 μm whereas that of coarse ash is about 490 μm . The diameter D_{50} for the minimal diameter is 535 μm for the bed material and 430 μm for the coarse ash.

Both samples showed a homogeneous particle size distribution. The bed material sample contained impurities from the feedstock with diameters above 1 mm. Those impure particles are referred to as coarse grains and were collected separately. The separation of the coarse grains from the rest of the bed material was performed so the samples could reasonably be compared with the coarse ash samples.

3.5. Fine ash

XRF analysis of fine ash is characterized by higher amounts of CaO and smaller amounts of SiO_2 and MgO than bed material and coarse ash samples. Higher K_2O amounts of around 3 wt.% could also be found. Results are shown in Table 2. Corresponding to findings from XRF analysis, XRD results show high amounts of CaO and CaCO_3 , as presented in Table 3. Two samples were examined. In addition, Ca–Mg compounds such as merwinite or bredigite could be detected in elevated amounts. No presence of forsterite could be found in fine ash. Mg could also be detected as periclase, MgO.

Table 5
Average elemental compositions on a C- and O free basis of attached melt fragments.

| | Deposit fragments A | Attached melt fragments |
|----|---------------------|-------------------------|
| | [wt.%] | [wt.%] |
| Na | 1.3 (+/-0.3) | 0.2 (+/-0.2) |
| Mg | 11.4 (+/-1.3) | 11.0 (+/-1.0) |
| Al | 3.7 (+/-0.4) | 3.6 (+/-1.0) |
| Si | 31.0 (+/-0.8) | 30.9 (+/-1.2) |
| P | 1.2 (+/-0.2) | 0.6 (+/-0.1) |
| S | 0.3 (+/-0.2) | 0.2 (+/-0.0) |
| Cl | 1.9 (+/-0.8) | 0.4 (+/-0.1) |
| K | 7.7 (+/-0.9) | 7.4 (+/-1.1) |
| Ca | 36.0 (+/-2.5) | 40.7 (+/-1.4) |
| Mn | 0.7 (+/-0.1) | 0.5 (+/-0.1) |
| Fe | 4.9 (+/-0.7) | 3.7 (+/-0.6) |

3.6. Fly coke

XRF analysis of fly coke, displayed in Table 2, also showed a resemblance to bed material samples. MgO, SiO_2 , CaO and Fe_2O_3 are the main compounds. The elemental composition of the main ash forming elements is displayed in Table 2. XRD analysis of fly coke showed a high variation of different components (Table 3). Two samples were investigated. Compounds containing Ca are dominant, but kalsilite was present in higher amounts than in the other samples. A comparably high variation of forsterite, Mg_2SiO_4 , could be detected between the two samples. Calcite, CaCO_3 , and portlandite, $\text{Ca}(\text{OH})_2$, were also detected in different amounts.

4. Discussion

Findings from analyses of inorganic streams in the process are discussed in detail. Deposition build-up in zones with elevated temperatures is connected with inorganic materials in the system. Mechanisms leading to deposits are explained by outlining the interaction between biomass ash, mineral impurities and bed material particles.

The logging residues which are used as feedstock showed relatively high amounts of potassium in comparison to average stemwood. This leads to comparably low melting temperatures of ash, making the char particles sticky at temperatures over 1000 °C, as chemical equilibrium calculations have shown. At calculated temperatures above 1000 °C, increasing amounts of molten fragments were present in coarse ash and deposit samples. These calculations allow a prediction of deposit build-up regarding temperature variation. However, melting

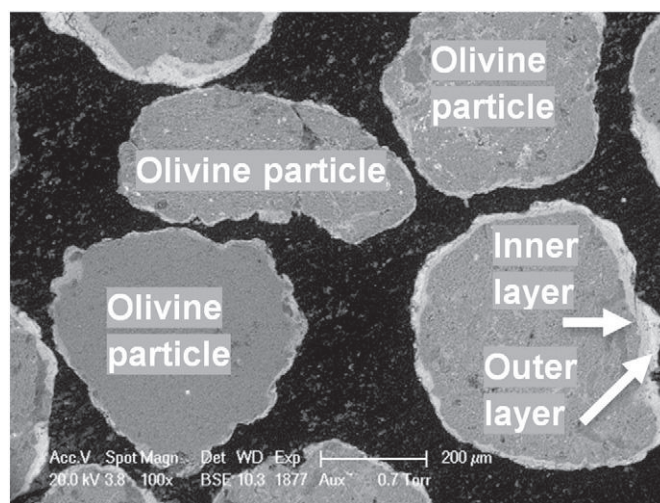


Fig. 3. ESEM image of the bed material.

Table 6
Average elemental compositions on a C- and O free basis in the bed and coarse ash samples.

| | Bed material inner layer [wt.%] | Bed material outer layer [wt.%] | Quartz particle inner layer [wt.%] | Quartz particle outer layer [wt.%] | Coarse ash fragments A [wt.%] | Coarse ash fragments B [wt.%] |
|----|------------------------------------|------------------------------------|---------------------------------------|---------------------------------------|----------------------------------|----------------------------------|
| Na | 1.4 (+/-0.0) | 0.3 (+/-0.2) | 0.9 (+/-0.1) | 0.7 (+/-0.0) | 1.5 (+/-0.2) | 1.1 (+/-0.1) |
| Mg | 29.6 (+/-0.5) | 9.2 (+/-0.4) | 3.9 (+/-0.3) | 3.7 (+/-0.5) | 5.0 (+/-0.8) | 6.5 (+/-0.6) |
| Al | 0.6 (+/-0.1) | 0.5 (+/-0.3) | 3.2 (+/-0.2) | 3.5 (+/-0.1) | 3.2 (+/-0.8) | 12.0 (+/-0.1) |
| Si | 18.5 (+/-0.3) | 6.0 (+/-0.2) | 61.4 (+/-2.5) | 42.1 (+/-1.3) | 55.9 (+/-1.5) | 51.2 (+/-0.8) |
| P | 0.5 (+/-0.0) | 2.0 (+/-0.2) | 0.1 (+/-0.0) | 0.7 (+/-0.0) | 0.3 (+/-0.1) | 0.5 (+/-0.1) |
| S | 0.1 (+/-0.0) | 0.1 (+/-0.0) | 0.2 (+/-0.0) | 0.2 (+/-0.0) | 0.2 (+/-0.0) | 0.0 (+/-0.0) |
| Cl | 0.2 (+/-0.0) | 0.1 (+/-0.1) | 0.4 (+/-0.0) | 0.5 (+/-0.0) | 0.6 (+/-0.0) | 0.4 (+/-0.1) |
| K | 0.5 (+/-0.4) | 0.6 (+/-0.1) | 20.0 (+/-1.0) | 6.7 (+/-0.5) | 19.7 (+/-0.6) | 19.6 (+/-1.7) |
| Ca | 41.8 (+/-0.3) | 75.8 (+/-0.7) | 7.0 (+/-0.4) | 39.4 (+/-0.8) | 8.8 (+/-1.2) | 5.6 (+/-1.1) |
| Mn | 1.3 (+/-0.1) | 1.8 (+/-0.1) | 0.7 (+/-0.0) | 0.4 (+/-0.1) | 0.9 (+/-0.1) | 0.9 (+/-0.1) |
| Fe | 5.5 (+/-0.4) | 3.5 (+/-0.2) | 1.6 (+/-0.6) | 1.8 (+/-0.4) | 3.9 (+/-0.9) | 2.3 (+/-0.2) |

processes highly depend on inorganic compounds, such as potassium, and therefore, predictions can only be made if representative fuel analysis is available. Higher amounts of e.g., potassium in the fuel result in ash melting at lower temperature levels, since the system approaches its eutectic point. Phase diagrams of relevant mixtures regarding biomass ash are discussed in length by [33]. After shut-down those fragments are typically found in the cyclone and post-combustion chamber as deposits. Potassium is released from the char particle and occurs in liquid form [34]. Since the gas stream is slowed down by a widening in the post-combustion chamber and is further redirected by 180°, particles can easily collide with the wall. These collisions lead to attachments of sticky particles. Operational experience in the gasification power plant in Senden, near Ulm, Germany, has shown noticeable deposition build-up in the post-combustion chamber after operation times of around 1000–1200 h when temperature levels exceeded 1000 °C. Depositions were mainly found in the post-combustion chamber, but also in the cyclone to some extent.

Furthermore, numerous impurities, such as quartz and feldspar particles, were brought into the gasifier together with the biomass feedstock. Potassium from the logging residues searches for reaction partners and can form silicates with the impurities. This leads to comparably high amounts of potassium in the layers of impurities. Potassium is involved in the layer formation of olivine, but is released from the particles during the process [28]. This could be verified, since the olivine layers did not show any potassium content. Therefore, the potassium which is bound in the feedstock has a high probability of reacting with impurities to form potassium-silicate compounds. Potassium reduces the melting temperature of the compound and is therefore critical as regards slagging and the build-up of deposits. Temperatures above

1000 °C in the post-combustion chamber lead to melting of the potassium-rich layers of the impurities and, as a consequence, make them sticky. Fragments with high amounts of silica, aluminum and potassium are most likely formed through an interaction between biomass ash and impurities. XRD analysis showed comparably high amounts of kalsilite, KAlSiO_4 , in the deposits, indicating that feldspars dissolved into the melt and formed new crystallite structures.

The composition of the deposit fragments C and D, as shown in Table 4, indicates impurity-driven melting processes. Deposit fragments C are characterized by higher amounts of aluminum and potassium, which indicates that they originate from feldspar particles interacting with biomass ash. Deposit fragments D seem to be formed from an interaction between quartz particles and biomass ash and therefore are characterized by higher amounts of silica and calcium.

Deposit fragments A and B with magnesium amounts of around 10 wt.% indicate the presence of olivine in the melt. Olivine itself is not prone to forming deposits; the particles are only embedded in a melt, as shown in Fig. 2. Therefore, depositions with significant amounts of magnesium (~10 wt.%) have to emerge from an interaction between olivine and impurity-driven melt, since significant amounts of Al and K could also be detected in those fragments. XRD analysis showed significant amounts of compounds with Si, Ca and Mg, such as akermanite, $\text{Ca}_2\text{MgSi}_2\text{O}_7$, merwinite, $\text{Ca}_3\text{Mg}(\text{SiO}_4)_2$ and bredigite, $\text{Ca}_7\text{Mg}(\text{SiO}_4)_4$, which also indicates an interaction between olivine and biomass ash. Two relevant observations regarding this interaction relate to the SEM analysis. First, on the surface of the outer layer of olivine particles, Mg-rich areas could be found. Since the morphology of those areas was less dense than that from the layers, it seems that the high Mg content originates from olivine attrition. This high Mg attrition accumulates on

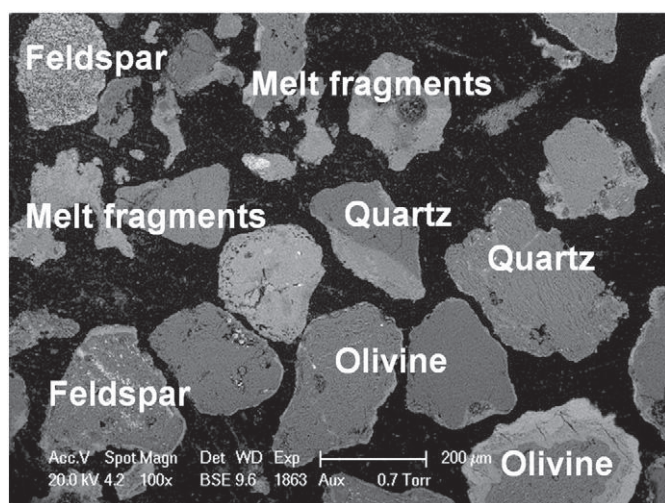


Fig. 4. ESEM image of the coarse ash.

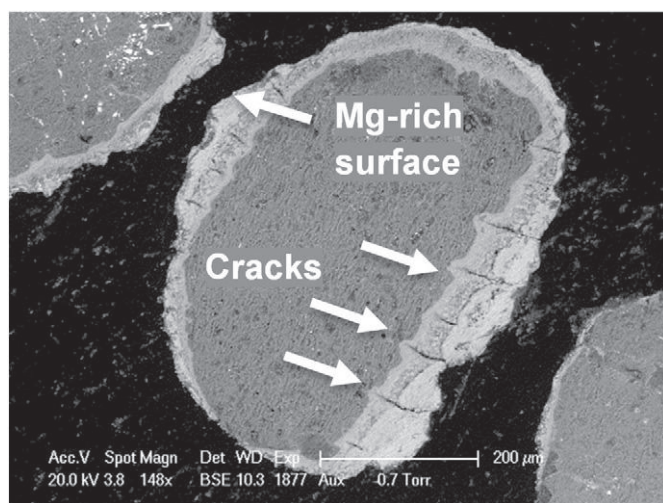


Fig. 5. ESEM image of cracks in the olivine bed particle layers.

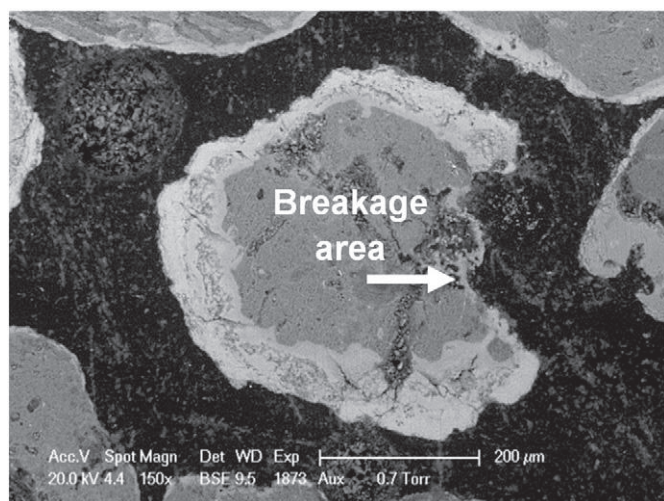


Fig. 6. ESEM image of breakage areas of the olivine bed particle layers.

the surface of the outer particle layer, a phenomenon observed in deposition samples as well as in bed material and coarse ash samples (see Fig. 5). Second, melt fragments attached to olivine particles showed exactly the same composition as deposition melt fragments A, as seen in Table 5, with about 10 wt.% of Mg. Therefore, it is likely that melts from biomass ash and layered impurities get stuck on the olivine particles. Reaction with Ca-rich layers and Mg-rich areas seems to proceed. These attached fragments can easily break off the olivine particle and be found as fragments in the deposits. A high probability of breakage of these fragments is further supported by another observation. Numerous breakage areas for aged olivine particles, as shown in Fig. 6, could be detected in the coarse ash. Olivine itself seems to be resistant to the formation of cracks. Therefore, the tension which is built up by the growth process of the layers results in cracks which lead to breakage of part of the layer itself. If, additionally, melt fragments are attached to the layers, breakage along the cracks seems probable.

SEM analysis showed a greater variety of different particles in the coarse ash than in the bed material. Numerous melt fragments and layered impurities with high amounts of potassium could be found, but XRD analysis did not detect the presence of potassium in crystalline structures. Therefore, potassium seems to exist in an amorphous state rather than in crystallite structures. This indicates that melting processes proceed in the post-combustion chamber. Chemical equilibrium calculations also showed comparably high amounts of melt at elevated temperatures for those fragments because of the relatively high content of potassium. Only the presence of aluminum stabilizes the compound and raises the melting temperature. However, even the fragments with higher aluminum content, such as coarse ash fragments B, have an estimated melt fraction of 33 to 43%, depending on the temperature. As a result they become sticky in zones with elevated temperatures, such as the cyclone or the post-combustion chamber. Melted fragments which do not stick on the walls and start building deposits but leave the post-combustion chamber are recirculated to the combustion chamber with the coarse ash. As a consequence, they can cause agglomeration of bed particles. Keeping those fragments in the system increases the probability of deposition build-up even further.

Coarse ash also showed higher amounts of older olivine particles, characterized by thicker layers. These layers have a positive and a negative side regarding biomass gasification. On the one hand, the layers increase the catalytic activity of the bed material [30]. On the other hand, since layers originate from melting processes of biomass ash [28], they have a high probability of causing agglomeration and deposit build-up in zones with higher temperature. Particle size fractionation of bed material and coarse ash showed that the average particle diameter is significantly smaller for particles recirculated with the coarse ash. As a

consequence, these particles have a higher probability of leaving the system through the cyclone and entering the post-combustion chamber before they can enter the gasification zone. Thus, a circulation of critical components in the coarse ash is created between the combustion chamber, the cyclone and the post-combustion chamber. This means that critical components, such as potassium-rich fragments leading to ash mixtures close to the eutectic point, are not only kept in the system, but seem to be mainly circulated in the combustion part of the dual fluidized bed. As a result, the recirculated particles have only a slight impact on the catalytic activity of the fluidized bed in the gasification zone as they are not frequently found there.

The cyclone is a critical area in this process regarding inorganic components. Temperatures between 950 °C and 1000 °C are typical in this area during operation of the gasification plant. Circulated bed material and circulated coarse ash both pass through the cyclone and therefore make it vulnerable to deposits in long-term operation. Deposits in the cyclone decrease the separation efficiency and as a result bed material consumption rises. This leads to higher amounts of mineral material in the post-combustion chamber and, as a consequence, a higher probability of deposition build-up. Controlling the temperature levels in the system is essential when logging residues are used. In long-term operation the cyclone needs to be operated at temperatures below 950 °C. To avoid an accumulation of critical compounds in the system, the coarse ash should be released from the system periodically.

5. Conclusions

Logging residues as lower-cost feedstock lead to higher amounts of potassium and therefore the melting temperature of the ash is lower than that from stemwood. Mineral impurities, e.g., quartz, are brought into the gasifier with the feedstock. Interaction between impurities and biomass ash increases the risk of deposit build-up.

In summary, the conducted work showed that dual fluid bed gasification of logging residues with high potassium amounts is possible and was successfully demonstrated at the CHP plant Senden, Germany. Knowledge of the above-described mechanism of deposit build-up helps to increase the operation time and reduces the risk of unplanned shutdowns.

Acknowledgments

This study was carried out in the frame of the Bioenergy2020+ project “C-II-1-24”. Bioenergy2020+ GmbH is funded within the Austrian COMET program, which is managed by the Austrian Research Promotion Agency (FFG) and promoted by the federal government of Austria as well as the federal states Burgenland, Niederösterreich and Steiermark. We are grateful for the support of our project partners HGA Senden (Stadtwerke Ulm), and the Institute of Chemical Engineering at the Vienna University of Technology. Furthermore, we would like to thank the Department of Energy Engineering, Division of Energy Science, at the Lulea University of Technology, Sweden, as well as the Department of Energy Technology and Thermal Process Chemistry at the Umea University, Sweden, for their support.

References

- [1] H. Hofbauer, R. Rauch, G. Löffler, S. Kaiser, E. Fercher, H. Tremmel, Six years experience with the FICFB-gasification process, Proc. 12th Eur. Conf. Technol. Exhib. Biomass Energy, Ind. Clim. Prot., 2002.
- [2] S. Kern, C. Pfeifer, H. Hofbauer, Synergetic utilization of renewable and fossil fuels: dual fluidized bed steam co-gasification of coal and wood, APCBEE Procedia 1 (2012) 136–140, <http://dx.doi.org/10.1016/j.apcbee.2012.03.022>.
- [3] S. Kern, C. Pfeifer, H. Hofbauer, Gasification of wood in a dual fluidized bed gasifier: influence of fuel feeding on process performance, Chem. Eng. Sci. 90 (2013) 284–298, <http://dx.doi.org/10.1016/j.ces.2012.12.044>.
- [4] V. Wilk, H. Hofbauer, Co-gasification of plastics and biomass in a dual fluidized-bed steam gasifier: possible interactions of fuels, Energy Fuels 27 (2013) 3261–3273, <http://dx.doi.org/10.1021/ef400349k>.

- [5] J.C. Schmid, T. Pröll, C. Pfeifer, H. Hofbauer, Improvement of gas–solid interaction in dual circulating fluidized bed systems, Proc. 9th Eur. Conf. Ind. Furn. Boil. (INFUB), Estoril, Port 2011, pp. 1–13.
- [6] J.C. Schmid, C. Pfeifer, H. Kitzler, T. Pröll, H. Hofbauer, A new dual fluidized bed gasifier design for improved in situ conversion of hydrocarbons, Proc. Int. Conf. Polygeneration Strateg. 2011, pp. 1–10.
- [7] C. Pfeifer, J.C. Schmid, T. Pröll, H. Hofbauer, Next generation biomass gasifier, Eur. Biomass Conf. Exhib. Berlin, Ger. 2011, pp. 1–7.
- [8] E. Brus, M. Öhman, A. Nordin, Mechanisms of bed agglomeration during fluidized-bed combustion of biomass fuels, Energy Fuels 19 (2005) 825–832, <http://dx.doi.org/10.1021/ef0400868>.
- [9] A. Grimm, M. Öhman, T. Lindberg, A. Fredriksson, D. Boström, Bed agglomeration characteristics in fluidized-bed combustion of biomass fuels using olivine as bed material, Energy Fuels 26 (2012) 4550–4559, <http://dx.doi.org/10.1021/ef300569n>.
- [10] J. Kaknics, R. Michel, A. Richard, J. Poirier, High-temperature interactions between molten miscanthus ashes and bed materials in a fluidized-bed gasifier, Energy Fuels 29 (2015) 1785–1792, <http://dx.doi.org/10.1021/ef502750t>.
- [11] H. He, D. Boström, M. Öhman, Time dependence of bed particle layer formation in fluidized quartz bed combustion of wood-derived fuels, Energy Fuels 28 (2014) 3841–3848, <http://dx.doi.org/10.1021/ef500386k>.
- [12] E. Brus, M. Öhman, A. Nordin, D. Boström, H. Hedman, A. Eklund, Bed agglomeration characteristics of biomass fuels using blast-furnace slag as bed material, Energy Fuels 18 (2004) 1187–1193, <http://dx.doi.org/10.1021/ef034095c>.
- [13] A. Grimm, N. Skoglund, D. Boström, M. Öhman, Bed agglomeration characteristics in fluidized quartz bed combustion of phosphorus-rich biomass fuels, Energy Fuels 25 (2011) 937–947, <http://dx.doi.org/10.1021/ef101451e>.
- [14] D. Serrano, S. Sánchez-Delgado, C. Sobrino, C. Marugán-Cruz, Defluidization and agglomeration of a fluidized bed reactor during *Cynara cardunculus* L. gasification using sepiolite as a bed material, Fuel Process. Technol. 131 (2015) 338–347, <http://dx.doi.org/10.1016/j.fuproc.2014.11.036>.
- [15] M. Öhman, L. Pommer, A. Nordin, Bed agglomeration characteristics and mechanisms during gasification and combustion of biomass fuels, Energy Fuels 19 (2005) 1742–1748, <http://dx.doi.org/10.1021/ef040093w>.
- [16] A.A. Khan, W. de Jong, P.J. Jansens, H. Spliethoff, Biomass combustion in fluidized bed boilers: potential problems and remedies, Fuel Process. Technol. 90 (2009) 21–50, <http://dx.doi.org/10.1016/j.fuproc.2008.07.012>.
- [17] M. Hupa, Ash-related issues in fluidized-bed combustion of biomass: recent research highlights, Energy Fuels 26 (2012) 4–14, <http://dx.doi.org/10.1021/ef201169k>.
- [18] D. Vamvuka, M. Pitharoulis, G. Alevizos, E. Repouskou, D. Pentari, Ash effects during combustion of lignite/biomass blends in fluidized bed, Renew. Energy 34 (2009) 2662–2671, <http://dx.doi.org/10.1016/j.renene.2009.05.005>.
- [19] Y. Shao, J. Wang, F. Preto, J. Zhu, C. Xu, Ash deposition in biomass combustion or co-firing for power/heat generation, Energies 5 (2012) 5171–5189, <http://dx.doi.org/10.3390/en5125171>.
- [20] M.S. Bashir, P.A. Jensen, F. Frandsen, S. Wedel, K. Dam-Johansen, J. Wadenbäck, et al., Ash transformation and deposit build-up during biomass suspension and grate firing: full-scale experimental studies, Fuel Process. Technol. 97 (2012) 93–106, <http://dx.doi.org/10.1016/j.fuproc.2012.01.018>.
- [21] T.R. Miles, T.R. Miles, L.L. Baxter, R.W. Bryers, B.M. Jenkins, L.L. Oden, Boiler deposits from firing biomass fuels, Biomass Bioenergy 10 (1996) 125–138, [http://dx.doi.org/10.1016/0961-9534\(95\)00067-4](http://dx.doi.org/10.1016/0961-9534(95)00067-4).
- [22] P.A. Jensen, F.J. Frandsen, J. Hansen, K. Dam-Johansen, N. Henriksen, S. Hörlyck, SEM investigation of superheater deposits from biomass-fired boilers, Energy Fuels 18 (2004) 378–384, <http://dx.doi.org/10.1021/ef030097l>.
- [23] G. Li, S. Li, X. Xu, Q. Huang, Q. Yao, Dynamic behavior of biomass ash deposition in a 25 kW one-dimensional down-fired combustor, Energy Fuels 28 (2014) 219–227, <http://dx.doi.org/10.1021/ef401530a>.
- [24] A.C. Tranvik, M. Öhman, M. Sanati, Bed material deposition in cyclones of wood fuel fired circulating fluidized beds (CFBs), Energy Fuels 21 (2007) 104–109, <http://dx.doi.org/10.1021/ef060175f>.
- [25] M. Öhman, A. Nordin, H. Hedman, R. Jirjis, Reasons for slagging during stemwood pellet combustion and some measures for prevention, Biomass Bioenergy 27 (2004) 597–605, <http://dx.doi.org/10.1016/j.biombioe.2003.08.017>.
- [26] S. Xiong, J. Burvall, H. Örberg, G. Kalen, M. Thyrel, M. Öhman, et al., Slagging characteristics during combustion of corn stovers with and without kaolin and calcite, Energy Fuels 22 (2008) 3465–3470, <http://dx.doi.org/10.1021/ef700718j>.
- [27] E. Lindström, M. Öhman, R. Backman, D. Boström, Influence of sand contamination on slag formation during combustion of wood derived fuels, Energy Fuels 22 (2008) 2216–2220, <http://dx.doi.org/10.1021/ef700772q>.
- [28] F. Kirnbauer, H. Hofbauer, The mechanism of bed material coating in dual fluidized bed biomass steam gasification plants and its impact on plant optimization, Powder Technol. 245 (2013) 94–104, <http://dx.doi.org/10.1016/j.powtec.2013.04.022>.
- [29] F. Kirnbauer, H. Hofbauer, Investigations on bed material changes in a dual fluidized bed steam gasification plant in Güssing, Austria, Energy Fuels 25 (2011) 3793–3798, <http://dx.doi.org/10.1021/ef200746c>.
- [30] F. Kirnbauer, V. Wilk, H. Kitzler, S. Kern, H. Hofbauer, The positive effects of bed material coating on tar reduction in a dual fluidized bed gasifier, Fuel 95 (2012) 553–562, <http://dx.doi.org/10.1016/j.fuel.2011.10.066>.
- [31] S. Kern, C. Pfeifer, H. Hofbauer, Reactivity tests of the water–gas shift reaction on fresh and used fluidized bed materials from industrial DFB biomass gasifiers, Biomass Bioenergy 55 (2013) 227–233, <http://dx.doi.org/10.1016/j.biombioe.2013.02.001>.
- [32] M. Kaltschmitt, H. Hartmann, H. Hofbauer, Energie aus Biomasse, Springer, Berlin, Heidelberg, 2001 <http://dx.doi.org/10.1007/978-3-662-07025-3>.
- [33] E. Roedder, Silicate melt systems, Phys. Chem. Earth 3 (1959) 224–297, [http://dx.doi.org/10.1016/0079-1946\(59\)90007-2](http://dx.doi.org/10.1016/0079-1946(59)90007-2).
- [34] F. Scala, R. Chirone, An SEM/EDX study of bed agglomerates formed during fluidized bed combustion of three biomass fuels, Biomass Bioenergy 32 (2008) 252–266, <http://dx.doi.org/10.1016/j.biombioe.2007.09.009>.

A.2 Paper II

Influence of bed material coatings on the water-gas-shift reaction and steam reforming of toluene as tar model compound of biomass gasification



Contents lists available at ScienceDirect

Biomass and Bioenergy

journal homepage: <http://www.elsevier.com/locate/biombioe>

Research paper

Influence of bed material coatings on the water-gas-shift reaction and steam reforming of toluene as tar model compound of biomass gasification

Matthias Kuba^{a,*}, Fabian Havlik^b, Friedrich Kirnbauer^a, Hermann Hofbauer^b^a Bioenergy 2020+ GmbH, Wiener Straße 49, 7540 Güssing, Austria^b Vienna University of Technology, Institute of Chemical Engineering, Getreidemarkt 9, 1060 Vienna, Austria

ARTICLE INFO

Article history:

Received 7 August 2015

Received in revised form

26 November 2015

Accepted 27 November 2015

Available online 17 December 2015

Keywords:

Biomass gasification

Bed material coating

Catalytic conversion

Water-gas-shift reaction

Steam reforming

ABSTRACT

A promising technology replacing fossil energy carriers for the production of electricity, heat, fuels for transportation and synthetic chemicals is steam gasification of biomass in a dual fluid bed (DFB). The principle of this technology is the separation into a gasification and a combustion reactor. Bed material, nowadays olivine, circulates between them, and has two functions. It acts as a heat carrier from the combustion to the gasification zone and as catalyst regarding gasification reactions. Today, an alternative to olivine does yet not exist.

In this work, experiments in a lab-scale test rig were performed investigating the catalytic activity of different fresh and used bed materials, such as olivine and quartz. The enhancement of the catalytic activity due to particle coatings was tested regarding the water-gas-shift reaction and steam reforming of toluene. Calcite is known as an active material in this respect and is therefore used as a benchmark substance.

Experiments revealed a correlation between the catalytic activity of bed particle coatings towards both the water-gas-shift reaction and the reduction of toluene by steam reforming. Results showed bed material particles with a calcium (Ca)-rich layer achieve satisfactory conversion of carbon monoxide and reduction of toluene. Furthermore, a qualitative comparison regarding hydrogen production relative to the benchmark material CaO is given for the water-gas-shift and steam reforming of toluene and ethene - used as model substance for lighter hydrocarbons. These results are the basis for further research on the catalytic properties of potential bed materials for DFB gasification of biomass.

© 2015 Elsevier Ltd. All rights reserved.

1. Introduction

Research on energy from renewable sources has risen considerably since the early 2000s. Substitution of fossil energy carriers by renewable sources plays an ever-increasing role in energy technology. The awareness of global warming caused by combustion of fossil fuels has increased the development of technologies using biomass since it is considered as a major source of renewable energy. Biomass is suitable for use in pyrolysis, combustion and gasification as CO₂-neutral feedstock [1]. Gasification transforms the solid feedstock into a gaseous secondary energy carrier, which is referred to as product gas. Chemical properties of biomass differ

from those of fossil fuels, triggering new challenges in the operation of such systems. Compared with fossil fuels biomass contains higher amounts of low melting ashes and it also produces a higher yield of heavier hydrocarbons, which are also referred to as tars, during gasification owed to higher volatile matter. The Tar Guideline (a standard for tar sampling and measuring) defines tar as follows: Generic (unspecific) term of entity of all organic compounds present in the producer gas excluding gaseous hydrocarbons (C1 to C6). Benzene is not included in tar [2].

During gasification of a biomass feedstock tars are primarily produced in the pyrolysis stage. The three main constituents of biomass, namely cellulose, hemicellulose and lignin, break down into primary tars. Typical primary tars include phenol and cresol. Above temperatures of 500 C these primary tars start to recombine into non-condensable gases and heavier molecules. These compounds are referred to as secondary tars. At further increased

* Corresponding author.

E-mail address: matthias.kuba@bioenergy2020.eu (M. Kuba).

temperatures primary and secondary tars may be destroyed and tertiary tars produced. Tertiary tars can either be alkyl tertiary products or condensable tertiary aromatics. Alkyl tertiary products include, for example, methylacenaphthalene, methylnaphthalene, toluene and 1H-indene. Condensed tertiary aromatics are mainly poly-aromatic hydrocarbons (PAHs), such as naphthalene or pyrene. These undesirable by-products cause operational problems in downstream equipment by forming depositions [3].

A gasification process using a dual fluid bed (DFB) system was developed at the Vienna University of Technology. Syngas gained from biomass feedstock can be further used to produce electricity, heat, fuels for transportation or synthetic chemicals. Thanks to the flexibility of the technology it can quickly react to changes in the energy market [4]. The technology is successfully demonstrated in Güssing, Austria. Industrial power plants using the same technology are in operation in Oberwart, Austria, Ulm, Germany, and Gothenburg, Sweden. New-generation DFB gasification of biomass using an improved reactor design where the contact of bed material and product gas is drastically increased is currently being investigated at the Vienna University of Technology [5–7]. Therefore, catalytic properties of bed materials will become more and more important for DFB gasification of biomass in the future.

Separating endothermic gasification from exothermic combustion into two different reactor zones is the main principle of the DFB process. Between those zones a bed material circulates, which has two major roles. First, it acts as a heat carrier to transport the energy released in combustion to the gasifier, where it is needed for the reactions. Second, it is catalytically active regarding the water-gas-shift reaction and decomposition of biomass tars. Olivine, a magnesium iron silicate, is currently used as bed material because of its catalytic activity, resistance to abrasion and satisfactory behavior in terms of agglomeration processes [4].

Catalytic activity of potential bed materials has been investigated in relation to different tar model compounds. Benzene, toluene and naphthalene are often used as model substances for either monocyclic or polycyclic aromatic hydrocarbons in steam reforming experiments. Usually, synthetically created or altered naturally occurring minerals have been investigated in lab-scale experiments regarding their activity for steam reforming reactions [8–15]. Furthermore, different natural minerals, e.g. ilmenite, have been investigated as potential alternative bed materials regarding their catalytic activity [16,17]. An extensive review of the literature on naturally occurring and synthetically created catalysts has been performed previously [18,19].

Biomass ash contains critical components which might lead to operational difficulties. One major issue is the interaction between ash and bed material in fluidized bed systems [20]. Through interaction between biomass ash and bed materials the development of layers can be observed for quartz particles in biomass combustion plants. These layers are initiated by potassium (K) attacking the particle surface. Over time calcium (Ca) diffuses into the first K-dominated layer and a second outer layer starts to grow outwards [21]. Since these layers on quartz particles originate from interaction with biomass ash they are critical in terms of agglomeration and slagging. Partly molten layers in zones of elevated temperatures act as glue and cause particles to stick together. Therefore, formation of particle layers is seen as critical in biomass combustion [22–24].

A similar layer build-up can be observed for olivine in biomass gasification. During long-term operation of the DFB biomass plant in Güssing two calcium-rich layers were formed on olivine particles. The inner layer mainly consisted of calcium silicates, whereas the outer layer had a more heterogeneous composition similar to fine ash [25–28]. Layer formation is caused by notable amounts of calcium in the feedstock and addition of calcium-rich additives to

the gasifier. These Ca-rich layers led to enhanced catalytic activity regarding tar decomposition in the gasifier. This observation showed that layers positively influence gasification processes and are therefore desirable [27]. Further investigations of olivine used in a pilot-scale plant showed an increase of the catalytic activity regarding the water-gas-shift reaction owed to layer formation [27], which was confirmed by lab-scale tests [29]. Calcium has been identified as playing an important role in terms of catalytic activity if present as CaO. Consequently, it is clear that layer formation has both negative (agglomeration, slagging) and positive (catalytic activity) effects regarding biomass gasification.

Knowledge of increasing catalytic activity through layer build-up on olivine raises the question of whether specific materials are necessary because of their catalytic characteristics. If the layer itself were catalytically active, all material could be used as a bed catalyst for decomposition of tars as long as a Ca-rich layer was built around it. Therefore, this paper focuses on the investigation of fresh and layered olivine and quartz particles and compares their catalytic activity. Calcite, which is known to be an excellent natural catalyst [29], is used as reference material. Furthermore, both the water-gas shift reaction and steam reforming of the tar model compound toluene are examined to see if the catalytic activity of bed particle coatings is increased in a similar manner for those different reactions. In addition, a qualitative comparison of the catalytic activity towards hydrogen production is given for the different materials. The comparison includes the water-gas-shift reaction and steam reforming of toluene and ethene - which is used as model compound for lighter hydrocarbons.

2. Materials and methods

2.1. Test rig for measurements of catalytic activity

Fig. 1 shows a flow chart of the employed test rig. Gases (3) are introduced into the reactor via mass flow controllers (MFCs). As it can be seen, there is a possibility of introducing six different gases into the reactor simultaneously. All gases as well as the mixture of steam and carrier gas can be directed into a bypass to avoid contact with the catalytically active material. This is important to calibrate the gas measurement system and verify its functionality immediately before the start of each experiment. Calibration and review of measurement accuracy was conducted by the certified Test Laboratory for Combustion Systems of the Vienna University of Technology.

Demineralized water (2) and the model tar toluene (1) were evaporated separately and transported together with carrier gas into the reactor. The mass flow controllers as well as the evaporator for the water were controlled by a computer which also recorded the data. Water was brought into the system from a reservoir through pressurized nitrogen. The nitrogen pushed liquid water out of the reservoir and into an evaporation unit. The amount of water which was brought to the evaporator was adjusted using a mass flow controller for liquids from Bronkhorst. Evaporation of water was realized with a controlled evaporator mixer (CEM) from Bronkhorst, which was heated up to a temperature of 135 °C. Steam became mixed with the carrier gas in the evaporator and was therefore continuously dragged through the reactor system. Tar was transported into an evaporator by a syringe pump and also mixed with carrier gas. The tar evaporator was heated up to a temperature of 165 °C. The pipes from the evaporators to the reactor were trace heated to ensure that no condensation took place. Trace heating was realized at temperatures of 135 °C for the steam pipes and 145 °C for the toluene pipes. In all experiments nitrogen, N₂, was used as inert carrier gas since it is not reactive with the used model compounds at the investigated conditions. It

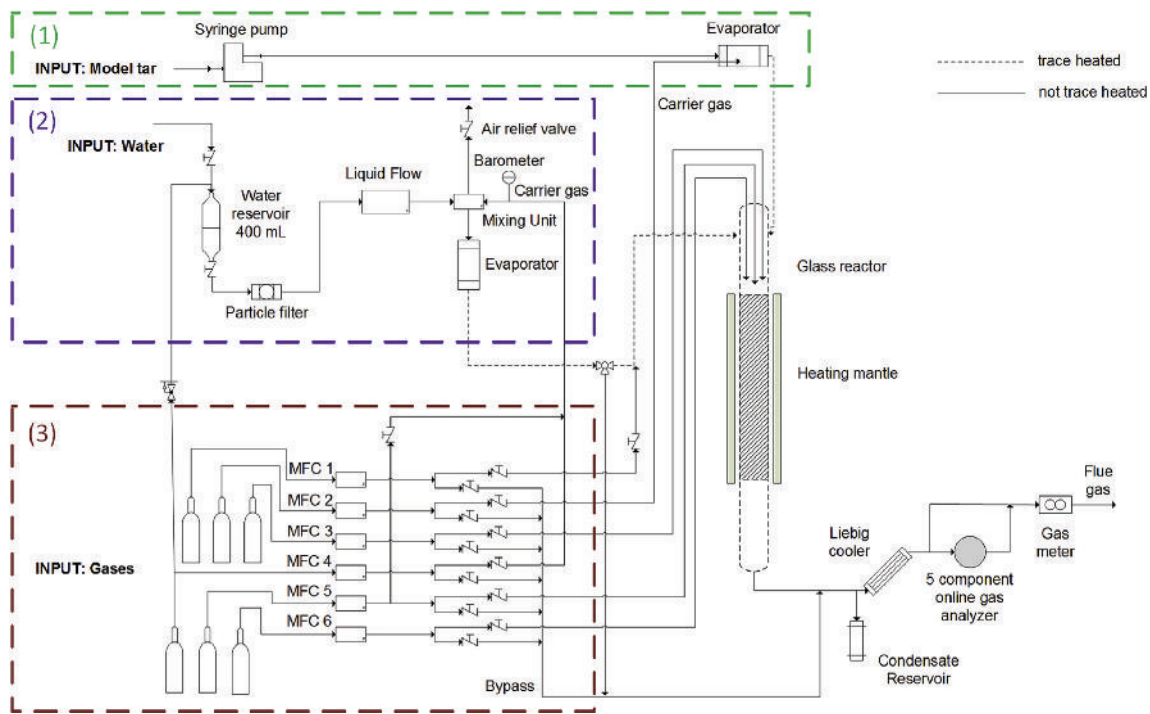


Fig. 1. Detailed flow sheet of the test rig.

rather leads to dilution of the produced gas.

After the reactor a Liebig cooler was installed to condensate both water and the model tar toluene. The temperature in the cooler was kept constant at 0.2 °C. Condensed liquid phases were collected in a reservoir for further measurement. The gas stream was then led to the measurement station. There, CO, CO₂, CH₄, H₂ and O₂ were measured with the Rosemount NGA 2000 five-component online gas analyzer. Data were recorded every 10 s with an automatic recording device. Before the gas was released through a vent the volume flow was measured by a gas meter.

Fig. 2 shows a more detailed scheme of the reactor part. A quartz glass tube with an inner diameter of 1.0 cm and an outer diameter

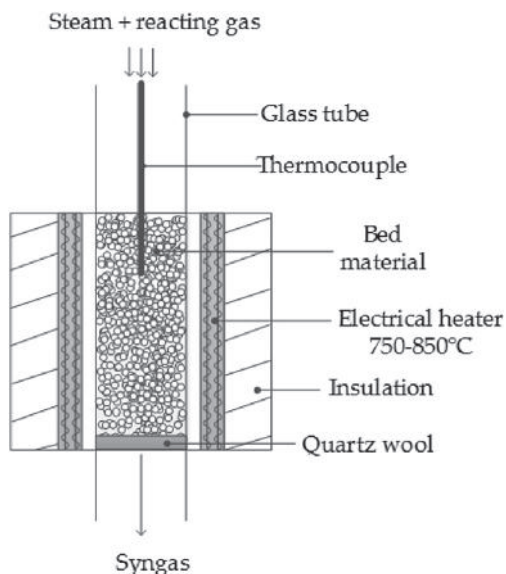


Fig. 2. Scheme of the reactor part.

of 1.2 cm was used as reactor. For the fixed bed 10 g of particles were inserted, resulting in a bed height of about 7.4 cm. Catalytic material was held in position by quartz wool inside the quartz glass tube. During experiments the gas flowed downwards from top to bottom through the catalytic bed. The reactor was placed inside a heating furnace and the bed temperature was continuously measured and controlled by a thermocouple, which was positioned as displayed in 2. The thermocouple was cleaned after each experiment to keep the measurement error to a minimum. Furthermore, a second thermocouple was placed outside the quartz glass reactor measuring the wall temperature outside of the fixed bed. This thermocouple was installed to constantly check the functionality of the thermocouple inside the reactor. If the two measured temperatures varied heavily from each other during the experiments, the test run was stopped and the thermocouple inside the reactor was cleaned before starting the experiment again. Temperature levels of 750 °C, 800 °C and 850 °C were investigated in this work. To avoid unnecessary heat losses glass wool was used as isolation.

Evaluation of gas compositions and conversion efficiencies were performed for steady state operation. Therefore, experiments were conducted until constant values were observed for a minimum of 40 min. Results from that time were then statistically evaluated. Each experiment was conducted three times to ensure reproducibility of the results.

2.2. XRF analysis

Analysis of elemental composition of the samples was carried out by means of X-ray fluorescence (XRF) and calculated as oxides. Samples were melted in a Merck Spectromelt at 1050 °C and placed on a stainless steel plate with a temperature of 400 °C. The Spectromelt ensures that no evaporation of e.g. sodium or potassium takes place. A PANalytical Axios Advanced analyzer was used to carry out the analysis. The analyzer worked under vacuum atmosphere with a rhodium anode, an excitation voltage of 50 kV, and a

tube current of 50 mA. Results of XRF analysis indicated the elemental composition of the total samples calculated in oxides.

Fresh and used quartz sand as well as fresh and used olivine were investigated by XRF.

2.3. SEM/EDS analysis

Collected samples were mounted in epoxy, cross-sectioned and polished. The chemical composition and morphology of the samples were determined by a scanning electron microscope (SEM) combined with energy dispersive X-ray spectroscopy (EDS).

Elemental composition of bed materials and their layers was determined by spot and line analysis. Spot analysis provided information about the composition of different particles. Numerous particles of each sample were analyzed and statistically evaluated, as described in more depth in chapter 2.4.

2.4. Bed material sampling

To investigate the catalytic activity of bed particle layers fresh and used materials were compared. Olivine, which is used as bed material in DFB gasifiers, was compared with quartz sand, a standard bed material in fluidized bed combustion. Olivine is a naturally occurring mineral with the formula $(Mg,Fe)_2SiO_4$. Quartz sand is a mineral which is made up of a continuous framework of SiO_4 silicon-oxygen tetrahedra. Each oxygen is shared by two tetrahedra, and therefore the overall formula is SiO_2 .

Quartz samples were collected from a bubbling fluidized bed (BFB) combustion plant in Austria, using wood chips as fuel. The combustion power plant has a fuel input of 48 MW. Operation of the BFB is realized at a target temperature of 740 °C. Fresh quartz samples were collected before the start-up of the power plant, whereas used quartz sampling was performed during steady state operation of the power plant by collecting bed material discharged from the bottom of the reactor.

Olivine samples were collected from the DFB power plant in Senden, close to Ulm, Germany, using logging residues as fuel. Detailed description of the biomass feedstock is given by Ref. [30]. Fresh olivine, collected before the start-up was already pretreated by calcination at 1200 °C, as described in literature [31]. Assessing the effect of this pretreatment on catalytic activity was not part of this work. Sampling of used bed material was also conducted during steady state operation. Bed material samples were collected at the bottom of the combustion reactor. Typical bed temperatures of the BFB in the gasifier are 840 °C to 860 °C, whereas temperatures in fast fluidized bed in the combustion reactor reach 940 °C.

Thus, used bed materials were coated from long-term operation of industrial biomass power plants.

Both fresh particle fractions - olivine as well as quartz sand - were contrasted with used ones, which were layered from long-term operation of industrial biomass power plants. To obtain representative values samples from five different days of the operation period were collected at both power plants.

As benchmark material burnt lime, CaO , was examined regarding its catalytic activity, because the active sites on the catalyst surface of the bed materials with Ca-rich layers are probably CaO sites [27]. Samples were obtained directly from a producer.

All bed material samples were sieved into a fraction of 400–800 μm for further investigations to obtain comparable samples. Materials were first sieved into three fractions between 400 and 800 μm , namely 400–500 μm , 500–630 μm and 630–800 μm . From those three fractions 3.33 g were taken as aliquot, to ensure similar diameters in the samples.

2.5. Bed material characterization

Since operation parameters in combustion in bubbling fluidized bed systems differ significantly from gasification in DFB systems, the two used bed materials were compared regarding their layers. Operating temperature, how long the bed material stayed in the system, and the composition of the biomass ash (amongst other parameters) have an influence on the formation of layers. Therefore, layers on particles from different industrial power plants can differ significantly from each other. Hence, layered bed materials were characterized and compared.

Table 1 shows the elemental composition of used quartz and olivine bulk samples. The main ash forming elements are displayed; the fraction referred to as others includes SnO , MoO_3 , Nb_2O_5 , ZrO_2 , PbO , As_2O_3 , ZnO , CuO , Co_3O_4 , Cr_2O_3 , V_2O_5 , TiO_2 , Cl and SO_3 . These are not of particular interest in terms of characterization because of the low amounts in particle layers and are therefore not included in further discussion.

Both materials show a significant amount of CaO , which is not present in the original, fresh materials. Used quartz contains notable amounts of K_2O . Used olivine, however, shows significantly lower amounts. The results of used olivine show a similar composition to that described in previous work [26,32].

Fig. 3 shows two images from SEM analysis of layered olivine particles. On the left the particle surface is displayed, and a cross-section of particle is shown on the right. As can be seen, there are two layers around the actual olivine particle. Previous work [26] showed the development of calcium-rich inner and outer layers owed to interaction between biomass ash and olivine. The olivine particles used in this work were characterized by thick layers.

Fig. 4 shows two images of a quartz particle. Similarly to Fig. 3, particle surfaces are shown on the left and a cross-section of a particle is presented on the right. The quartz particle also shows a calcium-rich layer around the particle; however, it is significantly thinner than the one on olivine. Furthermore, not all quartz particles showed complete coverage of layers. A close-up of the layer of the quartz sand particle is shown in Fig. 5. It can be seen that the thickness of the layer varies considerably, depending on the structure of the particle. Description of inner and outer layers together with their compositions from analyses in the cross-section has been published in previous work for both olivine [26] and quartz [21]. In this work, the surface composition of both used particles was further determined using EDS analyses. From each sample between 15 and 20 particles were investigated to obtain representative results. Table 2 shows the compositions on an oxygen free basis. The surface composition of the used particles is compared to both fresh bed materials and CaO . As it can be seen, fresh quartz and olivine particles possess significantly lower amounts Ca-amounts than used, layered, particles. Used quartz is

Table 1
Elemental composition (expressed as oxides) of used particles.

| Components | Used quartz | Used olivine |
|------------|-------------------|--------------|
| | Mass fraction (%) | |
| Fe_2O_3 | 1.6 | 11.1 |
| CaO | 11.9 | 15.4 |
| K_2O | 6.8 | 1.3 |
| SiO_2 | 69.7 | 28.5 |
| Al_2O_3 | 2.1 | 0.6 |
| MgO | 2.3 | 41.6 |
| Na_2O | 1.5 | 0.5 |
| NiO | 1.3 | 0.3 |
| P_2O_5 | 0.9 | 0.2 |
| Others | 1.9 | 0.5 |

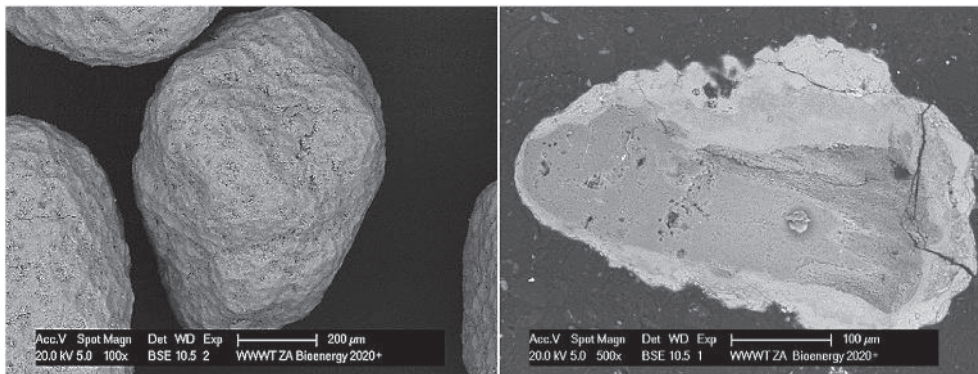


Fig. 3. SEM images of used olivine.

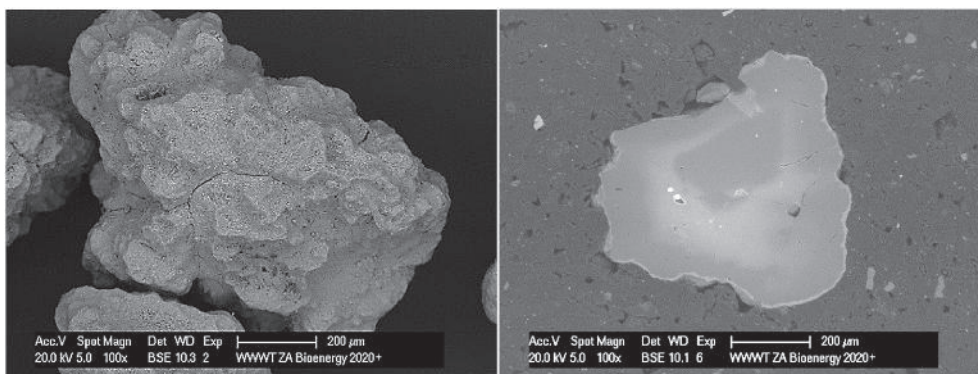


Fig. 4. SEM image of used quartz.

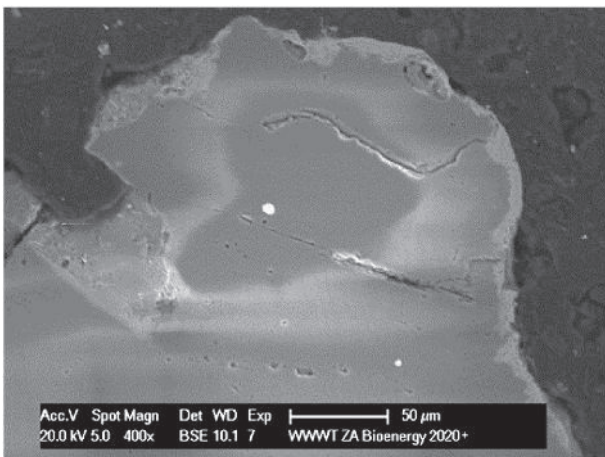


Fig. 5. Close-up SEM image of used quartz.

characterised by a lower Ca-amount on the surface than used olivine. This might be a consequence of the different operating conditions of the power plants. As described above, bed materials were benched to CaO in further investigations.

2.6. Model compounds and test reactions

Experiments to determine the catalytic activity of the materials were conducted by investigating three test reactions. Carbon monoxide, CO, was used to examine the water-gas-shift (WGS) reaction:

Table 2

Surface composition of main components of bed materials.

| | Fresh quartz | Fresh olivine | Used quartz | Used olivine | CaO |
|-------------------|--------------|---------------|-------------|--------------|------|
| Mass fraction (%) | | | | | |
| Mg | 0.7 | 46.8 | 11.7 | 6.4 | 0.8 |
| Al | 2.7 | 1.4 | 2.0 | 2.0 | 0.5 |
| Si | 90.4 | 39.8 | 8.9 | 10.6 | 1.8 |
| P | 0.4 | 0.1 | 5.8 | 3.2 | 0.1 |
| K | 0.8 | 0.3 | 1.9 | 1.0 | 0.2 |
| Ca | 1.0 | 1.1 | 64.7 | 73.0 | 95.9 |
| Mn | 1.2 | 0.2 | 3.2 | 1.0 | 0.2 |
| Fe | 2.8 | 10.3 | 2.0 | 2.8 | 0.5 |



The water-gas shift reaction (1) is an important gasification reaction and can easily be recreated, since no follow-up reactions occur and no intermediate products are formed [33]. Shifting CO in the presence of steam to increased amounts of CO₂ and H₂ is important for the production of pure hydrogen out of biomass feedstock. Secondary measures to further increase the H₂ amount and separate it from the product gas has been investigated by Ref. [34]. Enhancing the water-gas-shift reaction in-situ by coated bed material could lead to cost-reduction in secondary equipment, since lower amounts of CO had to be converted.

Fig. 6 shows simulated results for the equilibrium of the water-gas-shift reaction. Since the water-gas-shift reaction is slightly exothermic ($\Delta H_R = -41.2 \text{ kJ mol}^{-1}$) the production CO of CO₂ and H₂ is favored at lower temperatures. This can be explained through Le Chatelier's principle: a system in equilibrium reacts to a

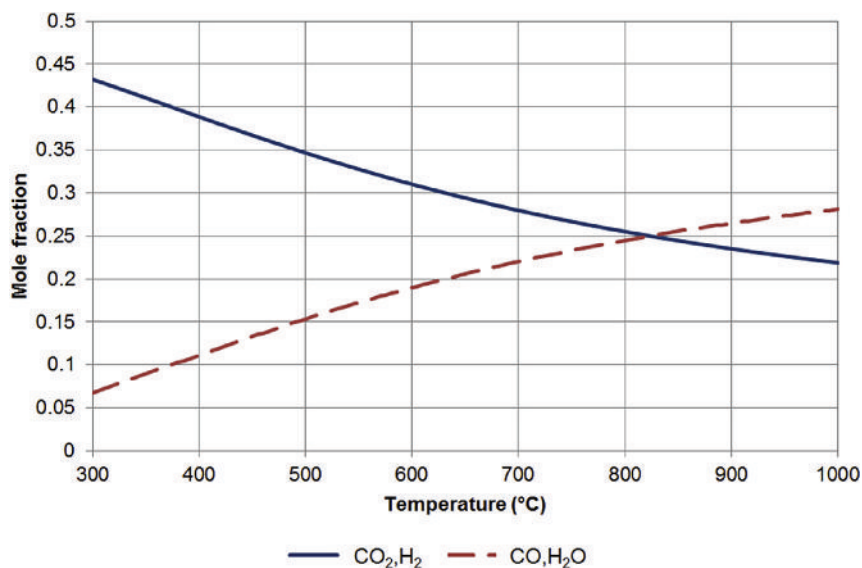


Fig. 6. Equilibrium of water-gas-shift reaction.

disturbance by adjusting itself to nullify the effect of the change.

For the tests here, the chosen volumetric flow rate of (measured at standard conditions of 101.3 kPa and 273.15 K) was $15 \text{ dm}^3 \text{ h}^{-1}$ and the corresponding mass flow rate of H_2O of 12.05 g h^{-1} . The desired carrier flow stream for the steam generator was nitrogen (N_2), with the same volumetric flow rate as CO . Thus, these input flow rates supply an input concentration of CO of 50% based on dry gas volume (CO and N_2) into the reactor.

Steam reforming of aromatic compounds was examined using toluene as educt:



Steam reforming of toluene (3) is a strongly endothermic reaction, and it has a standard enthalpy of $\Delta H_R = 869.5 \text{ kJ mol}^{-1}$. Toluene represents model compound for biomass tars and is often used as such in the literature [8,9,11].

Toluene is used to obtain information about the ability of materials to decompose tars in the produced gas. Since toluene is liquid at room temperature, it was evaporated before it was brought into contact with steam and the catalyst, as described before. For the experiments, the chosen volumetric flow rate of C_7H_8 was $10.6 \text{ cm}^3 \text{ h}^{-1}$, and the corresponding mass flow rate of H_2O of 25.2 g h^{-1} . The desired carrier flow stream for the evaporators was also nitrogen (N_2), with the volumetric flow (measured at standard conditions of 101.3 kPa and 273.15 K) rates of $1.5 \text{ dm}^3 \text{ h}^{-1}$ for the water evaporator and $1.0 \text{ dm}^3 \text{ h}^{-1}$ for the toluene evaporator, respectively.

Furthermore, steam reforming experiments using ethene as model compound for lighter gaseous hydrocarbons were conducted:



However, the conversion of ethene was not measured during the experiments. Therefore, in the following investigations a qualitative relation regarding H_2 production is given between the bed materials.

Since CO is a product, the water-gas-shift reaction (1) is connected and occurs as a follow-up reaction. Steam reforming of ethene (2) is an endothermic reaction.

For the tests, the chosen volumetric flow rate of C_2H_4 (measured

at standard conditions of 101.3 kPa and 273.15 K) was $11 \text{ dm}^3 \text{ h}^{-1}$ and the corresponding mass flow rate of H_2O of 17 g h^{-1} . The desired carrier flow stream for the steam generator was nitrogen (N_2), with the same volumetric flow rate as C_2H_4 . Thus, these input flow rates supply an input concentration of C_2H_4 of 50% based on dry gas volume (C_2H_4 and N_2) into the reactor.

3. Results

3.1. Catalytic activity regarding the water-gas-shift reaction

A comparison of the different materials based on the water-gas-shift reaction is presented. The focus is on the catalytic activity of fresh and used quartz and olivine particles in comparison with calcium oxide. Findings are presented for temperature levels of 750 °C, 800 °C and 850 °C.

Table 3 shows the gas composition of the outlet gas after the reactor. The content of H_2O was calculated from the equimolar reaction equation and the carrier gas nitrogen was subtracted. Thus, the values in the Table show actual compositions of the water-gas-shift reaction during steady state operation of the experiments.

Table 3

Wet gas composition at the outlet of the reactor by the water-gas-shift reaction, (*) H_2O content calculated from chemical equation (equimolar).

| | °C | $\text{H}_2\text{O}^{(*)}$ | CO | CO_2 | H_2 |
|------------------------|-----|----------------------------|-------------|---------------|--------------|
| Gas composition (100%) | | | | | |
| CaO | 750 | 24.0 | 24.0 | 25.7 | 26.3 |
| | 800 | 24.3 | 24.3 | 25.8 | 25.6 |
| | 850 | 25.6 | 25.6 | 24.5 | 24.4 |
| Used olivine | 750 | 36.0 | 36.0 | 14.1 | 13.9 |
| | 800 | 30.8 | 30.8 | 19.3 | 19.1 |
| | 850 | 28.1 | 28.1 | 22.0 | 21.8 |
| Used quartz | 750 | 40.4 | 40.4 | 9.7 | 9.5 |
| | 800 | 38.0 | 38.0 | 12.1 | 11.9 |
| | 850 | 35.8 | 35.8 | 14.3 | 14.1 |
| Fresh olivine | 750 | 45.7 | 45.7 | 4.4 | 4.2 |
| | 800 | 43.5 | 43.5 | 6.5 | 6.5 |
| | 850 | 41.8 | 41.8 | 8.2 | 8.2 |
| Fresh quartz | 750 | 49.7 | 49.7 | 0.3 | 0.3 |
| | 800 | 49.6 | 49.6 | 0.3 | 0.5 |
| | 850 | 49.3 | 49.3 | 0.7 | 0.7 |

Fresh quartz sand did not show significant catalytic activity. Fresh olivine showed some catalytic activity, however it was significantly lower than that of coated bed materials. Used quartz had notably higher catalytic activity than fresh olivine. Used olivine had a slightly higher activity than used quartz sand, however still lower than that of CaO . The difference between fresh and used quartz sand was especially notable since fresh quartz sand did not possess any catalytic activity. CaO almost reached the equilibrium of the reaction. As already mentioned, CaO was used as benchmark material for satisfying conversion. All materials except CaO showed higher production of H_2 at increased temperatures.

Furthermore, Fig. 7 shows the CO concentration on a dry basis in dependence of the temperature. As it can be seen, at a temperature of 850 °C used olivine almost reached the same catalytic activity as CaO towards the water-gas-shift reaction.

3.2. Catalytic activity regarding steam reforming of toluene

Results of experiments with the tar model compound toluene are presented in the following.

Table 4 shows the conversion efficiency for steam reforming of toluene of the different bed materials. For used, layered, particles a significantly higher catalytic activity towards toluene conversion could be observed than for fresh particles. The benchmark material CaO reached a conversion efficiency of 82% at 850 °C. All materials showed an increasing conversion efficiency with increasing temperature.

Table 5 shows the dry gas composition of steam reforming of toluene performed with the different bed materials. H_2 composition remained relatively constant between 60.6 and 69.7% depending on the bed material and slightly decreased with rising temperature. Materials with lower catalytic activity such as fresh olivine or fresh quartz showed significantly higher amounts of CO compared to CO_2 and vice versa for materials with higher catalytic activity such as used olivine or CaO . Used quartz showed amounts of both CO and CO_2 between 14 and 18.2% and the difference between them was much lower than that of the other particles. Between 1 and 3.5% of methane could be observed. The only exception was fresh olivine at 850 °C, where 6.6% could be observed.

Table 4

Conversion efficiency of bed materials regarding toluene steam reforming.

| °C | CaO | Used olivine | Used quartz | Fresh olivine | Fresh quartz |
|-----|------------|--------------|-------------|---------------|--------------|
| | η (%) | η (%) | η (%) | η (%) | η (%) |
| 750 | 60 | 19 | 12 | 5 | 2 |
| 800 | 75 | 35 | 30 | 10 | 3 |
| 850 | 82 | 56 | 45 | 22 | 5 |

Table 5

Dry gas composition of toluene steam reforming.

| | °C | CO | CO ₂ | CH ₄ | H ₂ |
|---------------|-----|------------------------|-----------------|-----------------|----------------|
| | | Gas composition (100%) | | | |
| CaO | 750 | 2.2 | 29.5 | 1.2 | 67.1 |
| | 800 | 4.2 | 28.1 | 1.2 | 66.5 |
| | 850 | 5.5 | 27.0 | 1.9 | 65.6 |
| Used olivine | 750 | 3.7 | 25.6 | 1.0 | 69.7 |
| | 800 | 4.4 | 25.1 | 1.1 | 69.4 |
| | 850 | 5.0 | 24.9 | 1.3 | 68.8 |
| Used quartz | 750 | 15.0 | 16.0 | 1.5 | 67.4 |
| | 800 | 17.0 | 14.4 | 1.7 | 66.9 |
| | 850 | 18.2 | 14.1 | 1.3 | 66.4 |
| Fresh olivine | 750 | 22.9 | 9.2 | 1.8 | 66.1 |
| | 800 | 26.7 | 7.5 | 2.7 | 63.0 |
| | 850 | 27.6 | 5.1 | 6.6 | 60.6 |

3.3. Qualitative comparison of H_2 yield relative to the benchmark CaO

A comparison of the H_2 yield relative to the yield achieved with the benchmark material CaO will be given in the following. The comparison shows a qualitative relation of the bed material coatings. Pure CaO possesses the maximal catalytic activity a Ca-coating can achieve. Thus, results in the following show the catalytic activity of the bed particle coatings compared to the maximal possible catalytic activity. Fig. 8 shows the comparison for the water-gas-shift reaction. Findings for steam reforming of ethene are presented in Fig. 9. As already observed during the experiments with the water-gas-shift reaction a significant increase in catalytic activity of layered materials could be observed compared with fresh particles.

Fig. 10 shows the H_2 production during steam reforming of

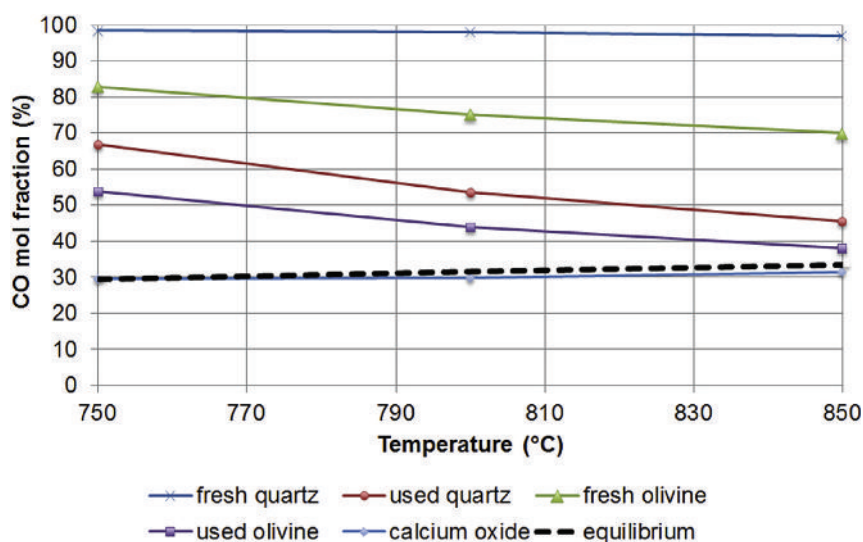


Fig. 7. CO mol ratio (dry gas) at the outlet of the reactor by the water-gas-shift reaction.

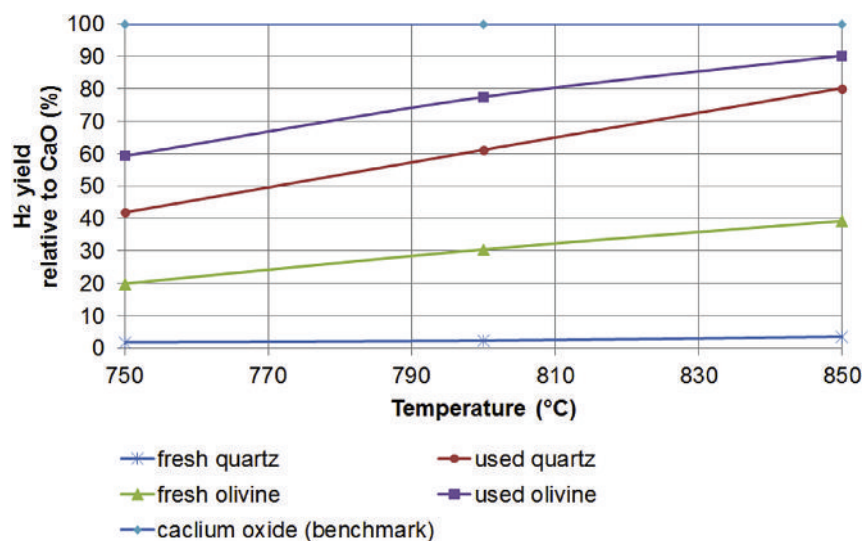


Fig. 8. H₂ yield by the water-gas-shift reaction relative to CaO (benchmark).

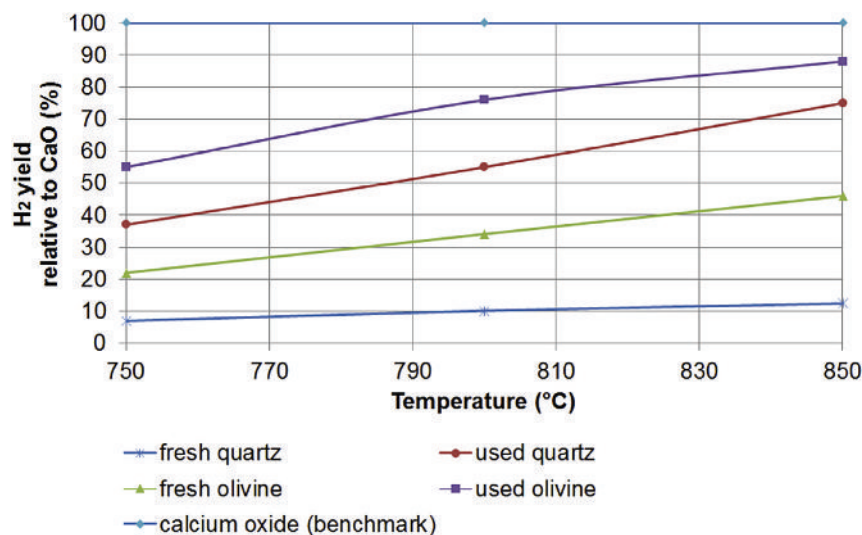


Fig. 9. H₂ yield by steam reforming of ethene relative to CaO (benchmark).

toluene relative to CaO. The H₂-yield increased for used, layered, bed materials compared to fresh ones in all investigated reactions.

4. Discussion

Findings from SEM analysis regarding layer formation are discussed and put into context regarding results from experimental investigations of catalytic activity.

Comparison of used quartz and olivine particles shows a significant difference in layer formation. Olivine is characterized by significantly thicker Ca-rich layers than quartz. In addition, the Ca-content on the surface is higher than that of used quartz. This could be caused by different operating conditions in the power plants, especially in relation to temperature. DFB gasification reaches temperatures of 950 °C in the combustion area of the process [4]. The conventional biomass combustion plant with a stationary fluidized bed, where quartz samples were collected for this work, is operated at bed temperatures between 730 °C and 750 °C. Layer formation is caused through the melting processes of biomass ash

and its interaction with bed particles, and therefore varying operating temperatures could have a major influence on the development of the layers.

CaO, used as benchmark material, showed high reactivity by almost reaching equilibrium in water-gas-shift test reactions. As expected, fresh quartz sand did not show any significant catalytic effect on the reaction. Therefore, these two materials constitute extreme cases regarding their catalytic activity. Fresh olivine is a known catalyst for biomass gasification reactions; however, it has significantly less influence on the regarding the water-gas-shift reaction than CaO, as seen in Table 3.

The investigated particles showed higher activity when the temperature increased, likely caused by increased reaction rates at higher temperatures, as described by the Arrhenius equation.

Conversion of toluene with CaO, shows a conversion of up to 82% at 850 °C. Coll and colleagues investigated the conversion of toluene by steam reforming using two commercial catalysts (containing about 15% nickel on a support consisting mainly of alumina) and achieve similar conversions with one of them [10].

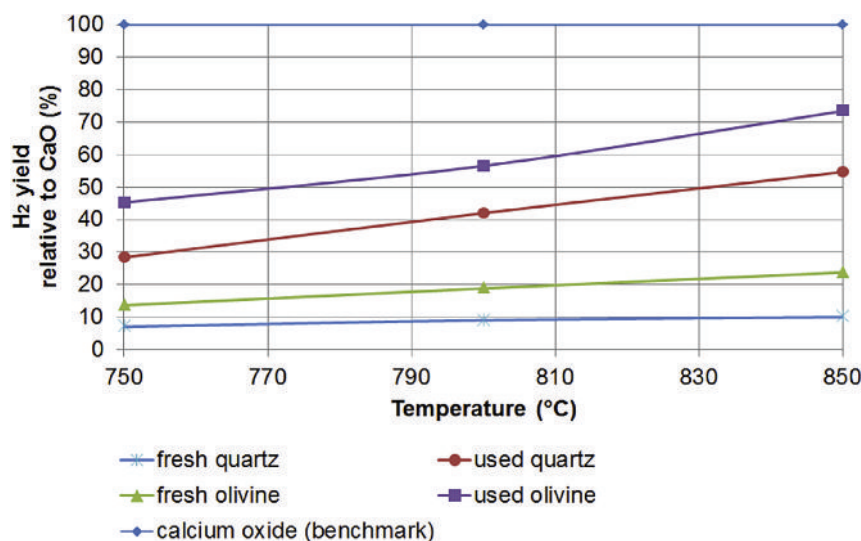


Fig. 10. H_2 yield by steam reforming of toluene relative to CaO (benchmark).

Swierczynski and colleagues measured higher conversion of toluene by steam reforming for Ni/olivine of around 90% at 850 °C [11]. Fresh quartz did not show any catalytic activity, low conversion of toluene is most likely a result of thermal rather than catalytic decomposition. Even though the catalytic activities of used olivine and quartz were significantly increased compared to the fresh particles, conversion of toluene was notably lower to when CaO was used.

Used, layered, quartz and olivine particles showed a much higher selectivity towards the production of CO_2 whereas fresh particles favored the production of CO , as displayed in Table 5. Therefore, it was shown that the higher the catalytic activity of the bed material, the higher is the content of CO_2 in the produced gas.

The qualitative comparison, displayed in Figs. 8–10, shows that the catalytic activity of used particles regarding the H_2 yield in the produced gas is increased for the water-gas-shift reaction and the steam reforming of the model compound for lighter hydrocarbons ethene and the tar model compound toluene. The catalytic activity seems to be related to the Ca-content on the surface of the particle, as a comparison with 2 shows. Since both olivine and quartz particles were characterized by Ca-rich surfaces, the catalytic activity could be assigned to the layer, independent of the original particle. Increasing amounts of CaO detected in XRF analysis of bulk samples, shown in 1, suggest that it is the active site responsible for increased catalytic activity of the coating. Pure CaO represents therefore the maximal catalytic activity a Ca-rich bed particle coating can theoretically achieve. Poorer performance of used quartz sand than that of used olivine could have been caused by reduced coverage of layers around the particles and a lower CaO-amount on the layer surface. Therefore, lesser active surface sites were available for catalytic reactions.

As a result, it was shown that Ca-rich particle layers are responsible for the catalytic activity of the material even if the material itself does not show any significant activity, as in the case of quartz sand. This leads to the conclusion that the catalytic activity of the original particle is substituted by that of the layer. Therefore, the activity of specific catalysts - whether (altered) naturally occurring or synthetically created - will eventually be replaced once a layer has developed. Hence, potassium and calcium containing feedstock will lead to substitution of the catalytic activity of the original catalyst thanks to their ability to develop particle layers. However, layer build-up on bed particles could

easily lead to agglomeration or slagging phenomena [23] and therefore to operational problems in DFB gasification of biomass when other materials than olivine are used. Non-quartz minerals were investigated regarding their agglomeration tendency by Ref. [35] and it was shown that the influence of different bed materials regarding layer build-up and slagging varies significantly.

Furthermore, it is not yet clear if the full potential of the catalytic activity of Ca-rich layers was tapped with the investigated samples. The difference between layered quartz and layered olivine shows the importance of sufficient coverage of Ca-rich layers around the particles. Moreover, it is not clear if the activity of fully covered particles could be further increased to reach the activity of pure CaO.

5. Conclusion

Formation of Ca-rich layers on bed particles caused by interaction with biomass ash leads to the development of a catalytic active surface concerning the water-gas-shift reaction as well as steam reforming of tars from biomass gasification, which were represented by the model compound toluene. An increased catalytic activity of the bed material coatings could also be observed for steam reforming of ethene. This catalytic activity is independent of the activity of the original particle. This substitution of the original catalytic activity suggests the possibility of using cheaper non-catalytic bed materials and activating them in-situ through interaction with inorganic compounds of biomass ash.

Acknowledgments

This study was carried out in the frame of the Bioenergy2020 + project C-II-1-24. Bioenergy2020 + GmbH is funded within the Austrian COMET program, which is managed by the Austrian Research Promotion Agency (FFG) and promoted by the federal government of Austria as well as the federal states Burgenland, Niedersterreich and Steiermark. We are grateful for the support of our project partners HGA Senden (Stadtwerke Ulm), and the Institute of Chemical Engineering at the Vienna University of Technology.

References

- [1] W. Van Swaaij, S. Kersten, W. Palz, *Biomass Power for the World - Transformations to Effective Use*, 1 ed., Pan Stanford Publishing, Singapore, 2015. ISBN 9789814613880.
- [2] W. Van de Kamp, P. De Wild, U. Zielke, M. Suomalainen, H. Knoef, J. Good, et al., Tar measurement standard for sampling and analysis of tars and particles in biomass gasification product gas, in: *Proceedings of the 14th European Biomass Conference and Exhibition*, 2005, pp. 791–794. Paris, France.
- [3] P. Basu, *Biomass Gasification and Pyrolysis*, Oxford: Elsevier Inc., 2010, <http://dx.doi.org/10.1016/B978-0-12-374988-8.00005-2>. ISBN 9780123749888.
- [4] H. Hofbauer, R. Rauch, G. Loeffler, S. Kaiser, E. Fercher, H. Tremmel, Six years experience with the FICFB-gasification process, in: *Proceedings of the 12th European Conference and Technology Exhibition on Biomass for Energy, Industry and Climate Protection*, Amsterdam, The Netherlands, 2002, pp. 982–985.
- [5] C. Pfeifer, J.C. Schmid, T. Pröll, H. Hofbauer, Next Generation Biomass Gasifier, in: *Proceedings of the 19th European Biomass Conference and Exhibition*, 2011, pp. 1–7. Berlin, Germany.
- [6] J.C. Schmid, T. Pröll, C. Pfeifer, H. Hofbauer, Improvement of Gas - Solid Interaction in Dual Circulating Fluidized Bed Systems, in: *Proceedings of the 9th European Conference on Industrial Furnaces and Boilers (INFUB)*, 2011, pp. 1–13. Estoril, Portugal.
- [7] J.C. Schmid, C. Pfeifer, H. Kitzler, T. Pröll, H. Hofbauer, A new dual fluidized bed gasifier design for improved in situ conversion of hydrocarbons, in: *Proceedings of the International Conference on Polygeneration Strategies (ICPS)*, 2011, pp. 1–10. Vienna, Austria.
- [8] I. Zamboni, C. Courson, D. Niznansky, A. Kiennemann, Simultaneous catalytic H₂ production and CO₂ capture in steam reforming of toluene as tar model compound from biomass gasification, *Appl. Catal. B Environ.* 145 (2) (2014) 63–72, <http://dx.doi.org/10.1016/j.apcatb.2013.02.046>.
- [9] B. Zhao, X. Zhang, L. Chen, R. Qu, G. Meng, X. Yi, et al., Steam reforming of toluene as model compound of biomass pyrolysis tar for hydrogen, *Biomass Bioenergy* 34 (1) (2010) 140–144, <http://dx.doi.org/10.1016/j.biombioe.2009.10.011>.
- [10] R. Coll, J. Salvadó, X. Farriol, D. Montané, Steam reforming model compounds of biomass gasification tars: conversion at different operating conditions and tendency towards coke formation, *Fuel Process. Technol.* 74 (1) (2001) 19–31, [http://dx.doi.org/10.1016/S0378-3820\(01\)00214-4](http://dx.doi.org/10.1016/S0378-3820(01)00214-4).
- [11] D. Swierczynski, C. Courson, A. Kiennemann, Study of steam reforming of toluene used as model compound of tar produced by biomass gasification, *Chem. Eng. Process. Process Intensif.* 47 (3) (2008) 508–513, <http://dx.doi.org/10.1016/j.cep.2007.01.012>.
- [12] R. Michel, A. Lamacz, A. Krzton, G. Djéga-Mariadassou, P. Burg, C. Courson, et al., Steam reforming of α -methyl-naphthalene as a model tar compound over olivine and olivine supported nickel, *Fuel* 109 (2013) 653–660, <http://dx.doi.org/10.1016/j.fuel.2013.03.017>.
- [13] D. Barisano, C. Freda, F. Nanna, E. Fanelli, A. Villone, Biomass gasification and in-bed contaminants removal: performance of iron enriched Olivine and bauxite in a process of steam/O₂ gasification, *Bioresour. Technol.* 118 (2012) 187–194, <http://dx.doi.org/10.1016/j.biortech.2012.05.011>.
- [14] H. Noichi, A. Uddin, E. Sasaoka, Steam reforming of naphthalene as model biomass tar over iron-aluminum and iron-zirconium oxide catalyst catalysts, *Fuel Process. Technol.* 91 (11) (2010) 1609–1616, <http://dx.doi.org/10.1016/j.fuproc.2010.06.009>.
- [15] F.L. Chan, A. Tanksale, Review of recent developments in Ni-based catalysts for biomass gasification, *Renew. Sustain. Energy Rev.* 38 (2014) 428–438, <http://dx.doi.org/10.1016/j.rser.2014.06.011>.
- [16] A. Larsson, M. Israelsson, F. Lind, M. Seemann, H. Thunman, Using ilmenite to reduce the tar yield in a dual fluidized bed gasification system, *Energy Fuels* 28 (4) (2014) 2632–2644, <http://dx.doi.org/10.1021/ef500132p>.
- [17] Z. Min, M. Asadullah, P. Yimsiri, S. Zhang, H. Wu, C.Z. Li, Catalytic reforming of tar during gasification. Part I. Steam reforming of biomass tar using ilmenite as a catalyst, *Fuel* 90 (5) (2011) 1847–1854, <http://dx.doi.org/10.1016/j.fuel.2010.12.039>.
- [18] Z. Abu El-Rub, E.A. Bramer, G. Brem, Review of catalysts for tar elimination in biomass gasification processes, *Industrial Eng. Chem. Res.* 43 (22) (2004) 6911–6919, <http://dx.doi.org/10.1021/ie0498403>.
- [19] D. Sutton, B. Kelleher, J.R.H. Ross, Review of literature on catalysts for biomass gasification, *Fuel Process. Technol.* 73 (3) (2001) 155–173, [http://dx.doi.org/10.1016/S0378-3820\(01\)00208-9](http://dx.doi.org/10.1016/S0378-3820(01)00208-9).
- [20] M. Hupa, Ash-related issues in fluidized-bed combustion of biomasses: recent research highlights, *Energy Fuels* 26 (1) (2012) 4–14, <http://dx.doi.org/10.1021/ef201169k>.
- [21] H. He, D. Boström, M. Öhman, Time dependence of bed particle layer formation in fluidized quartz bed combustion of wood-derived fuels, *Energy & Fuels* 28 (6) (2014) 3841–3848, <http://dx.doi.org/10.1021/ef500386k>.
- [22] A. Grimm, N. Skoglund, D. Boström, M. Öhman, Bed agglomeration characteristics in fluidized quartz bed combustion of phosphorus-rich biomasses, *Energy Fuels* 25 (3) (2011) 937–947, <http://dx.doi.org/10.1021/ef101451e>.
- [23] E. Brus, M. Öhman, A. Nordin, D. Boström, H. Hedman, A. Eklund, Bed agglomeration characteristics of biomass fuels using blast-furnace slag as bed material, *Energy Fuels* 18 (4) (2004) 1187–1193, <http://dx.doi.org/10.1021/ef034095c>.
- [24] A. Grimm, M. Öhman, T. Lindberg, A. Fredriksson, D. Boström, Bed agglomeration characteristics in fluidized-bed combustion of biomass fuels using olivine as bed material, *Energy Fuels* 26 (7) (2012) 4550–4559, <http://dx.doi.org/10.1021/ef300569n>.
- [25] F. Kirnbauer, M. Koch, R. Koch, C. Aichernig, H. Hofbauer, Behavior of inorganic matter in a dual fluidized steam gasification plant, *Energy & Fuels* 27 (6) (2013) 3316–3331, <http://dx.doi.org/10.1021/ef400598h>.
- [26] F. Kirnbauer, H. Hofbauer, Investigations on bed material changes in a dual fluidized bed steam gasification plant in Güssing, Austria, *Energy Fuels* 25 (8) (2011) 3793–3798, <http://dx.doi.org/10.1021/ef200746c>.
- [27] F. Kirnbauer, V. Wilk, H. Kitzler, S. Kern, H. Hofbauer, The positive effects of bed material coating on tar reduction in a dual fluidized bed gasifier, *Fuel* 95 (2012) 553–562, <http://dx.doi.org/10.1016/j.fuel.2011.10.066>.
- [28] F. Kirnbauer, H. Hofbauer, The mechanism of bed material coating in dual fluidized bed biomass steam gasification plants and its impact on plant optimization, *Powder Technol.* 245 (2013) 94–104, <http://dx.doi.org/10.1016/j.powtec.2013.04.022>.
- [29] S. Kern, C. Pfeifer, H. Hofbauer, Reactivity tests of the water-gas shift reaction on fresh and used fluidized bed materials from industrial DFB biomass gasifiers, *Biomass Bioenergy* 55 (2013) 227–233, <http://dx.doi.org/10.1016/j.biombioe.2013.02.001>.
- [30] M. Kuba, H. He, F. Kirnbauer, D. Boström, M. Öhman, H. Hofbauer, Deposit build-up and ash behavior in dual fluid bed steam gasification of logging residues in an industrial power plant, *Fuel Process. Technol.* 139 (2015) 33–41, <http://dx.doi.org/10.1016/j.fuproc.2015.08.017>.
- [31] C. Christodoulou, D. Grimekis, K. Panopoulos, E. Pachatouridou, E. Iliopoulou, E. Kakaras, Comparing calcined and un-treated olivine as bed materials for tar reduction in fluidized bed gasification, *Fuel Process. Technol.* 124 (2014) 275–285, <http://dx.doi.org/10.1016/j.fuproc.2014.03.012>.
- [32] T. Kyotani, S. Hayashi, A. Tomita, Study of calcium catalysis on carbon gasification with molecular oxygen-18, *Energy & Fuels* 5 (5) (1991) 683–688, <http://dx.doi.org/10.1021/ef00029a009>.
- [33] M. Kaltschmitt, H. Hartmann, H. Hofbauer, *Energie aus Biomasse*, Springer Berlin Heidelberg, Berlin, Heidelberg, 2001, <http://dx.doi.org/10.1007/978-3-662-07025-3>. ISBN 978-3-662-07026-0.
- [34] S. Fail, N. Diaz, F. Benedikt, M. Kraussler, J. Hinteregger, K. Bosch, et al., Wood gas processing to generate pure hydrogen suitable for PEM fuel cells, *ACS Sustain. Chem. Eng.* 2 (12) (2014) 2690–2698, <http://dx.doi.org/10.1021/sc500436m>.
- [35] S. De Geyter, M. Öhman, D. Boström, M. Eriksson, A. Nordin, Effects of non-quartz minerals in natural bed sand on agglomeration characteristics during fluidized bed combustion of biomass fuels, *Energy Fuels* 21 (5) (2007) 2663–2668, <http://dx.doi.org/10.1021/ef070162h>.

A.3 Paper III

Influence of coated olivine on the conversion of intermediate products from decomposition of biomass tars during gasification

Influence of coated olivine on the conversion of intermediate products from decomposition of biomass tars during gasification

Matthias Kuba^{1,2} · Friedrich Kirnbauer¹ · Hermann Hofbauer²

Received: 19 January 2016 / Revised: 13 March 2016 / Accepted: 15 March 2016
© The Author(s) 2016. This article is published with open access at Springerlink.com

Abstract Steam gasification of solid biomass in dual fluidized bed systems is a suitable technology for the production of chemicals, fuels for transportation, electricity, and district heating. Interaction between biomass ash and bed material leads to the development of Ca-rich bed particle layers. Furthermore, incomplete decomposition of biomass leads to the formation of tar components; among these are stable intermediate products such as 1H-indene and stable gaseous hydrocarbons such as methane. In this work, the influence of bed particle layers on the conversion of intermediate products such as 1H-indene and methane via steam reforming was investigated by conducting experiments in a lab-scale test rig. Satisfying conversion of 1H-indene into gaseous molecules (e.g., CO, CO₂, H₂) was achieved with used, layered olivine, whereas fresh olivine showed significantly poorer performance. Since steam reforming was connected to the water-gas-shift reaction for the tested hydrocarbons, investigations regarding carbon monoxide conversion in the presence of steam were conducted as well. Furthermore, a comparison of the influence of fresh and used bed material concerning the conversion of methane is presented, showing that methane is not affected by the bed material, independent of the presence of particle layers.

Keywords Biomass gasification · Bed material coating · Catalytic conversion · Steam reforming · 1H-indene · Methane

✉ Matthias Kuba
matthias.kuba@bioenergy2020.eu

¹ Bioenergy 2020+ GmbH, Wienerstraße 49, A-7540 Güssing, Austria

² Institute of Chemical Engineering, Vienna University of Technology, Getreidemarkt 9/166, 1060 Vienna, Austria

1 Introduction

The utilization of renewable energy carriers to substitute for fossil fuels plays an important role in meeting the worldwide aim to reduce greenhouse gas emissions, but requires innovative and efficient technologies. Climate change is partially a consequence of the combustion of fossil resources, and rising awareness of global warming has increased the necessity of developing “green technologies.” Biomass is the only renewable carbon source usable as a CO₂-neutral feedstock for pyrolysis, combustion, or gasification [1].

A dual fluid bed (DFB) gasification system was developed by the Vienna University of Technology, where the solid feedstock is transformed into a gaseous secondary energy carrier. Endothermic gasification and exothermic combustion are conducted in two separate reactors with the bed material circulating between those two reactors. This bed material acts both as a heat carrier and catalyst, as described in more detail in Sect. 2.1. While air is used for the fast fluidized bed in the combustion reactor, the gasifier is fluidized with steam. As a consequence, the product gas from this specific gasification is practically free of nitrogen and can be further used as a valuable synthesis gas for the production of a variety of different end products [2]. Examples of such products are bio-methane [3, 4], Fischer-Tropsch bio-diesel [5, 6], pure hydrogen [7–9], or mixed alcohols [10]. Therefore, this technology is also referred to as polygeneration. This flexibility of the process allows it to quickly react to changes in the energy market.

This technology has been successfully used in industrial-scale power plants since 2001. In Güssing, Austria, the first power plant started operation with a fuel power of 8 MW_{th}. Further, power plants using the same DFB setup are under operation in Oberwart, Austria (fuel power of 8.5 MW_{th}), Senden, close to Ulm, Germany (fuel power of 16 MW_{th}), and Gothenburg, Sweden (fuel power of 30 MW_{th}). A new

generation of DFB gasification is currently being developed at the Vienna University of Technology. A new design of the gasification unit increases the contact between the catalytically active bed material and gas released from the biomass feedstock [11–13].

Gas released from biomass feedstock contains heavier hydrocarbons, which are also referred to as tars. These tars are primarily produced in the pyrolysis stage due to breakage of the three main constituents of biomass: cellulose, hemicellulose, and lignin. As a result, primary tars, such as phenol and creosol, are formed. At temperatures above 500 °C, these primary tars recombine into heavier molecules, referred to as secondary tars. A further temperature increase leads to the destruction of primary and secondary tars, resulting in the production of tertiary tars, such as naphthalene or pyrene. These are highly undesirable by-products when they condense in downstream equipment [14]. Therefore, reducing these compounds is necessary to obtain a valuable product gas.

The mechanism behind tar decomposition has been investigated in the past [15–17]. Figure 1 shows the decomposition mechanism of naphthalene [15]. As it can be seen, stable intermediate products, such as 1H-indene, toluene, and benzene, are formed, which have to be further converted to produce small gaseous molecules. The reactivity of 1H-indene has not been addressed in the literature so far. A comparison of one-ring and poly-ring hydrocarbons has been published [18]. Furthermore, the conversion of toluene has been investigated [19–21]. The typical gaseous products that form during biomass steam gasification are carbon monoxide (CO), hydrogen (H₂), methane (CH₄), and carbon dioxide (CO₂). In lesser amounts, the product gas also contains larger molecules, such as ethene (C₂H₄). The molecules CO, H₂, and CO₂ are the result of steam reforming reactions and the water-gas shift reaction, which is explained in more depth in Sect. 2.3. The occurrence of CH₄ is most likely a consequence of both direct release from solid biomass feedstock [22] and the decomposition of heavier hydrocarbons [23].

Tar measurements from industrial-scale gasification power plants in Oberwart, conducted in earlier projects, and in Senden have shown notable differences regarding the distribution of tar components. The results from the power plant in Senden show significantly higher values of 1H-indene. A scrubber unit operated with rapeseed methyl ester (RME) is used for gas cleaning. Since the scrubber has a significantly lower separation efficiency for intermediate products, such as 1H-indene, than for heavier poly-cyclic hydrocarbons, as previously described [24], they might cause operational problems in downstream equipment due to condensation and the buildup of deposits. As a result, intermediate products such as 1H-indene from tar decomposition are highly undesirable.

As explained above, the conversion of tars into smaller gaseous molecules can be achieved through steam reforming reactions, since steam is used as the fluidization

medium in the gasifier. These reactions take place in the presence of a catalyst, which is the bed material, the ash, and additives in the case of the DFB process. The behavior of this inorganic matter in DFB gasification has been described by Kirnbauer et al. [25].

Through interactions between biomass ash and bed materials in the fluidized bed, the formation of calcium-rich layers on bed particles can occur during combustion [26] as well as for olivine particles in gasification [27]. Interactions between ash components and the bed material have different consequences. The formation of layers on bed particles can result in agglomeration, slagging, and deposit buildup [25, 28–32]. However, calcium-rich layers have shown a significant increase of the catalytic activity of bed particles [33–36] and are therefore highly desirable for gasification processes. Consequently, layer formation on bed particles has both positive and negative impacts on the gasification process.

In this work, lab-scale experiments were conducted to investigate the influence of calcium-rich bed particle coatings on the conversion of the intermediate tar decomposition products 1H-indene and methane. Thus, the catalytic activity of fresh and used, layered particles were compared to each other. Since the water-gas-shift reaction is linked to steam reforming of the investigated compounds and occurred as follow-up reaction, carbon conversion in the presence of steam was also addressed. In addition, experiments concerning the conversion of methane were performed to understand how the product gas composition can be influenced in situ with layered bed material. Understanding the catalytic activity of layered bed material regarding intermediates from tar decomposition offers the possibility of identifying indicator components for incomplete transformation, which can be caused by, e.g., problems with fuel mixing. Components which should be transformed in the presence of the bed material, but are still present in the product gas, are such indicator components.

These tests are follow-up experiments from previous work, where the influence of such coatings was investigated for steam reforming of toluene and C₂H₄ [34]. Both publications together give a comprehensive overview of the influence of calcium-rich bed particle layers on the reduction of tars and the product gas composition.

2 Materials and methods

2.1 Description of the dual fluid bed steam gasification of biomass

The DFB power plant in Senden has a fuel power of 16 MW_{th} and uses logging residues as feedstock. A detailed description of the feedstock was provided in a previous work [30].

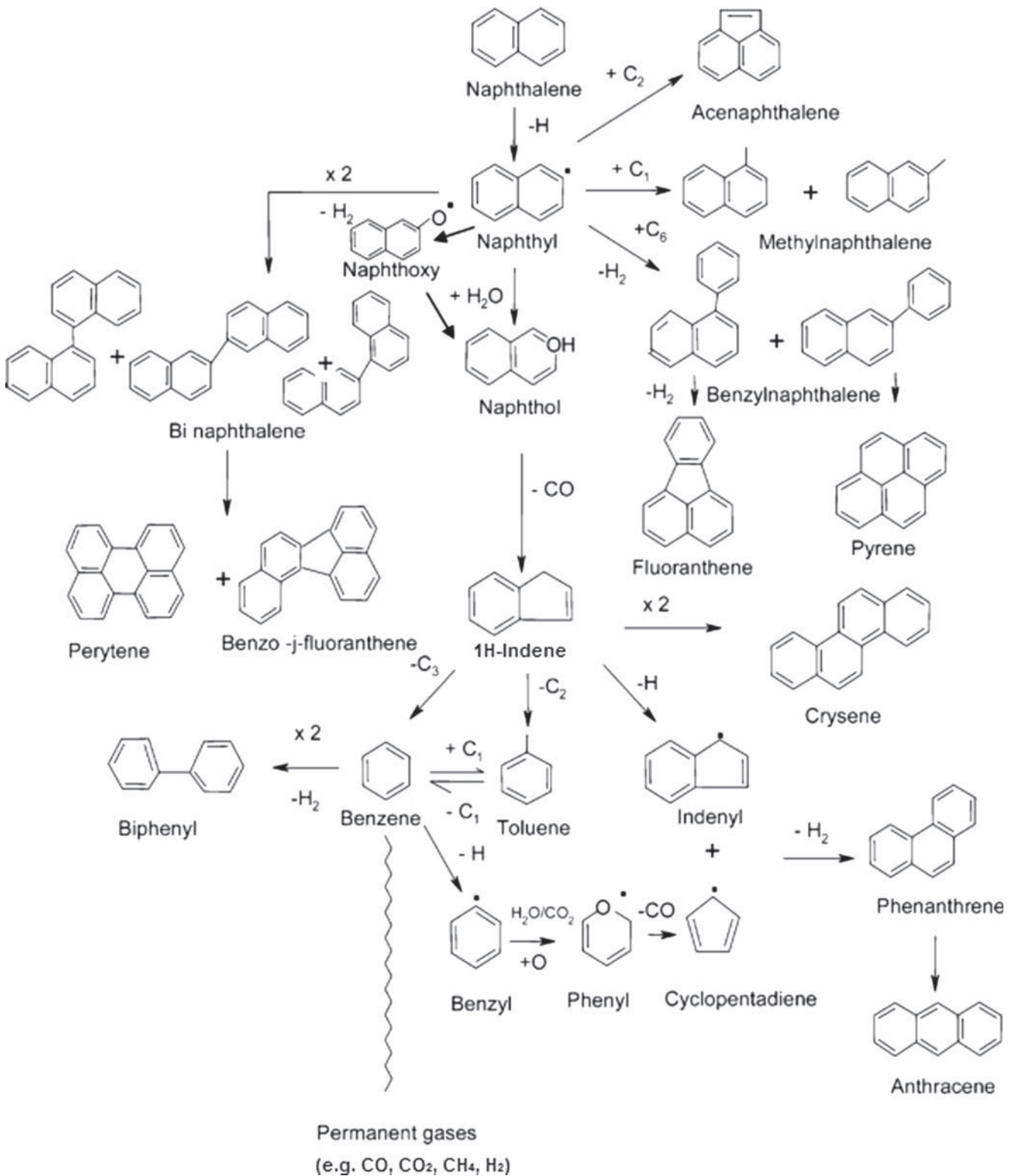


Fig. 1 Decomposition mechanism of naphthalene as proposed by Devi et al. [15] (adapted)

Figure 2 shows the flow sheet of the DFB gasification process as it occurs in the power plant in Senden, Germany. A screw conveyor system transports solid

feedstock into the bubbling fluidized bed of the gasifier. Therefore, volatile matter released from the biomass comes immediately into contact with the catalytically

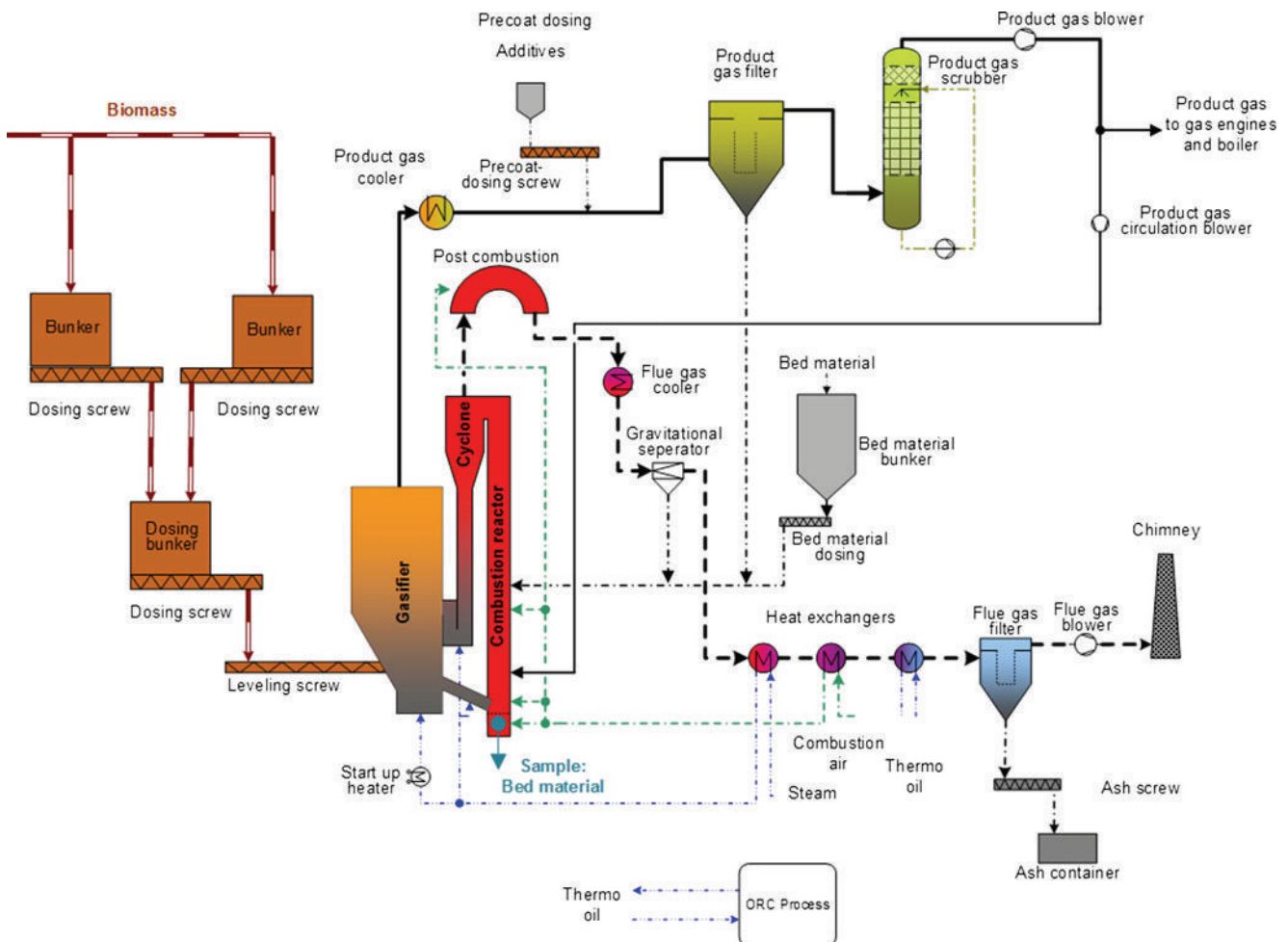


Fig. 2 Flow sheet of the DFB gasification plant in Senden

active bed material. Olivine is currently used as the bed material in all industrial power plants.

Gasification is conducted at a bed temperature of around 850 °C using steam as the gasifying agent. Calcium oxide is brought into the gasifier as an additive to further increase the catalytic activity toward tar reduction. Part of the biomass char enters into the combustion reactor via a chute where air is used as the fluidizing agent and combustion is performed at temperatures up to 930 °C. After the combustion reactor, bed particles are separated from the flue gas stream in a cyclone and transported back to the gasifier, thus providing the heat for gasification. Flue gas passes through a post-combustion chamber to ensure complete oxidation of the combustible compounds before it is cooled down in heat exchangers. Fine ash is separated from the gas stream in a flue gas filter and is removed from the system.

As a result of this separation of gasification and combustion, the valuable product gas is not mixed with the flue gas. The product gas is cooled down in a series of heat exchangers and cleaned after leaving the gasifier. Particles are separated from the gas stream in the product gas filter, and tars and water

are removed in the product gas scrubber. RME is used as the solvent for tars in the scrubber. After the scrubber unit, the clean product gas is then available for further usage. In the power plant in Senden, the product gas is used as fuel for two gas engines, resulting in the generation of electricity and district heating.

Fresh olivine samples were collected on site before start-up of the power plant. Used olivine samples were gathered during steady state operation from the bottom of the combustion reactor, as shown in Fig. 2. Samples were collected from four different days of operation.

2.2 Bed materials

To investigate the catalytic activity of bed particle coatings regarding the conversion of the compounds, fresh and used olivine samples were compared to each other. Fresh olivine was pretreated by calcination at 1200 °C. The detailed procedure of such a pretreatment has been previously described [37, 38]. The consequences of pretreatment itself regarding the catalytic activity of the material were not part of this work

and will therefore not be discussed further. An image from analysis in a scanning electron microscope (SEM) from a used olivine particle with a Ca-rich layer is shown in Fig. 3. As it can be seen, the surface is covered by the layer. Thus, the particle layer can be understood as catalytic coating on the olivine particle, which has the role of a support material. Detailed information on the interaction between olivine and biomass leading to such a layer has been presented by Kirnbauer et al. [27, 39].

Both olivine samples were compared to two benchmark materials. First, feldspar was used as a non-active inert material which does not influence the reactions. Second, calcium oxide (CaO) was used as natural material with high catalytic activity. Since the particle layers on olivine are Ca-rich, pure CaO serves as a benchmark for the highest activity due to active sites in the Ca-rich layer.

Bed material samples were sieved into a fraction of 400–800 μm to obtain comparable results. This was realized by first sieving the materials into three separate fractions, namely, 400–500, 500–630, and 630–800 μm . Then, 3.33 g was taken from each fraction and mixed together, resulting in samples with similar particle diameters. These samples were used for further investigations.

2.3 Test reactions

Experiments were conducted to determine the catalytic activity of the bed materials toward the conversion of hydrocarbons. Three reactions, which are relevant in gasification, will be discussed in detail.

The intermediate tar decomposition product 1H-indene was examined in detail. In-bed transformation of 1H-indene was investigated in lab-scale tests using the bed materials described above. On that account, steam reforming of 1H-indene was investigated, based on the following reaction formula:

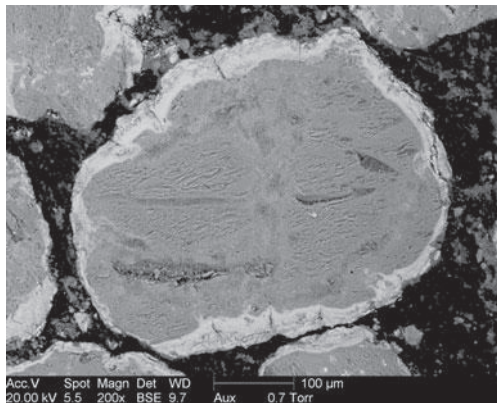


Fig. 3 SEM image of a used, layered, olivine particle

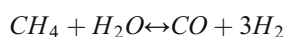
However, excess steam was used, resulting in input streams of $8.2 \text{ cm}^3\text{h}^{-1}$ of 1H-indene and a corresponding steam flow of 22.7 gh^{-1} . All gas volumes of the input streams were measured at standard conditions of 101.3 kPa and 273.15 K. The desired carrier flow stream for the evaporators was nitrogen (N_2) with volumetric flow rates of $1.5 \times 10^{-3} \text{ m}^3 \text{ h}^{-1}$ for the water evaporator and $1.0 \times 10^{-3} \text{ m}^3 \text{ h}^{-1}$ for the 1H-indene evaporator, respectively. Experiments with 1H-indene were performed for a temperature of 800 °C. This temperature was chosen, based on findings from previous work conducted by Kirnbauer et al. [40], where 800 °C was identified as the optimal operation temperature regarding the reduction of tars.

Since steam reforming of investigated hydrocarbons in this and previous work [34] was coupled with the water-gas-shift reaction, the influence of particle layers solely regarding this follow-up reaction was also addressed in this work to give a comprehensive overview:



For these tests, the chosen volumetric flow rate of CO was $1.5 \times 10^{-2} \text{ m}^3 \text{ h}^{-1}$ and the corresponding mass flow rate of H_2O was 12.05 gh^{-1} . The carrier gas for the steam generator was N_2 , with the same volumetric flow rate as that of CO. Thus, an input concentration of CO of 50 % based on the dry gas volume (CO and N_2) into the reactor was supplied. The water-gas-shift reaction was also addressed in previous work [34]; however, since it occurs as follow-up reaction in steam reforming of hydrocarbons, results are also shown in the present work to address the complete reaction path.

Furthermore, tests were conducted to investigate the transformation of CH_4 by steam reforming with fresh and used, layered olivine. As a result, the influence of the increased catalytic activity of Ca-rich layers on transformation of CH_4 , and therefore on the product gas composition was examined.



For the experiments, a volumetric flow rate of CH_4 was $1.1 \times 10^{-2} \text{ m}^3 \text{ h}^{-1}$ and a corresponding mass flow rate of H_2O of 17 gh^{-1} were applied. The carrier gas flow stream for the steam generator was N_2 with the same volumetric flow rate as that of CO. Therefore, the input flow rates supplied an input concentration of CH_4 of 50 % based on dry gas volume (CH_4 and N_2) into the reactor.

2.4 Lab-scale test rig for catalytic measurements

Figure 4 shows a flow chart of the employed test rig. The model tar component 1H-indene (Fig. 4(1)) was introduced in liquid state via a syringe pump. The liquid was pushed into an evaporator where complete transformation of 1H-indene into the gaseous state was achieved. The evaporator was operated at a temperature of 220 °C. A carrier gas stream was

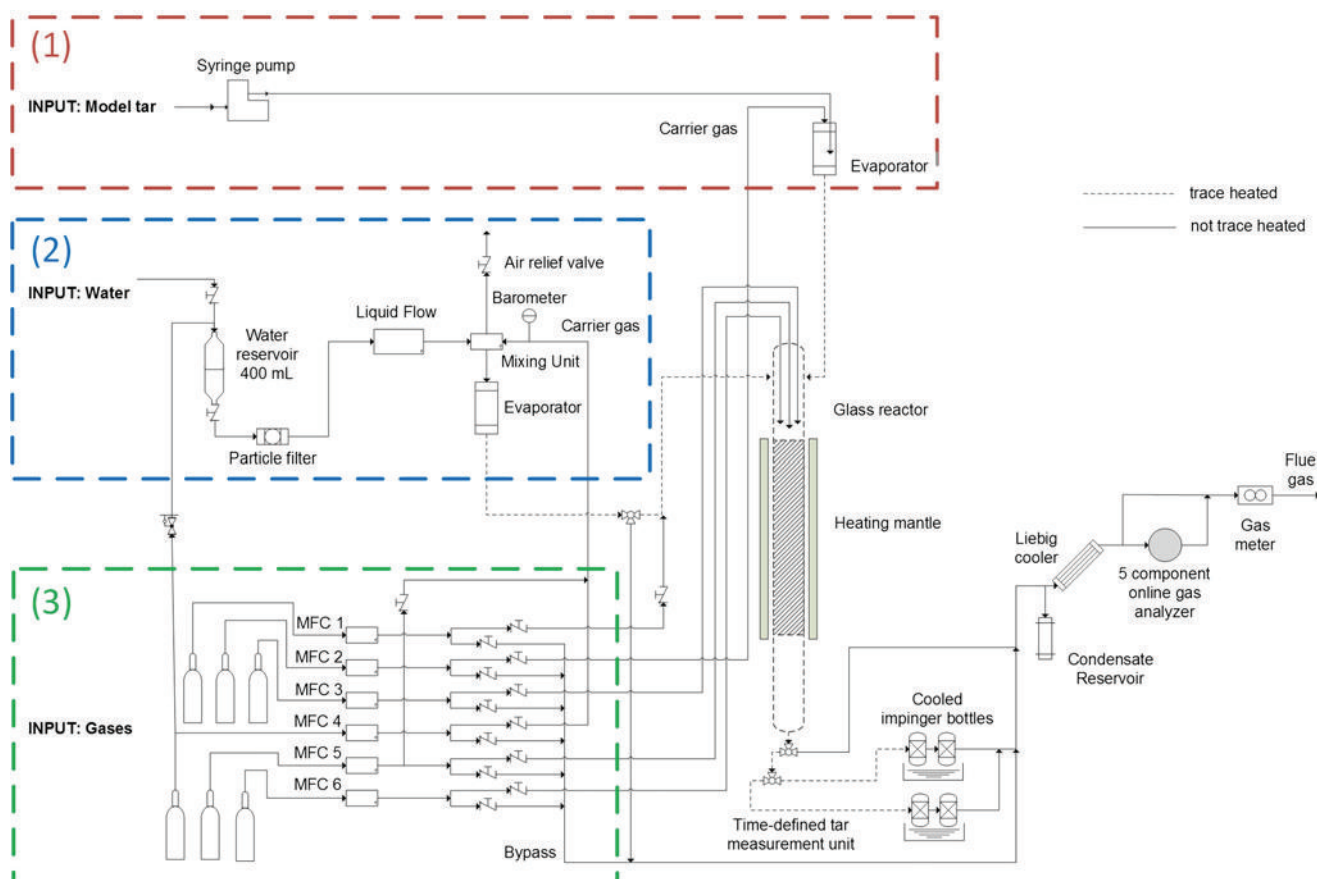


Fig. 4 Flow sheet of the lab-scale test rig for catalytic measurements

brought into the evaporator to drag the evaporated tar compound to the reactor zone. Nitrogen was used as the carrier gas for all experiments, since it is inert and therefore does not interfere with the reactions to a noteworthy extent but merely dilutes the produced gas. Demineralized water (Fig. 4(2)) was transported separately to the reactor zone. Pressurized N_2 pushed the water from a reservoir through a liquid mass flow controller. Then, it was brought to a controlled evaporator mixer (CEM) from Bronkhorst, where it was mixed with a carrier gas. The evaporator was operated at a temperature of $135\text{ }^\circ\text{C}$. Nitrogen was used as the carrier gas, analogous to the model tar carrier gas stream. A mixture of water and the carrier gas was either led directly to the reactor zone or switched to a bypass. All pipes leading to the reactor were trace heated to $200\text{ }^\circ\text{C}$ to avoid premature condensation.

It is possible to introduce up to six different gases (Fig. 4(3)) into the reactor simultaneously. The gas streams were introduced via mass flow controllers (MFCs). All gas streams could be separately switched to bypass or led to the reactor zone. Bypass mode was used to calibrate the measurement equipment and ensure its functionality. Calibration was conducted by the certified Test Laboratory for Combustion Systems of the Vienna University of Technology.

Figure 5 shows a more detailed scheme of the reactor part. A quartz glass tube with an inner diameter of 1.0 cm and an outer diameter of 1.2 cm was used as the reactor. Bed material particles of around 10 g were inserted as a fixed bed, resulting in a bed height of about 7.4 cm. Quartz wool inside the quartz

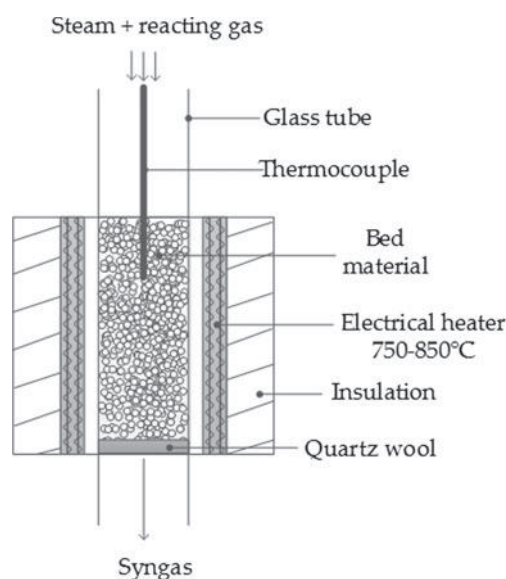


Fig. 5 Scheme of the reactor part

glass reactor held the particles in position. Gas streamed downward from top to bottom during the experiments. A heating furnace was placed around the quartz glass reactor, and a thermocouple continuously measured and controlled the bed temperature inside. A second thermocouple was placed outside the quartz glass reactor which continuously measured the wall temperature of the reactor outside of the fixed bed. This second thermocouple was used to constantly check the functionality of the thermocouple inside the reactor. When an increasing offset of the temperature measurement inside the reactor was observed, the experiment was stopped and the thermocouple was cleaned before starting again. Temperatures between 750 and 850 °C were investigated in this work. The temperature was continuously controlled, and therefore, constant temperature levels were ensured throughout the experiments. Quartz wool was installed as insulation outside of the reactor to reduce heat losses during operation.

Gas leaving the reactor was led through two impinger bottles, which were connected in series and were placed inside a cryostat. The cryostat was kept at a temperature of 0.1 °C. The exact procedure of tar sampling and measurement is explained in more depth in Sect. 2.5.

After the cryostat, a Liebig cooler was installed as a security measure to protect the measurement equipment in case of failure of the cryostat. The cooling medium of the Liebig cooler was also kept at a temperature of 0.1 °C. Condensed liquid phases were collected in a reservoir. The gas stream was then led to the measurement station, which consisted of a five-component Rosemount NGA 2000 online gas analyzer and an automatic data recording unit. Measurement of CO, CO₂, CH₄, H₂, and O₂ was carried out by the online analyzer, and data were recorded every 10 s. Before the off-gas was finally released through a vent, the volume flow was measured by a gas meter.

Experiments were conducted until a constant composition of the produced gas was observed. Afterwards, steady state operation was carried out for 30 min. Values for the evaluation of the catalytic activity were taken from steady state operation. Each experiment was repeated three times to ensure reproducibility of the results.

2.5 Tar sampling and measurement

Tar sampling from the lab-scale test rig was inspired by the Tar Sampling Guidelines [41], but was adapted for the apparatus. Figure 6 shows the setup as it was installed in the test rig. Gas was led through two consecutive impinger bottles in bypass mode at all times. The impinger bottles were filled with toluene as the solvent instead of a mixture of dry ice with isopropanol as suggested in the guidelines, since measuring 1H-indene was the primary goal. Time-defined tar sampling was performed by switching to two separate bottles, when a

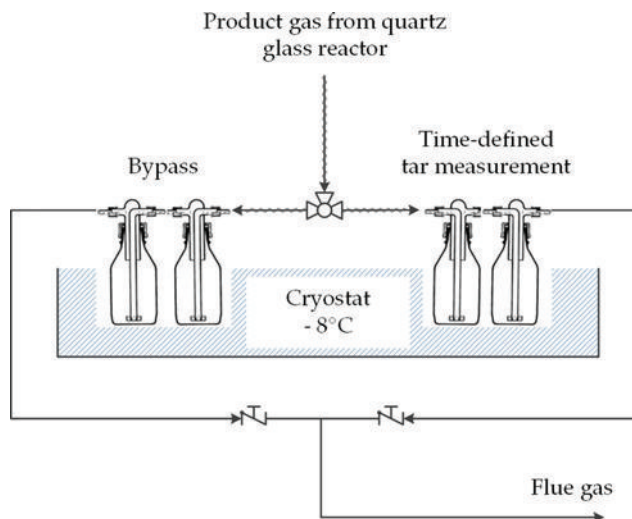


Fig. 6 Setup of the tar measurement unit in the lab-scale test rig

constant composition was measured for the produced gas. Time-defined tar sampling was conducted for 30 min. Pipes connecting the reactor outlet and the inlet to the bottles were constantly trace heated to a temperature of 200 °C to avoid losses through condensation.

Measurement of collected tar samples was performed by the certified Test Laboratory for Combustion Systems at the Vienna University of Technology using a GC/MS to identify single tar components.

3 Results

3.1 Catalytic activity of bed material particles

The influence of catalytic activity regarding the transformation of 1H-indene is presented. Conversion of 1H-indene at 800 °C in the presence of different bed materials is shown in Fig. 7. Feldspar did not show noteworthy catalytic activity.

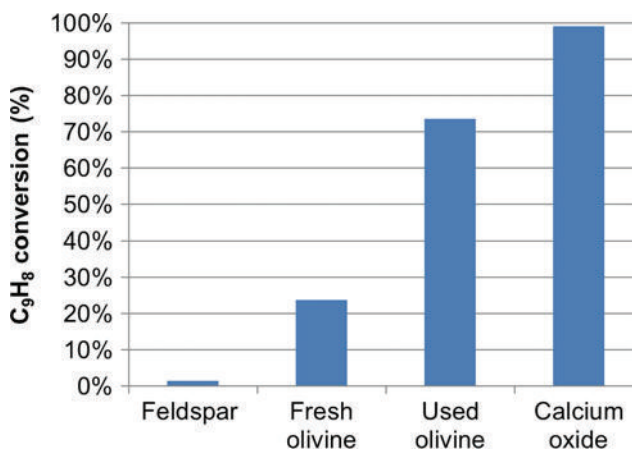


Fig. 7 Conversion of 1H-indene during steam reforming at 800 °C

Fresh olivine reached more than 20 % conversion; however, this was significantly less than used, layered olivine which converted more than 70 % of 1H-indene. Almost complete conversion could be achieved when using the benchmark material CaO.

Table 1 shows the dry gas composition (CO, CO₂, CH₄, H₂) of steam reforming of 1H-indene performed with the different bed materials. Moreover, the carrier gas N₂ is not included in the composition. The H₂ composition rose with increasing catalytic activity. Materials with lower catalytic activity, such as feldspar and fresh olivine, showed significantly higher selectivity toward CO compared to CO₂. In comparison, for used olivine and CaO, which possess higher catalytic activity, increased amounts of CO₂ compared to CO were observed. The amounts of CH₄ were close to the detection limit for all investigated samples.

Tar measurements during the experiments with the lab-scale test rig showed the presence of chrysene, a heavier poly-cyclic hydrocarbon. This polymerization, as described in Fig. 1, was observed during all test runs. The results are presented in Table 2. Increasing catalytic activity led to decreasing polymerization of 1H-indene. The amounts of chrysene were close to the detection limit when CaO was used as the catalyst.

Part of the CO produced during steam reforming reacts further with steam to form CO₂, and H₂. This water-gas-shift reaction occurred as a follow-up reaction to the investigated steam reforming reaction. Figure 8 shows the conversion of CO from separate experiments (see Sect. 2.3) at temperatures from 750 to 850 °C using feldspar, fresh, and used olivine as well as CaO. In those experiments, the water-gas-shift reaction was investigated isolated from any other reactions. Analogous to the steam reforming of 1H-indene, feldspar did not show any catalytic activity. Used olivine achieved significantly higher conversion of CO than fresh olivine. The equilibrium of the reaction was almost reached when the benchmark material CaO was used as the catalyst.

Steam reforming of methane was conducted using both fresh and used olivine according to the description in Sect. 2.3. In addition, the temperature dependency was investigated by conducting the experiments at 750, 800, and 850 °C. The conversion of methane is displayed in Fig. 9. As it can be seen, only minimal conversion of methane was achieved with both

Table 1 Dry gas composition of 1H-indene steam reforming at 800 °C

| | CO | CO ₂ | CH ₄ | H ₂ |
|---------------|-----------------------------|-----------------|-----------------|----------------|
| | Average gas composition (%) | | | |
| Feldspar | 22.0 | 5.7 | 0.4 | 71.9 |
| Fresh olivine | 15.8 | 9.6 | 0.2 | 74.4 |
| Used olivine | 6.0 | 18.5 | 0.5 | 75.0 |
| CaO | 3.1 | 18.8 | 0.2 | 77.9 |

Table 2 Polymerization of 1H-indene to chrysene at 800 °C

| | Feldspar (%) of total input | Fresh olivine | Used olivine | CaO |
|-----------------|--------------------------------|----------------|----------------|----------------|
| Chrysene | 2.1 +/- 0.3 | 1.9 +/- 0.4 | 1.1 +/- 0.2 | 0.2 +/- 0.1 |

materials. Fresh olivine did not show significant catalytic activity, and the coating of the used olivine did not increase it either. Increasing the temperature from 750 up to 850 °C promoted the conversion of CH₄ by less than 1 % and was still less than 2 % for both materials.

4 Discussion

In tar measurements from the DFB gasification of woody biomass, naphthalene is one of the major components [33]. Therefore, in this work, decomposition is discussed using naphthalene as a model compound for biomass tars. The decomposition mechanism of naphthalene, as described by Devi et al. [15] and presented in Fig. 1, shows that 1H-indene is a stable intermediate compound. Therefore, the detection of increased amounts of 1H-indene at the power plant in Senden could be explained by incomplete conversion of heavier hydrocarbons into smaller gaseous molecules. Lab-scale tests were conducted to clarify the catalytic activity of the normally used bed material, which is olivine. Steam reforming of 1H-indene is only possible in the presence of a catalyst, since no conversion was observed when feldspar was used. Fresh olivine did show higher catalytic activity; however, on average only 24 % of 1H-indene was converted. Analogous to experiments conducted in a previous work using other hydrocarbons, such as toluene and C₂H₄ [34], the calcium-rich bed particle coating of used olivine led to a significant increase in its catalytic activity. 1H-indene conversion of more than 70 % was achieved during these experiments. Pure CaO used as the benchmark showed conversion of almost 100 %. As a consequence, it can be stated that the bed material, once it is in

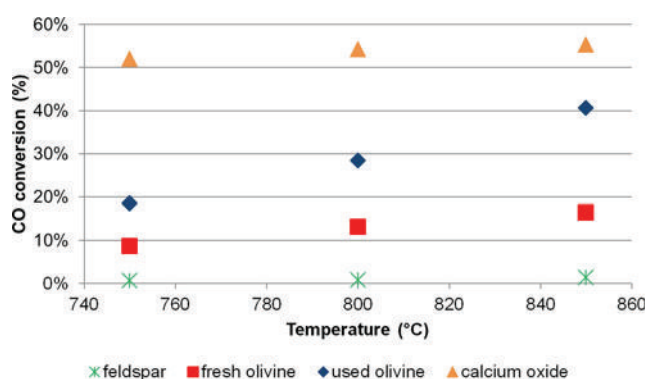


Fig. 8 Carbon monoxide conversion during the water-gas-shift reaction

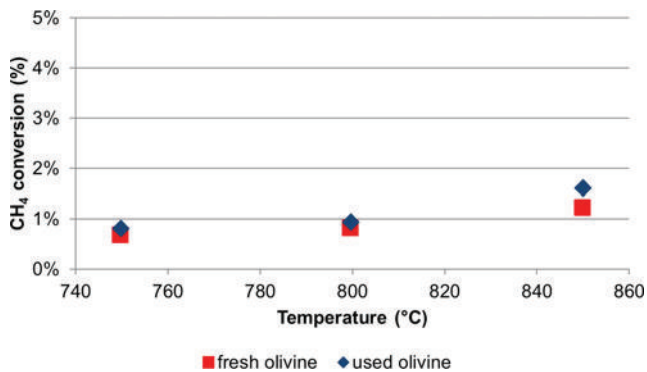


Fig. 9 Methane conversion during steam reforming

its active state with a calcium-rich coating, acts as an effective catalyst regarding the conversion of 1H-indene. If this active state is reached, ensuring sufficient contact time between tars and catalyst due to uniform mixing of solid biomass and bed material in the fluidized bed leads to decreasing amounts of intermediate tar decomposition products. The higher catalytic activity of the material leads to increased amounts of CO₂ compared to CO. This is most likely a consequence of the water-gas-shift reaction, which occurs as a follow-up reaction.

Polymerization of 1H-indene and as a result of the production of chrysene was observed during the lab-scale trials. The mechanism underpinning this recreation of five-membered to six-membered ring structures was investigated in detail by Lu and Mulholland [42]. It was found that the formation of chrysene is one possible outcome of aromatic hydrocarbon growth from 1H-indene. The lab-scale experiments conducted in the present study showed that the higher the catalytic activity of the bed material, the lower the formation of chrysene. Since higher amounts of 1H-indene are converted into smaller molecules, less 1H-indene is available for the polymerization step. Therefore, the recreation of intermediate tar decomposition products into heavier poly-cyclic molecules can be prevented in the presence of a catalyst.

The water-gas-shift reaction, which occurred as a follow-up reaction in the steam reforming of 1H-indene, was investigated in more depth. As shown in Fig. 8, this reaction also needs the presence of a catalyst, since feldspar did not lead to any conversion of CO. Similar to the findings for 1H-indene, used olivine showed increased catalytic activity compared to fresh olivine. Therefore, calcium-rich bed particle coatings also have a significant influence on the water-gas-shift reaction. Pure CaO showed the highest activity of the investigated materials and almost reached the equilibrium of the reaction, demonstrating the essential role of Ca in the bed particle coating. The findings discussed above strengthen the importance of sufficient contact time between coated (activated, used) bed particles and volatile matter from the biomass feedstock.

The typical product gas composition of the DFB gasifier shows the presence of 8–12 % methane, depending on the bed temperature [40]. Figure 9 shows that neither fresh nor used

olivine possesses high enough catalytic activity for noteworthy conversion of methane. Methane is, therefore, the only hydrocarbon investigated so far that is stable enough to withstand significant catalytic conversion in the presence of bed materials coated with a calcium-rich layer. Due to the stability of the methane molecule, only specific catalysts reduce the activation energy enough to enable the steam reforming process (e.g., Ni catalysts). This is of relevance when using DFB gasification for the production of bio-CH₄, where the presence of methane in the product gas is desired. Furthermore, it shows that there is not necessarily a causal correlation between the amount of methane and the amount of tar in the product gas, since tar is highly influenced by bed particle coatings in contrast to methane. Using methane as measurable tar indication compound during operation of an industrial power plant has therefore to be treated with caution until deeper understanding of reaction pathways is gained. In addition, a minor influence of the temperature was observed between 750 and 850 °C in comparison to the water-gas-shift reaction, where the temperature had a significantly greater influence.

CaO showed the best performance of the bed materials tested; however, a high attrition rate hinders its use as a bed material.

The collective results of these and previous investigations [33, 35, 36, 40] provide insight into the influence of calcium-rich bed particle coatings regarding the conversion of different hydrocarbons.

5 Conclusion

Based on these investigations, the following conclusions can be drawn:

1. The bed material has to be in its active state, which is achieved through the development of Ca-rich layers originating from interactions with biomass ash, to obtain satisfactory conversion of 1H-indene. Sufficient contact time between the catalytically active bed material and tars must be ensured.

2. Steam reforming of 1H-indene is linked to the water-gas-shift reaction. As a result, part of the CO produced during steam reforming is further converted into H₂ and CO₂ in the presence of H₂O. Analogous to the findings for 1H-indene, Ca-rich layers have a significant influence on the conversion of CO in the water-gas-shift reaction.

3. The increase of the catalytic activity of the bed material caused by the formation of Ca-rich layers does not affect the conversion of methane through steam reforming to a noteworthy extent. Due to the stability of the methane molecule, the increased activity is still too low to enable conversion under the investigated conditions.

In conclusion, understanding the influence of bed particle layers on the decomposition and conversion of hydrocarbons

is essential for stable and reliable operation and to obtain a specific product gas composition.

Acknowledgments Open access funding provided by TU Wien (TUW). This study was carried out in the framework of the Bioenergy2020+ project C20016016. Bioenergy2020+ GmbH is funded within the Austrian COMET program, which is managed by the Austrian Research Promotion Agency (FFG) and promoted by the Federal Government of Austria as well as the Federal States of Burgenland, Niederösterreich, and Steiermark. We are grateful for the support of our project partners HGA Senden (Stadtwerke Ulm) and the Institute of Chemical Engineering at the Vienna University of Technology.

Open Access This article is distributed under the terms of the Creative Commons Attribution 4.0 International License (<http://creativecommons.org/licenses/by/4.0/>), which permits unrestricted use, distribution, and reproduction in any medium, provided you give appropriate credit to the original author(s) and the source, provide a link to the Creative Commons license, and indicate if changes were made.

References

- Kaltschmitt M, Hartmann H, Hofbauer H. *Energie aus biomasse*. Berlin, Heidelberg: Springer Berlin Heidelberg; 2001. doi:10.1007/978-3-662-07025-3.
- Hofbauer H, Rauch R, Loeffler G, Kaiser S, Fercher E, Tremmel H. Six years experience with the FICFB-gasification process. Proc. 12th Eur. Conf. Technol. Exhib. Biomass Energy, Ind. Clim. Prot., Amsterdam, The Netherlands: 2002, p. 982–5.
- Rehling B, Hofbauer H, Rauch R, Aichernig C (2011) BioSNG—process simulation and comparison with first results from a 1-MW demonstration plant. *Biomass Convers Biorefinery* 1:111–119. doi:10.1007/s13399-011-0013-3
- Agerborg J, Lingehed E (2013) Integration of power-to-gas in gasendal and GoBiGas. Chalmers University of Technology, Master's Thesis
- Rauch R, Hrbek J, Hofbauer H (2014) Biomass gasification for synthesis gas production and applications of the syngas. *Wiley Interdiscip Rev Energy Environ* 3:343–362. doi:10.1002/wene.97
- Sauciuc A, Abosteif Z, Weber G, Potetz A, Rauch R, Hofbauer H, et al. (2011) Influence of pressure on the performance of biomass based Fischer-Tropsch synthesis. Vienna, Austria, Proc. Int. Conf. Polygeneration Strateg.
- Fail S, Diaz N, Benedikt F, Kraussler M, Hinteregger J, Bosch K, et al. (2014) Wood gas processing to generate pure hydrogen suitable for PEM fuel cells. *ACS Sustain Chem Eng* 2:2690–2698. doi:10.1021/sc500436m
- Benedikt F, Kraussler M, Konlechner D, Bosch K, Hackel M, Hofbauer H. polygeneration at the biomass steam gasification plant oberwart—evaluation of process chains to produce hydrogen, electricity and heat. Proc. 23rd Eur. Biomass Conf. Exhib., Vienna, Austria: 2015, p. 1–4.
- Chianese S, Loipersböck J, Malits M, Rauch R, Hofbauer H, Molino A, et al. (2015) Hydrogen from the high temperature water gas shift reaction with an industrial Fe/Cr catalyst using biomass gasification tar rich synthesis gas. *Fuel Process Technol* 132:39–48. doi:10.1016/j.fuproc.2014.12.034
- Weber G, Rauch R, Hofbauer H (2014) Influence of ethylene on the formation of mixed alcohols over a MoS₂ catalyst using biomass-derived synthesis gas. *Biomass Convers Biorefinery* 07:85–94. doi:10.1007/s13399-014-0140-8
- Schmid JC, Pfeifer C, Kitzler H, Pröll T, Hofbauer H. A new dual fluidized bed gasifier design for improved in situ conversion of hydrocarbons. Proc. Int. Conf. Polygeneration Strateg., Vienna, Austria: 2011, p. 1–10.
- Schmid JC, Pröll T, Pfeifer C, Hofbauer H. Improvement of gas-solid interaction in dual circulating fluidized bed systems. Proc. 9th Eur. Conf. Ind. Furn. Boil., Estoril, Portugal: 2011, p. 1–13.
- Pfeifer C, Schmid JC, Pröll T, Hofbauer H. Next generation biomass gasifier. Proc. 19th Eur. Biomass Conf. Exhib., Berlin, Germany: 2011, p. 1–7.
- Basu P (2010) *Biomass gasification and pyrolysis*. Elsevier Inc., Oxford. doi:10.1016/B978-0-12-374988-8.00005-2
- Devi L, Ptasiński KJ, Janssen FJJG (2005) Decomposition of naphthalene as a biomass tar over pretreated olivine: effect of gas composition, kinetic approach, and reaction scheme. *Ind Eng Chem Res* 44:9096–9104. doi:10.1021/ie050801g
- Devi L, Ptasiński KJ, Janssen FJJG, Van Paasen SVB, Bergman PCA, Kiel JHA (2005) Catalytic decomposition of biomass tars: use of dolomite and untreated olivine. *Renew Energy* 30:565–587. doi:10.1016/j.renene.2004.07.014
- Nair SA, Yan K, Pemen AJM, van Heesch EJM, Ptasiński KJ, Drinkenburg AAH (2004) Tar removal from biomass-derived fuel gas by pulsed corona discharges. A chemical kinetic study. *Ind Eng Chem Res* 43:1649–1658. doi:10.1021/ie034066p
- Coll R, Salvadó J, Farriol X, Montané D (2001) Steam reforming model compounds of biomass gasification tars: conversion at different operating conditions and tendency towards coke formation. *Fuel Process Technol* 74:19–31. doi:10.1016/S0378-3820(01)00214-4
- Zamboni I, Courson C, Niznansky D, Kiennemann A (2014) Simultaneous catalytic H₂ production and CO₂ capture in steam reforming of toluene as tar model compound from biomass gasification. *Appl Catal B Environ* 145:63–72. doi:10.1016/j.apcatb.2013.02.046
- Zhao B, Zhang X, Chen L, Qu R, Meng G, Yi X, et al. (2010) Steam reforming of toluene as model compound of biomass pyrolysis tar for hydrogen. *Biomass Bioenergy* 34:140–144. doi:10.1016/j.biombioe.2009.10.011
- Kong M, Yang Q, Fei J, Zheng X (2012) Experimental study of Ni/MgO catalyst in carbon dioxide reforming of toluene, a model compound of tar from biomass gasification. *Int J Hydrog Energy* 37:13355–13364. doi:10.1016/j.ijhydene.2012.06.108
- Biagini E, Barontini F, Tognotti L (2006) Devolatilization of biomass fuels and biomass components studied by TG/FTIR technique. *Ind Eng Chem Res* 45:4486–4493. doi:10.1021/ie0514049
- Swierczynski D, Courson C, Kiennemann A (2008) Study of steam reforming of toluene used as model compound of tar produced by biomass gasification. *Chem Eng Process Process Intensif* 47:508–513. doi:10.1016/j.cep.2007.01.012
- Kuba M, Kimbauer F, Hofbauer H (2015) The role of 1H-indene in product gas of biomass gasification. Shanghai, China, Contrib. to Int. Bioenergy Exhib. Bioenergy Conf.
- Kimbauer F, Koch M, Koch R, Aichernig C, Hofbauer H (2013) Behavior of inorganic matter in a dual fluidized steam gasification plant. *Energy Fuel* 27:3316–3331. doi:10.1021/ef400598h
- Öhman M, Pommer L, Nordin A (2005) Bed agglomeration characteristics and mechanisms during gasification and combustion of biomass fuels. *Energy and Fuels* 19:1742–1748. doi:10.1021/ef040093w
- Kimbauer F, Hofbauer H (2011) Investigations on bed material changes in a dual fluidized bed steam gasification plant in Güssing, Austria. *Energy and Fuels* 25:3793–3798. doi:10.1021/ef200746c
- Tranvik AC, Öhman M, Sanati M (2007) Bed material deposition in cyclones of wood fuel fired circulating fluidized beds (CFBs). *Energy and Fuels* 21:104–109. doi:10.1021/ef060175f
- Brus E, Öhman M, Nordin A (2005) Mechanisms of bed agglomeration during fluidized-bed combustion of biomass fuels. *Energy and Fuels* 19:825–832. doi:10.1021/ef040086g

30. Kuba M, He H, Kimbauer F, Boström D, Öhman M, Hofbauer H (2015) Deposit build-up and ash behavior in dual fluid bed steam gasification of logging residues in an industrial power plant. *Fuel Process Technol* 139:33–41. doi:10.1016/j.fuproc.2015.08.017
31. Scala F, Chirone R (2008) An SEM/EDX study of bed agglomerates formed during fluidized bed combustion of three biomass fuels. *Biomass Bioenergy* 32:252–266. doi:10.1016/j.biombioe.2007.09.009
32. Fryda LE, Panopoulos KD, Kakaras E (2008) Agglomeration in fluidised bed gasification of biomass. *Powder Technol* 181:307–320. doi:10.1016/j.powtec.2007.05.022
33. Kimbauer F, Wilk V, Kitzler H, Kern S, Hofbauer H (2012) The positive effects of bed material coating on tar reduction in a dual fluidized bed gasifier. *Fuel* 95:553–562. doi:10.1016/j.fuel.2011.10.066
34. Kuba M, Havlik F, Kimbauer F, Hofbauer H (2015) Influence of bed material coatings on the water-gas-shift reaction and steam reforming of toluene as tar model compound of biomass gasification. *Biomass Bioenergy*. doi:10.1016/j.biombioe.2015.11.029
35. Kuba M, Havlik F, Kimbauer F, H. Hofbauer. Investigations on the catalytic activity of bed material coating regarding the water-gas-shift reaction and steam reforming of model compounds for lighter and heavier hydrocarbons. *Proc. 23rd Eur. Biomass Conf. Exhib., Vienna, 2015*, p. 1–4.
36. Kern S, Pfeifer C, Hofbauer H (2013) Reactivity tests of the water-gas shift reaction on fresh and used fluidized bed materials from industrial DFB biomass gasifiers. *Biomass Bioenergy* 55:227–233. doi:10.1016/j.biombioe.2013.02.001
37. Devi L, Craje M, Thüne P, Ptasiński KJ, Janssen FJJG (2005) Olivine as tar removal catalyst for biomass gasifiers: catalyst characterization. *Appl Catal A Gen* 294:68–79. doi:10.1016/j.apcata.2005.07.044
38. Christodoulou C, Grimekis D, Panopoulos KD, Pachatouridou EP, Iliopoulou EF, Kakaras E (2014) Comparing calcined and untreated olivine as bed materials for tar reduction in fluidized bed gasification. *Fuel Process Technol* 124:275–285. doi:10.1016/j.fuproc.2014.03.012
39. Kimbauer F, Hofbauer H (2013) The mechanism of bed material coating in dual fluidized bed biomass steam gasification plants and its impact on plant optimization. *Powder Technol* 245:94–104. doi:10.1016/j.powtec.2013.04.022
40. Kimbauer F, Wilk V, Hofbauer H (2013) Performance improvement of dual fluidized bed gasifiers by temperature reduction: the behavior of tar species in the product gas. *Fuel* 108:534–542. doi:10.1016/j.fuel.2012.11.065
41. van de Kamp W, de Wild P, Zielke U, Suomalainen M, Knoef H, Good J, et al. Tar measurement standard for sampling and analysis of tars and particles in biomass gasification product gas. *Proc. 14th Eur. Biomass Conf. Exhib., Paris, France: 2005*, p. 791–4.
42. Lu M, Mulholland JA (2001) Aromatic hydrocarbon growth from indene. *Chemosphere* 42:625–633. doi:10.1016/S0045-6535(00)00236-8

A.4 Paper IV

**Thermal stability of bed particle layers on naturally occurring minerals from dual fluid
bed gasification of woody biomass**

Thermal Stability of Bed Particle Layers on Naturally Occurring Minerals from Dual Fluid Bed Gasification of Woody Biomass

Matthias Kuba,^{*,†,‡} Hanbing He,[§] Friedrich Kirnbauer,[†] Nils Skoglund,[§] Dan Boström,^{||} Marcus Öhman,[§] and Hermann Hofbauer[‡]

[†]Bioenergy 2020+ GmbH, Wiener Straße 49, A-7540 Güssing, Austria

[‡]TU Wien, Institute of Chemical Engineering, Getreidemarkt 9/166, 1060 Vienna, Austria

[§]Luleå University of Technology, Energy Engineering, Division of Energy Science, SE-971 87 Luleå, Sweden

^{||}Umeå University, Energy Technology and Thermal Process Chemistry, SE-901 87 Umeå, Sweden

ABSTRACT: The use of biomass as feedstock for gasification is a promising way of producing not only electricity and heat but also fuels for transportation and synthetic chemicals. Dual fluid bed steam gasification has proven to be suitable for this purpose. Olivine is currently the most commonly used bed material in this process due to its good agglomeration performance and its catalytic effectiveness in the reduction of biomass tars. However, as olivine contains heavy metals such as nickel and chromium, no further usage of the nutrient-rich ash is possible, and additional operational costs arise due to necessary disposal of the ash fractions. This paper investigates possible alternative bed materials and their suitability for dual fluid bed gasification systems focusing on the behavior of the naturally occurring minerals olivine, quartz, and K-feldspar in terms of agglomeration and fracturing at typical temperatures. To this end, samples of bed materials with layer formation on their particles were collected at the industrial biomass combined heat and power (CHP) plant in Senden, Germany, which uses olivine as the bed material and woody biomass as feedstock. The low cost logging residue feedstock contains mineral impurities such as quartz and K-feldspar, which become mixed into the fluidized bed during operation. Using experimental and thermochemical analysis, it was found that the layers on olivine and K-feldspar showed a significantly lower agglomeration tendency than quartz. Significant fracturing of particles or their layers could be detected for olivine and quartz, whereas K-feldspar layers were characterized by a higher stability. High catalytic activity is predicted for all three minerals once Ca-rich particle layers are fully developed. However, quartz may be less active during the buildup of the layers due to lower amounts of Ca in the initial layer formation.

1. INTRODUCTION

The substitution of fossil fuels with renewable energy carriers is being driven by rising greenhouse gas concentrations in the atmosphere which have reached levels unprecedented in at least the last 800 000 years. Rising concentrations of gases such as carbon dioxide and methane are likely to be the main cause of global warming.¹ Awareness of the consequences of climate change is leading to the development of technologies using renewable sources to cover the global demand of energy. Biomass is the only renewable carbon-based fuel and as such is CO₂-neutral.² Reducing CO₂, a long-lived climate pollutant, has been set as a major goal in the definition of the 2 °C goal, which was set by the Kyoto Protocol.³ In 2015, at the 21st session of the Conference of the Parties held in Paris, France, a new agreement was reached, where the limit of the temperature increase was set to 1.5 °C.⁴ Biomass needs to play a role in achieving this goal. It is suitable for use in pyrolysis, combustion, and gasification processes. Gasification is a key technology, since it transforms solid feedstock into a gaseous secondary energy carrier, also referred to as product or synthesis gas.²

A dual fluid bed gasification system was developed at the TU Wien, Austria. Separation of endothermic gasification from exothermic combustion is the main principle underlying this technology. Separation is achieved using two separate reactors connected by a circulating bed material which acts as both heat

carrier and catalyst in the process. Combustion provides the heat necessary for gasification.⁵ Syngas obtained from gasifying solid feedstock can be further used for the generation of electricity, district heat, or the production of hydrogen,^{6–9} methane,^{10,11} Fischer–Tropsch diesel,^{12,13} or mixed alcohols.¹⁴ As a result of the flexibility of the process, it can quickly react to a fast changing energy market.⁵

Olivine, a naturally occurring magnesium–iron–silicate, is currently the most commonly used bed material. It has good agglomeration performance¹⁵ and catalytic effectiveness in the reduction of tars.^{16–18} However, olivine contains heavy metals such as chromium and nickel which transfer to the ash due to abrasion of the olivine particles in the fluidized bed during long-term operation in industrial power plants. As a result, the biomass ash requires special disposal arrangements, and this leads to increased costs for the plant operator. In addition, the use of certain ash fractions is yet impossible. As a result, replacing olivine with a heavy-metal free bed material would be desirable as it would make possible the further use of some of the ash fractions, e.g., as fertilizer. Furthermore, it would reduce operational costs by avoiding special deposition of the ash, which is removed from the system. Therefore, alternative bed

Received: June 21, 2016

Revised: September 6, 2016

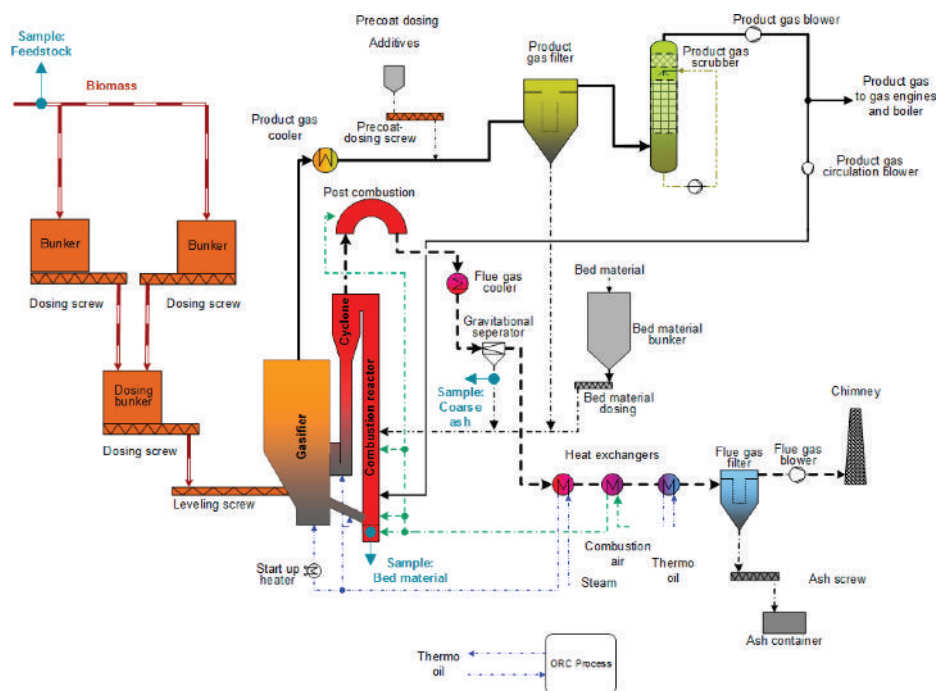


Figure 1. Simplified flow sheet of the power plant in Senden.

materials have to be considered. For this reason considerable research effort has gone into understanding the interactions between biomass ash and bed materials.

It has been found that biomass ash and bed materials interact at temperatures above 750 °C, leading to the formation of layers on the bed particles.^{19,20} Bed material layers were first found on quartz particles and have been identified as playing a major role in agglomeration. This prompted the search for alternative bed materials for combustion of problematic fuels.^{21–24} A comparison of the influence of different naturally occurring minerals used as bed materials on agglomeration during combustion was made by De Geyter et al.²⁵ It was shown that the tendency toward agglomeration cannot be solely attributed to bed materials but rather to the interaction between the bed materials and the ash components from the biomass feedstock. Depending on the biomass used, agglomeration, which leads to defluidization, varies significantly.^{26–29} Agglomeration in the combustion of woody biomass in quartz beds occurs mainly as a result of bed particle coatings and is therefore referred to as coating-induced.^{30–34}

Understanding the behavior of the main ash forming compounds is essential. An overview of important ash transformation chemistry related to this area of research was given by Boström et al.³⁵ Previous investigations have also demonstrated that fracturing due to layer fragmentation leads to deposit build-up.³⁶ Bed material thermal attrition in different combustion and gasification conditions have been investigated by Scala et al.^{37,38} In particular the influence of temperature on limestone attrition was investigated, finding a particle weakening effect when the operating temperature was increased from 850 to 900 °C. This led to a higher attrition rate.³⁹

Layers on olivine in dual fluid bed biomass gasification plants were investigated by Kimbauer and Hofbauer.⁴⁰ Calcium-rich layers around olivine particles had a positive effect on their catalytic activity in tar decomposition. This has been demonstrated in the industrial scale power plant in Güssing,

Austria,^{41,42} and in laboratory scale tests.⁴³ Similar results were observed in experiments conducted at the Chalmers' gasifier.⁴⁴ A laboratory scale test rig was also used to investigate the increase of the catalytic activity of quartz when layered from long-term operation in a biomass combustion plant. It was found that calcium-rich layers led to a significant increase of the activity for both olivine and quartz.⁴⁵ So the interaction with biomass ash during the process seems to be able to develop Ca-rich layers in other materials with similar catalytic effects as those in olivine. Any catalytic activity of the original particle will be substituted once a Ca-rich layer has developed.

Interactions between inorganic compounds in biomass ash and bed particles have been investigated for different possible bed materials, such as bauxite or ilmenite, and the different paths of ash-bed particle interaction explained in detail.^{46,47} In dual fluidized bed (DFB) gasification of biomass, layers formed on the bed material have to bestow on it three important characteristics: a low tendency toward coating-induced agglomeration, resistance against fracturing, and sufficient catalytic effectiveness in regarding the reduction of tars. Feldspar has also been investigated by Berguerand et al.⁴⁸ with a view to its use in gasification, using a reactor chamber downstream of the gasifier.

The influence of temperature in the combustion and postcombustion zone in DFB systems on alternative bed materials also needs to be understood to determine whether the layers are able to resist agglomeration and fracturing in various conditions. This paper therefore explores the thermal stability of the layers on bed particles of naturally occurring minerals by predicting the melting behavior of the bed particle layer material. We also investigate the resistance against fracturing by characterizing the corresponding bed particle layer morphology.

The bed particles originate from long-term interaction with biomass ash in dual fluid bed gasification. Samples were collected at the industrial scale combined heat and power (CHP) gasification plant in Senden, near Ulm, Germany, where

olivine is used as bed material. The CHP plant uses logging residues as feedstock, which contains mineral impurities, such as quartz and feldspars. During operation, they become mixed into the fluidized bed when transported into the gasifier together with the feedstock. Thus, olivine will be compared to quartz and K-feldspar, both widely available heavy-metal free minerals, which could be used as possible alternative bed materials. Feldspar has been investigated regarding its applicability in gasification by Berguerand et al.,⁴⁸ however, in a reactor chamber downstream of the gasifier. Investigations of different samples from an industrial scale DFB gasification plant have not been performed so far. Deriving information about the thermal stability under industrial scale conditions is an important basis for further research of alternative bed materials for DFB gasification. In this work, layer formation on those particles will be investigated regarding their compositions and predicted melting behavior as well as regarding their morphology and resistance against fracturing under process conditions typical for DFB systems. This approach is based on previous work regarding the enhancement of the catalytic activity once Ca-rich layers are developed, as described above. Resistance against fracturing is discussed on the basis of the bed particle/layer morphology. In addition, insights into the mechanism of layer formation of K-feldspars in gasification are given. A comparison of the findings to layer formation on olivine and quartz will be provided. Investigating impurities found in the olivine bed only shows tendencies of the layer formation and its characteristics and might differ from findings performed on pure quartz or pure K-feldspar beds. Thus, results presented in this work have to be considered first insights into the thermal stability of alternative bed materials when interacting with biomass ash in industrial scale DFB gasification of biomass.

Conclusions will be drawn regarding the suitability of the investigated minerals for DFB gasification of biomass.

2. MATERIALS AND METHODS

2.1. Description of Dual Fluid Bed Steam Gasification of Biomass. Figure 1 shows a simplified flow sheet of the DFB gasification process as installed in Senden, Germany. The feedstock enters directly into the bubbling fluidized bed of the gasifier via a screw conveyor. Gases released from biomass particles come immediately into contact with the catalytically active bed particles. Olivine is currently used as the bed material in all industrial scale power plants. Its main function is as the heat carrier between the combustion and gasification reactors, but it also acts as a catalyst in reducing the heavier hydrocarbons (tars). Steam is the gasifying agent in the bubbling fluidized bed. Calcium oxide is used as an additive to enhance the catalytic activity of olivine.

Part of the char from the solid biomass is transported, together with the bed material from the gasifier, to the combustion reactor via a chute. Combustion occurs in a fast fluidized bed using air as the fluidizing agent. After passing through the combustion reactor, bed particles are separated from the flue gas stream in a cyclone and transported back to the gasifier. Flue gas passes through a postcombustion chamber to ensure complete oxidation of the combustible compounds before being cooled in heat exchangers. Fine ash is separated from the gas stream by a flue gas filter and removed from the system. The resultant gas is passed through a scrubber unit filled with rapeseed methyl ester (RME) where impurities such as tars, ammonia, and sulfur components are captured and water is condensed out. The clean synthesis gas can then be used for various purposes. In Senden, the gas is delivered to gas engines to generate electricity and district heat. It is also used in this way in Güssing and Oberwart in Austria.

Figure 2 shows a more detailed illustration of the DFB reactors. The zones which are most likely to be critical regarding the thermal stability

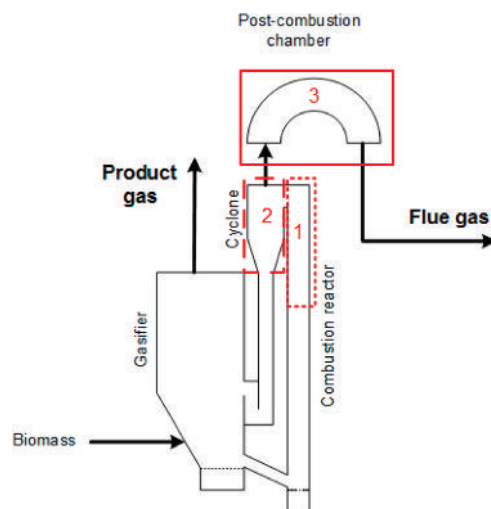


Figure 2. Zones with critically high temperatures: (1) upper part of the combustion reactor, (2) cyclone, (3) postcombustion chamber.

of bed particle layers are highlighted. Critically high temperatures of up to 1100 °C and consequently high potentials for deposit build-up and slagging occur in the combustion path, as has been observed and described in previous work.³⁶ Temperature profiles in these zones will be discussed later on in the context of long-term steady state operation of the power plant. Data used for the evaluation of these temperature profiles was provided by the CHP plant in Senden.

2.2. Sampling at the CHP Plant in Senden, Germany.

Feedstock and bed material samples were collected at the industrial scale CHP plant in Senden. This plant has a fuel power of 15 MW_{th}. It generates electricity of about 5.1 MW_{el} in two gas engines and an organic Rankine cycle (ORC) and provides about 6.4 MW_{th} of district heating. Logging residues, including cutoff root ends, branches, and tops, are used as feedstock. This fuel comprises on average 15% needles and 15% bark. More information about the feedstock used is given by Kuba et al.³⁶ As part of this feedstock, particles of impurities such as quartz and feldspar are transported into the gasifier and are mixed in with the olivine bed material. These particles behave, alongside olivine, as bed material and indeed are found to a certain extent in bed material samples as described in previous work.³⁶ Bed material samples were taken from the bottom of the combustion reactor as well as from coarse ash before its return to the combustion reactor during steady state operation of the power plant. The sampling positions are also shown in Figure 1. At the sampling time, the CHP plant had been in operation for around 1200 h without cooling down.

The quartz and K-feldspar samples are therefore not commercial materials. However, since the investigations in this work concentrate on the basic interactions of these materials with biomass ash, results derived from the sampled particles give a good insight into the basic suitability of the materials. Layer formation in a pure quartz or pure K-feldspar bed have to be addressed separately, as some components might behave slightly different without the presence of other materials. However, the samples show important information about the interaction tendency of inorganic components with the different materials.

2.3. Ashing and XRF Analysis of Feedstock. Feedstock samples were transformed into ash according to DIN CEN/TS 14775. Wood samples were heated up to a temperature of 250 °C. This temperature was maintained for 60 min. Then, the temperature was increased to 550 °C and maintained until transformation of the biomass into ash was completed. The ash produced from the feedstock was then subjected to X-ray fluorescence (XRF) analysis.

To do this, the ash samples were melted in a Merck Spectromelt at 1050 °C and placed on a stainless steel plate at a temperature of 400 °C. Using the Spectromelt ensured that no evaporation of, e.g., sodium or potassium took place. The XRF analysis was then carried out by a PANalytical Axios Advanced analyzer. This analyzer works in a vacuum with a rhodium anode, an excitation voltage of 50 kV, and a tube current of 50 mA. Results of XRF analysis indicated the elemental composition of the total sample, all of which is present as oxides. Unprocessed feedstock samples were also analyzed using XRF.

The composition of the feedstock ash is presented in Table 1. The composition listed is that of the woody biomass and not the mineral

Table 1. Elemental Fuel Ash Composition (Expressed As Oxides) Identified with XRF Analysis

| | feedstock ash mass fraction |
|--------------------------------|-----------------------------|
| Fe ₂ O ₃ | 0.7 |
| MnO | 0.0 |
| CaO | 55.6 |
| K ₂ O | 12.6 |
| SO ₃ | 2.9 |
| P ₂ O ₅ | 4.8 |
| SiO ₂ | 13.4 |
| Al ₂ O ₃ | 3.3 |
| MgO | 5.0 |
| Na ₂ O | 0.8 |
| Others | 0.8 |

impurities, such as quartz or feldspar particles, which are present in the feedstock. Mineral impurities are not present in every feedstock batch brought to the power plant, and levels vary significantly from batch to batch. Therefore, fuel ash analysis is confined to biomass ash components relevant for the interaction with bed material. Only the main elements are displayed, and the mathematical remainder (called “others”) includes the components SnO, MoO₃, Nb₂O₅, ZrO₂, PbO, As₂O₃, ZnO, CuO, Co₃O₄, V₂O₅, TiO₂, and Cl. They are of no further interest regarding the investigation of layer formation and are therefore not included in further results of this paper. As the power plant uses woody biomass as feedstock, components such as SO₃, Fe₂O₃, or Na₂O are present in a limited amount.

2.4. ESEM/EDS analysis. Bed material samples were mounted in epoxy, cross-sectioned and polished. Determination of the chemical composition and morphology of the samples was achieved using an environmental scanning electron microscope (ESEM) combined with energy dispersive X-ray spectroscopy (EDS). Elemental composition was determined by spot analysis in the cross-section of the particles and the corresponding layers. Spot analyses were performed for both inner and outer particle layers. For each particle investigated, between five and 10 spot analyses were conducted, and more than 30 particles of the different bed materials were investigated in every sample. The results obtained from these analyses were statistically evaluated.

2.5. Thermochemical Equilibrium Calculations. Thermochemical equilibrium calculations were carried out using FactSage 6.3 used to predict the melting behavior of the inner layers of the bed particles in DFB gasification conditions and thus gain a deeper understanding of the tendency toward agglomeration during layer formation. Agglomeration during initial layer formation has to be especially considered as once an outer layer is formed its high Ca levels typically protect the particle surface from further agglomeration.⁴⁹ Those calculations were based on results gained from EDS analysis of the samples. For the composition of the layers, average values which were gained from analyses were used.

FactSage 6.3 is based on the uses of the minimization of the total Gibbs free energy of a chemical system. The thermodynamic data required were taken from the Fact-database of gaseous compounds, stoichiometric condensed phases, and nonideal solutions. Table 2 shows the data used in FactSage 6.3. Calculations were performed for

temperatures between 700 and 1100 °C in 50 °C steps with an excess air ratio of 1.2.

Table 2. Elements and Solution Models Used in the Thermochemical Equilibrium Calculations

| elements | C, H, N, O, K, Na, Ca, Mg, Si, Fe, Al |
|-----------------|---|
| solution models | slag: SLAGA (MgO, SiO ₂ , CaO, K ₂ O, Fe ₂ O ₃ , FeO, Al ₂ O ₃) olivine (Mg, Fe, Ca//SiO ₃) MulF (mullite Al ₆ Si ₂ O ₁₃ , Fe ₆ Si ₂ O ₁₃) Mel (melilite Ca ₂ MgSi ₂ O ₇ , Ca ₂ Al ₂ SiO ₇ , Ca ₂ FeSi ₂ O ₇ , Ca ₂ Fe ₂ SiO ₇) salt melt: MELTA (K, Na//CO ₃ , OH salt melt) LCSO (K, Ca//CO ₃ melt) SCSO (K, Ca//CO ₃ solid solution) |

3. RESULTS

3.1. Temperatures in Industrial Scale DFB Gasification. This subsection will give an overview of temperature levels during steady state operation of the CHP plant in Senden. Data from 3 weeks of continuous operation were evaluated. After filtering the raw data so that only operation at full capacity was considered, a total of 25 655 data points for each temperature level were included for further evaluation. Table 3 shows the main average temperatures, which are

Table 3. Average Temperatures in the Gasifier and Combustion Reactor

| | gasifier bed, °C | upper part of the combustion chamber, °C | cyclone outlet, °C | outlet of the postcombustion chamber, °C |
|---------------------------|------------------|--|--------------------|--|
| average | 856 | 884 | 1018 | 922 |
| standard deviation (± 1σ) | 5.6 | 5.9 | 26.8 | 37.5 |

relevant to our analysis. The average bed temperature in the gasifier is around 856 °C, whereas 884 °C is the average in the upper part of the combustion reactor. The highest temperatures, averaging 1018 °C, are reached at the cyclone outlet, where the bed material has been separated from the flue gas stream.

However, to assess the thermal stability of bed particle layers in real process conditions, the temperature peaks have to be considered as well as the averages. Thus, a histogram of the frequency distribution of temperatures measured at the cyclone outlet is presented in Figure 3. This shows that temperature

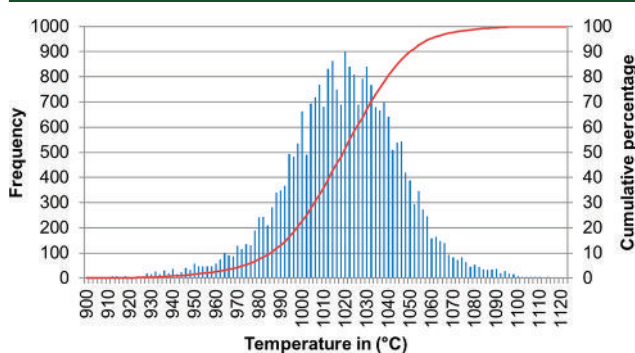


Figure 3. Frequency distribution of the cyclone temperature.

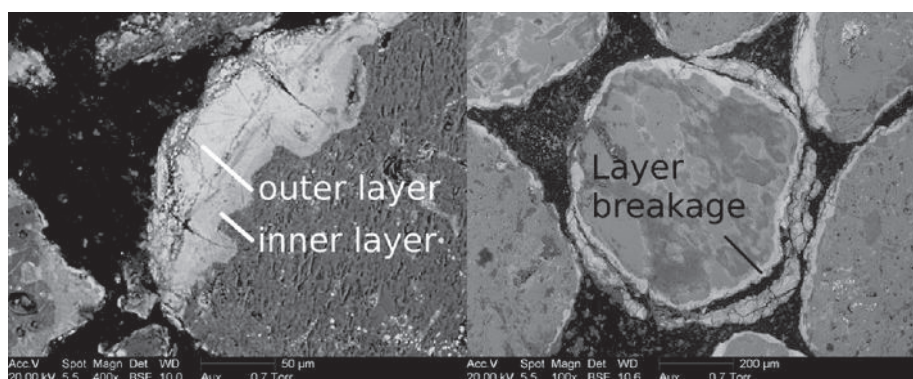


Figure 4. ESEM images of typical cross sections of olivine particles showing layers (left) and layer breakage (right).

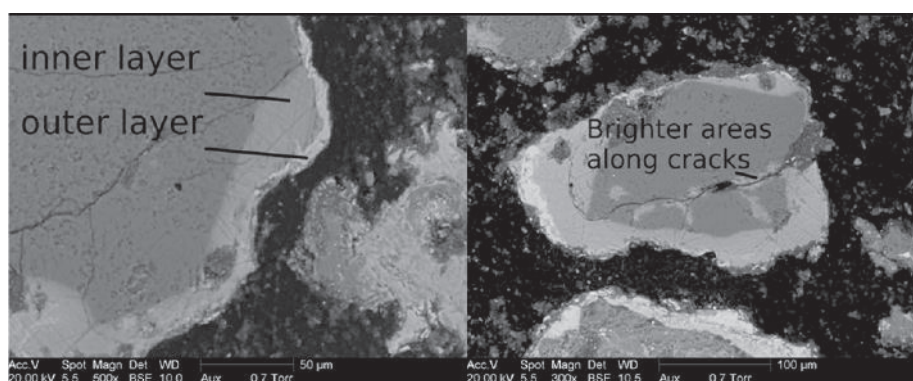


Figure 5. ESEM images of typical cross sections of the inner and outer layers on the surface of quartz particles (left) and particle crack layers (right).

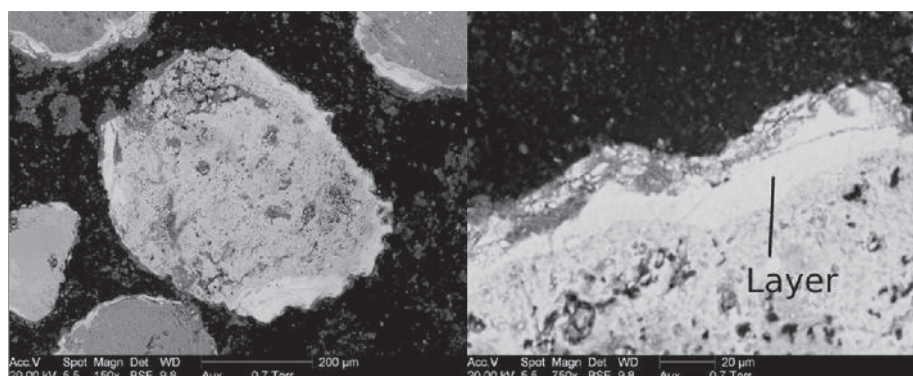


Figure 6. ESEM images of typical cross sections of feldspar layer (left) and as close-up (right).

fluctuations give rise to a spread in measurements of around 200 °C. We see that temperatures of up to 1100 °C are reached during steady state operation. The significance of temperature peaks is considered further below.

3.2. Morphology of Particles and Layers. This subsection focuses on the morphology of particle layers. The tendency toward cracking of the particles themselves and their layers will be addressed. As mentioned above and described in previous work,⁴⁰ the olivine particles which have been used in a fluidized bed are characterized by the formation of an inner and an outer layer which show up in ESEM images as brighter peripheries around the darker particle. Circumferential cracks spread through the particle layers, and for numerous particles breakage of the layers can be observed, as seen in Figure 4 (right). Parts of particle layers which have broken off were found as fragments in the samples.

Quartz particles with two layers differing significantly in size from each other are shown in Figure 5 (left). The inner layer is significantly thicker than the outer layer, which is visible as a lighter periphery surrounding the darker inner layer. Quartz particles also displayed cracking, along which the formation of brighter areas could also be observed as seen in Figure 5 (right). The brighter areas along the cracks are referred to as crack layers. These crack layers have only been found in aged particles with relatively thick layers.

K-feldspars showed a more uniform morphology with a brighter area surrounding the slightly darker particle as shown in Figure 6 (left). No separate inner and outer layers could be distinguished as for olivine and quartz particles. In addition, the visible layer around feldspar particles does not show any significant signs of crack development or layer breakage as seen in the close-up image in Figure 6 (right).

3.3. Bed Particle Layer Compositions and Predicted Melting Behavior. In this subsection, we focus on the inner layers of bed particles of olivine, quartz, and K-feldspar. Their elemental compositions are presented and discussed, and the melting behavior of the layers for temperatures typical in DFB gasification is predicted using thermochemical equilibrium calculations.

Two layers formed on olivine particles, as shown in Figure 4 and the compositions of the inner and outer layers are listed in Table 4. From this, we see that the outer layer has a

Table 4. Average Elemental Composition on a C- and O Free Basis of Olivine Particle Layers

| | olivine particle | inner layer | outer layer |
|----|-------------------|-------------------|-------------------|
| | | mass fraction (%) | |
| Na | 2.1 (\pm 0.1) | 1.2 (\pm 0.1) | 0.6 (\pm 0.2) |
| Mg | 42.4 (\pm 1.6) | 20.9 (\pm 0.4) | 10.3 (\pm 1.2) |
| Al | 1.0 (\pm 0.1) | 0.8 (\pm 0.1) | 1.1 (\pm 0.3) |
| Si | 36.2 (\pm 1.7) | 22.0 (\pm 1.1) | 7.8 (\pm 1.2) |
| P | 0.3 (\pm 0.1) | 0.7 (\pm 0.1) | 2.2 (\pm 0.2) |
| S | 0.1 (\pm 0.1) | 0.2 (\pm 0.1) | 0.1 (\pm 0.0) |
| Cl | 0.3 (\pm 0.1) | 0.2 (\pm 0.0) | 0.2 (\pm 0.1) |
| K | 1.3 (\pm 0.3) | 0.6 (\pm 0.1) | 0.7 (\pm 0.2) |
| Ca | 4.6 (\pm 0.9) | 47.2 (\pm 1.6) | 71.4 (\pm 3.2) |
| Cr | 0.2 (\pm 0.1) | 0.4 (\pm 0.1) | 0.4 (\pm 0.1) |
| Mn | 0.5 (\pm 0.1) | 0.5 (\pm 0.2) | 1.5 (\pm 0.2) |
| Fe | 11.0 (\pm 1.1) | 5.3 (\pm 0.5) | 3.7 (\pm 0.4) |

significantly higher content of Ca than the inner layer. Only limited amounts of potassium could be detected in the particle layers of olivine. The exact mechanism underpinning the layer formation has been investigated in parallel investigations.⁵⁰ The thermochemical equilibrium calculations for the inner particle layer showed a low tendency toward melting in the operational temperature range with the mass fraction of the melt in the layer varying between 0.5% and 3.7%. It is noteworthy that increasing the temperature did not significantly increase the predicted mass fraction of the melt. Even at 1100 °C, the calculation results predict minor melting of the layer.

Quartz particles also have two layers: an inner and an outer layer. The inner layer is characterized by high amounts of K and Si, whereas the outer layer contains higher amounts of Ca, as shown in Table 5. The Ca-rich outer layer was significantly thinner than the inner layer for the samples investigated.

Crack layers showed strong similarities with the inner particle layer but with slightly lower amounts of K and Ca and higher amounts of Si. The amount of Mg in crack layers is significantly lower than in the inner quartz particle layer. Figure 5 (right) shows an aged quartz particle with crack layers with increased amounts of K and Si, most likely present in the form of potassium silicate. Moreover, a graduation was visible along the crack formation for aged quartz particles.

The thermochemical equilibrium calculations for the inner potassium-silicate-rich particle layer predict a mass fraction for the melt of between 67.3% and 70.7%, depending on the temperature. The melt fraction of 67.3% was calculated for a temperature of 700 °C showing an already high tendency toward melting of the layer.

For K-feldspars, typically KAlSi_3O_8 , the formation of clearly separated particle layers could not be detected when investigating the elemental composition using EDS analysis. Therefore, a “mapping” approach was used as illustrated in

Table 5. Average Elemental Composition on a C- and O-Free Basis of Quartz Particle Layers (ESEM Measurements)

| | quartz particle | inner layer | outer layer | crack layers |
|----|-------------------|-------------------|-------------------|-------------------|
| | | mass fraction | | |
| Na | 0.7 (\pm 0.1) | 1.5 (\pm 0.4) | 0.7 (\pm 0.2) | 1.9 (\pm 0.3) |
| Mg | 3.9 (\pm 0.4) | 4.7 (\pm 0.5) | 3.7 (\pm 1.1) | 1.7 (\pm 0.2) |
| Al | 1.9 (\pm 0.1) | 1.8 (\pm 0.2) | 3.5 (\pm 1.0) | 2.6 (\pm 0.2) |
| Si | 85.1 (\pm 2.1) | 55.4 (\pm 1.7) | 42.1 (\pm 3.1) | 63.4 (\pm 2.7) |
| P | 0.3 (\pm 0.1) | 0.3 (\pm 0.1) | 0.7 (\pm 0.1) | 0.5 (\pm 0.1) |
| S | 0.3 (\pm 0.1) | 0.1 (\pm 0.1) | 0.3 (\pm 0.0) | 0.1 (\pm 0.1) |
| Cl | 0.5 (\pm 0.1) | 0.1 (\pm 0.1) | 0.5 (\pm 0.1) | 0.2 (\pm 0.1) |
| K | 2.7 (\pm 0.4) | 23.5 (\pm 1.1) | 6.7 (\pm 1.1) | 19.7 (\pm 1.3) |
| Ca | 2.4 (\pm 0.3) | 10.5 (\pm 1.6) | 39.4 (\pm 2.1) | 8.9 (\pm 1.1) |
| Cr | 0.3 (\pm 0.1) | 0.3 (\pm 0.1) | 0.2 (\pm 0.0) | 0.3 (\pm 0.1) |
| Mn | 0.3 (\pm 0.1) | 0.3 (\pm 0.1) | 0.4 (\pm 0.1) | 0.4 (\pm 0.2) |
| Fe | 1.6 (\pm 0.3) | 1.5 (\pm 0.3) | 1.8 (\pm 0.6) | 0.3 (\pm 0.1) |

Figure 7. Starting from within the bulk of the particle itself (x_1), numerous spot analyses were taken along a line going outward

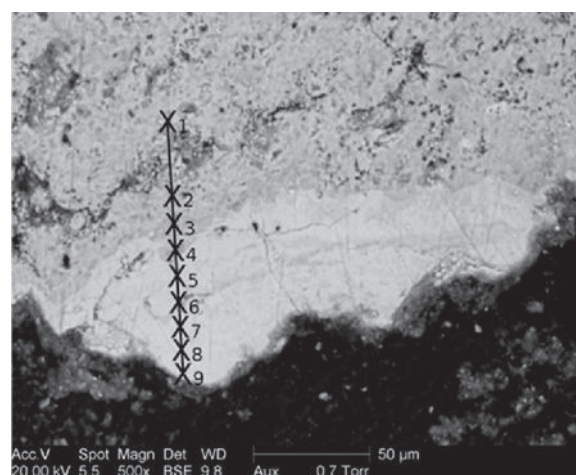


Figure 7. ESEM image of mapping along a typical cross-section of a K-feldspar layer.

toward the layer surface (x_2 – x_9). This was carried out for numerous K-feldspar particles. Table 6 shows the composition (average values) for the individual spots. The main components for K-feldspar are displayed in Figure 8, where the gradual reduction of silicon, potassium, and aluminum and the simultaneous increase of calcium can be seen. Especially the increase of calcium inside the particle, where no distinguishable layer can be detected in the SEM images, is noteworthy here. The issue of gradually increasing Ca contents without the establishment of clearly distinguishable particle layers will be addressed in further detail in the discussion.

This increase inside the particle (with rising amounts toward the surface) was observable for all K-feldspars, which had already developed a particle layer. Thus, K-feldspars differed significantly from olivine and quartz particles due to the makeup of the layer. All particles had a significant increase of Ca on the particle surface in common.

Since no clearly distinguishable inner layer could be observed, thermochemical equilibrium calculations were carried out for compositions around the middle of the sampled areas, namely x_4 and x_5 . Calculations using the composition x_4 resulted in mass fractions of the melt between 13.1% and

Table 6. Average Elemental Composition on a C- and O-Free Basis across K-Feldspar Particle Layers

| | x ₁ | x ₂ | x ₃ | x ₄ | x ₅ | x ₆ | x ₇ | x ₈ | x ₉ |
|----|-------------------|----------------|----------------|----------------|----------------|----------------|----------------|----------------|----------------|
| | mass fraction (%) | | | | | | | | |
| Na | 1.4 | 0.0 | 0.8 | 1.2 | 0.6 | 0.9 | 0.8 | 0.7 | 1.1 |
| Mg | 4.8 | 5.3 | 4.5 | 6.4 | 3.7 | 5.4 | 7.5 | 9.7 | 9.8 |
| Al | 14.1 | 11.6 | 11.1 | 3.4 | 4.2 | 2.9 | 2.5 | 2.7 | 2.7 |
| Si | 32.7 | 34.2 | 33.4 | 40.4 | 35.3 | 24.9 | 8.4 | 10.6 | 11.3 |
| P | 0.3 | 0.2 | 0.6 | 0.6 | 0.5 | 0.9 | 1.8 | 2.6 | 2.5 |
| S | 0.2 | 0.0 | 0.2 | 0.0 | 0.2 | 0.1 | 0.2 | 0.2 | 0.2 |
| Cl | 0.2 | 0.3 | 0.3 | 0.0 | 0.4 | 0.2 | 0.3 | 0.1 | 0.3 |
| K | 32.5 | 29.3 | 17.8 | 12.3 | 8.8 | 3.7 | 2.9 | 2.6 | 2.8 |
| Ca | 4.6 | 8.8 | 26.5 | 32.5 | 41.9 | 56.8 | 71.5 | 66.3 | 64.6 |
| Cr | 0.1 | 0.4 | 0.3 | 0.3 | 0.2 | 0.0 | 0.3 | 0.3 | 0.4 |
| Mn | 0.4 | 0.7 | 0.5 | 0.3 | 0.3 | 0.3 | 0.9 | 0.7 | 0.5 |
| Fe | 8.9 | 9.5 | 4.2 | 2.7 | 3.9 | 3.9 | 2.8 | 3.5 | 3.7 |

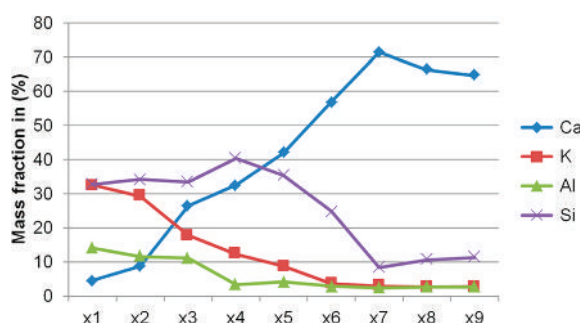


Figure 8. Main components in K-feldspar layers on C- and O-free basis.

14.8%, whereas those using the composition x₅ showed an even lower tendency toward melting with melt fractions between 5.3% and 8.4%, depending on the temperature. It was found that increasing the operational temperature in the modeling runs, even up to 1100 °C, did not increase the mass fraction of the melt significantly.

4. DISCUSSION

In this section, the findings described above will be explained in detail and critically evaluated. The layers formed on the surface and cracks of bed particles as a result of interaction between bed material and fuel ash will be reviewed in terms of their thermal stability at temperatures which are typical in industrial scale DFB gasification plants.

The results from ESEM and EDS analysis showed strong differences in the layer characteristics of the three naturally occurring materials investigated: olivine, quartz, and feldspar.

Thermochemical equilibrium calculations showed a low tendency toward coating-induced agglomeration for the inner layers of olivine particles due to high melting temperatures. This is due to the fact that only low amounts of alkalis such as potassium or sodium are found in olivine layers. The melting of olivine particle layers leading to agglomeration does not seem to be a major problem, even at temperatures up to 1100 °C.

The formation of particle layers on quartz occurs due to reaction between potassium and quartz, resulting in the formation of potassium silicates. Potassium levels of up to 25 wt % were observed in the inner layer. The thermochemical equilibrium calculations predict that this will lead to a melt fraction of more than 67% at 750 °C, which rises still further with increasing temperature. While no outer calcium-rich layer has yet formed, the melting of the potassium silicate layer leads

to a sticky particle surface resulting in agglomeration of the bed and deposit buildup in the combustion reactor, cyclone, and postcombustion chamber.

These sticky layers are a critical factor in agglomeration and, as a result, defluidization of beds. We have seen that in the upper part of the combustion zone of the dual fluid bed, process temperatures of around 883 °C are typical, but temperature fluctuations can cause peaks up to 1100 °C in the cyclone. Furthermore, smaller particles which are not separated from the flue gas stream by the cyclone pass through the postcombustion chamber, where the flue gas stream is redirected by 180°, as shown in Figure 2. Particles with sticky surfaces have a high probability of building up deposits through collision with the wall. Some of these particles are recirculated back to the combustion reactor after leaving the postcombustion chamber, where temperatures are still around 920 °C, and so stay in the system.^{36,51}

In combustion systems, counter-measures include the dilution of critical components such as potassium in the bed and the replacement of old bed particles by fresh ones.⁵² However, since the Ca-rich layers are necessary in gasification due to their catalytic activity, such replacement can be counter-productive in terms of tar reduction. For this reason, layer build-up is desirable, and therefore bed particles should be kept in the system as long as possible. Thus, using quartz sand as a bed material or quartz polluted fuel such as logging residues for dual fluid bed gasification is problematic as regards bed material agglomeration, slagging, and deposit build-up.

K-feldspar particles were characterized by increasing amounts of Ca and decreasing amounts of K toward the particle surface, which may be caused by replacement of K and incorporation of Ca into the crystal structure. These findings suggest that layer formation on K-feldspars follows a substantially different mechanism than that of quartz particles. As published recently by Kuba et al.,⁵³ the mechanism of layer formation can differ significantly for the already proposed mechanism for quartz.³⁰ Thus, the increasing amount of Ca in K-feldspars from interaction with biomass ash in an industrial-scale gasification plant suggest a similar substitution mechanism rather than a K-attack toward Si, as known for quartz particles. This substitution preserves a stable crystal structure.

Even though the exact mechanism is not yet known, the data for melting behavior combined with the findings of the Ca incorporation give a strong estimate about the thermal stability of K-feldspars in gasification plants. The thermodynamic equilibrium calculations predict that this composition should

have a significantly lower tendency toward coating-induced agglomeration than quartz, as the closer to the surface we get, the lower the melt fraction is. Feldspars used as bed material have been reported to decrease defluidization problems compared to quartz in fluidized bed combustion.^{23,54,55} In comparison to the inner layer of olivine, the melt fraction was slightly higher. However, due to the increasing Ca content near the surface, the tendency toward agglomeration is expected to be a minor issue.

In dual fluidized bed gasification of biomass, bed materials constantly change from a reducing atmosphere to an oxidizing atmosphere and back. Ash chemistry can be influenced by the changing atmospheres, as certain inorganic components form different compounds depending on the surrounding atmosphere. Kaknics et al.^{27,56} have observed that, e.g., sulfur is present in different forms in a reducing or oxidizing atmosphere. Moreover, Niu et al.⁵⁷ found that with the insufficient amounts of oxygen, e.g., chlorine is more likely to form metal-chlorides. These phenomena have to be considered when investigating ash chemistry in DFB gasification. Here in this work, bed material was sampled from the combustion chamber, where part of the biomass is burned in order to produce energy needed in gasification. The combustion part seems to have a major influence on the layer formation. No significant difference to studies in fluidized bed combustion has been identified for the samples. The layer formation due to interaction between biomass ash and bed material seems to play an important role in the zone of the higher temperature, in the combustion reactor. However, further research is needed to completely understand the influence of atmosphere changes.

Due to the development of layers on bed material particles the surface stability changes relative to the original particle. Thermal changes of bed particles and their layers can lead to fragmentation and as a result to an increase of undesired fines in the system. Even though olivine particles did not show any signs of crack formation inside, calcium-rich particle layers were characterized by the development of cracks which led to breakage of parts of the layer. As a result, fragments of the layers exist loosely in the dual fluid bed system, which increases the fines in the system.

Quartz particles showed two different characteristics related to their stability. Cracks were observed in the particles themselves, leading to fracturing. These could originate from well-known temperature dependent changes in the crystal structure.⁵⁸ The quartz inversion transforms α -quartz to β -quartz at 573 °C, where a linear expansion of 0.45% takes place. Therefore, during the heat-up phase, irreversible cracking of the bed material occurs. Above 870 °C, β -quartz further changes to tridymite. Crack layer formation seems to be a consequence of this. Those crack layers have strong similarities with the inner particle layer, which leads to the conclusion that the formation mechanism is the same. The presence of cracks results in potassium silicate rich areas along the cracks in the quartz particle, which can lead to the fracture of the quartz particles. This, combined with the predicted partial melting discussed above 750 °C, could lead to the production of sticky fragments of potassium silicates.^{36,58}

K-feldspar did not show any stability problems in DFB gasification. Furthermore, no crack formation was observed in K-feldspar or its layers, which should decrease fracturing of bed material compared to quartz and fracturing of bed particle layers compared to olivine, which mainly regard the particle surface and the layers. Olivine differs in this regard from quartz

as quartz particles show fracturing of particles and olivine only shows fracturing of the layers, which leads to an increase in layer fragments in the system. K-feldspar does not show either kind of fracturing and could therefore lead to an improvement in controlling inorganic streams in the system. The incorporation of Ca, which seems to be due to a similar layer formation mechanism to that of olivine, is an important finding regarding the suitability of the material.

Ca-rich layers are known to result in good catalytic activity.^{41,45} Olivine and K-feldspar particles show promising Ca-rich layers, whereas quartz only shows enrichment in Ca once an outer layer has formed. This has been described in detail by He et al.⁴⁹ Promising catalytic performance of both olivine and K-feldspars is also expected after initial formation of particle layers since Ca is already present in the inner layers and near-surface areas, respectively. In comparison to olivine and K-feldspar, Ca enrichment and the development of an outer layer on quartz particles take time.

5. CONCLUSION

To summarize, quartz and feldspar are both materials which are already present in fluidized bed combustion systems when using natural sand.^{25,59} Heavy metal concentrations are not critical and therefore do not contaminate the ash. Thus, they are possible candidates for alternative bed materials in dual fluid bed gasification. Results from this study indicate that K-feldspar is a promising alternative to olivine in dual fluid bed wood gasification, whereas usage of quartz would raise more severe challenges regarding agglomeration and deposit build-up. K-feldspar used as bed material could also lead to an improvement regarding layer fracturing as observed for olivine. However, the exact mechanism underpinning layer growth on K-feldspar is not yet fully understood. Therefore, the findings of this work provide the basis for further research into alternative bed materials for dual fluid bed gasification.

AUTHOR INFORMATION

Corresponding Author

*E-mail: matthias.kuba@bioenergy2020.eu.

Notes

The authors declare no competing financial interest.

ACKNOWLEDGMENTS

This study was carried out within the Bioenergy2020+ project "C20016016" framework. The COMET program is managed by the Austrian Research Promotion Agency (FFG) and promoted by the federal government of Austria as well as the federal states Burgenland, Niederösterreich, and Steiermark. We are grateful for the support of our project partners HGA Senden (Stadtwerke Ulm) and the Institute of Chemical Engineering at the TU Wien. Furthermore, we would like to thank the Department of Energy Engineering, Division of Energy Science, at the Luleå University of Technology, Sweden, as well as the Department of Energy Technology and Thermal Process Chemistry at the Umeå University, Sweden, for their support.

REFERENCES

- (1) *Climate Change 2014: Synthesis Report. Contribution of Working Groups I, II and III to the Fifth Assessment Report of the Intergovernmental Panel on Climate Change*; Pachauri, R. K., Meyer, L. A., Eds.; Core Writing Team, IPCC 2014: Geneva, Switzerland, 2014.

- (2) Kaltschmitt, M.; Hartmann, H.; Hofbauer, H. *Energie aus Biomasse*; Kaltschmitt, M., Hartmann, H., Eds.; Springer: Berlin, 2001.
- (3) *On Thin Ice - How Cutting Pollution Can Slow Warming and Save Lives*; The World Bank, The International Cryosphere Climate Initiative: Washington DC, 2013.
- (4) In *Conference of the Parties, 21st session*; United Nations - Framework Convention on Climate Change, Paris, 2015; Vol. 21932.
- (5) Hofbauer, H.; Rauch, R.; Loeffler, G.; Kaiser, S.; Fercher, E.; Tremmel, H. In *Proceedings of the 12th European Conference and Technology Exhibition on Biomass for Energy, Industry and Climate Protection*; Amsterdam, The Netherlands, 2002; pp 982–985.
- (6) Kraussler, M.; Binder, M.; Fail, S.; Bosch, K.; Hackel, M.; Hofbauer, H. *23rd European Biomass Conference and Exhibition*; Vienna, 2015; pp 1–4.
- (7) Benedikt, F.; Kraussler, M.; Konlechner, D.; Bosch, K.; Hackel, M.; Hofbauer, H. In *Proceedings of the 23rd European Biomass Conference and Exhibition*; Vienna, Austria, 2015; pp 1–4.
- (8) Fail, S.; Diaz, N.; Benedikt, F.; Kraussler, M.; Hinteregger, J.; Bosch, K.; Hackel, M.; Rauch, R.; Hofbauer, H. *ACS Sustainable Chem. Eng.* **2014**, *2* (12), 2690–2698.
- (9) Chianese, S.; Loipersböck, J.; Malits, M.; Rauch, R.; Hofbauer, H.; Molino, A.; Musmarra, D. *Fuel Process. Technol.* **2015**, *132*, 39–48.
- (10) Rehling, B.; Hofbauer, H.; Rauch, R.; Aichernig, C. *Biomass Convers. Biorefin.* **2011**, *1* (2), 111–119.
- (11) Agerborg, J.; Lingehed, E. *Integration of Power-to-Gas in Gasendal and GoBiGas*, Master's Thesis, Chalmers University of Technology, 2013.
- (12) Rauch, R.; Hrbek, J.; Hofbauer, H. *Wiley Interdiscip. Rev. Energy Environ.* **2014**, *3* (4), 343–362.
- (13) Sauciuc, A.; Abosteif, Z.; Weber, G.; Potetz, A.; Rauch, R.; Hofbauer, H.; Schaub, G.; Dumitrescu, I. In *Proceedings of the International Conference on Polygeneration Strategies (ICPS)*; Vienna, Austria, 2011.
- (14) Weber, G.; Rauch, R.; Hofbauer, H. *Biomass Convers. Biorefin.* **2014**, *5*, 85–94.
- (15) Grimm, A.; Öhman, M.; Lindberg, T.; Fredriksson, A.; Boström, D. *Energy Fuels* **2012**, *26* (7), 4550–4559.
- (16) Koppatz, S.; Pfeifer, C.; Hofbauer, H. *Chem. Eng. J.* **2011**, *175*, 468–483.
- (17) Christodoulou, C.; Grimekis, D.; Panopoulos, K. D.; Pachatouridou, E. P.; Iliopoulou, E. F.; Kakaras, E. *Fuel Process. Technol.* **2014**, *124*, 275–285.
- (18) Rauch, R.; Bosch, K.; Hofbauer, H.; Świerczyński, D.; Courson, C. Comparison of different olivines for biomass steam gasification. *Science in Thermal and Chemical Biomass Conversion*; CPL Press: United Kingdom, 2006; pp 799–809.
- (19) Barišić, V.; Hupa, M. *Fuel* **2007**, *86* (3), 464–468.
- (20) Valmari, T.; Lind, T. M.; Kauppinen, E. I.; Sfiris, G.; Nilsson, K.; Maenhaut, W. *Energy Fuels* **1999**, *13* (2), 379–389.
- (21) Nuutinen, L. H.; Tiainen, M. S.; Virtanen, M. E.; Enestam, S. H.; Laitinen, R. S. *Energy Fuels* **2004**, *18* (1), 127–139.
- (22) Davidsson, K. O.; Åmand, L. E.; Steenari, B. M.; Elled, a. L.; Eskilsson, D.; Leckner, B. *Chem. Eng. Sci.* **2008**, *63* (21), 5314–5329.
- (23) Almark, M.; Hiltunen, M. In *Proceedings of the 18th International Conference on Fluidized Bed Combustion*; Toronto, Ontario, Canada, 2005.
- (24) Kuo, J.-H.; Wey, M.-Y.; Lin, C.-L.; Chiu, H.-M. *Fuel Process. Technol.* **2008**, *89* (11), 1227–1236.
- (25) De Geyter, S.; Öhman, M.; Boström, D.; Eriksson, M.; Nordin, A. *Energy Fuels* **2007**, *21* (5), 2663–2668.
- (26) Skoglund, N.; Grimm, A.; Öhman, M.; Boström, D. *Energy Fuels* **2013**, *27* (10), 5725–5732.
- (27) Kaknics, J.; Michel, R.; Richard, A.; Poirier, J. *Energy Fuels* **2015**, *29* (3), 1785–1792.
- (28) Fryda, L. E.; Panopoulos, K. D.; Kakaras, E. *Powder Technol.* **2008**, *181* (3), 307–320.
- (29) Zevenhoven-Onderwater, M.; Backman, R.; Skrifvars, B.-J.; Hupa, M. *Fuel* **2001**, *80* (10), 1489–1502.
- (30) Brus, E.; Öhman, M.; Nordin, A. *Energy Fuels* **2005**, *19* (3), 825–832.
- (31) Gatternig, B.; Karl, J. *Energy Fuels* **2015**, *29*, 931–941.
- (32) Bartels, M.; Lin, W.; Nijenhuis, J.; Kapteijn, F.; van Ommen, J. R. *Prog. Energy Combust. Sci.* **2008**, *34* (5), 633–666.
- (33) Olofsson, G.; Ye, Z.; Bjerle, I.; Andersson, A. *Ind. Eng. Chem. Res.* **2002**, *41* (12), 2888–2894.
- (34) Zevenhoven-Onderwater, M.; Backman, R.; Skrifvars, B. J.; Hupa, M.; et al. *Fuel* **2001**, *80* (10), 1503–1512.
- (35) Boström, D.; Skoglund, N.; Grimm, A.; Boman, C.; Öhman, M.; Boström, M.; Backman, R. *Energy Fuels* **2012**, *26* (1), 85–93.
- (36) Kuba, M.; He, H.; Kirnbauer, F.; Boström, D.; Öhman, M.; Hofbauer, H. *Fuel Process. Technol.* **2015**, *139*, 33–41.
- (37) Scala, F.; Salatino, P.; Boerefijn, R.; Ghadiri, M. *Powder Technol.* **2000**, *107* (1–2), 153–167.
- (38) Scala, F.; Cammarota, A.; Chirone, R.; Salatino, P. *AIChE J.* **1997**, *43* (2), 363–373.
- (39) Montagnaro, F.; Salatino, P.; Scala, F. *Exp. Therm. Fluid Sci.* **2010**, *34* (3), 352–358.
- (40) Kirnbauer, F.; Hofbauer, H. *Energy Fuels* **2011**, *25* (8), 3793–3798.
- (41) Kirnbauer, F.; Wilk, V.; Kitzler, H.; Kern, S.; Hofbauer, H. *Fuel* **2012**, *95*, 553–562.
- (42) Kirnbauer, F.; Hofbauer, H. *Powder Technol.* **2013**, *245*, 94–104.
- (43) Kern, S.; Pfeifer, C.; Hofbauer, H. *Biomass Bioenergy* **2013**, *55*, 227–233.
- (44) Marinkovic, J.; Thunman, H.; Knutsson, P.; Seemann, M. *Chem. Eng. J.* **2015**, *279*, 555–566.
- (45) Kuba, M.; Havlik, F.; Kirnbauer, F.; Hofbauer, H. *Proceedings of the 23rd European Biomass Conference and Exhibition*; Vienna, 2015; pp 1–4.
- (46) Marinkovic, J.; Seemann, M. C.; Schwebel, G. L.; Thunman, H. *Energy Fuels* **2016**, *30*, 4044.
- (47) Corcoran, A.; Marinkovic, J.; Lind, F.; Thunman, H.; Knutsson, P.; Seemann, M. *Energy Fuels* **2014**, *28* (12), 7672–7679.
- (48) Berguerand, N.; Marinkovic, J.; Berdugo Vilches, T.; Thunman, H. *Chem. Eng. J.* **2016**, *295*, 80–91.
- (49) He, H.; Boström, D.; Öhman, M. *Energy Fuels* **2014**, *28* (6), 3841–3848.
- (50) Kuba, M.; He, H.; Kirnbauer, F.; Skoglund, N.; Boström, D.; Öhman, M.; Hofbauer, H. *Energy Fuels* **2016**, *30*, 7410.
- (51) Kirnbauer, F.; Koch, M.; Koch, R.; Aichernig, C.; Hofbauer, H. *Energy Fuels* **2013**, *27* (6), 3316–3331.
- (52) Llorente, M. J. F.; Cuadrado, R. E. *Fuel* **2007**, *86* (5–6), 867–876.
- (53) Kuba, M.; He, H.; Kirnbauer, F.; Skoglund, N.; Boström, D.; Öhman, M.; Hofbauer, H. *Energy Fuels* **2016**, *30*, 7410.
- (54) Vamvuka, D.; Zografos, D.; Alevizos, G. *Bioresour. Technol.* **2008**, *99* (9), 3534–3544.
- (55) Vamvuka, D. *Renewable Energy* **2009**, *34* (1), 158–164.
- (56) Kaknics, J.; Defoort, F.; Poirier, J. *Energy Fuels* **2015**, *29* (10), 6433–6442.
- (57) Niu, Y.; Tan, H.; Hui, S. *Prog. Energy Combust. Sci.* **2016**, *52*, 1–61.
- (58) Tranvik, A. C.; Öhman, M.; Sanati, M. *Energy Fuels* **2007**, *21* (1), 104–109.
- (59) Lindström, E.; Öhman, M.; Backman, R.; Boström, D. *Energy Fuels* **2008**, *22* (4), 2216–2220.

A.5 Paper V

**Mechanism of layer formation on olivine bed particles in industrial scale dual fluid bed
gasification of wood**

Mechanism of Layer Formation on Olivine Bed Particles in Industrial-Scale Dual Fluid Bed Gasification of Wood

Matthias Kuba,^{*,†,‡} Hanbing He,[§] Friedrich Kirnbauer,[†] Nils Skoglund,[§] Dan Boström,^{||} Marcus Öhman,[§] and Hermann Hofbauer[‡]

[†]Bioenergy 2020+ GmbH, Wienerstraße 49, A-7540 Güssing, Austria

[‡]Institute of Chemical Engineering, Technische Universität Wien, Getreidemarkt 9/166, 1060 Vienna, Austria

[§]Energy Engineering, Division of Energy Science, Luleå University of Technology, SE-971 87 Luleå, Sweden

^{||}Thermochemical Energy Conversion Laboratory, Umeå University, SE-901 87 Umeå, Sweden

ABSTRACT: Utilization of biomass as feedstock in dual fluidized bed steam gasification is a promising technology for the substitution of fossil energy carriers. Experience from industrial-scale power plants showed an alteration of the olivine bed material due to interaction with biomass ash components. This change results mainly in the formation of Ca-rich layers on the bed particles. In this paper, a mechanism for layer formation is proposed and compared to the better understood mechanism for layer formation on quartz bed particles. Olivine bed material was sampled at an industrial-scale power plant before the start of operation and at predefined times after the operation had commenced. Therefore, time-dependent layer formation under industrial-scale conditions could be investigated. The proposed mechanism suggests that the interaction between wood biomass ash and olivine bed particles is based on a solid–solid substitution reaction, where Ca^{2+} is incorporated into the crystal structure. As a consequence, $\text{Fe}^{2+/3+}$ and Mg^{2+} ions are expelled as oxides. This substitution results in the formation of cracks in the particle layer due to a volume expansion in the crystal structure once Ca^{2+} is incorporated. The results of this work are compared to relevant published results, including those related to quartz bed particles.

1. INTRODUCTION

Biomass used as a renewable, CO_2 -neutral carbon source is suitable for use in pyrolysis, gasification, and combustion systems.¹ Gasification transforms the solid biomass feedstock into a gaseous secondary energy carrier² or synthetic gas, which can be further used in a broad range of applications. A dual fluidized bed (DFB) gasification system has been developed at TU Wien (Wien, Austria). Endothermic gasification is separated from exothermic combustion: the two processes occur in separate reactors. The two reactors are connected through a circulating bed material that acts as both heat carrier and catalyst for the gasification reactions. The combustion provides the heat necessary for the gasification process.³ Syngas, the product of the gasification of the solid feedstock, can be used for a variety of other applications. Where several products are generated in one plant, this is referred to as poly-generation. In addition to the generation of electricity and district heat, the production of hydrogen,^{4–7} methane,⁸ Fischer–Tropsch diesel,⁹ or mixed alcohols¹⁰ is also possible and has been successfully demonstrated in the past using this technology. Because of the flexibility of the process, it can effectively react to fast changes in the energy market.

In fluidized bed systems using biomass, in both combustion and gasification applications, interactions between the bed materials and woody biomass ash have been observed to lead to the formation of layers on the surface of the bed particles.^{11–13} The layer formation is a result of the interaction between inorganic components and leads to changes in the composition of the particle surfaces.

In the combustion of biomass in fluidized beds, natural sand, mainly consisting of quartz, is normally used as the bed material. Potassium from woody biomass ash attacks the particle surface, forming potassium silicates that play an important role in agglomeration in the fluidized bed.^{14,15} The mechanism describing this interaction between wood ash and quartz particles has been identified and described.¹⁶ In simple terms, it can be explained as an attack by potassium on the particle surface mainly from the gaseous state. Therefore, the initial mechanism underpinning particle layer formation on quartz during wood combustion is based on a gas–solid reaction.

Öhman et al.¹³ have identified two routes for agglomeration. These are melt-induced and coating-induced agglomeration. When using quartz sand as the bed material in the combustion of wood-derived fuels, coating-induced agglomeration is dominant due to the significant decrease of the melting point of the outer layer caused by the formation of potassium silicates.^{17–19} This results in a sticky particle surface. Over time calcium diffuses into the initially potassium-rich layer, leading to the development of a calcium silicate-rich layer.²⁰ This can be viewed as a calcium shell protecting the layer from further potassium attack. The use of quartz as a bed material in fluidized beds has therefore been identified as a major factor in agglomeration and deposit buildup.^{21–25}

Received: June 21, 2016

Revised: August 2, 2016

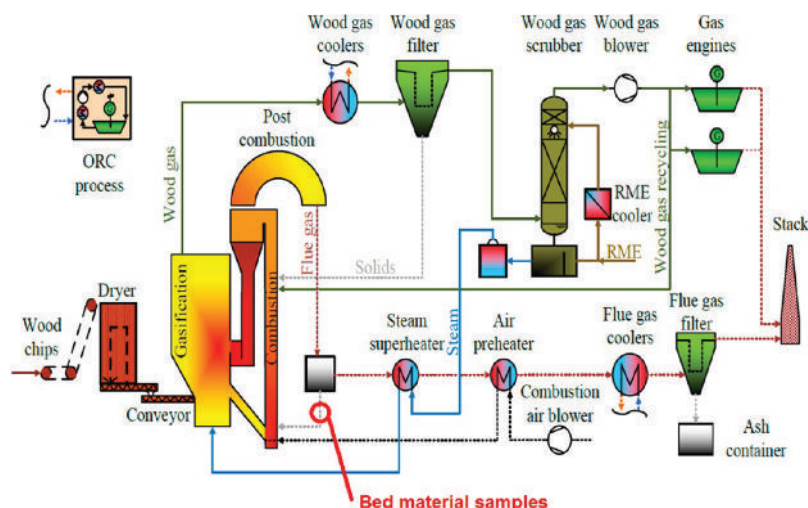


Figure 1. Simplified flow sheet of the CHP plant in Oberwart.

In DFB gasification, a naturally occurring magnesium iron silicate (olivine) is used as a bed material due to its catalytic activity.^{26–31} It has been observed that the long-term interaction between wood biomass ash and olivine particles also leads to the formation of particle layers.³² These layers are Ca-rich and enhance the catalytic activity of the olivine particles in tar reduction.³³ Similar results regarding the interaction between inorganic compounds in biomass ash and olivine bed material were found in later trials by Marinkovic et al.³⁴ The first insights into the mechanism for the formation of this layer on olivine particles were published by Kirnbauer and Hofbauer,³⁵ who proposed a different mechanism for layer formation than that involved in quartz. The initial layer buildup seemed primarily to lead to the formation of calcium–magnesium silicates rather than potassium silicates. Furthermore, Grimm et al.³⁶ found that low concentrations of potassium were retained in olivine bed particle layers, leading to the assumption that Ca is more likely to be involved in the initial layer formation.

Studies of the high-temperature interaction between miscanthus ash and olivine showed that agglomeration of olivine is caused by physical adhesion of molten ashes, i.e., melt-induced agglomeration rather than coating-induced agglomeration.^{37–39} This also sheds light on the mechanism underpinning layer formation on olivine particles.

Olivine is principally a solid solution of two main components: fayalite (Fe_2SiO_4) and forsterite (Mg_2SiO_4). The orthorhombic structure of olivine has two octahedral metal sites that are usually referred to as M1 and M2. These two positions are of major importance when discussing the layer formation on olivine and will be assessed in more detail later. Each position can be occupied by either a Mg^{2+} or a Fe^{2+} metal ion. At temperatures above 600 °C the exchange of ions at these positions is enabled.⁴⁰

The exact mechanism of layer formation on olivine particles in fluidized bed gasification has not yet been described in detail. This work assesses the time-dependent growth of the layers on olivine particles in an industrial DFB gasification power plant using woody biomass as feedstock. A mechanism based on a solid–solid substitution reaction, in which a Ca^{2+} replaces either a Mg^{2+} or a Fe^{2+} in the crystal structure, is proposed and explained. This mechanism is further able to explain the formation of the cracks that occur in particle layers if a particle

interacts with ash components over time. The discussion also includes findings from other published works regarding layer formation on olivine particles and addresses the implications of the newly proposed mechanism for those results. Since olivine has been found to be satisfyingly resistant to agglomeration and deposit formation in comparison to, for example, quartz,⁴¹ understanding the mechanism of layer formation on olivine is the first step toward finding alternative bed materials to olivine. The search for alternatives is essential when discussing the further utilization of biomass ash fractions of the DFB gasification process, since heavy metals from olivine abrasion make further use in, for example, agriculture impossible.

2. MATERIALS AND METHODS

2.1. Sampling at the Industrial Power Plant in Oberwart, Austria. Figure 1 shows a simplified flow sheet of the biomass gasification plant in Oberwart, Austria. This combined heat and power (CHP) plant has a fuel power of 8 MW, generates electricity of around 2.5 MW in two gas engines and in an organic Rankine cycle (ORC), and has the capacity to produce district heating of 4 MW. Fresh olivine was used as bed material for the start-up of the power plant. Following the heat-up phase, in which natural gas was burned by the gas burners but before biomass was transported into the system, calcium oxide was inserted into the gasifier as an additive for 7 h. This was done to increase the catalytic activity of the bed in the start-up phase. When starting up with fresh olivine, the catalytic activity of the bed material is significantly lower than that of used olivine.³³ Therefore, CaO is added during start-up to control tar amounts in the product gas. CaO is added as powder to the system. The feedstock was then added and the operation of the gasification process started. Sampling was carried out by collecting coarse ash before it was returned to the combustion reactor. The sampling position was chosen since sampling from the bottom of the reactor was not possible at the power plant. Bed material and ash leaving the combustion reactor are separated after the postcombustion chamber, and the larger particles—referred to as coarse ash—are transported back to the combustion chamber. Therefore, the coarse ash fraction contains mainly bed particles rather than fine ash. In the analysis with SEM, only bed particles were investigated and taken into account for statistical evaluation. Thus, investigating bed material by sampling coarse ash has been rated to be representative. A sample of fresh olivine was taken before it was introduced into the DFB reactor. Used olivine was collected at different times following the start of operation, which was taken at the point at which the biomass feedstock was introduced to the gasifier. The sampling times were after 4, 8, 16, 24, 32, 48, and 72 h of

operation at full capacity. During this time no fresh bed material was added into the system, so no dilution of the bed material took place.

Two longer time scale samples, one after 180 h and one after around 400 h of operation, were also collected to assess the long-term effects in the layer formation process. These samples were diluted with fresh bed material, which was periodically added to the system to compensate for bed material losses due to abrasion in the fluidized bed. However, aged bed material was clearly distinguishable from younger particles due to its layer thickness. Nevertheless, an exact age of bed particles cannot be stated with certainty for these two samples.

This time-dependent sampling was conducted to evaluate the particle layer growth through continuous interaction between wood biomass ash and olivine. Particle size distribution and information about the composition of fresh olivine have been published in previous studies by Kirnbauer et al.³³ Woody biomass in the form of wood chips was used as feedstock during the operation investigated in this work. Analysis of the fuel ash is shown in Table 1.

Table 1. Elemental Composition (expressed as oxides) Identified by XRF Analysis for Feedstock Ash

| oxides | fuel ash analysis, wt % |
|--------------------------------|-------------------------|
| Fe ₂ O ₃ | 1.5 |
| MnO | 2.0 |
| CaO | 35.4 |
| K ₂ O | 12.3 |
| SO ₃ | 4.4 |
| P ₂ O ₅ | 7.3 |
| SiO ₂ | 19.8 |
| Al ₂ O ₃ | 4.8 |
| MgO | 10.1 |
| Na ₂ O | 1.4 |
| others | 1.0 |
| total | 100.00 |

Gasification was realized at fairly constant temperatures of 850 °C, whereas the temperature at the outlet of the combustion reactor reached 935 °C. This temperature spread is necessary since energy in the form of heat has to be transported from the combustion reactor to the gasification reactor. This transport is done via the circulating bed material, which is heated up in the combustion reactor. In the gasification reactor, steam is used as the fluidizing agent and the gas stream is adapted so that the fluidized bed is in a bubbling regime. In comparison, the air used in the combustion reactor is adjusted so that the fluidized bed is in a transporting (fast fluidized) regime. Thus, bed material and char are transported from the gasifier to the combustion reactor via a chute and then transported upward. After leaving the combustion reactor, bed material is brought back to the gasifier via a siphon.

2.2. ESEM/EDX Analysis. Bed particle samples were mounted in epoxy, cross-sectioned, and dry polished. Environmental scanning electron microscopy (ESEM), combined with energy dispersive X-ray spectroscopy (EDS), was used for the determination of the chemical composition and morphology of the samples. The elemental composition was determined by spot analysis of the cross-section of the particles. For each sample that was investigated by ESEM, between 20 and 30 spot analyses were performed on the bed particle outer layer using EDS. Spot analyses were performed in different regions of the layer to examine the differences in composition. Samples taken at the different times following the start of operation, each containing numerous particles, were investigated. The results obtained were statistically evaluated.

2.3. Thermochemical Equilibrium Calculations. Calculations on the chemical equilibrium reactions of wood ash (represented by Ca and K) and bed material (olivine) were performed to further interpret the findings obtained from the experimental analysis. Fact-Sage 6.3 was used to perform the calculations. This software is based on the minimization of the total Gibbs free energy of a chemical system.

Thermodynamic data were employed from the Fact database regarding gaseous compounds, stoichiometric condensed phases, and nonideal solutions. Table 2 presents the data used in Fact-Sage 6.3. Calculations

Table 2. Elements and Solution Models Used in the Thermochemical Equilibrium Calculations

| | |
|-----------------|---|
| elements | C, H, N, O, K, Na, Ca, Mg, Si, Fe, Al |
| solution models | slag: SLAGA (MgO, SiO ₂ , CaO, K ₂ O, Fe ₂ O ₃ , FeO, Al ₂ O ₃) olivine (Mg, Fe, Ca//SiO ₃) MulF (mullite Al ₆ Si ₂ O ₁₃ , Fe ₆ Si ₂ O ₁₃) Mel (melilite Ca ₂ MgSi ₂ O ₇ , Ca ₂ Al ₂ SiO ₇ , Ca ₂ FeSi ₂ O ₇ , Ca ₂ Fe ₂ SiO ₇) salt melt: MELTA (K, Na//CO ₃ , OH salt melt) LCSO (K, Ca//CO ₃ melt) SCSO (K, Ca//CO ₃ solid solution) |

were performed at 800 °C using an excess air ratio of 1.2. The calculations were performed for different K/bed material as well as Ca/K molar ratios.

3. RESULTS

Findings from the analyses are presented in the following subsections, focusing first on morphology and then on composition. Each section will address the time dependence of the layer growth of olivine particles using the samples taken at different times.

3.1. Development of Olivine Bed Particle Layer Morphology. The morphology of the bed particle layers was seen to change with time. Images from SEM analysis of typical bed particle layers from samples taken at different times are shown in Figures 2 and 3.

The images of bed material samples taken after 4 and 8 h showed traces of a thin, brighter layer surrounding the original olivine particle. However, only limited parts of the particles' surfaces showed signs of layer formation; therefore, only incomplete coverage of the original particle surface had occurred. In comparison, samples taken after around 16 h of operation already showed layer coverage for the greater part of bed particles. The layers themselves, however, had not visibly changed much in appearance from the earlier samples.

The first separation of an inner and an outer layer could be observed after 24 and 32 h, as described in detail by Kirnbauer and Hofbauer.³² Samples taken after longer periods of operation showed an increase in the outer layer thickness, as seen in the samples from 48 and 72 h of operation. During this period the thickness of the inner layer did not notably change.

Samples collected after 180 h of operation showed a separation of the inner layer into two distinguishable zones. The inner zone is a bright band immediately surrounding the olivine particle, whereas the outer zone is visible as a darker, thin band on the borderline between the inner and outer layers. Over the same time scale we see the cracks start to form parallel to the particle surface (i.e., circumferential).

Figure 4 shows the layers of an aged olivine particle collected after an operation time of about 400 h. The separation of the inner layer into two distinguishable zones is now clearly visible and will be explained in more detail in terms of the compositions in the next section.

After long dwell times in the DFB reactor, olivine particle layers exhibit two different kinds of cracks. These cracks are either perpendicular or parallel to the particle surface. Cracks parallel to the surface were observed on the borderline between

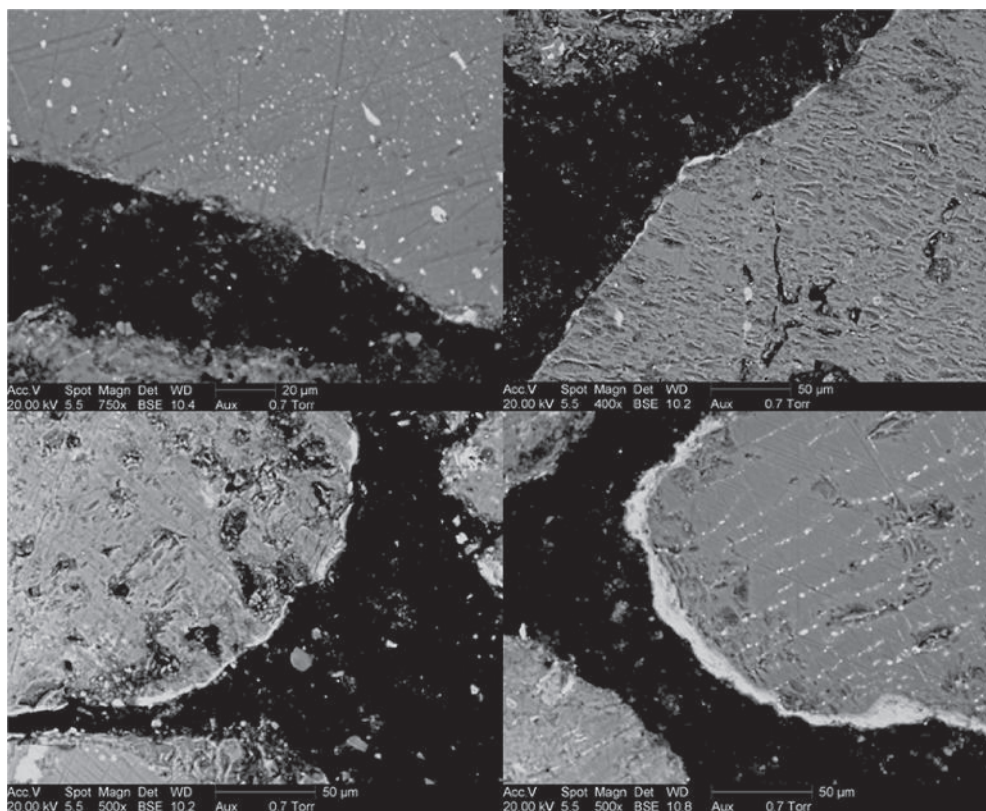


Figure 2. ESEM images of typical cross sections of olivine bed particle layers taken after 4 h (top left), 8 h (top right), 16 h (bottom left), and 24 h (bottom right) of operation.

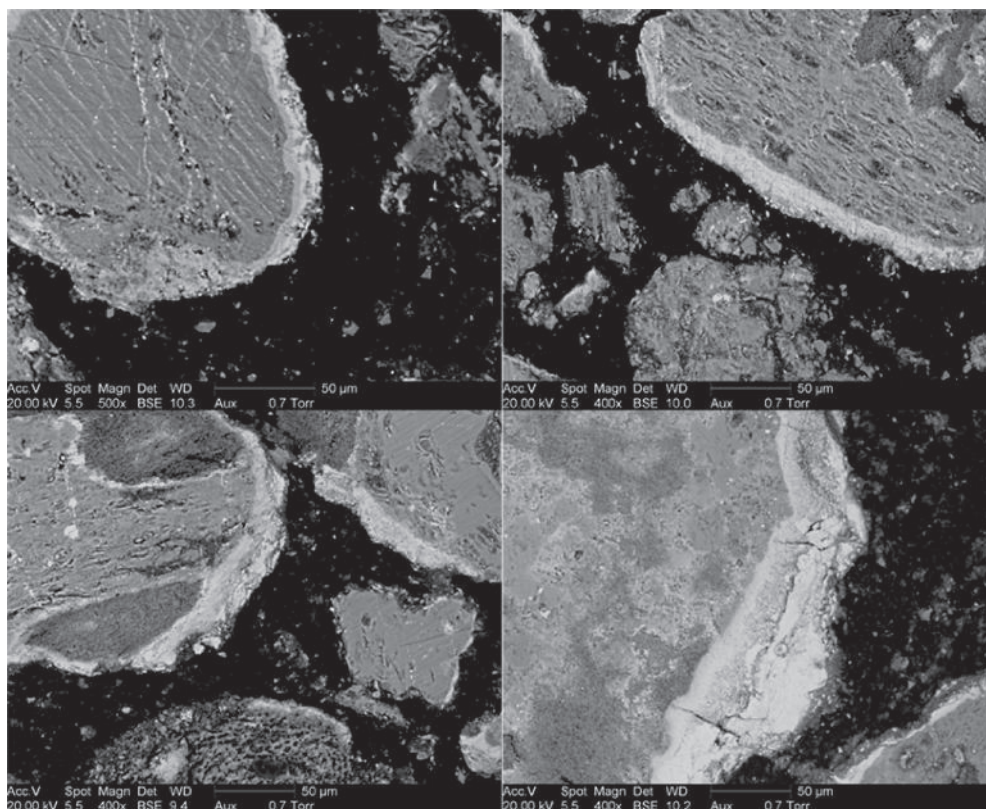


Figure 3. ESEM images of typical cross sections of olivine bed particle layers taken after 32 h (top left), 48 h (top right), 72 h (bottom left), and 180 h (bottom right) of operation.

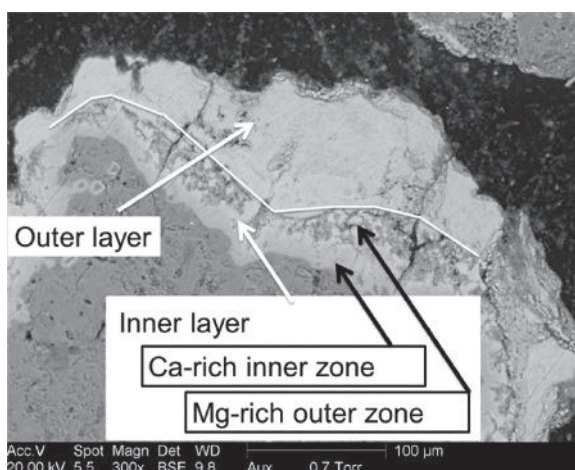


Figure 4. ESEM image of a typical cross section of the olivine bed particle layer taken after about 400 h showing distinguishable zones of the inner particle layer.

the outer zone of the inner layer and the outer layer. They appear to be continuous throughout the particle layer, as seen in Figure 5. Numerous particles with the outer layer broken off

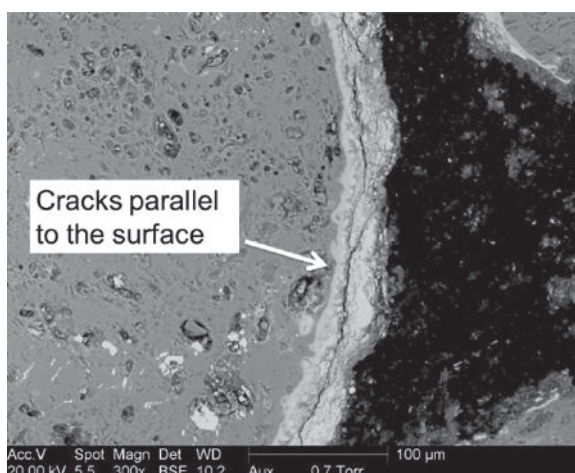


Figure 5. ESEM image of cracks in the olivine bed particle layer parallel to the surface (sample after 180 h of operation).

could be seen as in Figure 6. Where cracks perpendicular to the surface occur, an intrusion of a brighter area into the particle can be observed, as seen in Figure 7.

3.2. Development of Olivine Bed Particle Layer Composition. Changes in composition will be presented for particle layers found in samples taken after different operation times. Table 3 shows the composition of the initial layers on the olivine surface after 4–8 h of operation (Figure 2). The composition is compared to that of the original olivine particle. The thin surface layers showed increased amounts of Ca in comparison to the original olivine particle. It is noteworthy that no significant amounts of K could be detected in this initial layer. The absence of notable amounts of K in the initial layer on olivine particles when using woody biomass will be discussed in more detail later.

Table 4 gives the composition of the inner and an outer zones of the inner layer of an aged (400 h) particle as seen in Figure 4. While the inner zone is richer in Ca, the outer zone

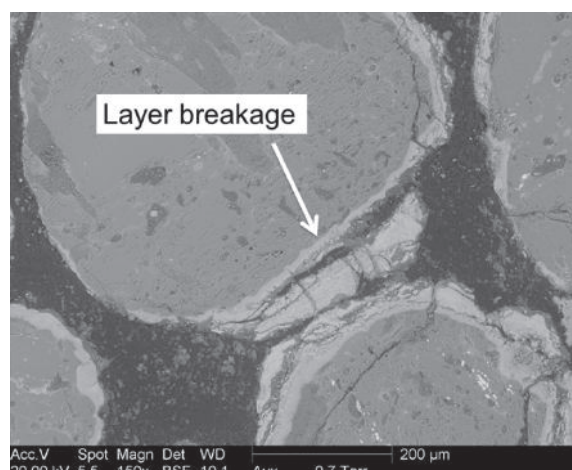


Figure 6. ESEM image of the olivine bed particle layer breakage (sample after 180 h of operation).

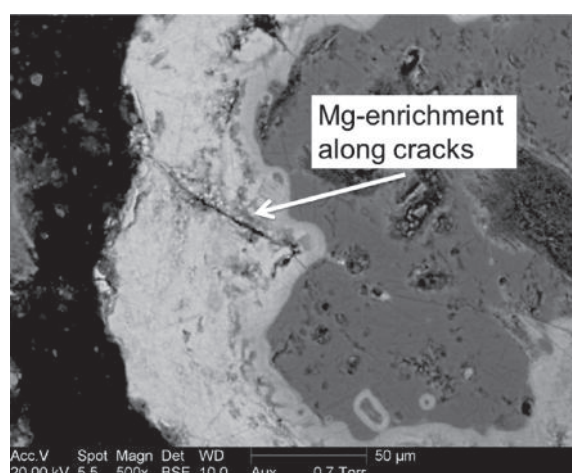


Figure 7. ESEM image of cracks in the olivine bed particle layer perpendicular to the surface (sample after 400 h of operation).

Table 3. Comparison of the Composition of the Original Olivine Particle and the Initial Layer Formed after 4–8 h of Operation

| | mass fraction (%) | |
|----|---------------------------|---------------|
| | original olivine particle | initial layer |
| Na | 2.2 ± 0.2 | 2.0 ± 0.1 |
| Mg | 44.4 ± 1.9 | 41.0 ± 0.6 |
| Al | 1.4 ± 0.2 | 1.2 ± 0.1 |
| Si | 37.1 ± 1.6 | 37.5 ± 1.4 |
| P | 0.1 ± 0.0 | 0.3 ± 0.1 |
| S | 0.1 ± 0.0 | 0.1 ± 0.0 |
| Cl | 0.3 ± 0.1 | 0.3 ± 0.0 |
| K | 0.9 ± 0.2 | 0.7 ± 0.1 |
| Ca | 1.8 ± 0.5 | 5.6 ± 0.7 |
| Cr | 0.2 ± 0.0 | 0.3 ± 0.1 |
| Mn | 0.3 ± 0.0 | 0.4 ± 0.0 |
| Fe | 11.5 ± 1.1 | 10.6 ± 0.8 |

shows higher amounts of Mg. This difference in composition was also observable in the composition of intrusions into the particle surface when cracks perpendicular to the surface were observed. These are also listed in Table 4. These intrusions

Table 4. Comparison of the Compositions in the Inner and Outer Zone of the Inner Layer and at the Intrusion into the Surface and along the Cracks (sampled after 400 h of operation)

| | mass fraction (%) | | | |
|----|-------------------|------------|----------------------------|------------------|
| | inner layer | | intrusion into the surface | along the cracks |
| | inner zone | outer zone | | |
| Na | 1.2 ± 0.1 | 1.6 ± 0.2 | 1.4 ± 0.2 | 1.7 ± 0.2 |
| Mg | 20.9 ± 0.4 | 29.3 ± 2.1 | 23.9 ± 1.2 | 29.9 ± 1.6 |
| Al | 0.8 ± 0.1 | 0.7 ± 0.1 | 1 ± 0.1 | 1 ± 0.2 |
| Si | 22.0 ± 1.1 | 18.9 ± 0.6 | 27.1 ± 0.8 | 25.6 ± 1.0 |
| P | 0.7 ± 0.1 | 0.6 ± 0.1 | 0.5 ± 0.1 | 0.5 ± 0.1 |
| S | 0.2 ± 0.1 | 0.1 ± 0.0 | 0.2 ± 0.0 | 0.2 ± 0.0 |
| Cl | 0.2 ± 0.0 | 0.2 ± 0.0 | 0.3 ± 0.0 | 0.3 ± 0.0 |
| K | 0.6 ± 0.1 | 0.7 ± 0.2 | 1.4 ± 0.2 | 0.8 ± 0.1 |
| Ca | 47.2 ± 1.6 | 40.8 ± 2.1 | 36.4 ± 2.7 | 31.9 ± 2.1 |
| Cr | 0.4 ± 0.1 | 0.3 ± 0.1 | 0.9 ± 0.2 | 0.3 ± 0.0 |
| Mn | 0.5 ± 0.2 | 0.7 ± 0.1 | 0.7 ± 0.1 | 0.7 ± 0.1 |
| Fe | 5.3 ± 0.5 | 6.1 ± 0.4 | 6.2 ± 1.2 | 7.1 ± 2.1 |

were characterized by increased amounts of Ca, whereas Mg enrichment was detected along the cracks, as seen in Figure 8. Both therefore seem to be based on a similar mechanism, as will be explained in the Discussion.

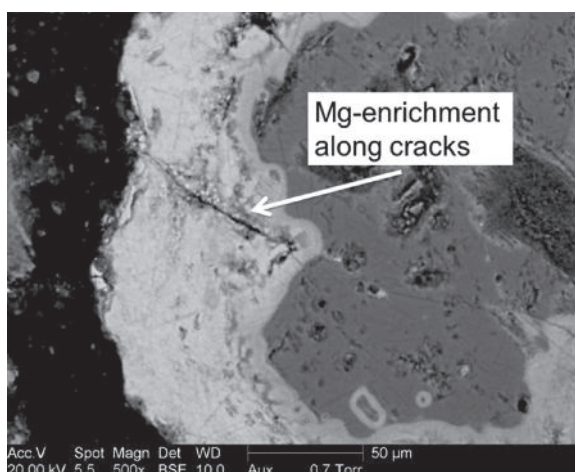


Figure 8. ESEM image of typical Mg-enrichment along cracks in the particle layer.

The time-dependent interaction between biomass ash and olivine particles was also investigated using thermochemical equilibrium calculations. These theoretical calculations predicted the quantities of various crystalline materials dependent on the Ca/K ratio. The calculations were performed for a K to bed material molar ratio of 1/200, which was characteristic of the CHP plant in Oberwart. Increasing the potassium to bed material ratio up to 1/20 did not lead to any significant changes in the results.

Figure 9 shows the crystalline material quantities predicted as Ca levels are increased. The Ca levels are expressed in terms of the Ca/K molar ratio. The baseline is the composition before the addition of Ca, i.e., for a Ca/K ratio of zero. When the fraction of Ca is increased, CaMgSiO₄ and MgO are formed. As more calcium is added, the amount of CaMgSiO₄ reduces and an increase of the mass fraction of Ca₃MgSi₂O₈ occurs. As the

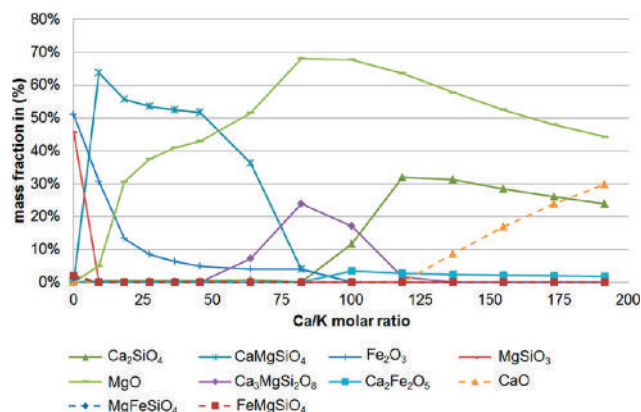


Figure 9. Mass fraction of crystal structures present at varying Ca/K molar ratios at a K to bed (olivine) molar ratio of 1/200.

total mass fraction of Ca–Mg–Si oxides approaches zero, the amount of Ca–Si oxides, such as Ca₂SiO₄, increases. At this stage, Mg is present only in the form of MgO. With further increases in the amount of Ca in the system, CaO becomes the dominant structure. It is notable that the fraction of Fe compounds, such as Fe₂O₃, decreases significantly with rising amounts of Ca.

4. DISCUSSION

In this section, the findings from the ESEM and EDS analyses will be discussed and put into context, along with the results from thermochemical equilibrium calculations. Crystallographic data will also be used. Combined, these results will be used to discuss the mechanisms underpinning the interaction between olivine particles and ash from woody biomass and to address its implications for the results found in the literature.

The first traces of layer formation after 4 and 8 h of operation showed increasing amounts of Ca, while no K was detected. The absence of K and the presence of Ca in the olivine layer formation was further confirmed by the chemical equilibrium calculations. These findings suggest that the initial step of layer formation is based on a solid–solid reaction between CaO and olivine. It should be noted that ash-forming elements introduced with the fuel may form melted K silicates that can act as an adhesive between surrounding ash and the olivine bed particles. Several K–Mg silicates exist that are conceivably products of such a reaction.⁴² Such initial melts may constitute an intermediate that facilitates Ca²⁺ transport into the olivine.

The low concentration of potassium retained in the particle layer is in good accordance with previous studies conducted by Kirnbauer and Hofbauer³⁵ and by Grimm et al.³⁶ This leads us to propose the following mechanism for olivine particle layer formation: This solid–solid reaction between CaO and olivine is a substitution reaction where Ca²⁺ is incorporated into the crystal structure of olivine.

The crystal structures in Figure 10 are taken from reference structures^{43,44} using Mercury 3.8⁴⁵ and show the changes in the crystal structure as the olivine bed material changes from olivine⁴³ to calcium magnesium silicate.⁴⁴ The calcium magnesium silicate monticellite (MgCaSiO₄) is shown in Figure 10. However, two other phases, merwinite [Ca₃Mg(SiO₄)₂] and bredigite [Ca₇Mg(SiO₄)₄] are also stable intermediates. In Figure 10, the yellow sphere in the middle of the structures represents a Si atom. The red spheres are O atoms.

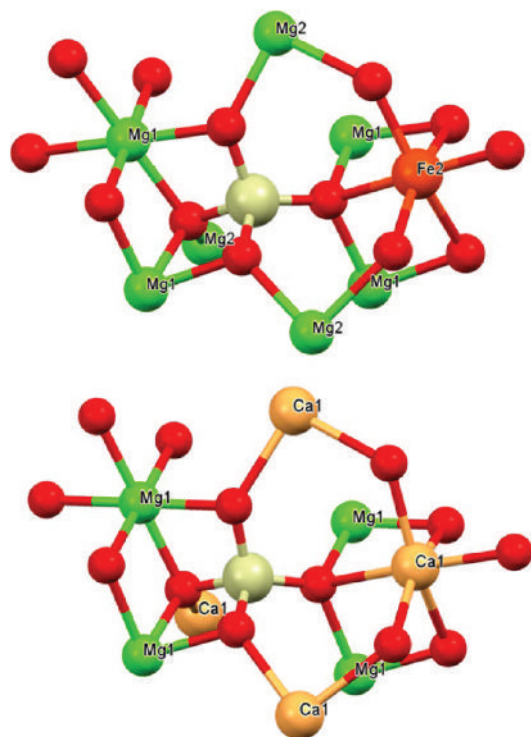


Figure 10. Steps of the substitution mechanism: (1) olivine, $\text{Mg}_{1.8}\text{Fe}_{0.2}\text{SiO}_4$ (top), and (2) CaMgSiO_4 (bottom).

The incorporation of Ca^{2+} into the crystal structure proceeds at one of the exchangeable sites M1 or M2, which are occupied by either Mg^{2+} or Fe^{2+} . Ca^{2+} will preferably occupy the site M2, as it is slightly larger than M1. For a Ca^{2+} ion to be incorporated, a Mg^{2+} or a Fe^{2+} ion has to be expelled from the structure, either accompanied by an O^{2-} from the SiO_4^{4-} or by reacting with the oxygen carried by CaO . This replacement is expected to be due to an ion substitution of a Mg^{2+} or Fe^{2+} by a Ca^{2+} ion. Fe^{2+} is statistically more likely to be replaced than Mg , as described by Smyth,⁴⁰ and is therefore statistically replaced first, before Mg is substituted. Fe is then not present in crystal form anymore and therefore not present in Figure 9 at rising Ca amounts. Besides, it should be noted here that the oxidation of Fe^{2+} , when exposed to air at elevated temperatures, is also likely to take place. As a consequence, so long as not every Mg^{2+} in the crystal structure is replaced by a Ca^{2+} atom, there exist intermediate states that are mainly composed of Ca-Mg silicates.

Substitution of Fe^{2+} by Ca^{2+} in the crystal structure is in good accordance with the results of the work of Kaknics et al.,³⁷ where agglomerates from miscanthus ash and olivine beds were investigated. Fe enrichment was observed in the melt phase once a Ca -rich layer had formed around the olivine particle. Fe diffused from the olivine structure (and was found in the ash attached to olivine particles), while Ca was incorporated by forming a particle surface layer. These findings are further supported by the thermochemical equilibrium calculations performed as part of the present work. These show that Fe levels quickly fall to nearly zero once Ca is added.

Further addition of calcium leads to a Ca silicate-dominated crystal structure, as Ca^{2+} is incorporated at all available exchangeable sites M1 and M2. Once all exchangeable sites are occupied by Ca^{2+} ions, the crystal structure α -dicalcium silicate⁴⁶ is present. This is shown in Figure 11. The three

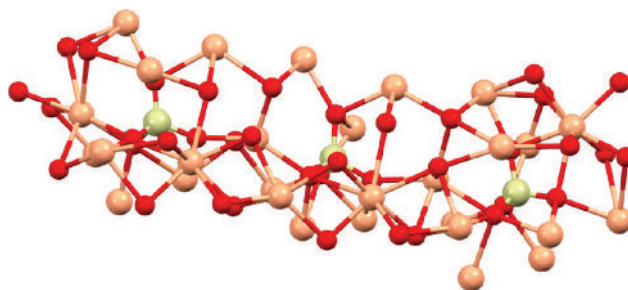


Figure 11. Crystal structure of α -dicalcium silicate.

yellow spheres shown in the figure are Si atoms, and red spheres are O atoms. The exchangeable sites M1 and M2 are now all occupied by Ca^{2+} , represented by the pink spheres.

The observed separation of the inner layer into an inner and an outer zone in the ESEM analysis therefore appears to be based on the substitution of Mg by Ca . As a result of being expelled from the olivine structure, Mg^{2+} accumulates and is trapped between the inner and the outer layers forming on the particle surface, and the outer zone of the inner layer is formed. EDS analysis confirms a relatively high amount of Mg in the outer zone of the inner layer. Thermochemical equilibrium calculations have shown the tendency of Mg^{2+} to form MgO . Therefore, EDS analysis in ESEM investigations has shown a comparably high amount of Mg in the outer zone of the inner layer. Kimbauer and Hofbauer,³⁵ using XRD analysis, also noted the presence of MgO in used, layered olivine particles. At the time this could not be explained.

Thermochemical equilibrium calculations suggest that further increases in Ca levels result in increasing amounts of $\text{Ca}_3\text{MgSi}_2\text{O}_8$, while CaMgSiO_4 concentrations decrease. This is further evidence of Ca incorporation into the originally Mg -rich olivine structure. The change from CaMgSiO_4 to $\text{Ca}_3\text{MgSi}_2\text{O}_8$ represents an increase of the $\text{Ca}:\text{Mg}$ ratio during ongoing substitution of Mg by Ca . With even further increases in Ca levels, no Ca-Mg structures will be present at all, but only Ca_2SiO_4 . At this stage, Mg has been completely expelled from the crystal structure and will only be present in the form of MgO . An increase in the level of CaO marks the last step of layer formation. Increasing amounts of Ca on the particle surface are essential for the catalytic effectiveness of the bed material in tar reduction.^{47,48}

The substitution of Mg by Ca also results in the formation of cracks perpendicular to the surface of the particles. It has to be stated at this point that it cannot be excluded with certainty that some of the cracks might have occurred during the polishing of the samples. However, as explained later on, certain chemical substitution reactions, which could be observed in the SEM, strongly indicate that most of these cracks were formed during operation. As can be seen in Table 5, the substitution of calcium into the olivine has a dramatic initial effect on the unit cell volume per formula unit, i.e., the volume of the smallest repeating unit in the crystal normalized against the amount of formula units in the unit cell. The 17% increase is a direct effect of the difference in bond lengths between metal ions and oxygen atoms in the silicate anion. The $\text{Mg}/\text{Fe-O}$ distance in olivine ranges from 2.075 to 2.145 Å in the Mg/Fe position M1 and between 2.062 and 2.225 Å in the Mg/Fe position M2. In CaMgSiO_4 , the corresponding distance for Mg-O is 2.086–2.191 Å, but it is significantly longer for Ca-O at 2.301–2.480 Å. As Mg^{2+} is fully substituted by Ca^{2+} to form Ca_2SiO_4 (most

Table 5. Unit Cell Data for the Crystal Structure of Olivine,⁴³ Monticellite,⁴⁴ and α -Dicalcium Silicate⁴⁶ Displaying Changes In Unit Cell Dimensions and Volume per Formula Unit

| | Mg _{1.81} Fe _{0.19} SiO ₄ | CaMgSiO ₄ | α -Ca ₂ SiO ₄ |
|--|--|----------------------|--|
| space group | <i>Pbnm</i> | <i>Pbnm</i> | <i>Pna2₁</i> |
| Unit Cell Dimensions (Å) and Volume Per Formula Unit (Å ³) | | | |
| <i>a</i> | 4.7641(7) | 4.822(1) | 20.5266(16) |
| <i>b</i> | 10.2669(17) | 11.108(3) | 9.49636(7) |
| <i>c</i> | 5.9952(8) | 6.382(2) | 5.5897 (5) |
| volume per formula unit | 73.31 | 85.46 | 190.80 |
| | Unit Cell angles (deg) | | |
| α | 90 | 90 | 90 |
| β | 90 | 90 | 90 |
| γ | 90 | 90 | 90 |

likely α -Ca₂SiO₄ at the relevant process temperatures), the volume per formula unit increases by 6% compared to CaMgSiO₄. Also, the unit cell axis changes significantly, creating a further strain in the structure that may promote crack formation.

There are several other modifications of Ca₂SiO₄ that may also induce further strain in the layers formed on the surface of fluidized bed particles. As can be seen in Figure 10, this change is probably induced by going from an octahedral configuration of oxygens surrounding Ca²⁺ in CaMgSiO₄, where four oxygen atoms are located in the same plane and the other two oxygen atoms are almost orthogonal to that plane. This symmetrical configuration surrounding the Ca²⁺ is lost in α -Ca₂SiO₄, as seen in Figure 11. These changes in bond distances and angles are the likely causes of crack formation and will be further exacerbated by physical conditions, such as temperature changes and abrasion.

Due to these cracks, the surface becomes exposed and further intrusion of Ca into the particle is possible. The mechanism of the intrusion is identical to the proposed layer formation mechanism, since Ca²⁺ is again substituting for either Fe²⁺ or Mg²⁺ at the same exchangeable sites in the crystal structure. This phenomenon can be observed in the ESEM and EDS analyses as the separation of Ca and Mg can be detected at the intrusion area and along the cracks. Ca²⁺ is incorporated into the crystal structure at the exposed surface and Mg accumulates along the cracks, indicating that it has been expelled from the olivine structure. This accumulation of Mg along the cracks is therefore equivalent to the outer zone of the inner layer.

Crack formation can also be observed on the borderline between the Mg-rich outer zone of the inner layer and the Ca-rich outer layer. Those cracks, which spread out parallel to the particle surface, seem to be critical regarding layer breakage. They originate at the borderline of Mg, which is present in the form of oxide, and the Ca-rich outer ash layer, since there is no interaction between those two stable structures. They result in a clear physical separation of the outer layer, which is likely to break off during operation.

Thus, the fine share is increased in the system and this can have an impact on the buildup of deposits, as described by Kuba et al.⁴⁹ The increase of fines in the bed material is made even worse by the perpendicular cracks, as these lead to further fragmentation of the already broken outer layer. Moreover, the outer layer is essential regarding the catalytic activity of the particles, since the outer layer possesses the highest amounts of

Ca in the form of CaO, as was also confirmed by the thermodynamic equilibrium calculations.

According to the above description and explanation, no K-rich layers are formed on olivine particles, as is the case for quartz particles. This is due to the low driving force of K to react with olivine. Layers on olivine particles are therefore characterized by higher melting temperatures, and coating-induced agglomeration is a minor issue when using olivine as a bed material. However, K from the biomass ash is likely to react with free Si, also from the ash, leading to melt-induced agglomeration. This is especially so when using fuel high in K and Si and can lead to a buildup of deposits, as described by Kuba et al.⁴⁹ One possible approach to prevent melt-induced agglomeration is to use fuel blends to introduce controlling inorganic substances such as phosphorus and this has been investigated by Grimm et al.⁵⁰ and Skoglund et al.^{51,52} Clearly, a detailed knowledge of the pathways of inorganic matter in DFB gasification is essential to control agglomeration.⁵³

5. CONCLUSION

In summary, an updated and detailed mechanism for olivine particle layer formation in fluidized bed gasification (also applicable to combustion) due to the interaction between woody biomass ash and olivine has been proposed. The proposed mechanism is based on a solid–solid substitution reaction. However, a possible enabling step in the form of a Ca²⁺ transport via melts may occur. Ca²⁺ is incorporated into the crystal structure of olivine by replacing either Fe²⁺ or Mg²⁺, which are located at the exchangeable sites M1 or/and M2. This substitution occurs via intermediate states where Ca–Mg silicates, such as CaMgSiO₄, are formed. Mg²⁺ released from the crystal structure is most likely to form MgO, which can be found in a distinguishable zone between the main particle layers. Due to a difference in the bond lengths between Mg/Fe and their neighboring O's and between the incorporated Ca²⁺ and its neighboring O's, the crystal structure shifts, resulting in formation of cracks.

The proposed mechanism is in good accordance with previous published results. Understanding the mechanisms underpinning the growth of layers is essential to the evaluation of potential alternative bed materials for DFB gasification.

■ AUTHOR INFORMATION

Corresponding Author

*E-mail: matthias.kuba@bioenergy2020.eu.

Notes

The authors declare no competing financial interest.

■ ACKNOWLEDGMENTS

This study was carried out within the Bioenergy2020+ project “C20016016” framework. Bioenergy2020+ GmbH is funded within the Austrian COMET program, which is managed by the Austrian Research Promotion Agency (FFG) and promoted by the federal government of Austria as well as the federal states of Burgenland, Niederösterreich, and Steiermark. We are grateful for the support of our project partner, the Institute of Chemical Engineering at the TU Wien. Furthermore, we would like to thank the Department of Energy Engineering, Division of Energy Science, at Lulea University of Technology, Lulea, Sweden, as well as the Department of Energy Technology and Thermal Process Chemistry at Umea University, Umea, Sweden, for their support. In addition, we would like to

express our thanks to Energie Burgenland for the sampling of olivine at the industrial-scale power plant in Oberwart.

REFERENCES

- (1) Van Swaaij, W.; Kersten, S.; Palz, W. *Biomass Power for the World—Transformations to Effective Use*, 1st ed.; Van Swaaij, W., Kersten, S., Palz, W., Eds.; Pan Stanford Publishing: Singapore, 2015.
- (2) Kaltschmitt, M.; Hartmann, H.; Hofbauer, H. *Energie aus Biomasse*; Kaltschmitt, M., Hartmann, H., Eds.; Springer: Berlin, 2001.
- (3) Hofbauer, H.; Rauch, R.; Loeffler, G.; Kaiser, S.; Fercher, E.; Tremmel, H. In *Proceedings of the 12th European Conference and Technology Exhibition on Biomass for Energy, Industry and Climate Protection*; 2002; pp 982–985.
- (4) Fail, S.; Diaz, N.; Benedikt, F.; Kraussler, M.; Hinteregger, J.; Bosch, K.; Hackel, M.; Rauch, R.; Hofbauer, H. *ACS Sustainable Chem. Eng.* **2014**, *2* (12), 2690–2698.
- (5) Kraussler, M.; Binder, M.; Fail, S.; Bosch, K.; Hackel, M.; Hofbauer, H. *Biomass Bioenergy* **2016**, *89*, 50.
- (6) Kraussler, M.; Binder, M.; Hofbauer, H. *Int. J. Hydrogen Energy* **2016**, *41* (15), 6247–6258.
- (7) Benedikt, F.; Kraussler, M.; Konlechner, D.; Bosch, K.; Hackel, M.; Hofbauer, H. In *Proceedings of the 23rd European Biomass Conference and Exhibition*; 2015; pp 1–4.
- (8) Rehling, B.; Hofbauer, H.; Rauch, R.; Aichernig, C. *Biomass Convers. Biorefin.* **2011**, *1* (2), 111–119.
- (9) Rauch, R.; Hrbek, J.; Hofbauer, H. *Wiley Interdiscip. Rev. Energy Environ.* **2014**, *3* (4), 343–362.
- (10) Weber, G.; Rauch, R.; Hofbauer, H. *Biomass Convers. Biorefin.* **2015**, *5*, 85–94.
- (11) Nuutinen, L. H.; Tiainen, M. S.; Virtanen, M. E.; Enestam, S. H.; Laitinen, R. S. *Energy Fuels* **2004**, *18* (1), 127–139.
- (12) Öhman, M.; Pommer, L.; Nordin, A. *Energy Fuels* **2005**, *19* (4), 1742–1748.
- (13) Öhman, M.; Nordin, A.; Skrifvars, B.-J. J.; Backman, R.; Hupa, M. *Energy Fuels* **2000**, *14* (1), 169–178.
- (14) Brus, E.; Öhman, M.; Nordin, A. *Energy Fuels* **2005**, *19* (3), 825–832.
- (15) Brus, E.; Öhman, M.; Nordin, A.; Boström, D.; Hedman, H.; Eklund, A. *Energy Fuels* **2004**, *18* (4), 1187–1193.
- (16) He, H.; Ji, X.; Boström, D.; Backman, R.; Öhman, M. *Energy Fuels* **2016**, *30* (3), 2227–2232.
- (17) Gatterner, B.; Karl, J. *Energy Fuels* **2015**, *29*, 931–941.
- (18) Montes, A.; Ghiasi, E.; Tran, H.; Xu, C. *Powder Technol.* **2016**, *291*, 178–185.
- (19) Montes, A.; Hamidi, M.; Briens, C.; Berruti, F.; Tran, H.; Xu, C. *Powder Technol.* **2015**, *284*, 437–442.
- (20) He, H.; Boström, D.; Öhman, M. *Energy Fuels* **2014**, *28* (6), 3841–3848.
- (21) Niu, Y.; Tan, H.; Hui, S. *Prog. Energy Combust. Sci.* **2016**, *52*, 1–61.
- (22) Sevonius, C.; Yrjas, P.; Hupa, M. *Fuel* **2014**, *127*, 161–168.
- (23) Lin, W.; Dam-Johansen, K.; Frandsen, F. *Chem. Eng. J.* **2003**, *96* (1–3), 171–185.
- (24) Scala, F.; Chirone, R. *Biomass Bioenergy* **2008**, *32* (3), 252–266.
- (25) Chirone, R.; Miccio, F.; Scala, F. *Chem. Eng. J.* **2006**, *123* (3), 71–80.
- (26) Rauch, R.; Bosch, K.; Hofbauer, H.; Świerczyński, D.; Courson, C. *Science in Thermal and Chemical Biomass Conversion*; CPL Press, 2006; Vol. 1, pp 799–809.
- (27) Corella, J.; Toledo, J. M.; Padilla, R. *Energy Fuels* **2004**, *18* (3), 713–720.
- (28) Devi, L.; Ptasinski, K. J.; Janssen, F. J. J. G. *Ind. Eng. Chem. Res.* **2005**, *44* (24), 9096–9104.
- (29) Devi, L.; Ptasinski, K. J.; Janssen, F. J. J. G.; Van Paasen, S. V. B.; Bergman, P. C. A.; Kiel, J. H. A. *Renewable Energy* **2005**, *30* (4), 565–587.
- (30) Devi, L.; Craje, M.; Thüne, P.; Ptasinski, K. J.; Janssen, F. J. J. G. *Appl. Catal., A* **2005**, *294* (1), 68–79.
- (31) Rapagnà, S. *Biomass Bioenergy* **2000**, *19* (3), 187–197.
- (32) Kirnbauer, F.; Hofbauer, H. *Energy Fuels* **2011**, *25* (8), 3793–3798.
- (33) Kirnbauer, F.; Wilk, V.; Kitzler, H.; Kern, S.; Hofbauer, H. *Fuel* **2012**, *95*, 553–562.
- (34) Marinkovic, J.; Thunman, H.; Knutsson, P.; Seemann, M. *Chem. Eng. J.* **2015**, *279*, 555–566.
- (35) Kirnbauer, F.; Hofbauer, H. *Powder Technol.* **2013**, *245*, 94–104.
- (36) Grimm, A.; Öhman, M.; Lindberg, T.; Fredriksson, A.; Boström, D. *Energy Fuels* **2012**, *26* (7), 4550–4559.
- (37) Kaknics, J.; Michel, R.; Richard, A.; Poirier, J. *Energy Fuels* **2015**, *29* (3), 1785–1792.
- (38) Kaknics, J.; Michel, R.; Poirier, J. *Fuel Process. Technol.* **2016**, *141*, 178–184.
- (39) Michel, R.; Kaknics, J.; de Bilbao, E.; Poirier, J. *Ceram. Int.* **2016**, *42*, 2570–2581.
- (40) Smyth, J. R. *Am. Mineralogist* **1975**, *60*, 1092–1097.
- (41) Kuba, M.; He, H.; Kirnbauer, F.; Skoglund, N.; Boström, D.; Öhman, M.; Hofbauer, H. *Energy Fuels* **2016**, submitted.
- (42) Roedder, E. *Am. J. Sci.* **1951**, *249*, 81–130.
- (43) McCormick, T. C.; Smyth, J. R.; Lofgren, G. E. *Phys. Chem. Miner.* **1987**, *14* (4), 368–372.
- (44) Onken, H. *Naturwissenschaften* **1964**, *51* (14), 334.
- (45) Macrae, C. F.; Bruno, I. J.; Chisholm, J. A.; Edgington, P. R.; McCabe, P.; Pidcock, E.; Rodriguez-Monge, L.; Taylor, R.; van de Streek, J.; Wood, P. A. *J. Appl. Crystallogr.* **2008**, *41* (2), 466–470.
- (46) Mumme, W.; Cranswick, L.; Chakoumakos, B. *Neues Jahrb. Mineral.* **1996**, *170* (2), 171–188.
- (47) Kuba, M.; Havlik, F.; Kirnbauer, F.; Hofbauer, H. *Biomass Bioenergy* **2016**, *89*, 40.
- (48) Kuba, M.; Kirnbauer, F.; Hofbauer, H. *Biomass Convers. Biorefin.* **2016**, DOI: 10.1007/s13399-016-0204-z.
- (49) Kuba, M.; He, H.; Kirnbauer, F.; Boström, D.; Öhman, M.; Hofbauer, H. *Fuel Process. Technol.* **2015**, *139*, 33–41.
- (50) Grimm, A.; Skoglund, N.; Boström, D.; Öhman, M. *Energy Fuels* **2011**, *25* (3), 937–947.
- (51) Skoglund, N.; Grimm, A.; Öhman, M.; Boström, D. *Energy Fuels* **2014**, *28* (2), 1183–1190.
- (52) Skoglund, N.; Grimm, A.; Öhman, M.; Boström, D. *Energy Fuels* **2013**, *27* (10), 5725–5732.
- (53) Kirnbauer, F.; Koch, M.; Koch, R.; Aichernig, C.; Hofbauer, H. *Energy Fuels* **2013**, *27* (6), 3316–3331.